Chapter One

Introduction

1.1 Introduction

The restoration of endodontically treated teeth is a challenging task as it usually involves the rehabilitation of teeth with significant loss of tooth structure. Tooth fracture has been described as a major failure for endodontically treated teeth, and is the third most common cause of tooth loss after dental caries and periodontal disease. It has been suggested that a post should only be used when the remaining coronal tooth tissue can no longer provide adequate support and retention for the restoration (Assif et al., 1993; Torbjörner and Fransson, 2004a).

Various metallic and non-metallic materials such as gold, titanium, stainless steel, carbon, ceramic, zirconia and fibre reinforced composites are being used for dental posts to provide retention to the core that replaces lost coronal part of the tooth structure. Until the mid-1980s, the indirect cast post core system was considered to be the safest way to restore an endodontically treated tooth (Shillingburg et al., 1970). The fabrication of cast posts and cores is time consuming and could be expensive as it requires an intermediate restorative phase. The utilization of prefabricated posts in combination with different types of core materials is much easier and can be performed in one visit (Baraban, 1988; Stockton, 1999; Torbjörner, 2000; Torbjörner and Fransson, 2004a).

It was earlier thought that posts reinforced endodontically treated teeth (Silverstein, 1964; Baraban, 1967), however, other studies have reported otherwise; a post may be a predisposing factor for root fracture (Hunter et al., 1989; Whitworth et al., 2002; Peroz et al., 2005). The most appropriate post material has been widely discussed in the literature (Torbjörner and Fransson, 2004b), and this issue remains controversial. A finite element analysis study by Cailleteau et al. (1992) indicated that a post restored model results in a decreased level of the stress along the coronal facial portion of the root surface which peaked abruptly near the apical end of the posts. These findings contradict the belief that the conventional posts strengthen the tooth by evenly distributing the external forces acting on the tooth. On the other hand, the utilization of flexible materials having dentine-like Young's modulus such as fibre reinforced composite posts has been recommended (King and Setchell, 1990; Asmussen et al., 1999) to reduced the risk of root fracture. However, stress concentration may be focused at the post-dentine interface causing debonding of posts and movement of the core resulting in microleakage (Schwartz and Robbins, 2004). On the other hand, the utilization of rigid posts allow minimal tooth preparation as smaller post diameters can be used, however it may lead to root fracture (Raygot et al., 2001; Sorensen et al., 2001).

The development of the different post and core systems goes along with a paradigm shift in the restorative philosophy of treatment (Morgano et al., 1994). Whilst the traditional approach of treatment concepts is focused on the durability of the restoration, aims for tooth survival. Long term follow up studies on the post and core technique reported highly variable survival rates, demonstrating that root fractures do occur in clinical practice (Sorensen and Martinoff, 1984b; Torbjörner et al., 1995; Yamada et al., 2004).

There is significant mismatch between material properties such as stiffness of the posts and surrounding dental tissues. Moreover, the difference between thermal properties of these dental posts covered by an artificial crown and tooth structure gives rise to thermo-mechanical stresses. High stress concentration can develop at the restorative-materials/tooth interfaces and thus increasing the susceptibility of fracture in endodontically treated teeth (Yang et al., 2001a; Toparli and Sasaki, 2003; Genovese et al., 2006). Therefore, the ideal dental post should have high stiffness at the cervical region and it should be gradually reduced apically.

In order to overcome these shortcomings of dental posts, the concept of Functionally Graded Materials (FGMs) can be applied. Compositional gradient of multilayer materials achieved in FGM has been identified as a possible solution for this problem. The concept of FGM has been conceived as a new material design approach to improve performance compared to traditional homogeneous and uniform materials (Watanabe et al., 2002). This technique allows the production of a material with very different characteristics within the same material at various interfaces. FGM is an innovative material technology, which has rapidly progressed both in terms of materials processing and computational modeling in recent years (Watanabe et al., 2002). Development of functionally graded biomaterials for implants for medical and dental applications has been reported (Hedia and Mahmoud, 2004; Watari et al., 2004; Hedia, 2005a,b; Wang et al., 2007; Yang and Xiang, 2007; Huang et al., 2007; Niu et al., 2009; Rahbar and Soboyejo, 2011). FGM allows the integration of dissimilar materials without formation of severe internal stress and combines diverse properties into a single material system. Therefore, this study aimed to be evaluated at fabricating and characterising functionally graded multilayered composite with various combinations of metal and ceramic materials; titanium, zirconia, alumina, and hydroxyapatite for the fabrication of a novel dental post.

This study is presented in four different chapters according to the different work process; where the early chapters describe the fabrication and characterization of functionally graded multilayered composite (FGMC) based on the preliminary finite element analysis results leading to the fabrication of a functionally graded structured dental post prototype and the determination of fracture resistance and failure mode in restored bovine teeth.

Chapter Two
Literature review

2.1 Teeth structure and its properties

2.1.1 Introduction

Tooth structure has been researched for many decades and both its physical and mechanical properties are major factors to be considered in the quest of finding the ideal replacement materials. Knowledge of the physical properties of teeth and the tissues from which they are formed is important to aid understanding of their mechanical behaviour under clinical loading conditions. The most important of these properties include hardness and elastic properties. Braden (1976) and Waters (1980) reviewed much of the work that has been carried out to determine the physical properties of enamel and dentine. Diseases of teeth result in both structural and mechanical degradation of the tooth. In order to reconstruct the damaged structure, restoration is needed to regain proper functions to the tooth. In order to appreciate the behaviour of a mechanically loaded system, a basic understanding of the mechanical properties of the materials that constitute them is required.

2.1.2 Enamel

2.1.2.1 Compositional structure

Enamel is the hardest tissue in the human body. It has the ability to retain its shape and resist fracture during severe load-bearing events. Enamel is a highly mineralised crystalline structure. It contains on average 95% inorganic substance, 4% water and 1% organic substance by weight or 87% inorganic, 11% water and 2% organic component by volume (Simmelink, 1987). Hydroxyapatite substituted with carbonate and hydrogen phosphate ions are the largest mineral constituent, 90-92% by volume.

2.1.2.2 Mechanical behaviour of enamel

As the outer layer of teeth, enamel must retain its shape as well as resist fracture and wear during load-bearing function for the life of the individual. Understanding the fracture properties and crack propagation within enamel is important for both clinicians and material scientists.

Featherstone et al. (1983) found that hardness of enamel have a correlation with that of the mineral content. Meredith et al. (1996) reported that enamel hardness varied depending on its location. Hardness decreased inward with distance from the surface, having least hardness at the dento-enamel junction (DEJ). The same authors also reported that modulus of elasticity was the highest at the outer surface of the enamel and decreases towards the DEJ. He & Swain (2009) investigated the nanoindentation mechanical behaviour of the inner and outer regions of human enamel. They reported that inner enamel has lower stiffness and hardness but higher creep and stress redistribution abilities than their outer counterpart. They attributed this observation to the gradual compositional change throughout the enamel from the outer region near the occlusal surface to the inner region near EDJ. They suggested that enamel can be regarded as a functionally graded natural biocomposite.

2.1.3 Dentine

2.1.3.1 Compositional structure

Dentine is approximately composed of 60% inorganic by weight, 30% organic and 10% water (Kinney et al., 1993; Gale and Darvell, 1999a; Kinney et al., 1999). The organic phase consists of approximately 90% densely arranged; insoluble proteins containing the inorganic mineral phase which is composed of hydroxyapatite crystallites.

2.1.3.2 Mechanical behaviour of dentine

Dentine has relatively higher compliance or lower elasticity, than enamel and hence provides a more flexible substrate when supporting enamel under function. It is less hard and can sustain more tensile strain than enamel. Fracture of dentine is less catastrophic than enamel and more energy is required to fail a dentine since the dentine is considerably tougher than enamel (Rasmussen et al., 1976).

Gradient distribution in the hardness and elastic modulus of dentine has been also attributed to the distribution of the inorganic mineral phase. Kishen et al. (2000) stated that the degree of mineralization of the collagen substrate in dentine varies continuously with location, and this gradient in the mineralization is believed to optimize the functionality of the overall tooth structure. Pashley et al. (1985) showed that the microhardness of coronal dentine is higher in superficial than in deep dentine. They indicated the variation in mechanical properties of dentine to be associated with the change in dentine structure. Kinney et al. (1996) reported that the hardness and elastic modulus of the peritubular dentine were much higher than those of the intertubular dentine. The decrease in hardness may be due to a decrease in the stiffness of the intertubular matrix.

The mechanical properties and microstructural features of enamel and dentine are important in order to understand the stress dissipation within the tooth and for the development of biomimetic restorative materials.

2.2 Differences between sound and endodontically treated teeth

2.2.1 Introduction

Walton & Torabinejad (1996) stated that endodontically treated teeth differ from teeth with a viable pulp. Tang et al. (2010) summarized the various potential risks of tooth fracture after endodontic treatment. The risks included loss of tooth structure, stresses attributed to endodontic and restorative procedures, access cavity preparation, instrumentation and irrigation of the root canal, obturation of the root canal, post canal preparation, post selection, coronal restoration, and inappropriate selection of tooth abutments for prostheses.

There are three main changes that can occur in a tooth following root canal therapy, namely (i) changes in the physical properties and in the chemical composition, (ii) changes in the morphology and in the biomechanical behaviour under stress and (iii) possible elevation of pain threshold and loss of pressoreceptors.

2.2.2 Changes in the physical and chemical properties of the dentine

Healthy dentine can be described as a biological composite of collagen matrix (Marshall et al., 1997). Helfer et al. (1972) postulated that the increase in brittleness of dentine was due to loss of moisture after root canal therapy. They found that the moisture content of dentine from endodontically treated teeth decreased by approximately 9% compared to teeth with vital pulp. The reduction of moisture content in endodontically treated teeth is an often quoted reason for their increased fracture susceptibility (Johnson et al., 1976; Wagnild and Mueller, 2002). Weaker collagen intermolecular cross-links have also been reported to be one of the reasons why endodontically treated teeth may be more susceptible to fracture (Rivera et al., 1988). Huang et al. (1992) found that dehydration of human dentine increased its modulus of elasticity and that wet dentine specimens from treated pulpless teeth generally showed lower modulus of elasticity and proportional limit in compression than those of sound teeth. Kinney et al. (2003a) also found that dehydration of human dentine increases its modulus of elasticity. Kahler et al. (2003) reported that the brittleness of root after root canal therapy is a manifestation of a change in modulus of elasticity.

Sakaguchi et al. (1992) reported that if collagen fibrils are removed after root canal treatment, fracture is more likely to take place. Mason (2001) demonstrated that the percentage of collagen present in crown and root dentine decreases following the root canal treatment. The percentage of collagen in crown dentine of healthy sound teeth is 21.7% and it reduce to 20.1% following root canal treatment after 2 years, and was further reduce to 16.8% after 10 years. In root dentine the percentages are 25.5%, 23.5% and 19.3% respectively. Depletion of collagen fibrils was also reported in specimens that were aged in an oral environment (Hashimoto et al., 2000). These findings were confirmed by Ferrari et al. (2004), who showed that a decline in the distribution of the collagen fibrils within root dentine three to nine years after root canal therapy. However, Lewinstein & Grajower (1981) observed no difference in the modulus of elasticity and hardness between vital teeth and teeth that were endodontically treated 5 or 10 years before.

Irrigating solutions that are used in root canal therapy have been reported to have a negative effect on the physical and chemical properties of dentine (Grigoratos et al., 2001; Goldsmith et al., 2002). Sodium hypochlorite, a very reactive chemical with desirable disinfecting effect, however when applied at a high concentration for a long period it can cause detrimental effects on the root canal dentine. There have been several studies on the adverse effects of sodium hypochlorite on the mechanical properties of dentine such as flexural strength, elastic modulus, and microhardness (Grigoratos et al., 2001; Goldsmith et al., 2002). The changes in the inorganic and the organic phases of the dentine also lead to changes in the mechanical properties of dentine (Di Renzo et al., 2001a, b). Different concentrations of sodium hypochlorite can also reduce tooth surface strain; even if no difference was found in the strain recorded after different irrigation regimes (Goldsmith et al., 2002). Ethylenediaminetetraacetic acid (EDTA) is a chelating agent utilized to remove the smear layer formed after root canal preparation. Calt & Serper (2002) applied 10 mL of 17% EDTA for 1 min and 10 min followed by 10 mL of 5% sodium hypochlorite irrigation. They reported that the 1 min EDTA application was enough to remove the smear layer; however, the 10 min EDTA showed extreme peritubular and intertubular dentinal erosion.

Chemical treatments can alter biological substrates and render them amenable to bacterial adherence or susceptible to degradation. Kayaoglu et al. (2005) found that high prevailing pH caused by alkaline medicaments such as calcium hydroxide leads to increased bacteria adhesion to collagen in the root canal. Besides thin dentine, long term calcium hydroxide medication has also been alluded as a cause of root weakening (Andreasen et al., 2002). The same authors pointed out that calcium hydroxide may, due to its alkaline nature, neutralize, dissolve, or denature some of the acidic protein components in dentine and thereby weaken it. Their results showed a marked reduce in fracture strength with increasing storage time.

2.2.3 Changes in the morphology and in the biomechanical behaviour

In 1976, Tidmarsh described the intact tooth as a hollow, laminated structure that deforms under load; this structure may undergo permanent deformation following excessive or sustained loads. It might therefore be expected that the removal of dental substance during access cavity preparation would significantly weaken the tooth. Therefore, the presence of intact roofs of pulp chambers are important in avoiding root fractures in a healthy tooth (Fuzzi, 1993), however this is not done clinically as it contradict the principles of endodontics.

The endodontic procedure in itself can also be considered as an additional morphological modification. Canal preparation involves dentine removal, and therefore, it may compromise the fracture strength of the roots. Canal preparation has been repeatedly stated (Bender and Freedland, 1983; Gher et al., 1987; Tamse, 1988) as a cause of vertical root fracture. Another *in vitro* study showed that hand instrumented mandibular premolars were more susceptible to fracture than their uninstrumented counterparts, while canal preparation in canine teeth did not caused any detrimental effect (Wu et al., 2004). The authors concluded that canal shaping and remaining dentine thickness must play an important role in determining fracture strength of root treated teeth.

Obturation, both vertical and lateral compaction techniques, involves load application through spreaders and pluggers onto the root canal wall and radicular dentine. It is another step in the root canal treatment procedure that has been implicated as a cause of vertical root fracture (Tamse, 1988). Stresses are closely associated with structural failure or fracture, because structural failure will occur once the applied load produces stress that exceeds the ultimate strength of a material (Callister, 2003). Stresses in roots as a result of obturation have been studied utilizing finite element analysis. These studies have shown that it is very unlikely for root fractures to occur if it is solely due to root canal obturation (Yaman et al., 1995; Telli and Gülkan, 1998).

In addition, post space preparation and post placement was also considered as risk factors that weakened the remaining tooth structure and predisposed teeth to fractures. Many studies have showed that restoring endodontically treated teeth using cast metal, prefabricated metal and fibre posts had negative effects on the fracture resistance and therefore, increase the incidence of vertical root fractures (Fuss et al., 2001; Butz et al., 2001; Lertchirakarn et al., 2003; Pilo et al., 2008). This was greatly attributed to stress concentration within the radicular dentine during post placement and, consequently, the altered pattern of stress distribution upon loading (Lertchirakarn et al., 2003).

Soares et al. (2008) reported that the loss of dentinal structures and the presence of fibre posts caused more stress concentration in the tooth and restoration thus decreasing the fracture resistance. However, Fokkinga et al. (2005) reported that the presence or absence of metal/fibre posts did not affect the fracture resistance of endodontically treated premolar even when the whole coronal structure was replaced with resin composite crowns. Therefore, they suggested that posts are not necessary for the restoration of such teeth. Mohammadi et al. (2009) also found no difference in fracture resistance of premolars restored with direct resin composite in the presence or absence of fibre post and cuspal coverage.

2.2.4 Possible elevation of pain threshold and loss of pressoreceptors

Randow & Glantz (1986) and Ingle & Bakland (2002) stated that it is possible that endodontically treated teeth will be able to bear heavier loads without triggering a protective response due to the loss of pressoreceptors in blood vessels of the pulp or an elevated pain threshold. They hypothesized that the pressure receptors or pressoreceptors are sensitive to the stretching of the vessel walls in the dental pulp and this is likely to increase the risk of fracture of endodontically treated teeth.

2.3 Restoration of endodontically treated tooth

2.3.1 Evidence based selection of dental materials

The biomechanical behaviour of biologic structures as well as restorative systems is influenced by several factors that interacts with one another other (Zarone et al., 2005; Zarone et al., 2006). In the oral environment several variables contribute to the long term success of restorations. Some of them are dependent on the individual, just like occlusion, load intensity and direction, temperature, moisture, wear, presence of sound tooth structure and quality of supporting tissues, whereas other factors are not controllable, such as structural integrity, microleakage, fatigue and time. Furthermore, teeth and restorative materials are characterized by intrinsic physical characteristics which are responsible for their mechanical performances during functions over time (Van Noort, 2002).

Restoration of an endodontically treated tooth often needs additional support from the root canal by means of a post and core system (Christensen, 2004). Dental post is often used after root canal treatment when restoring a damaged tooth with extensive loss of coronal tooth structure (Morgano and Brackett, 1999). The main purpose of this treatment is to provide retention for a crown or a fixed partial denture (Morgano, 1996; Heydecke et al., 2001). Post insertion should be avoided if adequate retention can be achieved from the remaining coronal tooth structure (Torbjörner and Fransson, 2004b). Unfortunately, these teeth that have been restored endodontically have been shown to exhibit a significantly shorter service life when compared with vital teeth (Palmqvist and Soderfeldt, 1994; Leempoel et al., 1995). Williams & Edmunson (1987) indicated that the success of restored teeth is related to the design and materials of posts and cores. This has become clearer, when Vire (1991) reported that failure of the majority of restored pulpless teeth was due to the prostheses rather than biological.

Over several decades, many literatures have been published regarding the restoration of endodontically treated teeth with various post and core systems. Since then, modifications to these systems and introduction new systems have flooded the more recent literature.

2.3.2 Biomechanical considerations for using dental post and core systems

2.3.2.1 Overview

Studies showed that the dental post does not reinforce an endodontically treated tooth (McDonald et al., 1990; Heydecke et al., 2001). Post and core systems should provide sufficient retention to the final restoration, showing acceptable fracture resistance and protecting the remaining tooth. The biomechanical consideration for the restoration of endodontically treated teeth utilizing post and core system are as follows:

2.3.2.2 Retention and Resistance factors

Post retention refers to the ability of a post to resist vertical dislodging forces. Post retention is influenced by the post’s length, design, diameter, post fitting and the luting cement used, tooth type and its position and ferrule effect.

a. Post length

There are various recommendations in the dental literature concerning the post length. The dental post should equal the incisocervical or occlusocervical dimensions of the crown (Harper and Lund, 1976). If possible the dental post should be equal or longer than the crown (Silverstein, 1964; Peroz et al., 2005) or be as long as possible without distrusting the apical seal (Hirschfeld and Stern, 1972). It should end halfway between the crestal bone and the root apex. However, Jacoby (1976) suggested that the post length should be equal to half the length of the root. Other studies have suggested that the post length should be equal to two thirds of the root length (Larato, 1966) or at least half way between the apex of the root and the alveolar crest of supporting bone (Stern and Hirshfeld, 1973).

Standlee et al. (1978) reported that longer dental posts are more retentive. Posts with a length of at least ¾ of the length of the root offer the greatest rigidity and the least deflection of the root when compared with shorter dental posts (Leary et al., 1987). The length of the post influences stress distribution in the root, and thereby affects its resistance to fracture. When the length of the post is increased, the retentive capacity increases (Nergiz et al., 2002), as well as resists bending (Leary et al., 1987). Cecchin et al. (2010) found that longer fibre posts (12 or 8 mm long) were associated with higher fracture resistance of teeth when compared with shorter ones (4 mm long). However, Guzy & Nicholls (1979) suggested that long posts can affect root resistance because of the removal of tooth structure at the deepest part of the root itself and Sorensen & Martinhof (1984a, b) reported a high risk of tooth fracture for teeth with short posts. On the contrary, Giovani et al. (2009) found that post length does not have an effect on the fracture resistance of teeth restored with metal cast post and core.

Other criteria for the success of restored endodontically treated teeth are the amount of gutta-percha left at the apical area after post preparation. It has been suggested that leaving at least 4-5 mm of root filling material is necessary to maintain the apical seal (Mattison et al., 1984). Camp & Todd (1983) demonstrated that at least 5 mm of gutta-percha filling should remain in the apical portion of the canal. Kvist et al. (1989) recommended that post should be as long as possible leaving a minimum of 4-5 mm undisturbed apical seal. They reported that roots with posts where the remaining gutta-percha was shorter than 3 mm exhibited significantly higher frequency of periapical radiolucencies compared to those with longer gutta-percha.

b. Post design

Parallel-sided posts are more retentive than tapered posts (Torbjörner et al., 1995), and they distribute stress more uniformly along their length during function. Parallel-sided posts create the highest stress areas apically around the post end while tapered posts function as wedges and initiate stress areas coronally (Asmussen et al., 2005). Signore et al. (2009) found that the survival rate of parallel-sided glass fibre posts was more than that recorded for tapered ones over up to 8 years of function.

The surface designs of posts can be divided into serrated, threaded and smooth surface designs. According to Standlee et al. (1978), a serrated post increases the retention of the post compared to a smooth post. Sorensen & Martinoff (1984b) recorded that teeth restored with the parallel-sided serrated posts and an amalgam or resin composite core had the highest success rate. The tapered cast post and core displayed a higher failure rate than teeth treated without intracoronal reinforcement. The parallel-sided serrated post did not show any failures caused by root fracture, whereas root fractures caused extractions of teeth restored with tapered cast posts and cores.

The threaded post design was first evaluated by Kurer in 1983. The presence of threads enhances the retention of the post over the smooth-sided and serrated typed posts (Kurer, 1983). However, the added retention afforded by these threaded posts systems must be weighed against potential problems that may result from their insertion. Threaded metal posts have been associated with stress concentration at the dentine-thread interface. Such areas can predispose to crack formation and jeopardize the fracture resistance of post restored teeth (Mentink et al., 1998). Decreasing the number of threads and increasing the spaces between them produces less harmful stresses (Deutsch et al., 1985). Stockton (1999) also reported that the active self threaded posts distribute higher stress in the root than other types. Uddanwadiker et al. (2007) proposed a finite model of threaded fibre post and found that increased stress concentration cause reduced the fracture resistance of teeth restored with these type of posts.

c. The post diameter

The diameter of the post and the remaining dentine also play a major role in preventing the root from fracturing. Several *in vitro* studies have confirmed the importance of the remaining bulk of the tooth structure with regards to strength and resistance to root fracture (Lang et al., 2006; Naumann et al., 2006). When the diameter of the post is increased, the surface of the post that is in contact with the tooth is increased. This does not influence the retentive capacity significantly (Nergiz et al., 2002) but, it is related to the remaining tooth structure. As an increase in post diameter did not provide increasing in post retention, conservation of remaining tooth structure by avoiding the use of posts with a large diameters have been recommended (Standlee et al., 1980). The post diameter must be selected according to the root diameter in order to preserve radicular dentine, accordingly increasing the fracture resistance (Standlee et al., 1980).

Therefore, the narrower roots are not very suitable for post preparation such as mesial roots of lower molars and the buccal roots of upper molars (Gutmann, 1992).

It was suggested that post diameter should not exceed 1/3 of the root diameter at any given point along the root length (Goodacre and Spolnik, 1995). Data from previous studies indicated that the diameter of the post at the apical tip should be 1 mm (Abou-Rass et al., 1982; Goodacre and Spolnik, 1995). The canal preparation should minimally alter the internal anatomy of the root canal (Goerig and Mueninghoff, 1983). The diameter of the post should be as small as possible while retaining the necessary rigidity (Robbins, 1990). In order to reduce failures and fractures, Mou et al. (2009) recommended that the optimum post to root diameter ratio should be approximately 1:4.

d. Post fitting

Goracci et al. (2005) concluded that sliding friction was the main factor that affected resistance to dislocation of resin bonded fibre posts. Also, the use of dentine adhesive did not improve dislocation resistance when compared with the use of resin cement without dentine adhesive. The presence of interfacial gaps and the incomplete removal of smear layer might be the reason for these findings.

Poorly fitted posts might create levers within the root canal, making the tooth more liable to fracture (Turner, 1982). Close adaptation of posts to the canal walls was found to increase the fracture resistance of restored teeth significantly (Sorensen and Engelman, 1990). Santos et al. (2009) showed that lacking effective bonding between the root and posts with different elastic modulus was associated with a higher risk of vertical root fracture in upper premolars. Schmitter et al. (2010) concluded that when fibre post restored teeth were crowned, centrally positioned fibre reinforced posts did not contribute to load transfer as long as the bond between the tooth and composite core was intact and resin cement was used to bond the fibre post. However, Büttel et al.

(2009) found that the fracture resistance of teeth restored with fibre posts and composite crowns without ferrules was not affected by post fit within the root canal. Therefore, excessive post canal preparation to achieve optimal circumferential post fit is unjustifiable because it will not increase the fracture resistance of teeth.

e. Luting cement

Zinc phosphate, zinc polycarboxylate, glass-ionomer and resin cements are the most commonly used luting cements for posts. Zinc phosphate cement has been commonly used for decades for most conventional fixed prostheses due to its easy handling characteristics and adequate long term clinical results (Jokstad and Mjör, 1996).

Glass-ionomer cement is defined as "water-based materials and are susceptible to dissolution in a wet environment and dehydration in a dry environment" by Ricketts et al. (2005). Microcracking during setting is not rare and this will lead to crack propagation during function. To overcome this problem, resin was added to form resin-modified glass-ionomers. Mitchell & Orr (1998) compared the retention of posts cemented with glass-ionomer and resin-modified glass-ionomer cements under fatigue loading. They reported that there was no statistical difference between the both cements used. However, Love & Purton (1998) showed a reverse trend, where resin-modified glass ionomers showed inferior retention to conventional glass ionomer.

Adhesive dental materials offer clinicians an opportunity to reinforce the endodontically treated tooth through the use of bonded sealers in the root canal system. The interest in reinforcing the root canal system have lead to the development of many adhesive root canal sealers with the potential to increase resistance to root fracture (Boone et al., 2001). Junge et al. (1998) reported that resinous cements have higher retention values and resistance to fatigue compared to zinc phosphate cements. Furthermore, the modulus of elasticity of resinous cements approaches that of dentine, and therefore they may have the potential to clinically reinforce roots with thin walls (Mendoza et al., 1997). However, resinous cements have some limitations such as short working time, the number of operating steps involved, and the sensitivity to moisture compared to zinc phosphate cements. To overcome this problem, some of the newest self-etching resinous cements were introduced to overcome the technique-sensitiveness of conventionally bonded resinous cements (Nergiz et al., 1997). Schwartz et al. (1998) and Boone et al. (2001) found that resin cement had higher retentive values compared to zinc phosphate and glass ionomer cements. Dietschi et al. (2008) recommended the use of specific combinations of adhesives and cements to overcome the problems of ovoid canal shape and dentine moisture that might reduce the efficacy of adhesion between the tooth and the post. Kivanc & Gorgul (2008) concluded that self-etching adhesives were better to use than etch and rinse adhesives for luting dental posts. An increased ferrule height coupled with resin cement resulted in higher fracture loads.

f. The ferrule effect

A ferrule is defined as "a vertical band of tooth structure at the gingival aspect of a crown preparation". It was described as a 360-degree ring in cast restoration apical to junction of the core (Rosenstiel et al., 2001). It adds some retention, but primarily provides resistance form (Mezzomo et al., 2003) and enhances longevity (Cheung and Chan, 2003). The ferrule, which should be at least between 1.5 and 2 mm above the crown margin area, embraces the circumference of the root, thus protecting it from fracture (Naumann et al., 2007).

Tan et al. (2005) reported in an *in vitro* study that a tooth restored with a crown with a uniform ferrule of 2 mm in height was significantly more resistant to fracture than a tooth restored with a crown with a no uniform ferrule. Al-Omiri & Al-Wahadni (2006) reported that retaining coronal dentine did increase the fracture resistance of teeth.

However, they found that increasing the amount of retained dentine more than 2 mm did not improve the tooth fracture resistance any further. Dorriz et al. (2009) recommended the use of ferrule or bonding with an opaque porcelain layer (if cast metal post was used) to improve the fracture resistance of grossly destroyed teeth. Schmitter et al. (2010) concluded that increased ferrule height and resin bonding of the crown resulted in higher fracture loads of teeth. They recommended the use of resin-bonding agents with crowns when optimum ferrule height cannot be achieved.

Conversely, some researchers questioned the benefit of ferrules because they did not seem to provide additional support for restored teeth. Gegauff (2000) investigated the effect of crown lengthening for ferrule purposes on the failure loads of simulated analog teeth restored with post and core retained crowns impeded within simulated periodontal ligament and alveolar bone. He reported significantly lower failure loads of teeth that received crown lengthening and ferrules. The reduction of supporting tissues combined with the altered crown: root ratio seemed to weaken the restored teeth even with the incorporation of ferrules. Al-Hazaimeh & Gutteridge (2001) investigated the effect of ferrule preparation on the fracture resistance of the central incisors restored with prefabricated posts and cemented with resin cement. They found no difference in fracture resistance of the central incisors with or without a 2 mm ferrule. However, the fracture patterns were more favourable when a ferrule was present. Mezzomo et al. (2003) reported no significant difference in fracture resistance of non-ferruled specimens restored with resin-cemented posts and ferruled ones.

2.3.2.3 Tooth type and its position

Tamse et al. (1999) evaluated vertically fractured endodontically teeth clinically and radiographically before and after extraction. They noticed that most fractured teeth were maxillary second premolars (27.2%) and mesial roots of the mandibular molars (24%).

They found that susceptibility of these teeth to root fracture increased when the residual sound tooth structure was less than 1-2 mm, however, there was no mention if any of these teeth were restored with dental posts. Chapman et al. (1985) suggested that oval shaped canals caused roots to be more susceptible to fracture, because there are large spaces filled with luting cements. When the cement dissolves, unintentional spaces are created causing for the post to move inside the canal. These micro-movements may finally result in cementation failure, dislodgement of the post, fatigue of the tooth and root fracture.

2.4 Types of the dental post systems

2.4.1 Cast posts

Cast posts became an established treatment option due to their superior physical properties (Creugers et al., 1993). The post preparation should be slightly tapered and free from undercuts to allow easy withdrawal of the impression and insertion of the casting (Baraban et al., 1988). They can be fabricated from gold alloys, base-metal alloys (DeDomenico, 1977), silver-palladium alloys (Dale and Moser, 1977), and other non-precious alloys. They are indicated in teeth with relatively large root canals. Their disadvantage is that they have strict requirement regarding their fabrication. These dental posts can be fabricated directly or indirectly.

Cast post and cores were the standard for many years and are still used by some clinicians today. Generally, they do not perform as well as other types of posts during *in vitro* tests (Isidor and Brøndum, 1992) and clinical studies (Torbjorner et al., 1995). They have fallen from favour because they require two appointments, temporization, and a laboratory fee. Nevertheless, there are studies that report high rate of success with cast post and cores (Weine et al., 1991; Walton, 2003), and they offer advantages in certain clinical situations. Post reproduces the contours of the prepared canal, the adaptation to the canal is good and it can be designed to resist torsional forces. One distinct advantage with a cast post and core is that if a tooth is misaligned, the core may be angled in relation to the post to achieve proper alignment with the adjacent tooth. A cast post and core also may be indicated when there is minimal coronal tooth structure available for anti-rotation features or bonding. When the morphology of the canal is critical, e.g. in the case of an oval canal, it is indicated to use a cast post. In these cases, using a prefabricated post would result in minimal contact with the canal walls and would lead to loosening of the post due to the large cement layer. Moreover, if a prefabricated post is used and an extensive preparation is made to improve the adaptation of the post, it would lead to increased root fracture risk due to the weakened tooth structure. Despite the above-mentioned features, cast posts also have their disadvantages. They have low retentive abilities and the technique is both time consuming and expensive. Furthermore, a temporary restoration is also always required, increasing the risk of contamination of the root canal system (Fox and Gutteridge, 1997). In addition, in certain cases, the need for more aesthetic solutions has launched the development of new alternative post materials.

There are conflicting reports on the outcome of cast metal post systems. A 6-year retrospective study of 96 endodontically treated teeth with extensive loss of tooth structure and restoration with the use of cast post and cores showed a success rate of 90.6% (Bergman et al., 1989). Significantly higher fracture thresholds were recorded for cast post and cores compared to carbon fibre posts in another study (Martinez-Insua et al., 1998). In a clinical study where 1273 endodontically treated teeth with six different intracoronal reinforcement methods were evaluated, the tapered cast post and core displayed a higher failure rate than teeth without intracoronal reinforcement (Sorensen and Martinoff, 1984a). However, this study was later criticized and the data were re-evaluated in a retrospective review study where the high failure rate of the cast posts and cores was concluded to be due to the fact that almost half of the cast posts were half the desired length or less (Morgano and Milot, 1993). In a study where restored teeth were intermittently loaded and the adaptation of the posts to the root was measured, it was found that the adaptation was better for teeth restored with parallel-sided prefabricated posts and composite cores than that of teeth restored with tapered individually cast posts (Isidor and Brøndum, 1992).

2.4.2 Prefabricated posts

A great variety of prefabricated posts has been developed either metallic or non-metallic. The variations in post design are attempts to satisfy various root configurations and retention needs. Prefabricated posts have several advantages compared to cast posts, better retentive abilities, time saving and also economical. When a large amount of coronal dentine remains, a prefabricated post with a composite core may be recommended (Torbjörner, 2000). However, the prefabricated posts have the disadvantage that they usually require more dentine removal than cast posts, because the natural shape of the canal is tapered. In addition, the round design of the prefabricated posts offers little resistance to rotational forces. Also, the strength of composite, nowadays commonly used as core material with prefabricated posts, is not as high as that of a cast core. Clinical studies have indicated higher survival rates for serrated prefabricated posts than cast posts and cores (Sorensen and Martinoff, 1984b; Torbjörner et al., 1995). In a prospective study where 325 single-rooted and multi-rooted teeth were restored with and without posts, it was concluded that cast posts and prefabricated titanium posts yielded similarly favourable results (Salvi et al., 2007).

2.4.2.1 Metallic posts

Most typically, metallic prefabricated posts are made of stainless steel or titanium alloy. The stainless steel commonly used in prefabricated posts contains chromium (18%) and nickel (8%) (Anusavice, 2003). Because of the concerns about the allergenic potential of stainless steel posts, and also the risk of corrosion and the high risk of root fracture (Silness et al., 1979), titanium posts were introduced.

Isidor et al. (1996) compared the fracture resistance of cast gold, titanium, and carbon fibre posts and found higher fracture resistances for metal posts compared to carbon fibre post. Purton & Love (1996) reported higher retention with stainless steel than carbon fibre posts when both were cemented with resin luting cement. Sidoli et al. (1997) evaluated the fracture resistance of cast gold, stainless steel, and carbon fibre and reported that teeth restored with metal posts had significantly higher fracture resistance compared to those teeth restored with carbon fibre posts. Drummond (2000) compared the shear strength of stainless steel and three commercial brands of fibre posts cemented with the same resin luting agent. They found no difference in shear strength among the groups. Butz et al. (2001) compared the survival rates and fracture strength of cast gold, titanium with a composite core, and zirconium with composite or ceramic cores using cyclic loading, followed by continuous loading. They found that zirconium/composite group was worse than the other posts. Cormier et al. (2001) investigated the fracture resistance of gold, stainless steel, and four commercial brands of fibre posts and reported that teeth restored with stainless steel posts had the highest fracture resistance, whilst teeth restored with one of the quartz fibre post systems had the lowest. Raygot et al. (2001) reported no difference in fracture resistance between stainless steel, cast gold, and carbon fibre posts. Gallo et al. (2002) found that stainless steel posts cemented with zinc phosphate cement had higher retention than a variety of fibre posts luted with resin cement. Akkayan & Gulmetz (2002) compared the fracture resistance of titanium, glass fibre, quartz fibre and zirconium posts. They reported the highest fracture resistance were for the teeth restored with quartz fibre posts. Ottl et al. (2002) reported the highest fracture resistance for teeth restored with carbon fibre, followed by non-palladium metal and ceramic posts. Zirconia ceramics had the lowest values. Newman et al. (2003) compared the fracture resistance of stainless steel posts with three brands of fibre posts and found higher fracture resistance in teeth restored with the stainless steel posts. Reid et al. (2003) compared the fracture resistance of titanium posts with three carbon fibre posts and one quartz fibre post and found no differences amongst groups. Cormier et al. (2001), Akkayan & Gulmez (2002) and Newman et al. (2003) reported more repairable failures with fibre posts than metal posts. Qualtrough et al. (2003) reported that quartz fibre post is more retentive than titanium, glass fibre, or carbon fibre posts.

2.4.2.2 Ceramic posts

Aesthetics is one factor that has reduced the use of metal posts today due to its visibility through the more translucent all-ceramic restorations. Even with less translucent restorations metal posts may cause the marginal gingiva to appear darkish. These concerns have led to the development of posts that are tooth coloured or translucent. Among the materials used to achieve the aesthetic value for posts are zirconium and other ceramic material. Stabilized zirconia ceramics have been introduced for the fabrication of posts and cores (Kwiatkowski and Geller, 1989, Meyenberg et al., 1995, Zalkind and Hochman, 1998), because they have higher strength and fracture toughness than other ceramics.

Zirconia posts offer possible advantages with respect to aesthetics and biocompatibility (Purton et al., 2000), but they have several disadvantages. Zirconia posts are rigid, but at the same time very brittle (Asmussen et al., 1999). Therefore, it is of great importance to make a deep post preparation when using zirconia posts. Zirconia posts are not yet available in small a diameter, which makes it difficult to use minimal invasive preparation on the tooth with this kind of post. In addition, if endodontic retreatment is necessary, retrieval of zirconia and ceramic posts are very difficult. One *in vitro* study recorded poor resin bonding capabilities of the zirconia posts to radicular dentine after dynamic loading and thermocycling (Dietschi et al., 1997). In another study, the zirconia posts exhibited lower retention values than serrated metal posts (Purton et al., 2000). Zirconia posts also showed poor retention to composite resin cores, and this combination was therefore not recommended for clinical use (Butz et al., 2001). However, Paul and Werder (2004) observed good clinical success of zirconia posts with direct composite cores after a mean clinical service of 4.7 years

2.4.2.3 Fibre posts

Fibre posts were first introduced by Duret at the beginning of the 90's (Duret et al., 1990). Fibre posts can be considered as composite reinforced materials where fibres are embedded in a matrix of epoxy-resin or methacrylate-resin, and an interfacial agent such as silane is used to optimize the link between the two components. The post is fabricated through a semi-automated industrial process called pultrusion. The diameter and density of the fibres as well as the adhesion between them and the matrix strictly influence the quality of the post and its mechanical properties. The resinous matrix (epoxy or methacrylate) is injected into the pre-tensioned fibre bundle to completely fill the spaces between fibres. Alternatively, fibres can be simply immersed in a resin bath. Differences in manufacturing processes are related to the quality, mechanical and clinical behaviour of posts (Grandini et al., 2005). The translucent fibres (glass or quartz) was utilised as alternative to dark fibres to improve aesthetics (Vichi et al., 2000; Ferrari et al., 2001), and are today better accepted than carbon post, especially when restoring anterior teeth to provide support for all-ceramic crowns. Moreover, they are translucent thus facilitate luting cement polymerization process. The mechanical behaviour of the new generation of posts does not seem to differ from the traditional carbon post (Grandini et al., 2005).

The main advantage of fibre posts is the variability of their modulus of elasticity depending on the loading direction; in particular, during transversal loading, the modulus of elasticity has a value close to sound dentine (Ferrari and Scotti, 2002). This property reduces stress transmission to the root canal walls thus reduces the risk of vertical fractures (Asmussen et al., 1999). The most common failure that can occur with a fibre post is a “debonding” of the post, especially during the removal of temporary restoration. However, this failure can be dealt with by repeating the adhesive procedures. In the event of failure, endodontically teeth restored with fibre reinforced posts are more likely to be restorable as the failure occur more coronally (Cormier et al., 2001). This type of failure may be due to the amount of tooth structure preserved compared to the tooth structure that must be sacrificed when a metallic post is placed (Stankiewicz and Wilson, 2002). When failure occurs, favourable fractures are seen in teeth restored with fibre posts and resin cores, whereas unfavourable fractures or failures are usually encountered with the use of a metal post (Heydecke et al., 2002).

2.5 Survival rate of endodontically treated teeth restored with dental posts

Clinical studies can be used to explore the characteristics of clinical problems and assist clinicians in decision making. Many studies reported high percentage of survival rate for metal posts. Tables 2.1 and 2.2 summarize survival rate of some retrospective and prospective studies for metal and fibres dental posts.

Table 2.1 Long term clinical studies on metal post and core build ups

Authors	Study design	Number of the teeth	Follow-up (year)	Survival (%)
Sorensen & Martinof (1984b)	Retrospective	420	1-25	91
Weine et al. (1991)	Retrospective	138	6	99
Mentink et al. (1993)	Retrospective	112	7.9	92
Ellner et al. (2003)	Prospective	50	10	94
Creugers et al. (2005a)	Prospective	319	5	96
Creugers et al. (2005b)	Prospective	99	5	96
Balkenhol et al. (2007)	Retrospective	802	10	50

Table 2.2 Long term clinical studies on fibre posts

Author	Study design	Number of the teeth	Follow-up (years)	Survival (%)
Ferrari et al. (2000a)	Retrospective	130	3.8	96.8
Ferrari et al. (2000b)	Retrospective	100	4	95
Glazer (2000)	Prospective	59	2.3	89.6
Hedlund et al. (2003)	Retrospective	65	2.1	97
King et al. (2003)	Prospective	16	7.25	71
Naumann et al. (2005)	Prospective	105	2	88.6
Segerström et al. (2006)	Retrospective	99	6.7	65

2.6 Evaluation methods for performance of dental posts

2.6.1 Introduction

Several methods have been used to analyze the effects of the post and core system on the stress distributions in endodontically treated tooth when restored with various dental posts. Experimental methods and the finite element analysis are most commonly used.

2.6.2 Experimental methods

According to Van Noort (2002), several kinds of forces can act on a material: tensile, compressive, flexural and/or shear loads. Subsequently, laboratory tests can also be carried out to determine the tensile, compressive, flexural and shear strength. For example, as adhesive link different interfaces together, bond strength can be considered as the force an adhesive system opposes to tensile loading. The performances of a material could also be different if tested in either static or dynamic mode. When an experimental test is designed, the main goal should be a definition of the study variables. On this basis, the proper investigation can be chosen correctly.

2.6.2.1 Fracture resistance evaluation

Several studies have been performed to assess the fracture resistance of endodontically treated human or bovine teeth restored with various type of posts (Akkayan and Gulmez, 2002; Yamada et al., 2004; Bortoluzzi et al., 2007; Soares et al., 2007; Santos-Filho et al., 2008; Martelli et al., 2008; Clavijo et al., 2009; Soares et al., 2010; Nothdurft et al., 2011). Most studies have tried to identify the best technique and combination of materials to be used to increase the strength of the tooth-restoration complex (Ferrari et al. 2000a, b; Hannig et al. 2005).

Most experimental studies used static loading (Akkayan and Gulmez, 2002; Newman et al., 2003; Fokkinga et al., 2005), whereas only few investigators adopted dynamic loading (Heydecke et al., 2002; Krejci et al., 2003). Such a choice depends on the objective of the study as well as other factors; time and costs. The use of static forces can simplify a study and most likely require simpler instrumentations.

Static tests allow the investigation of the mechanical properties of a material using different types of loading (Salameh et al., 2006) whereas dynamic assessments could be used to study the mechanical performances of materials or restorative systems during function over time (Heydecke et al., 2002).

Bortoluzzi et al. (2007) evaluated the fracture resistance of bovine incisors treated with different reinforcement treatments using mineral trioxide aggregate (MTA). They reported that the use of MTA and metallic post as an intra-radicular reinforcement treatment increased the resistance to fracture of weakened bovine teeth in an experimental immature tooth model. Hinckfuss & Wilson (2008) evaluated the fracture resistance of bovine teeth restored with one-piece cast core/crowns with no ferrule and compared to those restored with amalgam cores and full coverage crowns with and without ferrule. They reported that the maximum load resistance was significantly improved in the groups with 2 mm ferrule. Teeth restored with one-piece cast core/crowns were significantly more resistant to loading than teeth restored with amalgam cores and crowns without a ferrule. Marchi et al. (2008) evaluated the influence of remaining dentine thickness around post and core systems and the thermo-mechanical stresses on fracture resistance of bovine teeth. They reported that although cast cores had higher fracture resistance when compared to the other techniques, the results were highly dependent on remaining dentine thickness. Nothdurft et al. (2008) examined the influence of fatigue and cementation mode on the fracture behaviour of endodontically treated bovine teeth restored with zirconia posts and crowns. They found that most specimens fractured in a repairable way, regardless of the type of cementation. Santos-Filho et al. (2008) investigated *ex vivo* the effects of different post systems and lengths (5 mm, 7.5 mm, 10 mm) on the strain and fracture resistance of filled bovine teeth. They reported that the cast post (10 mm) and core exhibited the highest fracture resistance. However, the fibre glass post was effective for all post lengths, with highest fracture resistance when the length was 5 mm. Cecchin et al. (2010) investigated the fracture resistance of the bovine teeth restored with intra-radicular posts of different length. They concluded that post lengths influenced the fracture resistance of restored bovine teeth.

Clavijo et al. (2009) evaluated the fracture strength and failure mode of flared bovine teeth restored with different intraradicular posts. They found that the use of direct anatomic posts which comprised of fibre post relined with composite resin and indirect anatomic post fabricated using glass fibres and flowable resin could be an alternative for flared root canals compared to cast metal post and core. da Silva et al. (2010) evaluated the effect of post, core, crown type, and ferrule presence on the deformation, fracture resistance, and fracture mode of endodontically treated bovine teeth. They found that core type did not affect the deformation and fracture resistance of endodontically treated teeth restored with alumina-reinforced ceramic crowns. The presence of a ferrule improved the mechanical behaviour of teeth restored with metal crowns, regardless of core type.

2.6.2.2 Photoelastic method

Photoelastic method based on the property of double refraction has been widely used to evaluate the stress distribution within the post systems. The specimens under investigation are fabricated using transparent plastic sheet that possesses the property of the double refraction either in two or three dimensions. When the specimens are stressed in a polariscope and examined in white light, colour patterns known as the fringes can be observed (Mahler and Peyton, 1955). The fringe pattern scan will then be evaluated to determine the stress distributions in the specimen. Each fringe order can be considered as a gradient of the differences in the principle stresses of the model. Fringes can be highly concentrated at some focal areas, such as the apical end of posts, where the stress gradient is so high thus distinguishing the various fringe orders can be difficult (Caputo and Standlee, 1987).

The stress distributions surrounding posts were studied by Burns et al. (1990) using the two dimensional (2D) photoelastic method. Test blocks from photoelastic materials were prepared incorporating simulated root canals. Posts of different designs, diameters and lengths were cemented into the canals. Using a circular polariscope, the fringes were photographed when each specimen was loaded. The loads used were 0 N, 135 N compressive loads, and oblique loads of either 90 N or 135 N applied at 26 degree angulation. The results showed that the Para post and the Para post plus produce evenly distributed stress of similar patterns. The Flexi post produced asymmetric stress patterns with stress concentrations at each thread. After cementation and during compressive loading, the Flexi posts caused higher stresses along the coronal surface than those with the Para posts and the Para post plus. They also found that the apical stress distributions were similar for the Flexi posts, Para posts and Para post plus during compressive loading. Loney et al. (1990) used three dimensional (3D) photoelastic stress analysis to study the effect of metal collar on stress distribution in cast post and cores. In both groups the highest stress concentration was found at the apical part of the post on the lingual side.

The 3D photoelastic stress analysis although expensive is more realistic than 2D, because the full geometric fidelity and stress distributions can be achieved. Nevertheless, photoelastic stress analysis is still questionable as the properties of the photoelastic materials are not able to perfectly model the teeth, bone and periodontal ligament (Loney et al., 1990). The variation in material properties could have a significant effect on the magnitude of stresses observed in the region of interest.

2.6.3 Finite element method

2.6.3.1 Introduction

Finite element method is (FEM) is a computer-based numerical method developed to solve the different equations. The geometric model of the structure is built and subdivided into small elements. In each of the elements, element equations are formed according to the relationship between the displacement and loading. The equations are assembled together to form the global FE equations. The global equations are then solved using a computer. With the FEM, the parameters of the geometry of the structure, post design, material properties, and the magnitude and direction of the load can be changed easily in simulations, which is a significant advantage over experimental methods. It can be used to calculate many phenomena such as vibration, deflection, stress, buckling behaviour. It can be used to analyze either small or large scale deflection under loading or applied displacement. It can also analyze elastic deformation, or “permanently bent out of shape” plastic deformation. In the FE method, a structure is broken down into many small simple blocks or elements (NISA-II User's Manual, 1997).

2.6.3.2 Application of finite element method in dentistry

Ledley & Huang (1968) developed a linear displacement force analysis model of a human tooth based on an experimental data where the tooth was considered to be a homogeneous structure. However, in reality the human tooth is highly non-homogeneous, especially the modulus of elasticity of the enamel is about three times higher than dentine.

Thresher & Saito (1973) used FEM to analyse the stresses of homogeneous and non-homogeneous human teeth model. They concluded that the enamel bear the major portion of the load before transfering to the surrounding bone structure. They also reported that high stress was observed in the root. Darendeliler et al. (1992) built a 3D FE model to determine the stress distributions in a maxillary central incisor. The tooth was considered to compose of only enamel and dentine since the thickness of periodontal ligament and cementum were very small. The effect of pulp on stress distributions was neglected. The tooth model was assumed to be isotropic, homogenous and elastic. The values and directions of the principle stresses were calculated from nodal displacements using the stress-strain and strain-displacement relations. Their results showed that the stresses were highest around the cervical line and the incisal margin. Ukon et al. (2000) investigated the influence of elastic moduli of the post and core combination on the stress distribution in the root under vertical and 45 degree oblique loading. They reported that peak dentinal stress adjacent to the luting cement layer depended only on the post material for vertical loading. Joshi et al. (2001) evaluated the stress distribution of endodontically treated teeth using 3D FE method when restored with stainless steel, titanium and carbon fibre posts. They reported that stainless steel post showed the highest stress followed by titanium post. Al-Omiri et al. (2011) compared the stress distribution of endodontically teeth restored with post retained crown and crown only using 3D FE method. They observed that dental posts caused higher dentinal stress than those of crowns without posts. Du et al. (2011) analyzed the stress distributions of posts with various diameters during masticatory loading using 3D FE method. They reported that when the diameter of the post was 50% of that of the root, the stress distributions in the post and the root surface were most favourable.

2.7 Hydroxyapatite and its applications

2.7.1 Overview

Hydroxyapatite (HA) is the most documented calcium phosphate ceramic, and can be used in bulk form or as a coating material. All forms of HA have excellent biocompatibility and are able to promote osteoconduction and osseointegration and it is the biomaterial of choice in both dentistry and orthopaedics (Sakkers et al., 1997). It is the main crystalline component of the mineral phase in bone and teeth. Table 2.3 shows the structural similarities between HA, enamel, dentine and bone (Dorozhkin, 2007). This similarity makes it the most clinically used as biomaterial for medical and dental applications (Dorozhkin and Epple, 2002).

Table 2.3 Chemical and structural comparison of teeth, bone and HA

Composition, wt%	Enamel	Dentine	Bone	HA
Calcium	36.5	35.1	34.8	39.6
Phosphorous	17.1	16.9	15.2	18.5
Ca/P ratio	1.63	1.61	1.71	1.67
Total inorganic (%)	97	70	65	100
Total organic (%)	1.5	20	25	--
Water (%)	1.5	10	10	--

2.7.2 Structure of hydroxyapatite

HA has a hexagonal symmetry and unit cell lattice parameters, a = 0.94 nm and c = 0.68 nm (Figure 2.1). Taking into account the lattice parameters and its symmetry, its unit cell is considered to be arranged along the c-axis. This would justify a preferred orientation that gives rise to an oriented growth along the c-axis and a needle-like morphology. Table 2.4 shows the similarities in crystallographic properties: Lattice parameters (±0.003 Å) between enamel, dentine, bone and HA as reported by Dorozhkin (2007).

Table 2.4 Crystallographic properties: Lattice parameters (±0.003 Å)

Composition, wt%	Enamel	Dentine	Bone	HA
a-axis (Å)	9.441	9.421	9.41	9.430
c-axis (Å)	6.880	6.887	6.89	6.891
Crystallinity index, (HA=100)	70-75	33-37	33-37	100

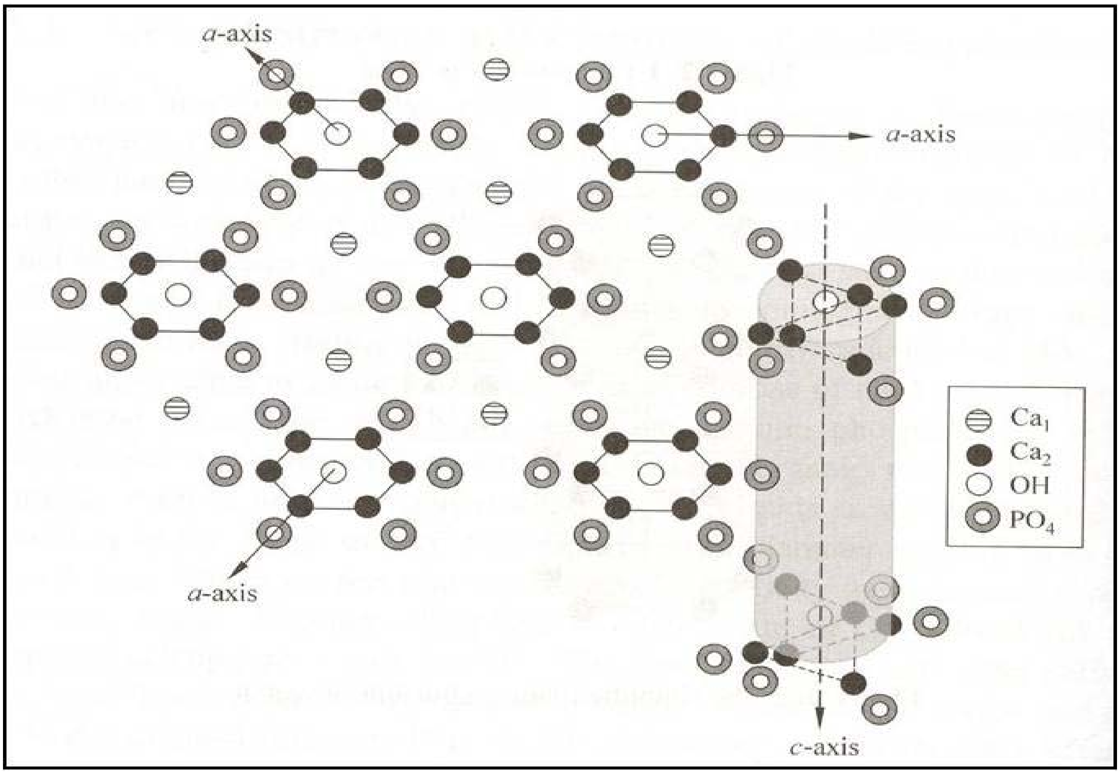

Figure 2.1 Schematic representation of hydroxyapatite crystal structure.

2.7.3 Properties of hydroxyapatite

Although, HA has favourable bioactive and osteoconductive properties that results in rapid bone formation in a host body and strong biological fixation to bony tissues (Martz et al., 1997), it possess low mechanical strength, which is an obstacle to its applications in load bearing areas (Choi et al., 1998). Thus, the enhancement of the mechanical properties of HA would extend its scope of applications. HA is either used as a bioactive coating on implants or reinforced with tough phases such as metal or ceramic phases for biomedical applications.

HA have been used successfully in clinical and animal studies for endodontic treatment including pulp capping, repair of mechanical bifurcation perforation, apical barrier formation and repair of periapical defects (Jean et al., 1988; Pissiotis and Spangberg, 1990; Chohayeb et al., 1991; Liu et al., 1997). Jean et al. (1988) suggested that the degree of mineralization of reparative dentine obtained with tricalcium phosphate-hydroxyapatite was quicker and thicker when compared with that produced by calcium hydroxide. In addition, HA has been used as fillers for the reinforcement of dental composite resins (Leinfelder, 1985; Arcís et al., 2002), coating in both orthopaedic and dental implant (Munting et al., 1990; Chang et al., 1997), restoration of edentulous atrophic ridges (Piecuch, 1986), perio infrabony pockets (Meffert et al., 1985), periodontal defects (Yukna et al., 1985), under and around failing sub-periosteal metal implants (Golec, 1985), ridge augmentation prior to implantology for metal prosthetics (Linkow, 1984).

Calcium phosphate cement is a bioactive cement that sets as HA when moistened (Takechi et al., 1998). The use of calcium phosphate cement may improve the prognosis of the treatment. The calcium phosphate cements were developed for furcation sealing (Chau et al., 1997), root surface desensitization and sealer for root canal filling materials

(Sugawara et al., 1990; Bilginer et al., 1997). The self-setting ability, satisfactory compressive strength and biocompatibility made calcium phosphate to be a useful material for pulp capping or lining materials (Yoshimine and Maeda 1995; Chaung et al., 1996).

New synthetic HA materials have been introduced into the market in the recent years to mimic the mineral component and the microstructure of natural bone and teeth. These new development would benefit various biomedical applications such as bone substitute materials, constituent implants and dental materials. Kim et al. (2004) developed new HA based sealers (calcium phosphate cement) and trade named them as CAPSEAL I, CAPSEALII and compared with another type of commercially available calcium phosphate sealer (SARCS I, SARCS II). They reported that new sealers showed lower tissue response than commercially available calcium phosphate sealers. However, all the experimented sealers showed acceptable biocompatibility.

2.7.4 Reinforcement of hydroxyapatite

Many reinforcements materials including particles, platelets, whiskers, long fibres, partially stabilized zirconia, metal dispersoids, and polymers have been used in HA bioceramic to improve their reliability (Bonfield, 1988; Silva and Domingues, 1997; Silva and Lameiras, 2000; Miao et al., 2001 Silva et al., 2001a,b). HA matrix composites containing 20–30% Fe-Cr alloy long metal fibres has been shown to exhibit the highest values of fracture toughness and fracture strength as reported by Suchanek and Yoshimura (1997). Ramires et al. (2001) tested TiO_2 and HA as a composite material, formed by sol-gel method, for biocompatibility and cell response. Their results showed that the combination was biocompatible and excellent at promoting cell activity. Volceanov et al. (2006) investigated the influence of zirconia when added to HA matrix on the mechanical properties and the interaction mechanism between zirconia and its polymorphs with calcium phosphates after sintering in air at 1250^{o}C. Their results highlighted that the mechanical properties for the HA matrix composites were improved. It has also been shown that the inclusion of phosphate based glasses produced significant improvement in mechanical properties (Lopes et al., 1998; Tancred et al., 1998). While others added small amounts of glass into HA ceramic to improve its sinterability, biological and mechanical properties (Ferraz et al., 1999; Franks et al., 2001). Ferraz et al. (1999) fabricated glass-HA composite coatings, using a plasma spraying technique. They showed favourable cellular responses in their *in vitro* experiment with osteosarcoma cells.

2.8 Functionally graded materials

Functionally graded materials (FGMs) are a group of new materials that have recently attracted much attention. According to Khor and his co-workers, FGM is a material with engineered gradients of composition, structure and/or specific properties aiming to become superior over homogeneous material composed of same or similar constituents (Khor et al., 2003). The aim of producing FGM is to obtain a material with two different characteristics in its two opposite faces. A FGM is obtained by varying the composition from one side of the material to the other side either continuously or stepwise. This graded structure allows the integration of dissimilar materials such as ceramics and metals without severe internal stress and combine diverse properties into a single material system. Thus, it can perform specific functions and meet performance requirements (Koizumi and Niino, 1995, Koizumi, 1997). According to Narayan et al. (2006), FGM was proposed in 1984 at the National Aerosapace Laboratory of Japan by Niino and his co-workers, as a preparation method for thermal barrier material for space plane application. This concept has been later expanded for different application such as coatings, packing, optical, biomedical etc. In the biomedical field, several approaches have been used to develop FG biomaterials for implants (Kon et al., 1995). FGMs can also be made into bulky specimens with strong interfacial bonding and reduced thermal stresses unlike coatings on substrates. Wong et al. (2002) fabricated the FG tricalcium phosphate/fluoroapatite composites and later prepared to combine the bioactive fluoroapatite with the bioresorbable tricalcium phosphate

The importance of the FGM concept in biological applications and functions was reported by several studies (Manjubala and Sastry, 2002; Ozeki et al., 2002). Fundamentally, the combination of mechanical properties and biocompatibility are very important factors in application of any biomaterial to medical or dental fields. The characteristics of the surface govern the biocompatibility of the material, and the mechanical strength is determined by the average mechanical strength of the materials. According to Chu et al. (1999) and Lim et al. (2002), the combinations of HA and Ti-6Al-4V can form an excellent FGM. Since the surface layer is HA, the resultant FGM exhibits excellent biocompatibility and bone-bonding ability or dental-bonding ability and the improved mechanical strength in the FGM is contributed by Ti-6Al-4V phase.

Miyao et al. (2001) fabricated titanium/hydroxyapatite FGM by spark plasma sintering (SPS) and later the mechanical properties and biocompatibility as an implant were evaluated. They showed that the Ti/HA FGM implants made by the SPS method had satisfactory strength, excellent biocompatibility and controllability for graded bio-reaction.

Matsuo et al. (2001) fabricated functionally graded dental post using laser lithography, one of the photo-curing type CAD/CAM system. The elastic modulus of the post could be changed longitudinally at the apical end of post by decreasing the filler content of ceramic powders from 64% to 0% in polymer matrix. They used FE method and showed that stress was reduced further by 30% in functionally graded dental post compared with the uniform one.

Foppiano et al. (2004) evaluated the biocompatibility of functionally graded bioactive coating of novel glasses using mouse osteoblast-like cells *in vitro*. Their result showed that functionally graded bioactive coating performed at least as well as tissue culture polystyrene and Ti6Al4V alloy. In addition, they hypothesized that functionally graded bioactive coating may affect gene expression favourably for osseointegration.

Fujihara et al. (2004) fabricated functionally graded dental post and analysed the stress distribution by FEA. They showed that the peak tensile and shear stresses for a functionally graded dental post were less than that of stainless steel post. They suggested that the modulus elasticity of the post material should be as close as possible to the modulus of the dentine and crown at the apical part and the coronal part respectively, in order to minimize the chance of interfacial debonding.

Hedia (2005b) introduced the optimal design of FGM dental implant by incorporating a thin layer of collagen/hydroxyapatite around the implant. Her results exhibited that the optimal design of collagen/hydroxyapatite FGM implant reduced the stresses concentration in the cortical bone, cancellous bone and implant compared with conventional titanium. She also showed that collagen/hydroxyapatite FGM had excellent biocompatibility and controllability.

Huang et al. (2007) added bioinspired FGM layer between the dental ceramic and the dental cement and investigated the effects of the functionally graded layer on the stress in the crown and its surrounding structures. From their results, the functionally graded layer was shown to promote significant stress reduction and improvements in the critical crack size. From their study, they concluded that the low stress concentrations were associated with the graded distributions in the dentin-enamel junction (DEJ). This provided new insights into the design of functionally graded crown architecture that can increase the durability of future dental restorations.

Rahbar & Soboyejo (2011) used computational and experimental effort to develop crack-resistant multilayered crowns that are inspired by the functionally graded DEJ structure. The computed stress distributions showed that the highest stress was concentrated at the ceramic outer layer of crown and reduced significantly towards the DEJ when bioinspired functionally graded architecture was used. They reported that the bioinspired functionally graded layers were also shown to promote improvements in the critical crack size.

Chapter Three
Fabrication, Optimization and Characterization of Gradient Architecture of Functionally Graded Multilayered Composites: Compositional Analysis, Physical and Mechanical Properties

3.1 Introduction

Designing functionally graded materials (FGMs) is a novel concept to achieve improved properties that cannot be achieved by conventional homogeneous-type materials (Lannuttia, 1994; Koizumi, 1997). FGMs are materials with a smooth gradient in one or more properties, which is essential for their function. The change in property is usually caused by a gradient in chemical microstructure or composition. Generally, this material consists of one material at one end, a second material on the other, and intermediate layers of materials between them whose structure, composition and morphology vary gradually from one layer to the other (Kawasaki and Watanabe, 1997).

The concept of FGMs was first proposed in 1984 by Niino. Originally the purpose for development of these materials was to produce superheat-resistant materials for propulsion systems and airframes of space planes (Niino and Maeda, 1990). The development of FGMs has now been extended to electronic, optical, biomedical and other applications (Hirai, 1996). Features of the FGMs are as follows:

1. Gradual transition in microstructure/composition.
2. "Smoothening" the transition for reduction of thermal stress.
3. Minimize or eliminate stress concentration.
4. Tailored functional performance.

The fabrication of FGMs has been successfully demonstrated through a variety of methods. The most important objective in the fabrication of a FGM is to achieve a well-controlled not only distribution of various materials but also other necessary elements such as its microstructure, crystal structure, and pores (Hirai, 1996).

The following types of gradients for FGM can be processed using the powder metallurgy route as quoted from Kieback et al. (2003);

1. “Porosity and pore-size gradients: Porosity gradients may be created either by the deposition of powder mixtures with different particle shape or by varying the deposition parameters including the use of space holders”.
2. “Gradients in chemical composition of single phase materials: The deposition of powders with a continuous change in the composition of the mixture during sintering will lead to a single phase material with a smooth change in the distribution of elements”.
3. “Gradients of the volume content of phases and grain size gradients in two or multiphase materials: The resulting microstructure consists of two or more phases with gradients in volume content or in grain size which were predetermined during the deposition of the powders. The combinations of phases can include metal-metal, metal-ceramic and ceramic-ceramic systems”.

Many researchers have fabricated FGMs using hot isostatic pressing (Rabin and Heaps, 1993; Winter et al., 2000). In this method, pressure is applied to the specimen during the heating cycle. The externally applied pressure helps to restrict deformation and alleviate the stresses that lead to fracture and at the same time reduce the porosity and increase the relative density leading to an improvement of mechanical properties. However, hot isostatic pressing is expensive and requires a lot of work to prepare samples before they can be heated.

Others used pressureless sintering (Pines and Bruck, 2006a, b) where preconditioning of the materials is not required as it only require a high temperature furnace. Depending on the materials combination utilized, an inert gas may be necessary to prevent oxidation. As preconditioning of the FGM is not required, there are less time and cost requirements. However, crack and deformation of materials may occur as there is no external pressure applied to the specimen, and there is no force to mitigate the differential stresses between layers.

The existence of a designed concentration and structural profile is the most exclusive characteristic of FGMs. In order to define the characteristics of a graded profile, the starting point of FGMs characterization is the determination of its microstructure and chemical composition. Scanning electron microscopy (SEM), energy dispersive X-ray analysis (EDX)-elemental analysis and X-ray diffraction (XRD) phase analysis are the most convenient techniques for this purpose. The physical and mechanical properties of the FGM such as densities, porosities, shrinkages, microhardness, flexural strength and modulus of elasticity represents an important field of study relevant to a wide variety of materials systems.

3.2 Aim

The aim of this chapter was to fabricate, characterize and optimize functionally graded multilayered composite (FGMC) for possible applications as dental post.

3.3 Objectives

3.3.1 Fabrication and optimization of functionally graded multilayered composite

a. To fabricate the FGMC based on preliminary finite element analysis (FEA) through stacking layers of metal-ceramic powders.

b. To optimize the FGMC so that it is free from cracks during sintering process.

3.3.2 Characterization and optimization of the functionally graded multilayered composite using pressureless sintering and hot isostatic press

I. Characterization functionally graded multilayered composite using pressureless sintering

a. To characterize the compositional and microstructure feature of FGMC by using scanning electron microscopy (SEM), energy dispersive X-ray analysis (EDX)-elemental analysis and X-ray diffraction (XRD) phase analysis.

b. To determine selected physical properties of the FGMC such as experimental density, mathematical densities (initial and final densities), theoretical density, experimental porosity, mathematical porosities (initial and final porosities), relative density, shrinkage and relative shrinkage.

c. To create porosity models in order to estimate and predict porosity distribution during the fabrication of FGMC and compared to experimental porosity.

d. To determine the microhardness of FGMC.

e. To determine the flexural strength and modulus of elasticity of FGMC.

II. Optimization of the functionally graded multilayered composite using hot isostatic press

a. To optimize the compositional and microstructure of FGMC by using scanning electron microscopy (SEM), energy dispersive X-ray analysis (EDX)-elemental analysis and X-ray diffraction (XRD) phase analysis,.

b. To determine and refine selected physical properties of the FGMC such as experimental density, mathematical densities (initial and final densities), theoretical density, experimental porosity, mathematical porosities (initial and final porosities), relative density, shrinkage and relative shrinkage.

c. To determine the microhardness of FGMC.

d. To determine the flexural strength and modulus of elasticity of FGMC.

3.3.3 Comparison of hot isostatic press and pressureless sintering processes

a. To compare the efficiency of pressureless sintering and hot isostatic press methods in the fabrication of FGMC.

3.4 Materials and method

3.4.1 Fabrication of the functionally graded multilayered composite

A crucial goal for the processing strategy of FGMC was to produce composites of high density and good phase distribution to obtain the desired microstructure. The designed and fabricated FGMC was in accordance to the results of preliminary FEA (Appendix I, Figures A-D). The various steps used to produce the required materials are outlined in the following sections.

3.4.1.1 Powders preparation

The fabricating of FGMC was divided into two steps:

1. Layer by layer cladding of various components by physico-chemical process to produce multilayered composite.
2. Fabricating functionally graded structured bulk sample via sintering.

The specifications of materials used to prepare FGMC were listed in Table 3.1.

Table 3.1 Specification of green powders in the study

Properties	Alumina (Al_2O_3)	Zirconia (ZrO_2)	Titanium (Ti)	Hydroxyapatite (HA)
Physical state	Powder	Powder	Powder	Powder
Particle size	~10 µm	~5 µm	<45 µm	~5 µm
Purity	~99.7%	~99 %	~99%	≥90%
Density	4.000	5.89	4.510	--
Molecular weight	101.96	123.22	47.88	502.31
Boiling point	2980°C	5000°C	3287°C	N/A
Melting point	2038°C	2700°C	1660°C	N/A
Solubility in water	Insoluble	Insoluble	Insoluble	Solvent
Manufacturer	Sigma-Aldrich	Sigma-Aldrich	Sigma-Aldrich	Sigma-Aldrich
Batch No.	265497	19052-2500	42107-0000	04238

3.4.1.2 Powder processing technique

FGMC were prepared using a powder metallurgy route schematically as shown in Figures 3.1 and 3.2.

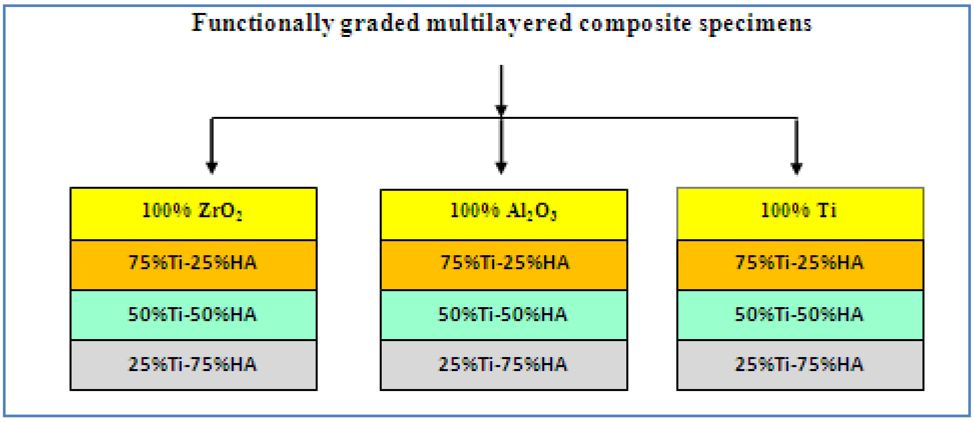

Figure 3.1 Schematic diagram of multilayers and composition of each layer of the fabricated specimens.

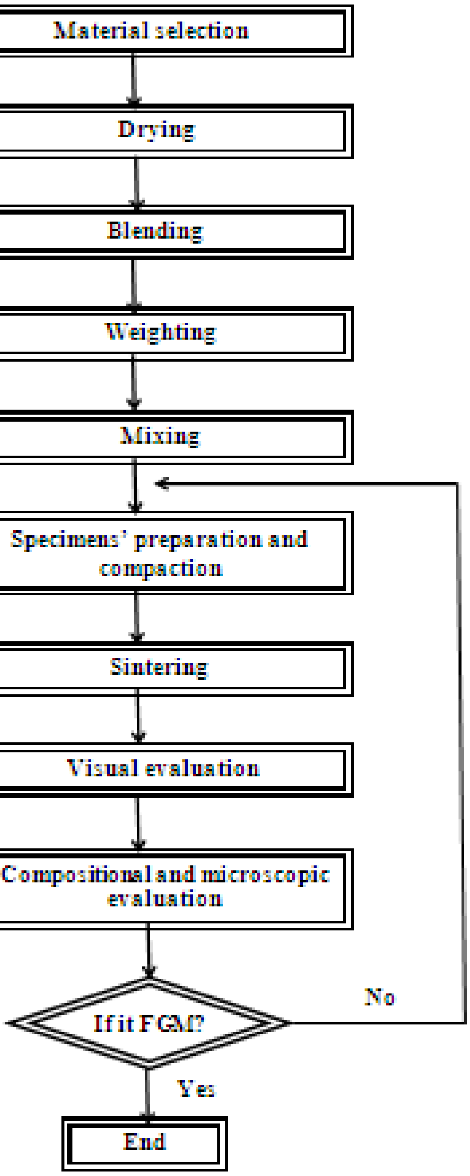

Figure 3.2 Flow chart for fabrication of FGMCs.

The powder processing technique was divided into 5 steps as follows:

a. Drying

ZrO_2, Ti, Al_2O_3 and HA powders were dried in an oven at 110°C overnight to prevent the particles from being sticky during mixing, thus minimizing the formation of agglomerates of the particle during mixing.

b. Blending of pure powder

Once the selected powders had been weighed (10-12 g), the raw powders were thoroughly blended together to ensure maximum particles dispersion for optimal mechanical properties. The objectives of the blending are to reduce the particle size and to obtain a more homogenous shaped particle. The blending process of raw powders was achieved by using a planetary ball mill (Retsch, Germany) filled with ten zirconia ceramic balls of half an inch in diameter. The blending process was carried out at 300 rpm with reverse action for an hour.

c. Powders mixing and milling

Milling and mixing are the crucial steps in specimens' preparation. Effective mixing and milling process will result in lower amount of agglomerates and a uniform composition in the mixture.

The powders were poured into the bowl of the ball mill and the top is then closed tightly. The ZrO_2, Ti, Al_2O_3 and HA of various combination powders were then mixed for five hours. In order to minimize or prevent particle agglomeration, the planetary ball mill was allowed to rest every one hour and to allow removal of powders sticking onto the wall of the bowl.

d. Preparation and compaction of the specimens using uni-axial hydraulic press

Stainless steel compaction die (Figure 3.3) was used to produce the individual graded specimens. The die consisted of five parts as illustrated in Figure 3.3. Prior to specimen fabrication, the mould was cleaned using ethanol and cotton tissue to remove any contamination. The mould was lubricated using zinc stearate and this will facilitate the removal of specimen from the mould after compaction.

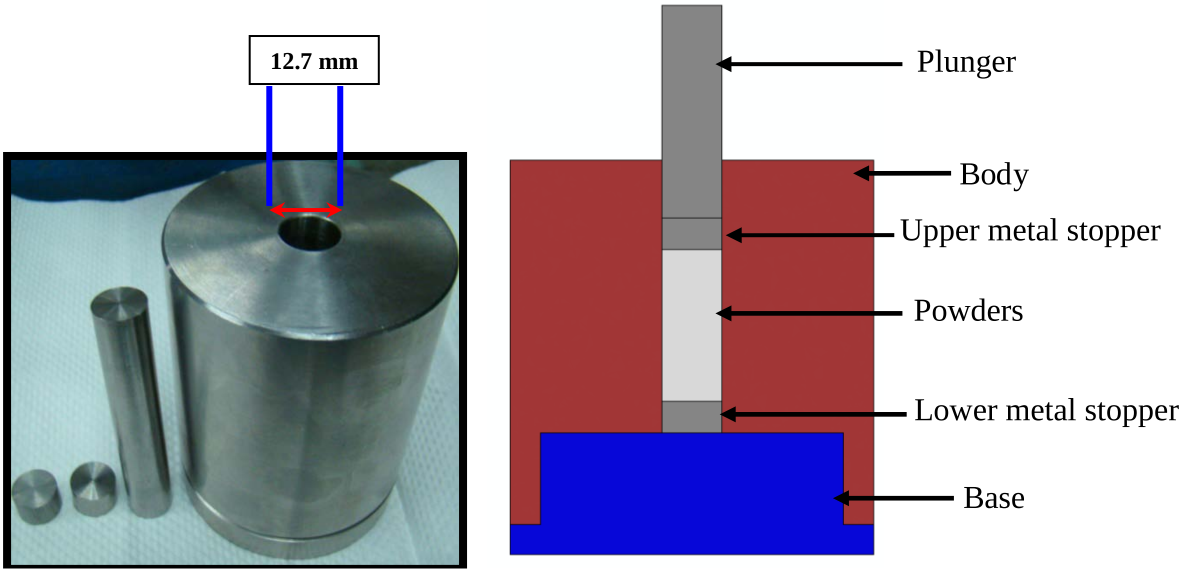

Figure 3.3 Stainless steel die compaction mould used for fabrication of powder processed graded structure.

In order to determine the amount of powder to be placed into the mould, the desired sintered layer thickness, *t*, was multiplied by the cross-sectional area, *A*. This will determine the final sintered volume of the layer. This volume was then multiplied by the theoretical density of the powder composition ρ_{layer} based on a rule of mixture formulation, to ultimately determine the mass of the powder to be added m_{layer}:

$$m_{layer} = \rho_{layer} A t \tag{3-1}$$

The specimen was then placed layer by layer into the mould. It was found that layering with combination of 25% Ti and 75% HA powders first, made removal of the specimen after compaction easier and efficient without causing any damage to the specimen. After each layer had been placed, the plunger was inserted to flatten each layer using gentle figure pressure. This pressing stage does not constitute enough force to consolidate the powders, but it is just enough to flatten the layer to allow for the formation of smooth interfaces. Once all of the powders had been added into the mould, the plunger was placed on top for final compaction. The powder was then compacted using uni-axial hydraulic pressing machine (Figures 3.4) at 8 tones for 10 minutes forming a rod shaped specimens and then ejected from the mould. The FGMC green specimens' height was approximately 8-9 mm (Figure 3.5). The finished green specimens were then ready for sintering in the furnace.

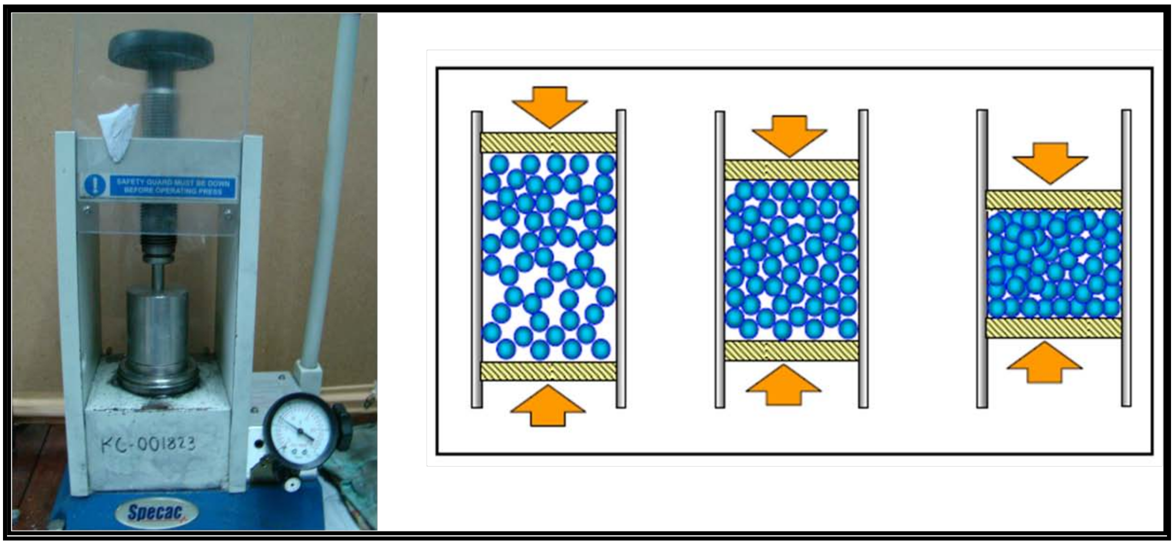

Figure 3.4 Hydraulic pressing machine and schematic diagram of the powder compaction.

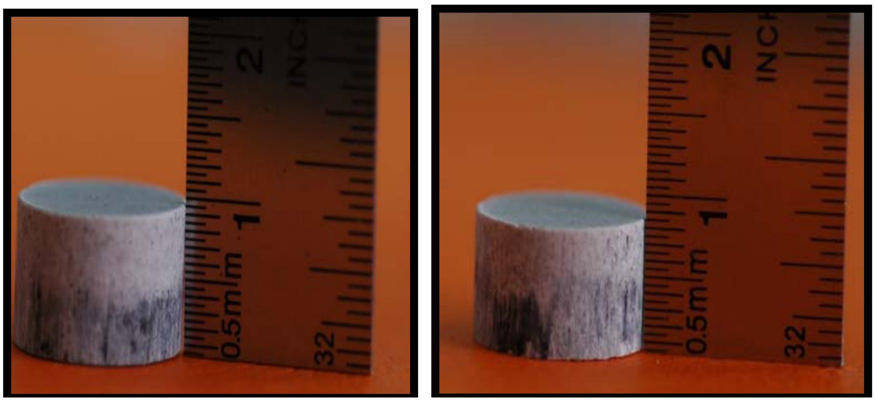

Figure 3.5 The green specimens.

e. Sintering of specimens

Sintering is a process whereby compacted powder are heated so that particles fused together, thus resulting in a solid particle with improved mechanical strength. After compaction all specimens were sintered either by using pressureless sintering and hot isostatic press.

I. Pressureless sintering

The prepared specimens were placed into the furnace as shown in Figure 3.6 (Yamatake Corporation, Japan). The specimens were sintered under flowing inert argon gas to prevent oxidation of Ti at high temperatures.

i. Sintering schedule and densification of the functionally graded multilayered composite

A sintering cycle was selected as shown in Figure 3.6. The temperature of the furnace was set and monitored using the digital program controller. The initial temperature of 30^{o}C was maintained for 1 minute, then the temperature was increased gradually to 440^{o}C within 82 minutes (increment of 5^{o}C/min). This stage is to precondition the specimens for high temperature sintering. Once the temperature reached 440^{o}C, it was then maintained for 120 minutes. After that, the temperature was increased gradually to 1100^{o}C within 66 minutes for the sintering process. The temperature of 1100^{o}C was again maintained for 60 minutes. This stage allows densification of the specimens. Finally, the temperature was decreased gradually from 1100^{o}C to 30^{o}C within 107 minutes, following which the specimens were kept in the furnace overnight. The furnace was set to cool down to 20-30^{o}C.

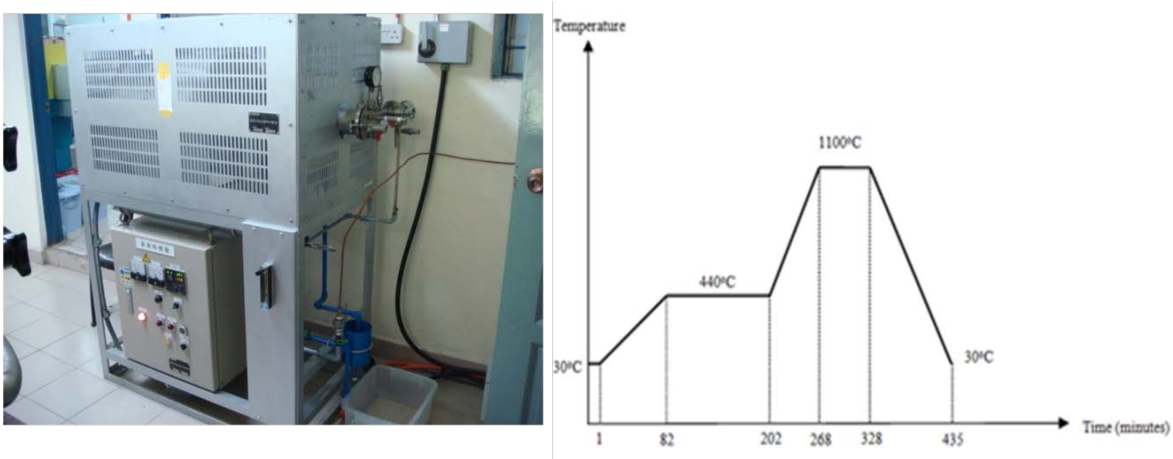

Figure 3.6 Furnace and sintering cycle used for pressureless technique.

II. Hot isostatic press

The prepared specimens were placed into the hot isostatic press machine (American Isostatic Press, USA) as shown in Figure 3.7. The specimens were sintered under flowing inert argon gas and vacuum to prevent oxidation of the Ti and under high pressure and to produce highly densed specimens. The sintering cycle for hot isostatic press used in the current study is illustrated in Figure 3.7.

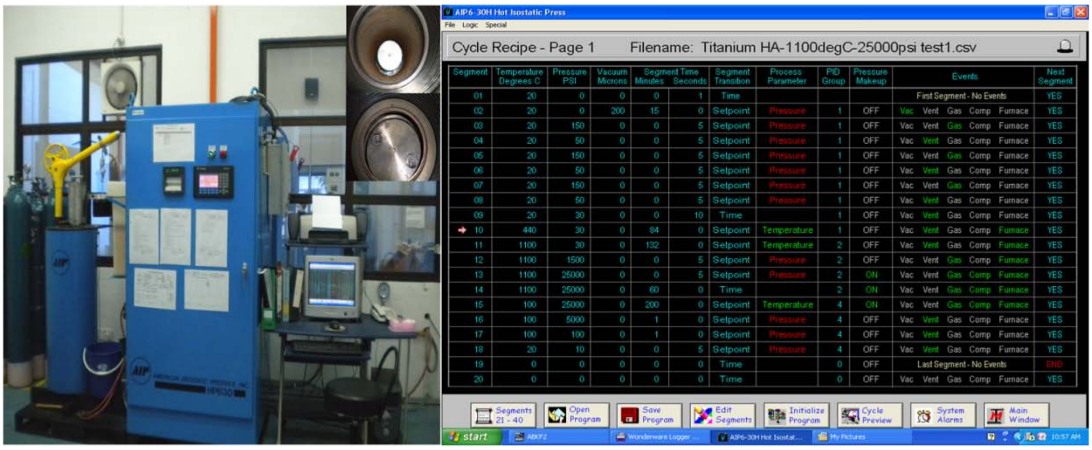

Figure 3.7 Hot isostatic press machine and sintering cycle.

3.4.2 Characterization and optimization of the functionally graded multilayered composite using pressureless sintering and hot isostatic press

In order to define the characteristics of the graded specimen, the starting point of FGMC was the determination of the microstructure and chemical composition. Scanning electron microscopy (SEM), energy dispersive X-ray analysis (EDX)-elemental analysis and X-ray diffraction system (XRD) phase analysis are the most convenient techniques for this purpose. The second part of the experiment assessed the physical and mechanical properties. The assessment of physical properties includes the determination of the experimental density, mathematical densities (initial and final densities), theoretical density, experimental porosity, mathematical porosities (initial and final porosities), shrinkage, relative density and relative shrinkage. The evaluation of the mechanical properties such as microhardness, flexural strength and modulus of elasticity was also carried out.

3.4.2.1 Microstructure analysis

Microstructural characterization is an important feature of this study in view of the pronounced influence of microstructure on various properties of FGMC. These characterization are important to determine if the microstructure depicted shows particles reinforcement or interpenetrating phase between different particle composition; which will not only determine the sintering behaviour but also have an impact on the mechanical properties.

The microstructure, morphology, and distribution of particles were investigated by using SEM (Low Vacuum Operating Mode, Quanta 200 F, FEI, USA). Prior to mounting on the aluminium stub, the surface of the specimens was polished and then cleaned with ethanol. Each specimen was then mounted on the aluminium stub using adhesive carbon tape and was subsequently mounted on the 7-holder specimen stage. Imaging was done under 10 and 20 kV accelerating voltage at magnification between 200× to 4000× using both the secondary electron and backscattered electron signals.

Micrographs were taken by focusing on the various regions of each layer. It is important to observe different locations within each layer, since the materials are likely to be non homogeneous on the microscale, and there may be features that are not present throughout the material.

3.4.2.2 Elemental analysis (EDX)

Elemental analysis was performed by using the energy dispersive X-ray spectroscopy analyzer (EDX) equipped in the same SEM.

3.4.2.3 X-ray diffraction (XRD) phase analysis

X-ray diffraction (X-Ray Diffraction (XRD), Frankfurt, Germany) was used to determine the phase stability and composition of FGMC. Specimens were mounted onto holders using a viscous adhesive and adjusted to the correct height with a glass slide. In order to obtain the graded composition profile, the specimens were cut using a diamond blade into consecutive slices of 2 mm thick at each layer representing the different composition. The peaks obtained were then compared to the standard reference JCPDS-ICCD (Joint Committee of Powder Diffraction Standard-International Center for Diffraction Data) files to assess the phases in specimens.

3.4.2.4 Physical properties evaluation

a. Experimental measurements of density and porosity

I. Experimental density

The bulk densities of ten specimens for each layer of FGMC were determined by water immersion techniques based on the Archimedes principle using an electronic densitometer (SD-200L, Japan).

For density measurement, first the temperature of the distilled water was recorded using a thermometer. Once the room temperature of 23±2^{o}C was achieved, the balance was set to zero. The balance set the density of the water according to the temperature value automatically. Then specimen was inserted into the upper cup and the weight was recorded in the balance, following, which the specimen was removed and then placed into the lower cup which was also filled with water. Again the weight was recorded. Based on Archimedes' principle, the difference between the two recorded values is equal to the weight of the water displaced by the specimen. The balance automatically calculates the density of the specimen using the recorded data. The previous procedures were repeated four times to reduce any errors and to produce a repeatability of the measurement.

The equation to measure bulk density;

$$\text{Sintered density} = \frac{W_a}{W_a - W_w} \times \rho_{water} \tag{3-2}$$

where;

ρ : Bulk density of the specimen, gcm^{-3}

W_a: dry weight of specimen.

W_w: specimen weight in water.

ρ_{water} : ~1.0 gcm^{-3}

Temperature effects on the water density were taken into consideration (Appendix II, Table A).

b. Theoretical and relative densities

The theoretical density of the composite was calculated by the rule of mixture, assuming that the total volume of each ingredient remained unchanged after mixing and sintering.

$$\rho_{th} = \sum f_i \rho_i \qquad (3\text{-}3)$$

where;

ρ_{th} is the theoretical density of the composite,

f_i and ρ_i are the volume fraction and the density of the initial theoretical ingredient of the composite, respectively.

The relative density was calculated using the experimental density divided by the theoretical density.

II. Experimental porosity

Porosity is the measurement of the void spaces in a material. Saturated surface dry technique was used to measure the void spaces by the open pores. This measurement specifically measure values fraction representing of 0 to 1 or as percentage from 0-100%. The specimens were treated in vacuum desiccators at 1 atm. This is to ensure air bubbles trapped in the specimens were removed. The experimental porosity was calculated using the following formula;

$$\text{Porosity} = \frac{W_s - W_a}{W_s - W_w} \times 100 \qquad (3\text{-}3)$$

where;

W_a: Weight of the specimens in air, g.

W_s: Weight of the saturated surface dry specimen, g.

W_w: Weight of the specimens in water, g.

c. Mathematical measurements of density, porosity and shrinkage

The mathematical density and shrinkage of specimens was determined by measuring the mass and the dimensions of the specimens. Measurement was taken on each specimen using a digital vernier caliper (Mitutoyo/Digimatic, Tokyo, Japan) to an accuracy of ±0.01 mm. Measurements were taken for each specimen and repeated four times to ensure a repeatability of the measurement.

Calculations of porosity are made directly from measurements of density change between sintered specimens based on each formulation of the layers instated the FGMC. This was done to ensure accurate measurements of the final mass, as the compositional gradient within FGMC may cause distortion due to shrinkage stress. It was also anticipated that both of these effects will be negligible given the rapid rate at which the thinner disc could be cooled down without retaining the stress that was induced during sintering the discs.

Each disc measuring 5 mm in height and 12.7 mm in diameter was fabricated using the combination of the following materials which represent each layer of the FGMC; 75%Ti-25%HA, 50%Ti-50%HA, 25%Ti-75%HA, 50%Al_2O_3-25%Ti-25%HA, 50%ZrO_2-25%Ti-25%HA and 100%Ti.. The initial measurements of the diameter and thickness of each specimen were recorded prior to placing them into the furnace. All specimens were then sintered in the furnace using pressureless and hot isostatic press sintering cycles. Following removal from the furnace, the final mass, diameter and thickness of sintering specimens were measured.

The density was obtained by first calculating the initial volume, V_i, of the disc using the following formula:

$$V_i = \frac{1}{4}\pi d_i^{\,2} h_i \tag{3-5}$$

where; d_i is the initial diameter of the disc and h_i is the initial height of the disc.

Shrinkage is measured in the radial direction, since that is the direction that causes the most stress in a graded material. Shrinkage of the disc, α, was calculated based on the difference between the initial and final diameters of the specimen.

$$\alpha = \frac{d_i - d_f}{d_i} \times 100 \tag{3-6}$$

The relative shrinkage was also calculated based on the relationship between the shrinkage of the first disc to the shrinkage of the second one.

The shrinkage (α) calculated from above equation was applied to determine the changes in the volume of the specimens to achieve final volume to ascertain the final density. Assuming isotropic shrinkage of the composite, this can be used to correlate the initial volume to the final volume, V_f, using the following equations;

$$\rho_i V_i = \rho_f V_f \tag{3-7}$$

$$V_f = V_i (1 - \alpha)^3 \tag{3-8}$$

Measuring the sintered final mass, M_f, allows the final density, ρ_f to be calculated.

$$\rho_f = \frac{M_f}{V_f} \tag{3-9}$$

The shrinkage (α) then was used again to calculate the initial density, ρ_i, in following equation (Pines and Bruck, 2006b):

$$\rho_i = \rho_f (1 - \alpha)^3 \tag{3-10}$$

The initial and final porosity in the sintered discs was then calculated using the theoretical maximum-fired density, ρ_{th}. This theoretical fired density is based on a rule of mixtures formulation shown in following equation:

$$\rho_{th} = \rho_1 v_1 + \rho_2 v_2 \tag{3-11}$$

where;

v = volume fraction.

ρ = density of the specific material.

The initial and final percent porosity, P_i and P_f respectively, were calculated using following equations:

$$P_f = \left(\frac{\rho_{th} - \rho_f}{\rho_{th}} \right) \times 100 \quad (3\text{-}12)$$

$$P_i = \left(\frac{\rho_{th} - \rho_i}{\rho_{th}} \right) \times 100 \quad (3.13)$$

d. Porosity reduction Models

Two porosity models were fabricated using Ti and HA. The porosity within these models will be calculated mathematically. These models then are used to predict the porosity reduction in the each layer of the FGMC. The component with greater volume fractions; either Ti or HA, is considered as the matrix, while the other component played the role of reinforcement particles. There are two proposed models according to the porosity distribution in the disc; Model I, the pores are observed in the matrix only, while in Model II the pores are associated with both matrix and particles, simultaneously.

I. Porosity reduction in Model I: Porosity observed only in matrix

In this model the porosity was calculated with the assumption that the particle reinforcement phase is pore free and does not introduce additional porosity into the disc due to their size and shape. It was assumed that volume fraction of the reinforcing particles remained constant before and after sintering. Therefore, the calculations were based on the volume fraction of the matrix component can be used to determine the porosity. The total volume fractions of all the components are:

$$v_{Ti} + v_{HA} + v_{porosity} = 1 \quad (3\text{-}14)$$

As the porosity is assumed to be associated with the matrix only, therefore the ratio of the initial and final partial volume fractions of porosity should be equal to the ratio of initial and final volume fractions for the matrix material (Pines and Bruck, 2006b). This equation could be rewritten in terms of volume fractions of the matrix:

$$v_{matrix_f} + (v_{matrix_f} v^*) + (v_{matrix_f} \, x \frac{1 - v_{partial_f}}{v_{partial_f}}) = 1 \qquad (3\text{-}15)$$

where; the ratio v^* defines the relationship between Ti and HA and in the equation it converts the final volume fraction of the matrix into the volume fraction of the reinforcing particles.

$$v^* = (\frac{v_x}{1 - v_x}) \qquad v_x \quad \text{if} \quad x_{(\text{Ti or HA})} = 0.25,\ 0.50 \qquad (3\text{-}16)$$

$$v^* = (\frac{1 - v_x}{v_x}) \qquad v_x \quad \text{if} \quad x_{\text{Ti or HA})} = 0.75,\ 1 \qquad (3\text{-}17)$$

The final volume fraction of porosity was then calculated by subtracting the Ti and HA volume fractions in equation (3-18), as follows (Pines and Bruck, 2006b):

$$P_f = 1 - v_{matrix_f} (1 + v^*) \qquad (3\text{-}18)$$

II. Porosity reduction Model II: Porosity associated with both matrix and reinforcement particles

Assuming the volume fraction of porosity associated with the matrix does not change with volume fraction of the matrix, the amount of porosity caused by the matrix can be calculated from the known volume fraction of the matrix material, v_{matrix}, and the amount of porosity in the pure matrix material P_{pure} (Pines and Bruck, 2006b).

$$\frac{(v_{porosity})_{matrix}}{v_{matrix}} = \frac{P_{pure\,matrix}}{1 - P_{pure\,matrix}} = \textit{Constant} \qquad (3\text{-}19)$$

Next, the porosity associated with the presence of the reinforcing inclusion phase, $(v_{porosity})_{particle}$, can simply be calculated from the difference between the porosity in the composite material, P, and the partial volume fraction of the porosity due to the matrix phase.

$$v_{Ti} + v_{HA} + (v_{porosity})_{particle} + (v_{porosity})_{matrix} = 1 \qquad (3\text{-}20)$$

However, in this model the porosity is associated with both matrix and particle agglomeration. Therefore, the final porosity, P_f, was determined as follows (Pines and Bruck, 2006b).

$$P_f = (v_{matrix})_f \left[\left(\frac{P_{pure\ matrix}}{1 - P_{pure\ matrix}} \right)_f + \frac{((v_{porosity})_{particle})_i}{(v_{matrix})_i} \right] \tag{3-21}$$

3.4.2.5 Mechanical properties

The mechanical properties evaluated were microhardness, flexural strength and modulus of elasticity. These tests, together with compositional analysis, would allow investigation of the correlation between graded compositional characteristics and mechanical properties.

a. Microhardness

Microhardness was determined using an automatic Vickers microhardness testing machine (Shimadzu, Japan) as shown in Figure 3.8, which is ideal for both sintered disc specimens representing layer of the FGMC and the FGMC specimens. Ten specimens were prepared for each group.

The indenter is pyramidal in geometry with known angles on each side. Using 500 g load for 15 seconds, the microhardness was calculated automatically by measuring the length of the diagonals of the indent on the surface of the material (Figure 3.8).

The hardness was determined using

$$H_v = 1.854\frac{L}{d^2} \tag{3-22}$$

where;

L = the load.

d = the longer diagonal of the indentation impression.

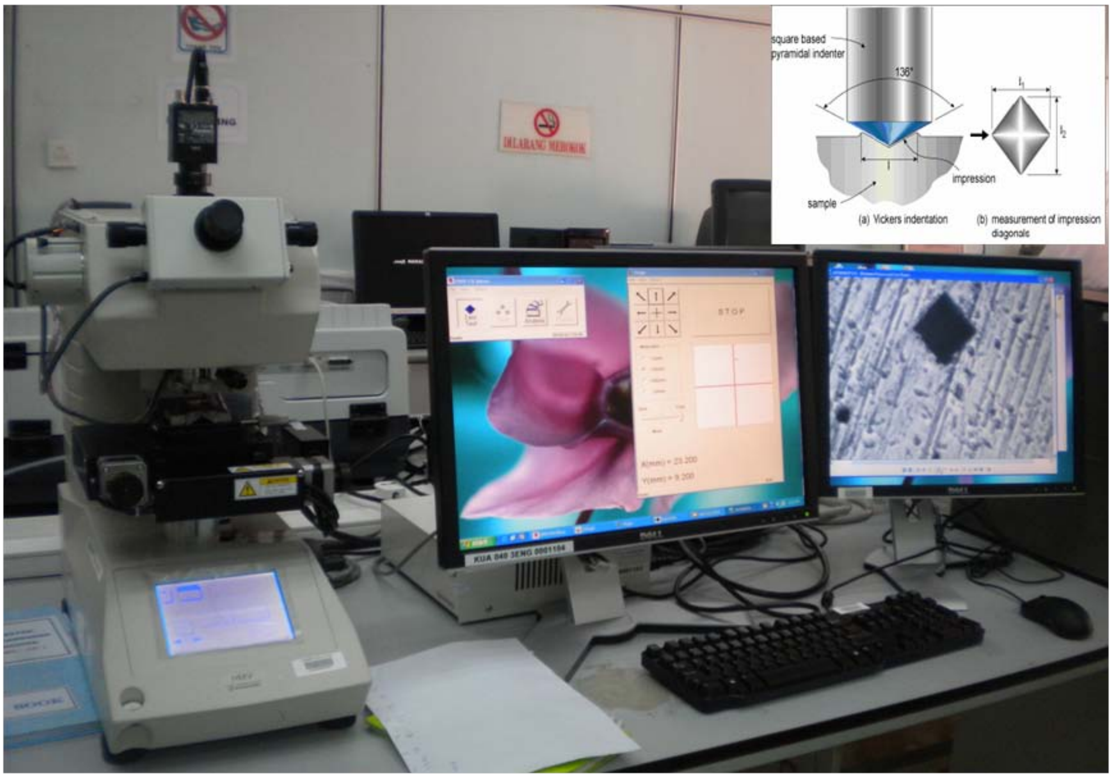

Figure 3.8 Microhardness testing machine and schematic hardness measurement imprint according to Vickers hardness method.

b. Flexural strength and modulus of elasticity

Ten rectangular-shaped specimens for each formulation representing each layer of FGMC were prepared according to ISO 6872:1995 Dental ceramic materials. A steel mould was used to prepare the specimens as illustrated in Figure 3.9. The three point bending test was used to determine the flexural strength and modulus of elasticity of FGMC on a universal testing machine (Shimadzu, Japan) at a crosshead speed of 0.5 mm/min.

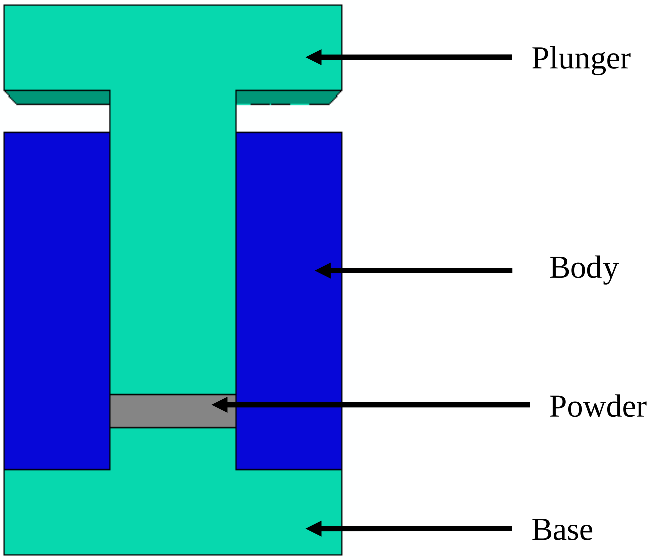

Figure 3.9 Schematic diagram for stainless steel die compaction for flexural strength and modulus elasticity.

The parallelism and flatness of opposing surface of each specimen was checked visually. In this test, the specimens were placed on two parallel supporting pins. The loading force was applied in the middle by means of a loading pin. Flexural strength was calculated using following formula:

$$\sigma = \frac{3Fl}{2bh^2} \qquad (3\text{-}23)$$

where;

F is the load at failure, in Newton’s;

L is the inner test span (centre to centre distance between inner support rollers), in millimeters;

b is the width of the specimen, i.e., the dimension of the side at right angles to the direction of the applied load, in millimeters;

h is the thickness of the specimens, i.e., the dimension of the side parallel to the direction of the applied load, in millimeters.

During the test, vertical displacement was recorded. These pre-failure load values were used to determine the modulus elasticity. Modulus elasticity was determined using the slope of the load-displacement curves, *E* in, which calculated from the following equation:

$$E = \frac{F_1 l^3}{4bh^3 d} \tag{3-24}$$

where;

E is the modulus elasticity;

F_1 is the pre-failure load (in Newton's);

d is the displacement of the crosshead at load *F1* (in millimeters);

l is the distance between the supports;

b is the width, and h is the height of the specimen (in millimeters).

3.4.3 Data analysis

The descriptive analysis will be carried out and the parametric independent sample *t*-test will determine the significance difference between the physical and mechanical properties of the FGMC sintered by pressureless sintering and hot isostatic press using SPSS, version 12 (SPSS Inc., Chicago, USA). However, if the collected data does not meet the normal distribution, the non-parametric Mann-Whitney *U* test will be employed.

3.5 Results

3.5.1 Fabrication and optimization of functionally graded multilayered composite

After removing each specimen from the furnace, cracks were seen in two of sintered specimens, whereas crack was not obvious in one specimen of Ti-HA-Ti formulation (Figure 3.10).

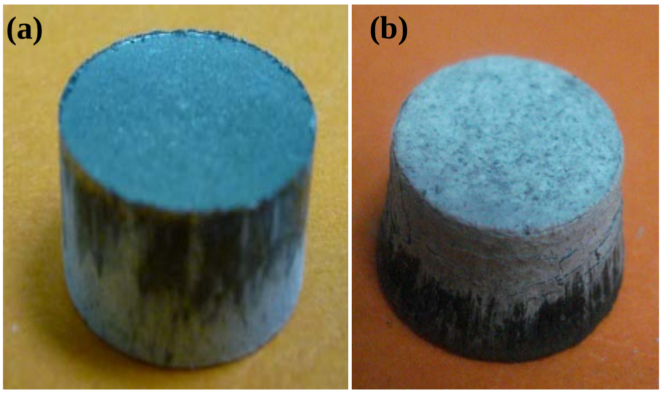

Figure 3.10 Macroscopic feature of specimen a) before sintering b) after sintering from Ti-HA-Ti formulation.
.

For the two specimens that cracked, the cracks were generally obvious between layers of materials. This may be attributed to the differences in the gradient shrinkage of each material composition (Figure 3.1). As seen in Figure 3.11, the cracks were obviously seen between the first and the second layers for specimens which consisted of:

a. Pure ZrO_2 and 75% Ti- 25% HA.
b. Pure Al_2O_3 and 75% Ti- 25% HA.

However, no cracks were evident in the third and fourth layers.

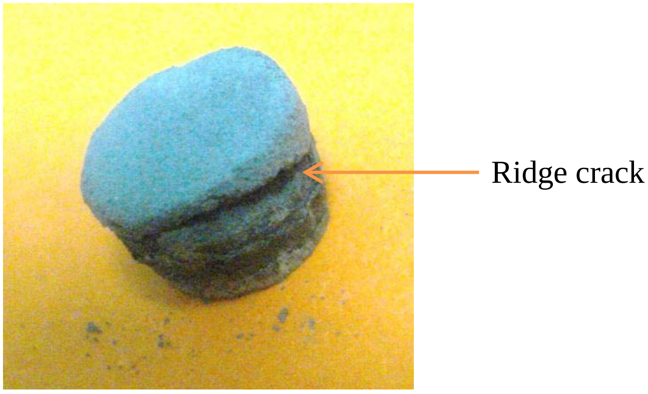

Figure 3.11 Macroscopic feature of sintered specimen from the first batch

Since the pure material (ZrO_2 or Al_2O_3) in the first layer did not prevent the occurrence of ridge cracks, a new composition at the interface between first and second layers was introduced as schematically shown in Figure 3.12.

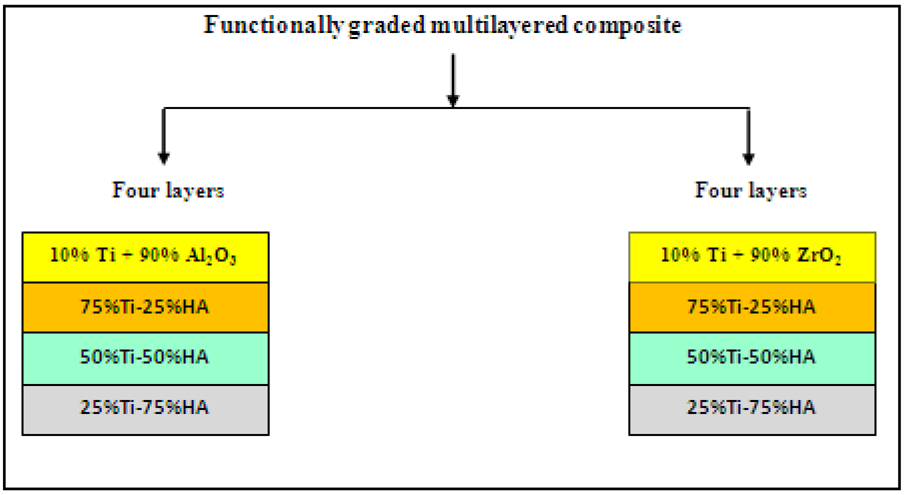

Figure 3.12 Composition of the second batch of functionally graded multilayered composite.

.

Two specimens of approximately 8-9 mm thick and 12.7 mm in diameter with compositions as shown in Figure 3.12 were fabricated in an attempt to match the thermo-mechanical stress at interfaces between layers. After sintering, ridge cracking was still seen at interface layers between first and second layers. However, the depth of the crack was less than before (Figure 3.13).

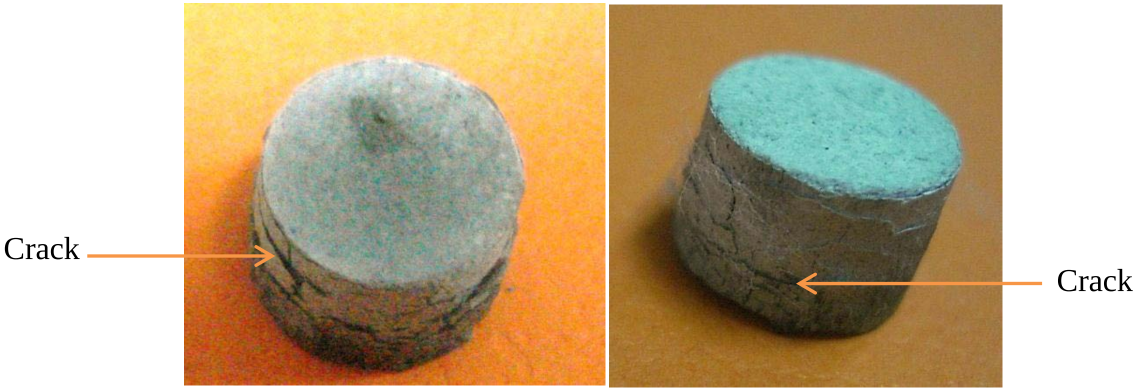

Figure 3.13 Macroscopic feature of sintered specimen from the second batch.

For this reasons, a third batch of specimens with different compositions (Figure 3.14) were fabricated in an attempt to optimize and integrate the properties at the interface between these layers.

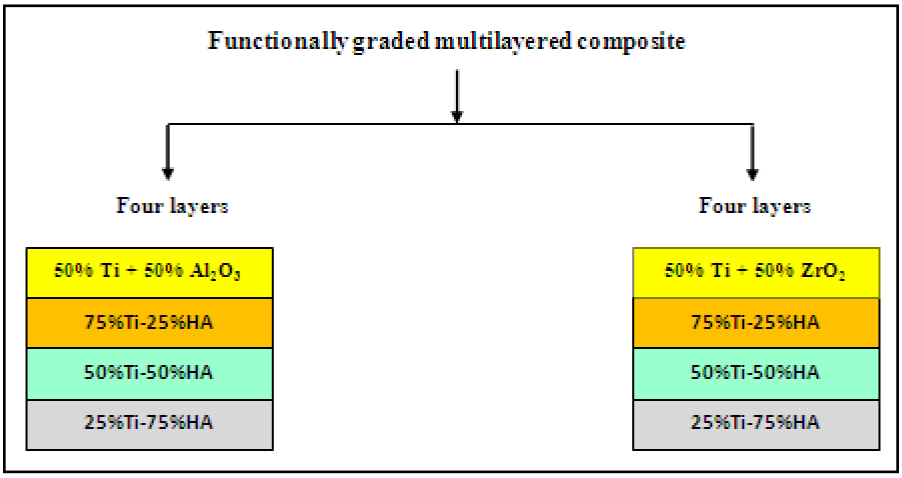

Figure 3.14 Composition of the third batch of functionally graded multilayered composite.

New specimens were fabricated based on the aforementioned formulation. Although ridge crack was not observed between layers, delaminating cracks was evident. However, the severity of the cracks was reduced (Figure 3.15).

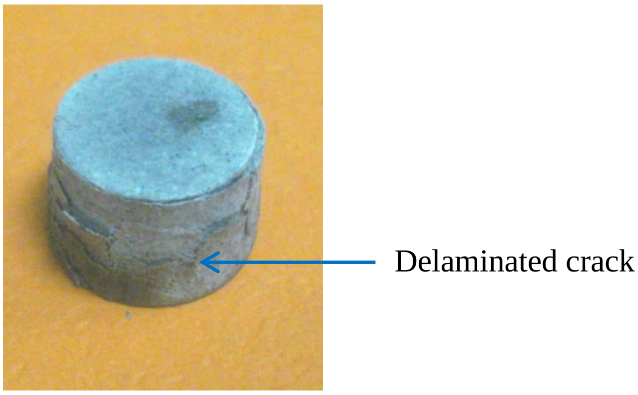

Figure 3.15 Macroscopic feature of sintered specimen from the third batch.

It was again necessary to alter the powder distributions between the first and second layers in order to achieve the proper thermal matching for sintering process. Identical specimens were fabricated with the addition of 25% to first layer to achieve matching composition with second layer (Figure 3.16).

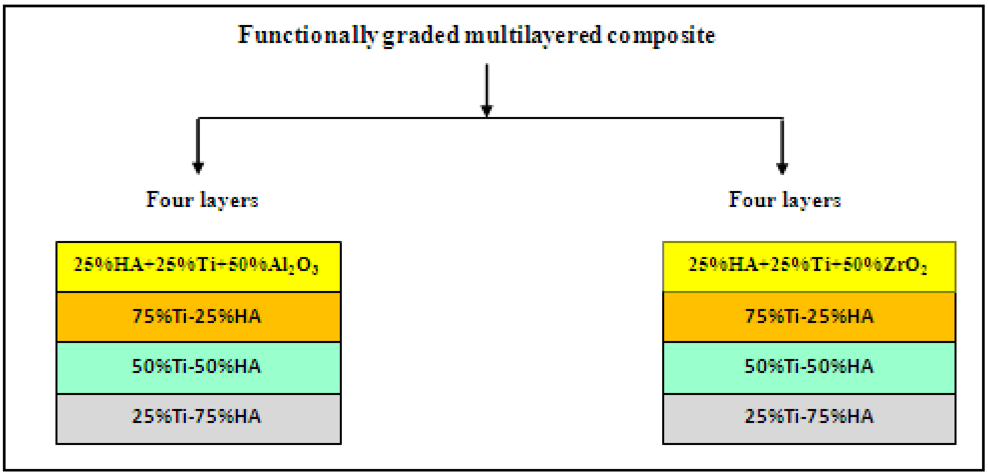

Figure 3.16 Composition of the functionally graded multilayered composite.

These formulations seem to produce the best specimens as delaminating cracks at interfacial layers were eliminated (Figurers 3.17 and 3.18).

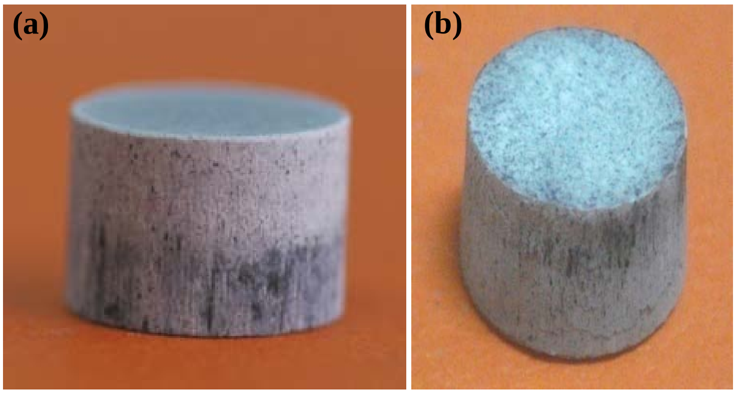

Figure 3.17 Macroscopic feature of ZrO_2-HA-Ti specimen a) before sintering b) after sintering.

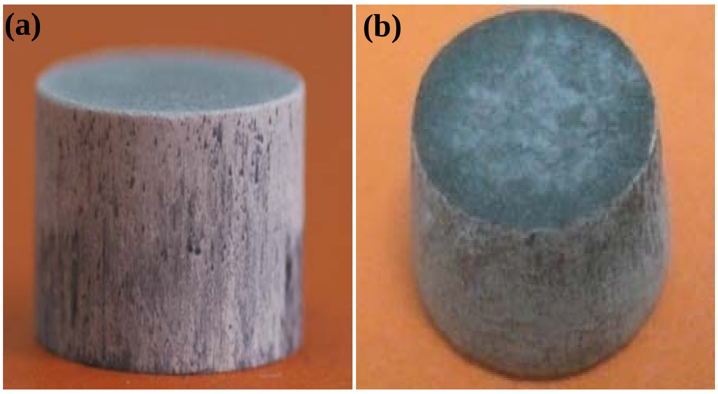

Figure 3.18 Macroscopic feature of Al_2O_3-HA-Ti specimen a) before sintering b) after sintering.

3.5.2 Characterization and optimization of gradient architecture of functionally graded multilayered composites: compositional analysis and physical properties fabricated by pressureless sintering and hot isostatic press

3.5.2.1 Microstructure and elemental analysis using scanning electron microscopy

Two micrographs were taken for each layer using both the secondary electron and backscattered electron signals. In each micrograph, the white and black phases indicated the distribution of the Ti and HA in each layer respectively, while the alumina were the smaller particles. Zirconia grains in darker colour dispersed within the HA grains. Specifically, each composite layer had a distinct appearance depending on the volume fractions of each constituent material. EDX analyses from different areas of the microstructures of ZrO_2-HA-Ti, Al_2O_3-HA-Ti and Ti-HA-Ti specimens confirmed the presence Ca, P, Ti, O, Al and Zr elements. Not any additional elements were observed. The EDX intensity of the elements in each layer was in accordance to the percentage of each material before sintering.

The first layer for Al_2O_3-HA-Ti (Figure 3.19) and ZrO_2-HA-Ti (Figure 3.20) can be differentiated easily from second layer in the micrograph. The border between both layers was distinct and no evidence of cracks suggesting that the sintering process was performed satisfactorily. The EDX from the first layer of Al_2O_3-HA-Ti formulation showed the presence of Ti, Al, Ca, P and O atoms (Figure 3.19). The EDX from the first layer of ZrO_2-HA-Ti showed the presence of Ti, Zr, Ca, P and O atoms (Figure 3.20). The porosity in all specimens sintered by hot isostatic press was considerably reduced compared to those sintered by pressureless sintering.

Figure 3.21 shows Ti layer with numerous cavities indicating that microspores existed in this layer. The EDX from this layer showed the presence of Ti atoms only. The reduction in porosity in this layer sintered by hot isostatic press compared to that sintered by pressureless sintering was noticeable.

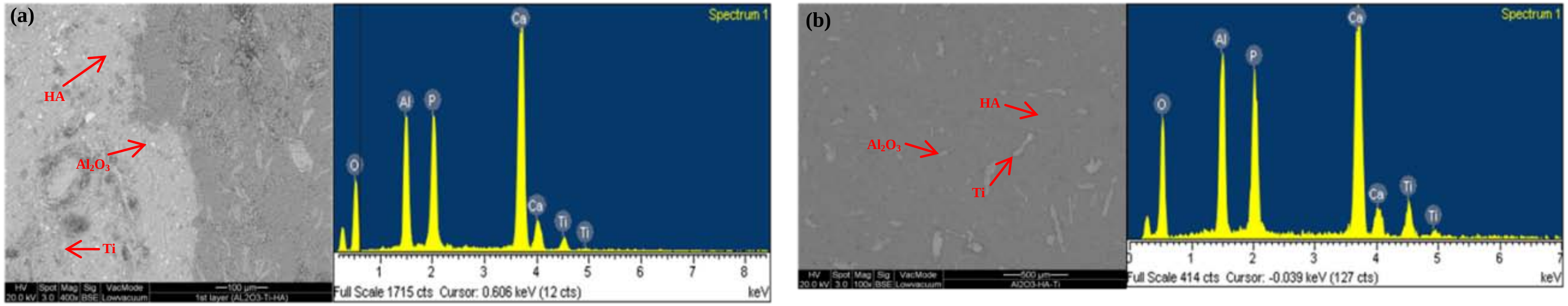

Figure 3.19 Micrograph and elemental analysis for 50%Al_2O_3-25%Ti-25%HA formulation sintered under a) pressureless sintering and b) hot isostatic press.

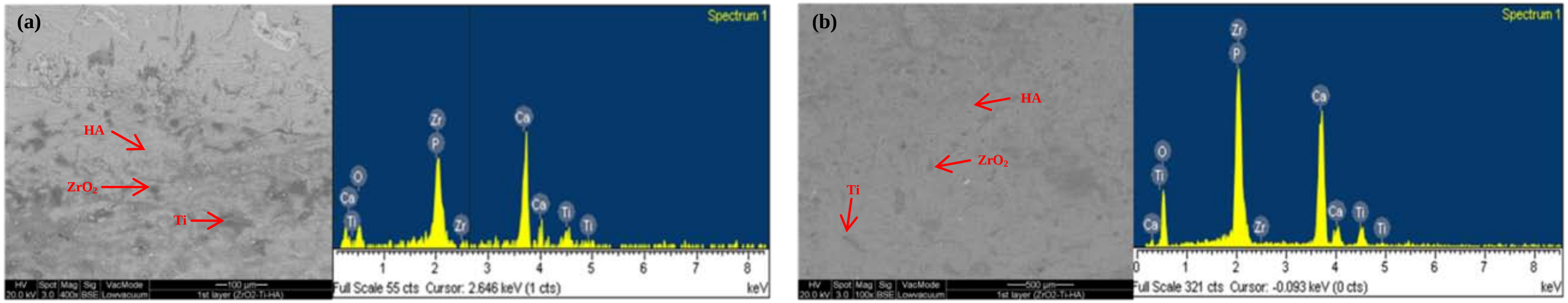

Figure 3.20 Micrograph and elemental analysis for 50%ZrO_2-25%Ti-25%HA formulation sintered under a) pressureless sintering and b) hot isostatic press.

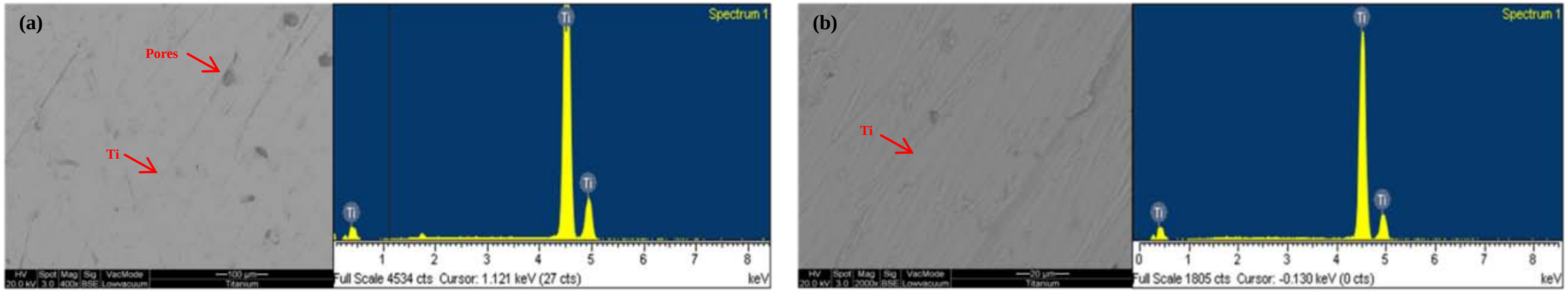

Figure 3.21 Micrograph and elemental analysis for Ti layer sintered by pressureless sintering sintered under a) pressureless sintering and b) hot isostatic press.

In the second, third and fourth layers, the microstructures were quite similar. The only difference among them was the amount of the Ti dispersed throughout the HA. Microstructure of the second, third and fourth layers show a gradual reduction in the Ti concentration from the second to the fourth layers. The EDX from these layers showed the presence of Ti, Ca, P and O atoms with the different intensity. It was observed that each element in the layers exhibits a graded distribution where the contents of Ti decrease gradually from second into fourth layers (Figures 3.22-3.24). The reduction in porosity in the second, third and fourth layers sintered by hot isostatic press compared to that sintered by pressureless sintering was obvious (Figures 3.22-3.24).

Secondary electron micrograph and back scattered electron analysis of the interface between first and second layers showed a complete continuous sintering and uniform graded phase distribution that confirms FGMC architecture (Figure 3.25). The interface between first and second layers was well defined, and no considerable residual porosity was observed in the interface layers. The adjacent layers of the graded composites seemed to be firmly bonded to each other.

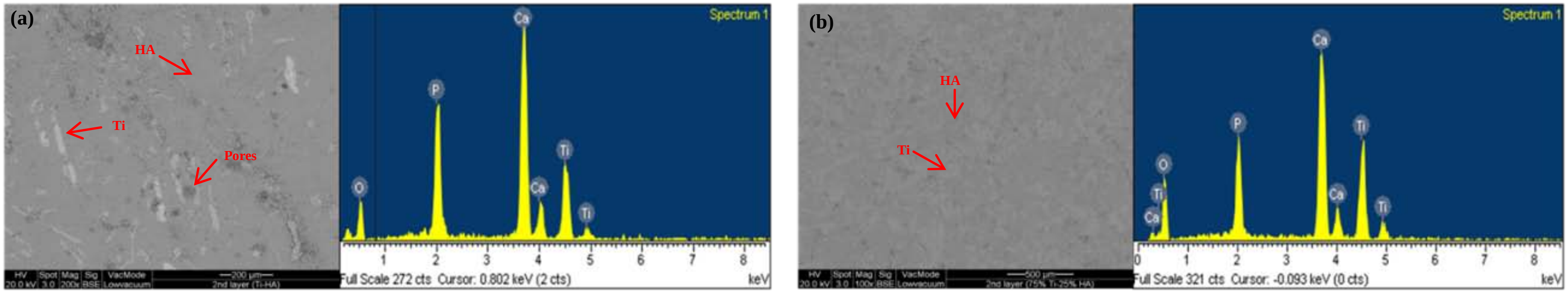

Figure 3.22 Micrograph and elemental analysis for 75%Ti-25%HA formulation sintered under a) pressureless sintering and b) hot isostatic press.

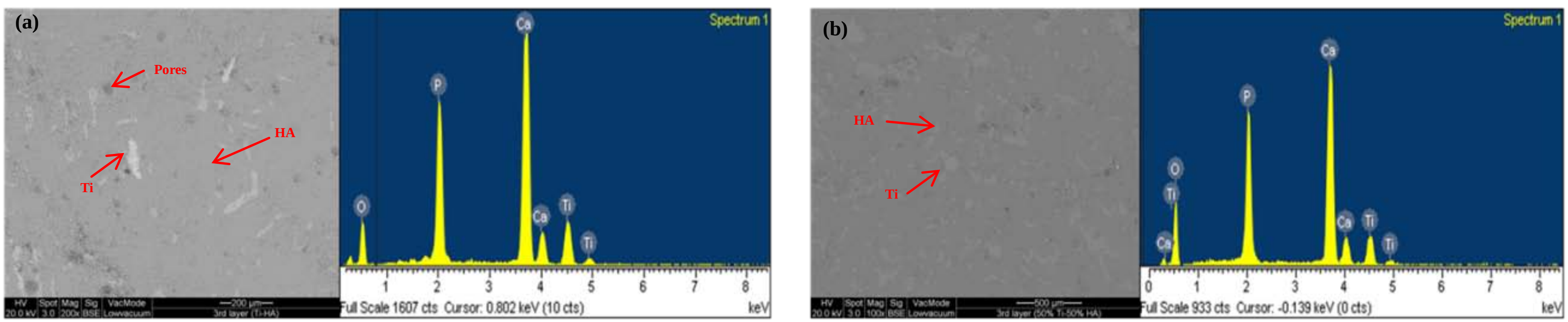

Figure 3.23 Micrograph and elemental analysis for 50%Ti-50%HA formulation sintered under a) pressureless sintering and b) hot isostatic press.

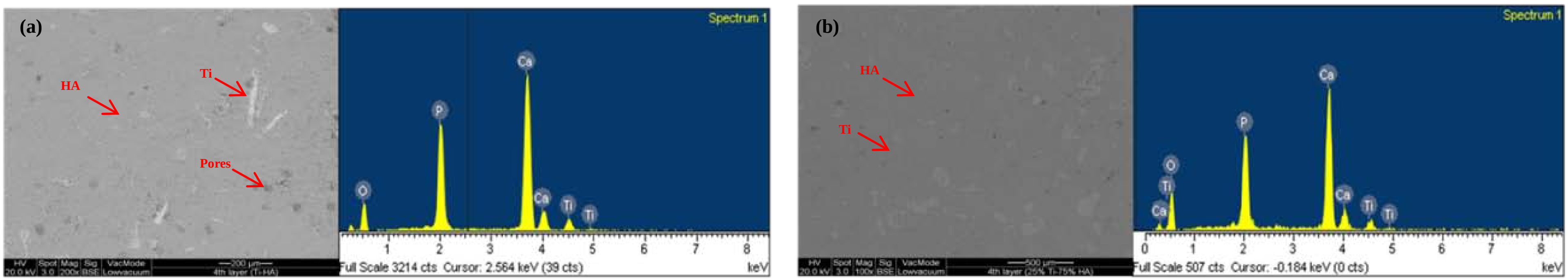

Figure 3.24 Micrograph and elemental analysis for 25%Ti-75%HA formulation sintered under a) pressureless sintering and b) hot isostatic press.

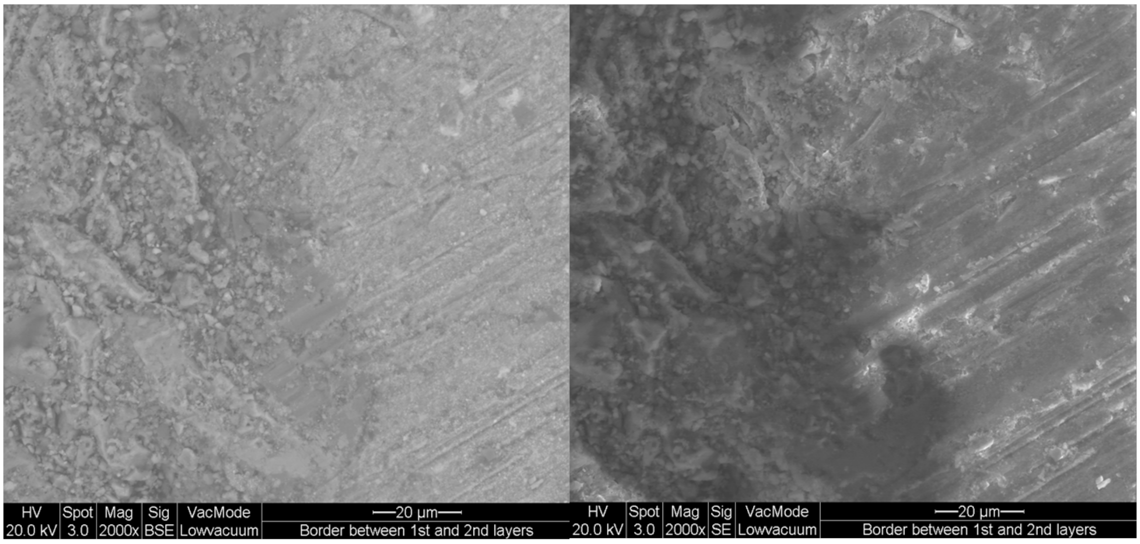

Figure 3.25 Micrograph shows sharp border between first and second layers. No crack evident between both layers.

Figure 3.26 represents the EDX analysis taken from the white spot representing the Ti and it showed high intensity peaks of Ti atoms. Peaks of Ca, P and O were also detected. It is possible that HA grains nucleate at lower temperature around the periphery of Ti.

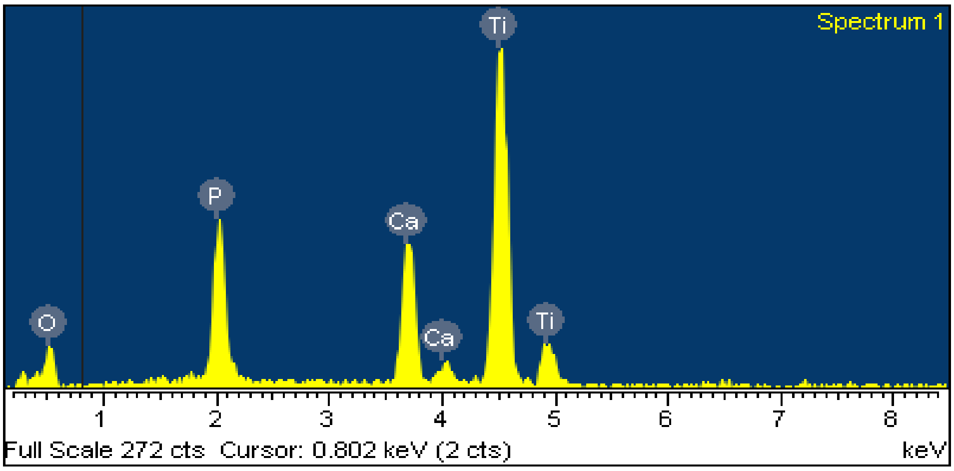

Figure 3.26 Elemental analysis taken from the Ti.

3.5.2.2 X-ray diffraction (XRD) phase analysis

Figure 3.27 shows the XRD patterns of the first layer of ZrO_2-HA-Ti FGMC sintered under pressureless sintering and hot isostatic press. There was no evidence of any chemical contamination and reaction that had taken place between the elemental phases as no additional phases was detected except for those present at the green stage; ZrO_2, HA and Ti. Figures 3.28 and 3.29 display the XRD patterns of the first layer of Al_2O_3-HA-Ti and Ti-HA-Ti FGMCs sintered under same condition. Similarly, no additional phase was detected, suggesting no chemical contamination or reactions had taken place. XRD diffraction patterns of second, third and fourth layers for formulation of Al_2O_3-HA-Ti, ZrO_2-HA-Ti HA and Ti-HA-Ti respectively (Figures 3.30-3.32) where only HA and Ti were detected.

XRD analyses from different areas of the microstructures confirmed the presence and gradual change of Ti-HA-ZrO_2-Al_2O_3 elements and phases in all the specimens. The gradual change in compositions and microstructure of Ti-HA-ZrO_2-Al_2O_3 is likely to lead to a gradual change in material properties.

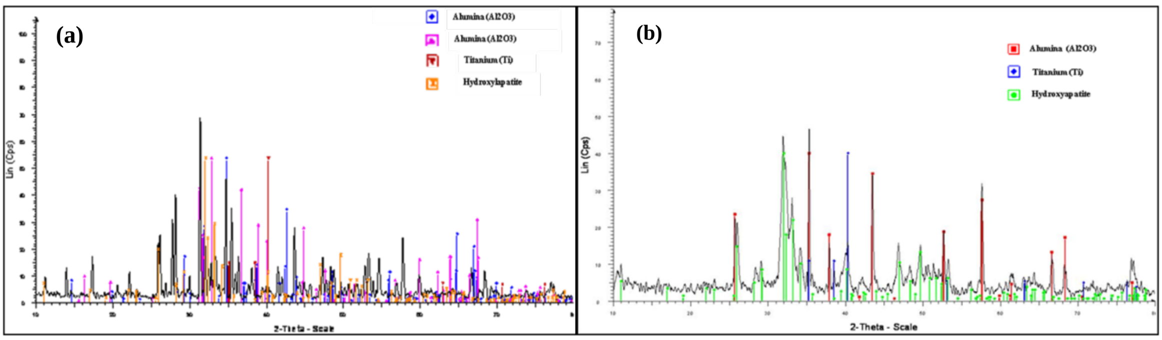

Figure 3.27 XRD spectra of first layer for FGMC formulation of 50%Al_2O_3-25%Ti-25%HA sintered under a) pressureless sintering and b) hot isostatic press.

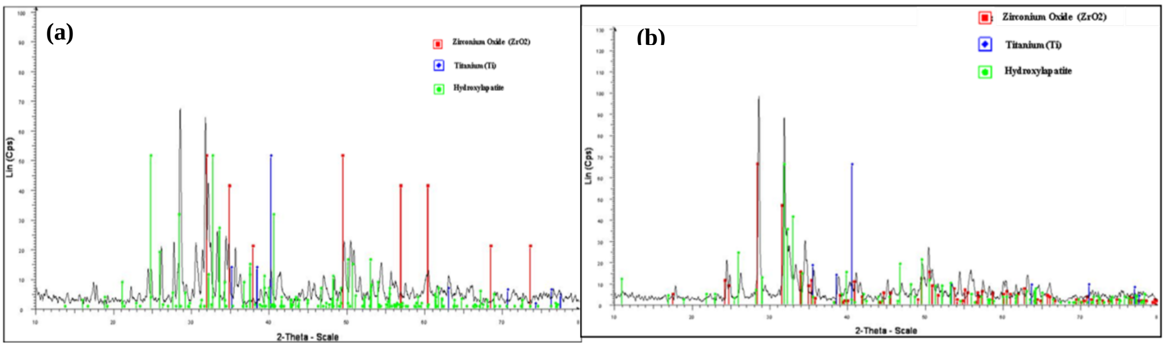

Figure 3.28 XRD spectra of first layer for FGMC formulation of 50%ZrO_2-25%Ti-25%HA sintered under a) pressureless sintering and b) hot isostatic press.

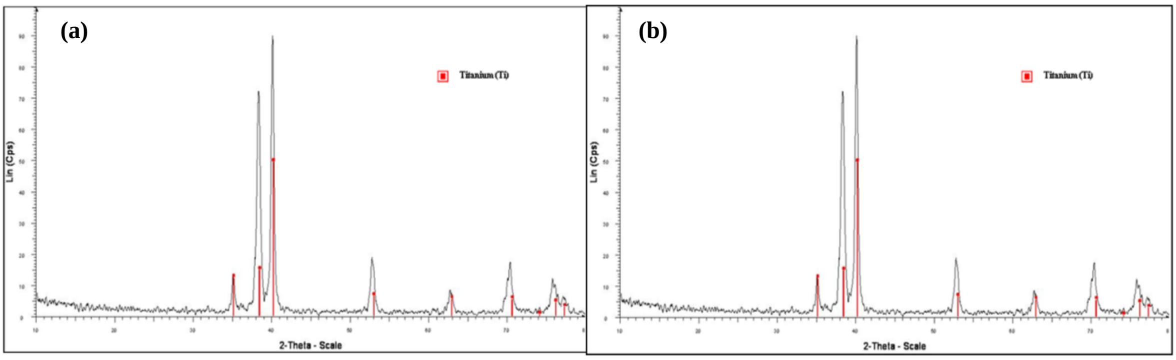

Figure 3.29 XRD spectra of first layer for FGMC formulation of Ti sintered under a) pressureless sintering and b) hot isostatic press pressureless sintering.

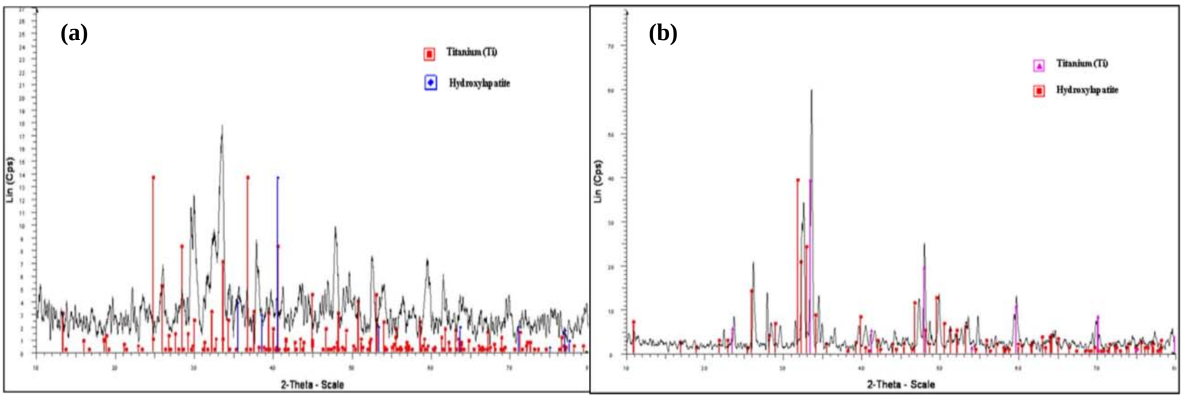

Figure 3.30 XRD spectra of second layer for FGMC formulation of 75%Ti-25%HA sintered under a) pressureless sintering and b) hot isostatic press.

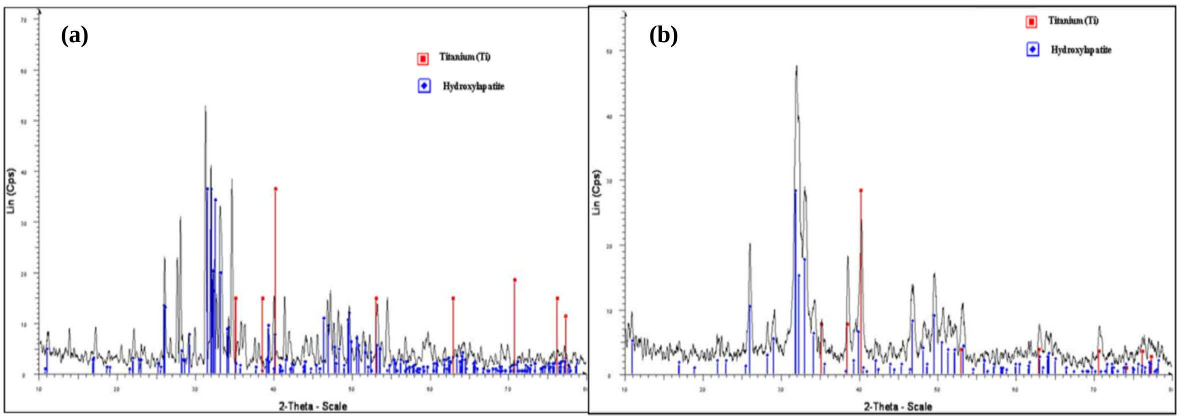

Figure 3.31 XRD spectra of third layer for FGMC formulation of 50%Ti-50%HA sintered under a) pressureless sintering and b) hot isostatic press.

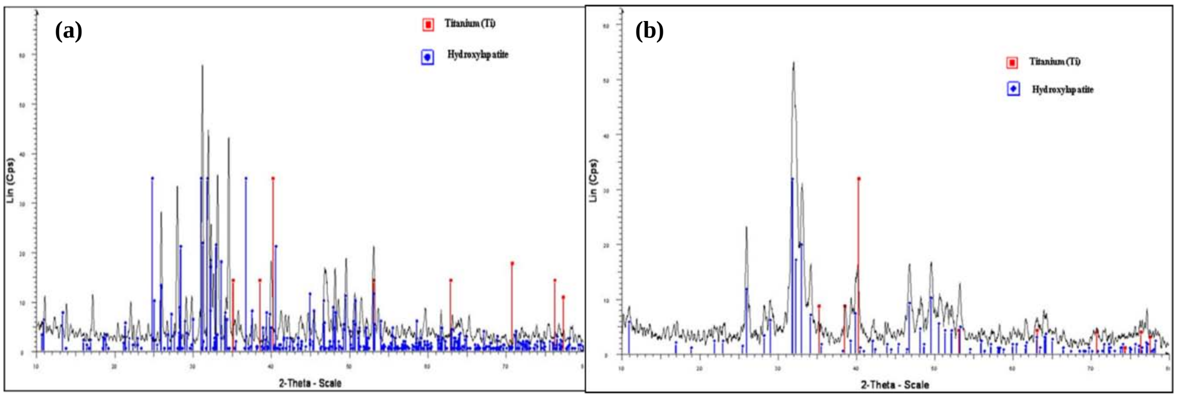

Figure 3.32 XRD spectra of fourth layer for FGMC formulation of 25%Ti-75%HA sintered under a) pressureless sintering and b) hot isostatic press.

3.5.2.3 Density and porosity characteristics

The densities and porosities of FGMCs with varying contents of Ti, ZrO_2, Al_2O_3 and HA were measured and plotted in Figures 3.33-3.35. The densities and porosities of the specimens exhibited graded distributions corresponding to its compositional change. In general, the data plotted in Figures 3.33-3.35 revealed that densities of the FGMCs decrease with increasing amount of HA, however, an increase in porosities was observed. The change in densities and porosities between the different layers of materials was gradual except for the first layer of Al_2O_3-HA-Ti FGMC where the densities values of first layer was lower than the second layer. However, gradual changes continued in the same trend for the following layers. The experimental density for FGMC sintered under hot isostatic press was higher than that observed for specimens sintered under pressureless sintering. The experimental density results for FGMC sintered under hot isostatic press approximate the theoretical density (Figures 3.33-3.35).

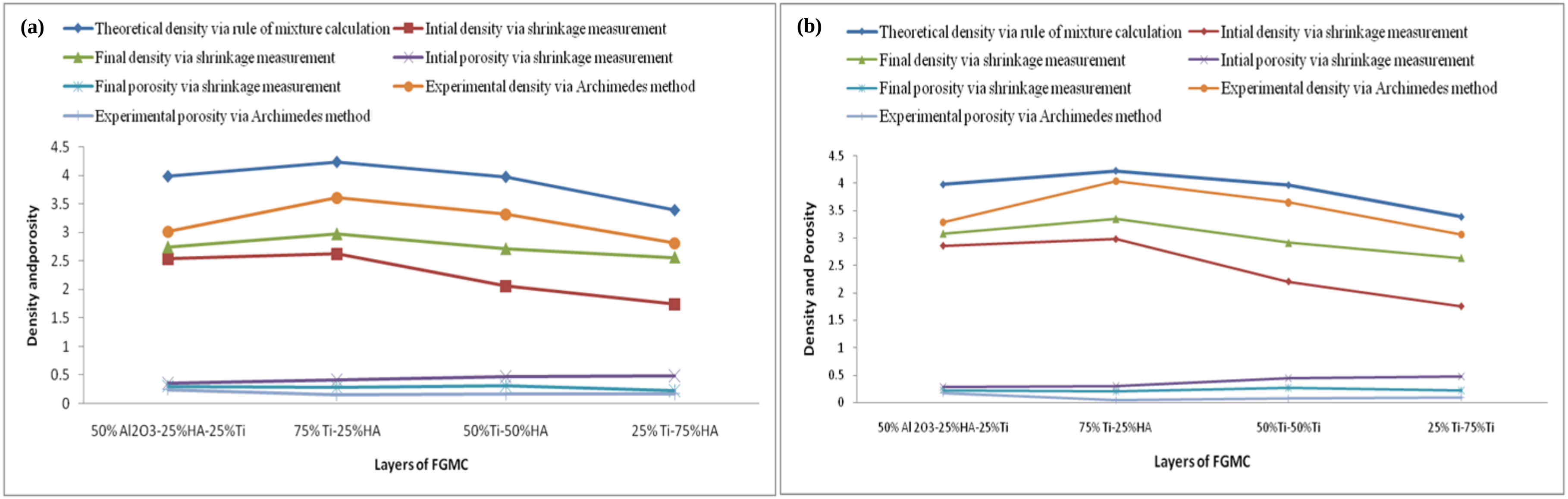

Figure 3.33 Densities and porosities with varying volume fraction of Ti in layers of Al_2O_3-Ti-HA FGMC sintered under a) pressureless sintering and b) hot isostatic press.

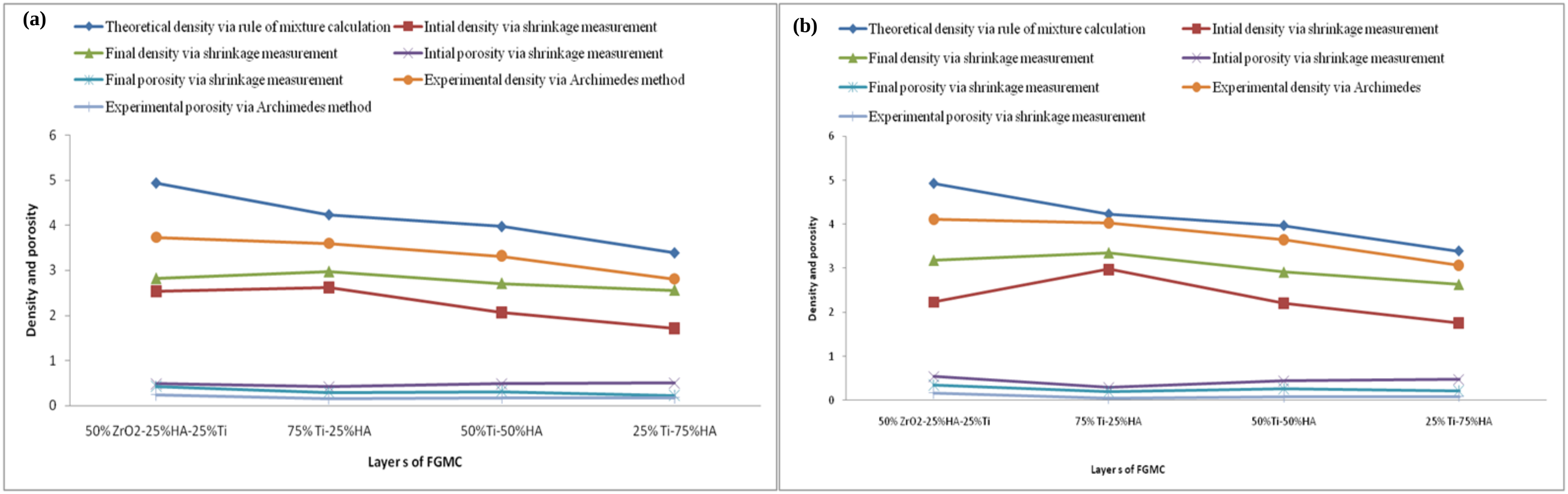

Figure 3.34 Densities and porosities with varying volume fraction of Ti in layers of ZrO_2-Ti-HA FGMC sintered under a) pressureless sintering and b) hot isostatic press.

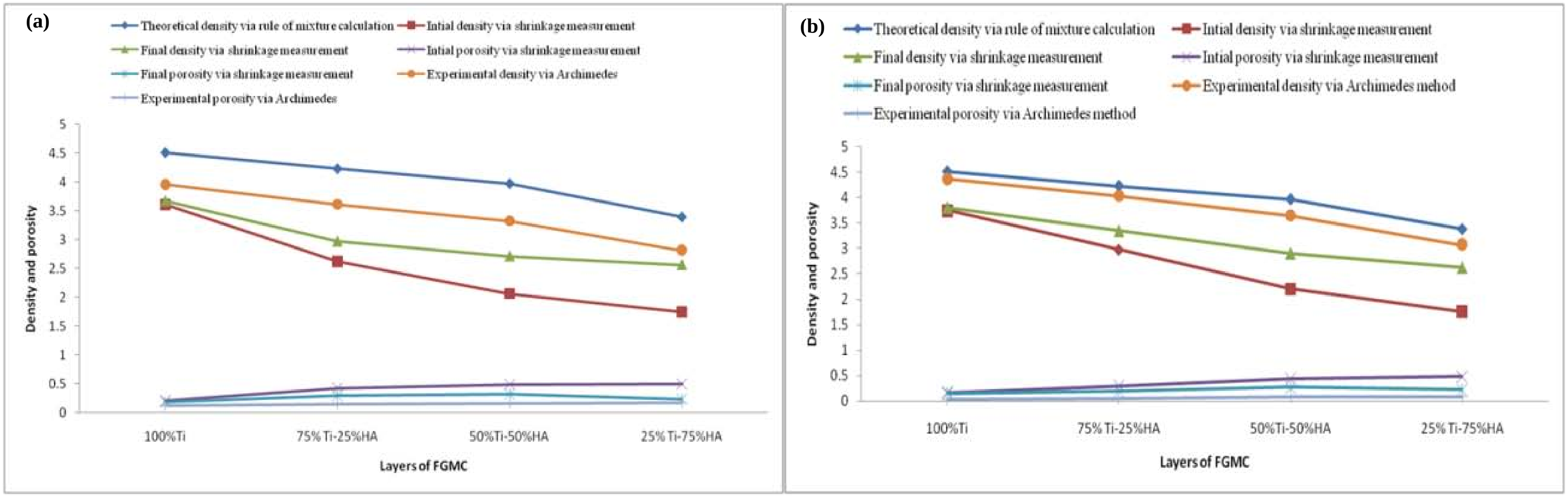

Figure 3.35 Densities and porosities with varying volume fraction of Ti in layers of Ti-HA FGMC sintered under a) pressureless sintering and b) hot isostatic press.

3.5.2.4 Relative experimental density

The relative experimental density data of FGMCs with varying contents of Ti, ZrO_2, Al_2O_3 and HA are measured and illustrated in Figures 3.36-3.38. The relative densities of 50%Al_2O_3-25%Ti-25%HA, 50%ZrO_2-25%Ti-25%HA, 100% Ti, 75% Ti-25%HA, 50% Ti-50%HA and 25% Ti-75%HA sintered under pressureless sintering were 0.75, 0.76, 0.88, 0.85, 0.84 and 0.83 respectively. However, the relative densities of 50%Al_2O_3-25%Ti-25%HA, 50%ZrO_2-25%Ti-25%HA, 100% Ti, 75% Ti-25%HA, 50% Ti-50%HA and 25% Ti-75%HA sintered under hot isostatic press were 0.83, 0.84, 0.97, 0.95, 0.92 and 0.91 respectively. The relative density for all specimens sintered under hot isostatic press was higher compared to those sintered under pressureless sintering.

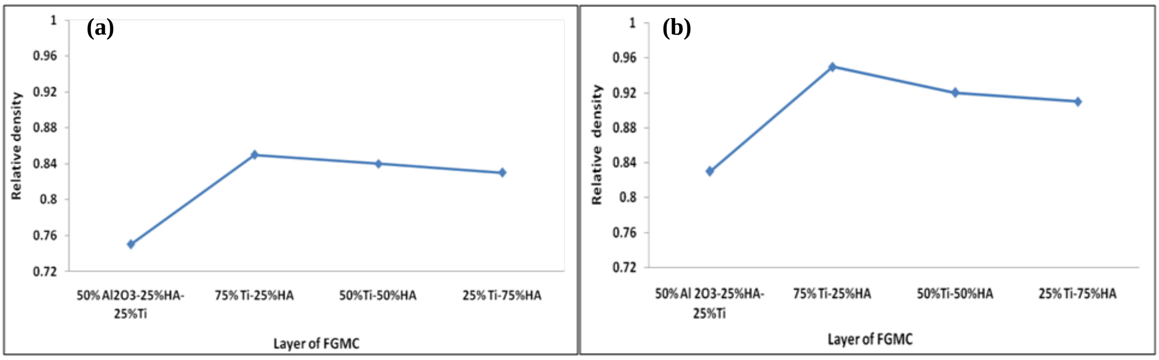

Figure 3.36 Relative experimental density with varying volume fraction of Ti in layers of the Al_2O_3-Ti-HA FGMC sintered under a) pressureless sintering and b) hot isostatic press.

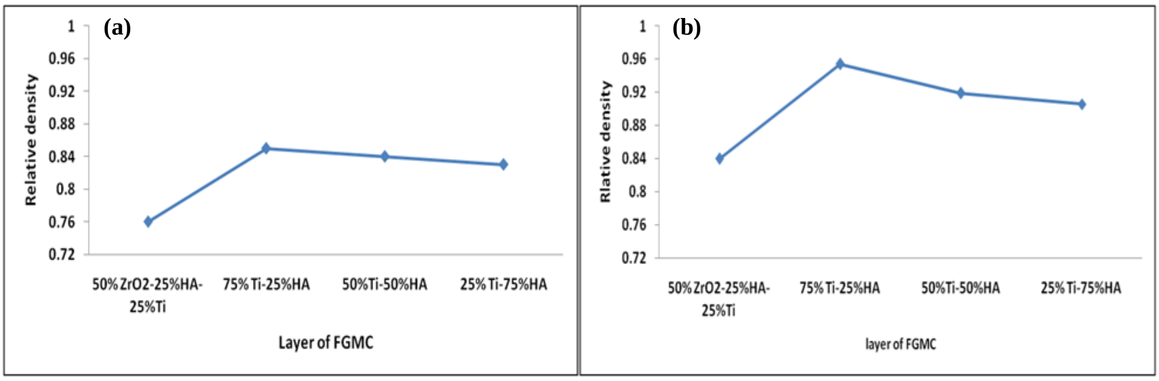

Figure 3.37 Relative experimental density with varying volume fraction of Ti in layers of the ZrO_2-Ti-HA FGMC sintered under a) pressureless sintering and b) hot isostatic press.

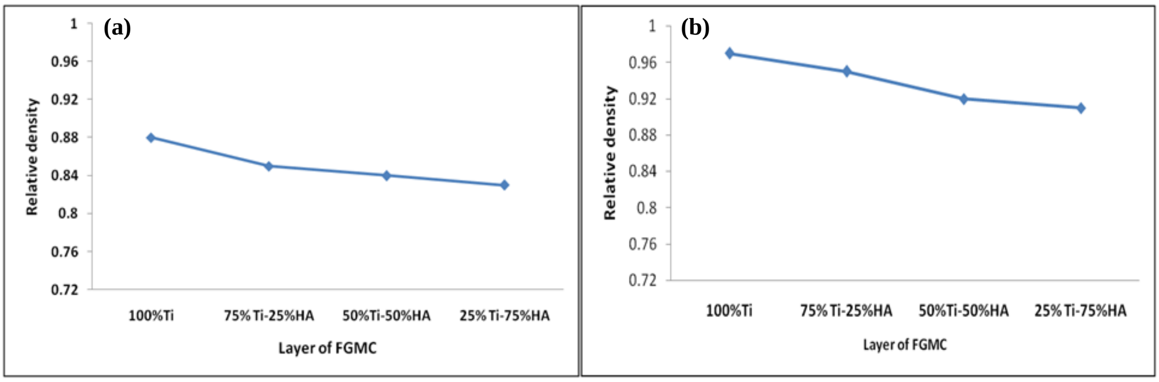

Figure 3.38 Relative experimental density with varying volume fraction of Ti in layers of the Ti-HA FGMC sintered under a) pressureless sintering and b) hot isostatic press.

3.5.2.5 Shrinkage characteristics

The shrinkage of the FGMCs is illustrated in Figures 3.39-3.41. The shrinkage can be considered as linear for each specimen especially for Ti-HA-Ti specimen, thus confirming the linearity of properties changes inside the FGMCs. The shrinkage of the specimen proved to be dependent on the amount of Ti and this was elucidated by the diameter of specimen which decreases as the amount of Ti decreased (Figure 3.42). The shrinkage behaviour for all specimens sintered under pressureless sintering and hot isostatic press was similar.

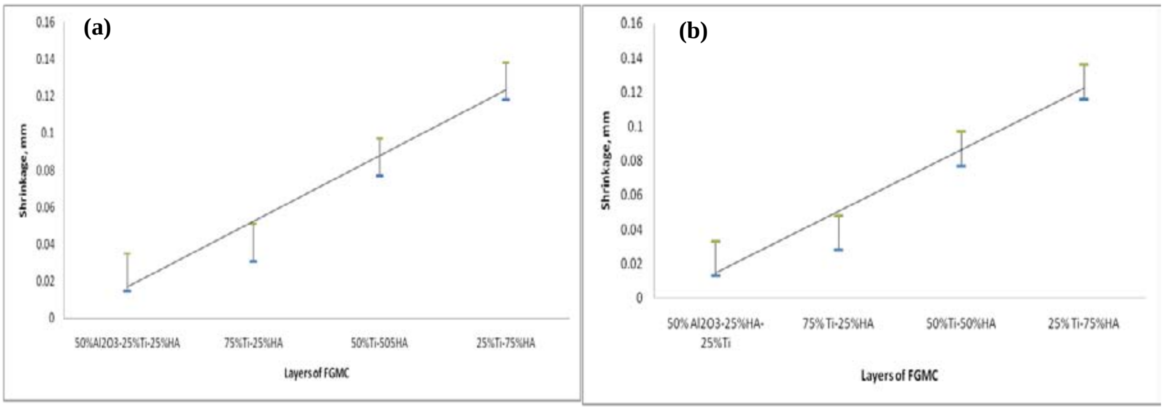

Figure 3.39 Shrinkage of Al_2O_3-Ti-HA FGMC sintered under a) pressureless sintering and b) hot isostatic press.

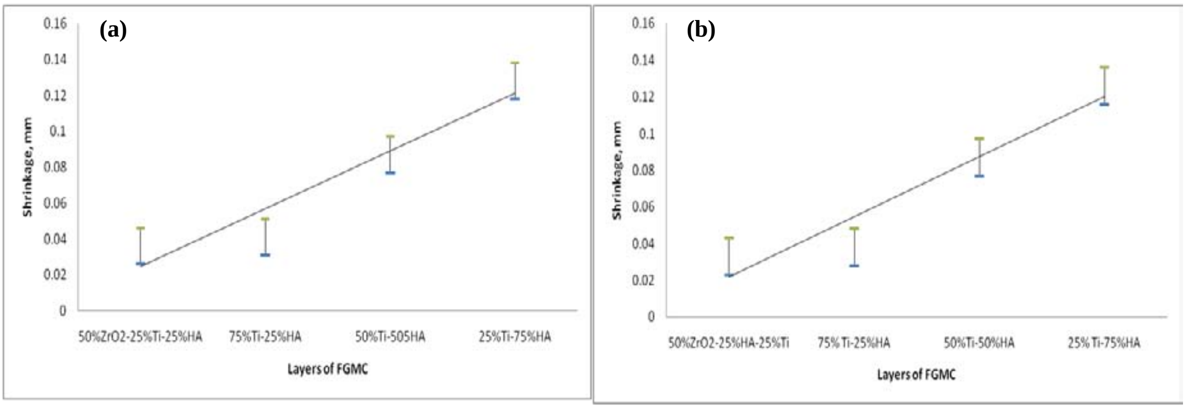

Figure 3.40 Shrinkage of ZrO_2-Ti-HA FGMC sintered under a) pressureless sintering and b) hot isostatic press.

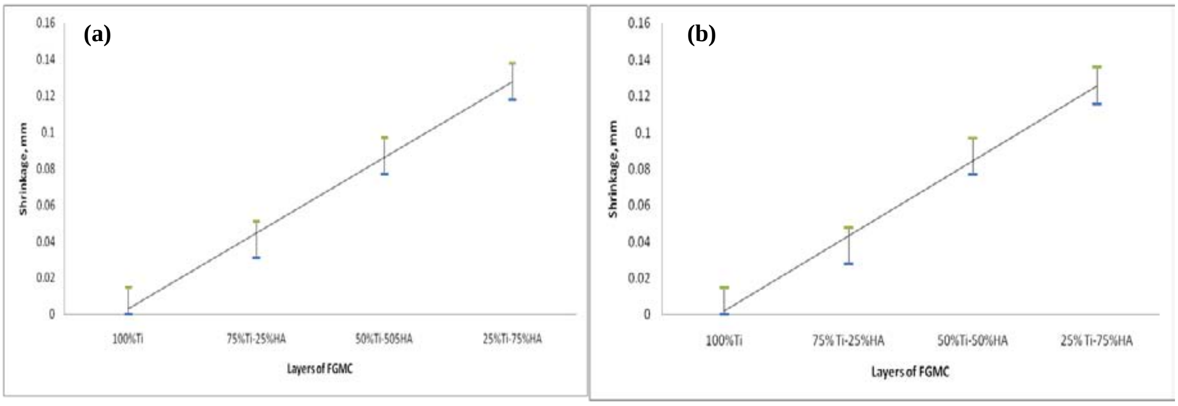

Figure 3.41 Shrinkage of Ti-HA-Ti FGMC sintered under a) pressureless sintering and b) hot isostatic press.

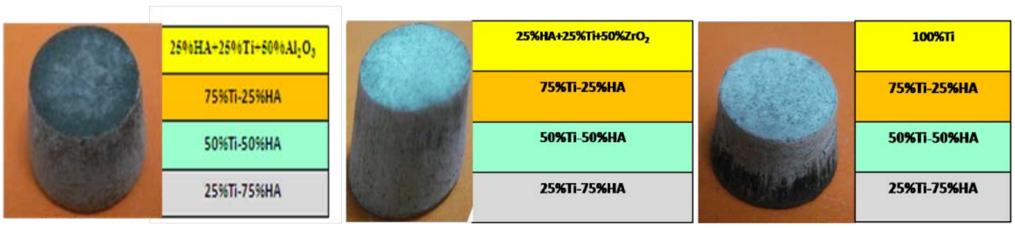

Figure 3.42 Shrinkage behaviour of FGMCs in terms of diameter.

3.5.2.6 Relative shrinkage

Relative shrinkage of each layer of the FGMCs are calculated and plotted as shown in Figures 3.43-3.45. The relative shrinkage for all specimens sintered under pressureless sintering and hot isostatic press was relatively linear particularly for Ti-HA-Ti specimen. It can be considered that the overall relative shrinkage of the specimens uniform and changed gradually in the different layers.

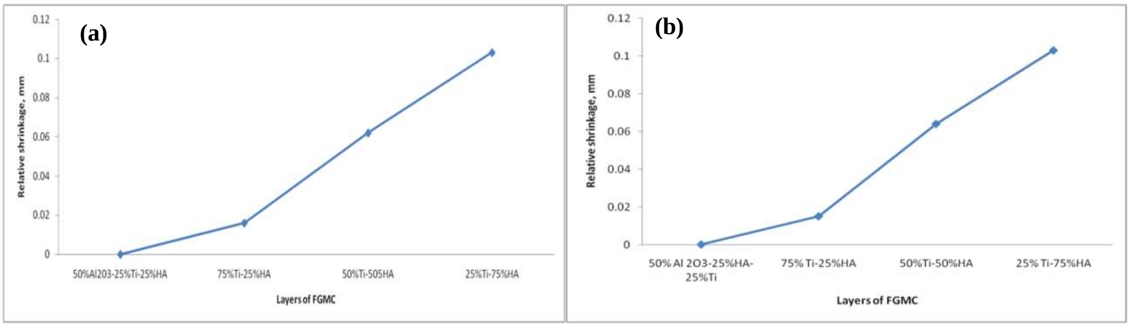

Figure 3.43 Relative shrinkage of Al_2O_3-Ti-HA FGMC sintered under a) pressureless sintering and b) hot isostatic press.

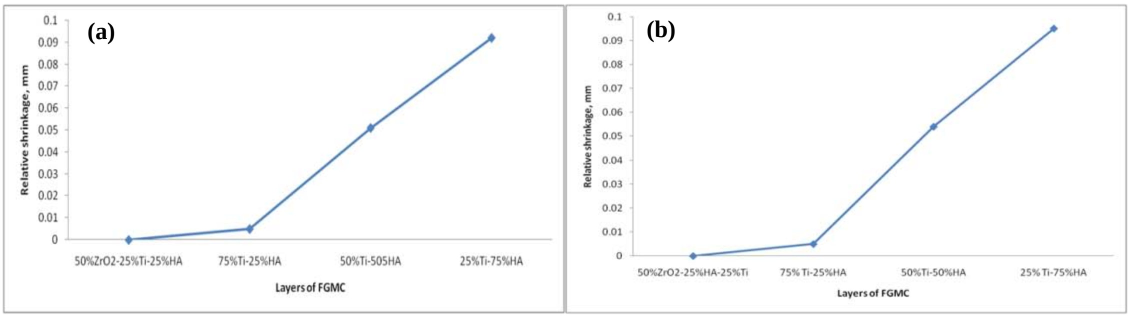

Figure 3.44 Relative shrinkage of ZrO_2-Ti-HA FGMC sintered under a) pressureless sintering and b) hot isostatic press.

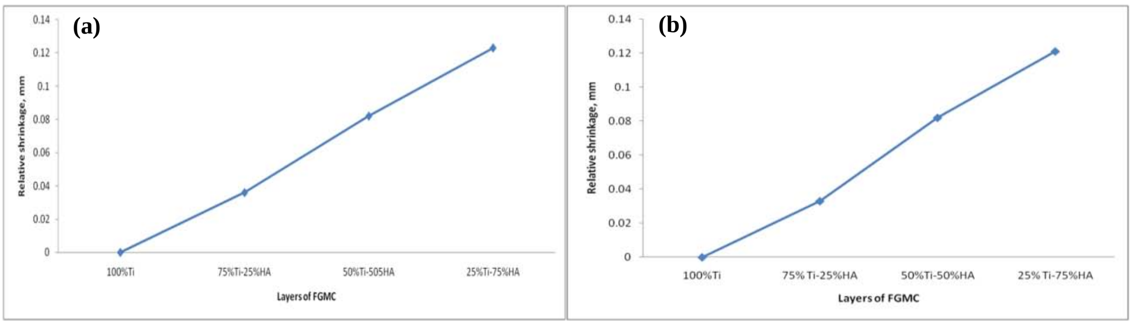

Figure 3.45 Relative shrinkage of Ti-HA-Ti FGMC sintered under a) pressureless sintering and b) hot isostatic press.

3.5.2.7 Comparison of porosities measurements and proposed Models I and II

The results of the proposed porosity reduction models (I and II) and experimental measurements are shown in Figure 3.46. The highest volume fraction for porosity was observed when the volume fraction of Ti is 0.50 in both models and experimental measurements. In addition, the differences between the estimated values in both models and measured porosities were also largest. When the results of the experimental measurements were compared to both models, they approximate each other except at Ti = 0.50 and Model II appeared to be a more accurate model for estimation of the porosity reduction.

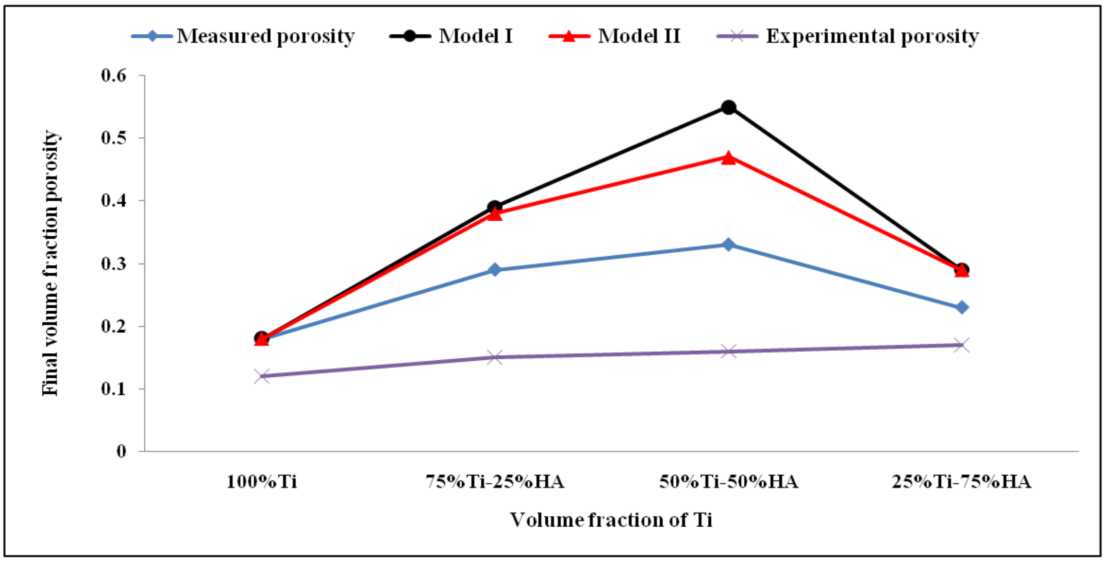

Figure 3.46 Porosity in models I, II and experimental results of four layers for Ti-HA FGMC.

3.5.2.8 Microhardness

Vickers microhardness specimens are presented in Figures 3.47-3.49. Reviewing the results, the FGMC microhardness profile showed that the microhardness of FGMCs and identical layers representing of FGMCs is similar. From the plots, it has been seen that the microhardness increase with increasing content of HA. The difference in microhardness between the each layers was gradual except for the first layer in Al_2O_3-HA-Ti and ZrO_2-HA-Ti FGMC specimens where the microhardness values of first layer was larger than second layer. However, gradual changes continued in the same trend for the subsequent layers. The microhardness for FGMCs sintered under hot isostatic press was significantly higher than that observed for the specimens sintered under pressureless sintering ($p < .05$).

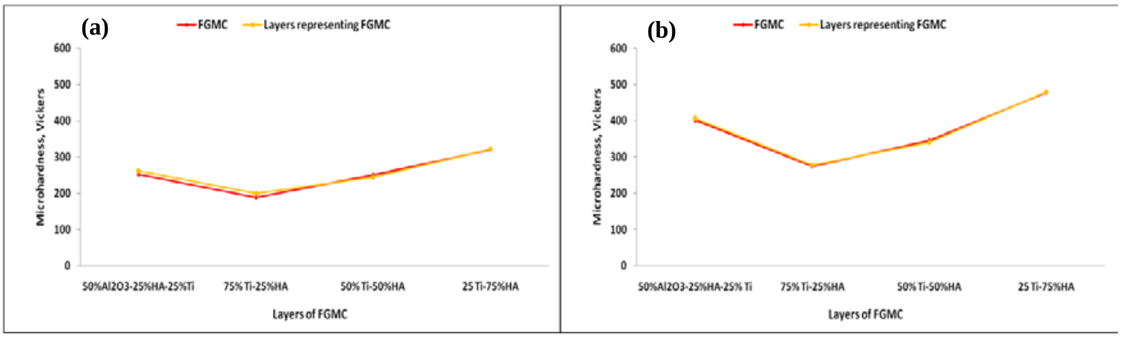

Figure 3.47 Vickers microhardness of FGMC (Al_2O_3-Ti-HA) sintered under a) pressureless sintering and b) hot isostatic press.

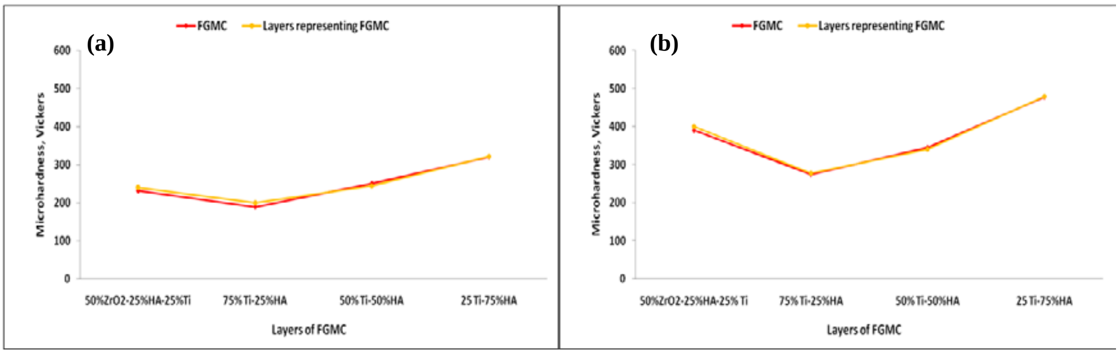

Figure 3.48 Vickers microhardness of FGMC (ZrO_2-Ti-HA) sintered under a) pressureless sintering and b) hot isostatic press.

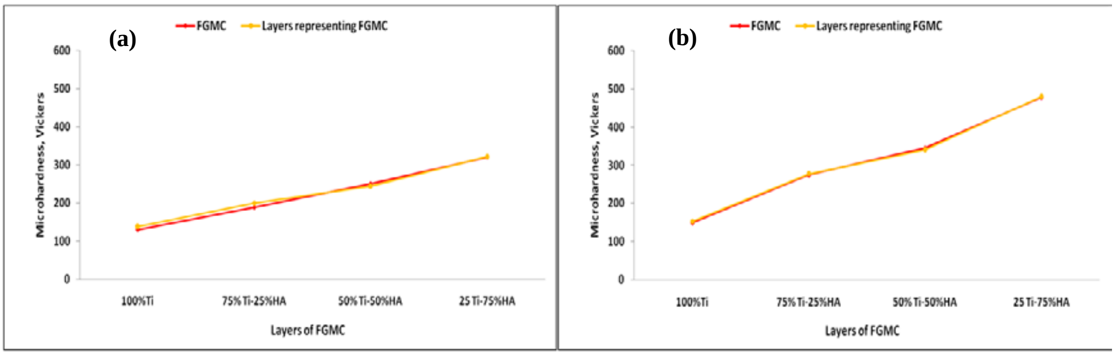

Figure 3.49 Vickers microhardness of FGMC (Ti-HA-Ti) sintered under a) pressureless sintering and b) hot isostatic press.

3.5.2.9 Flexural strength

The graded changes of the chemical compositions in FGMC also lead to a continuous gradual change in flexural strength as demonstrated in Figures 3.50-3.52. The flexural strength for FGMCs sintered under hot isostatic press was significantly higher than that observed for specimens sintered under pressureless sintering ($p < .05$). It was also obvious that flexural strength increase markedly with the increase of Ti content, especially in Ti riched region.

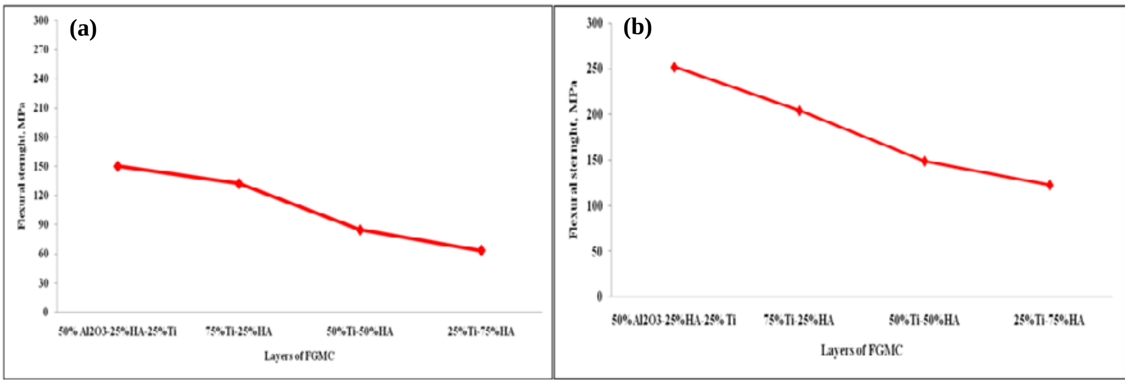

Figure 3.50 Flexure strength of FGMC (Al_2O_3-Ti-HA) sintered under a) pressureless sintering and b) hot isostatic press.

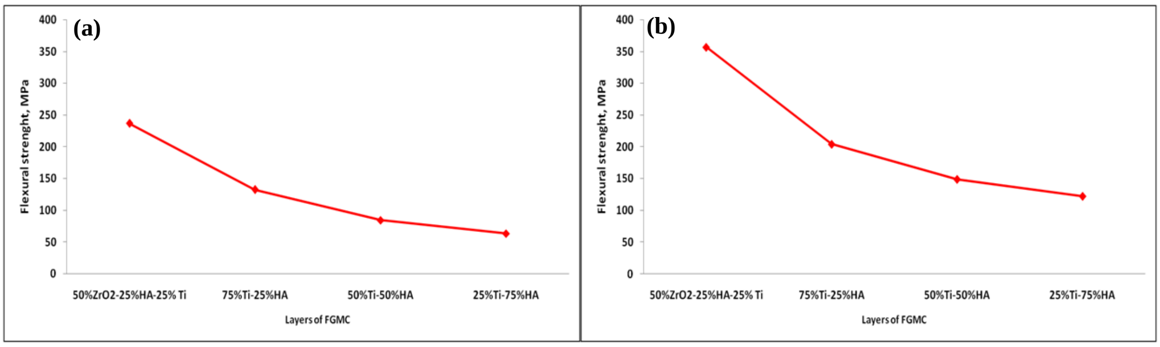

Figure 3.51 Flexure strength of FGMC (ZrO_2-Ti-HA) sintered under a) pressureless sintering and b) hot isostatic press.

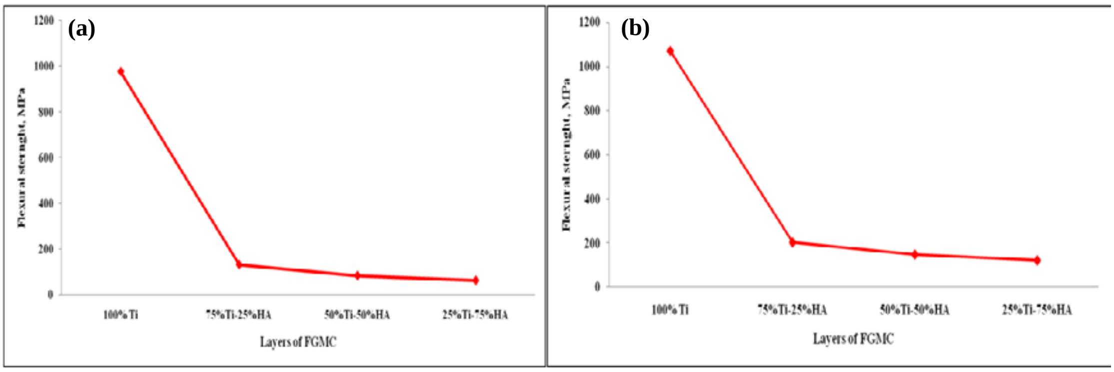

Figure 3.52 Flexure strength of FGMC (Ti-HA-Ti) sintered under a) pressureless sintering and b) hot isostatic press.

3.5.2.10 Modulus of elasticity

Modulus of elasticity of FGMCs specimens of Al_2O_3-Ti-%HA, ZrO_2-Ti-HA and Ti-HA-Ti were calculated and illustrated in Figures 3.53-3.55. The same trend was observed for all specimens. The modulus of elasticity for FGMCs reduced gradually with increased amount of the percentage of HA. The modulus of elasticity for FGMCs sintered under hot isostatic press was significantly higher than that observed for specimens sintered under pressureless sintering ($p < .05$).

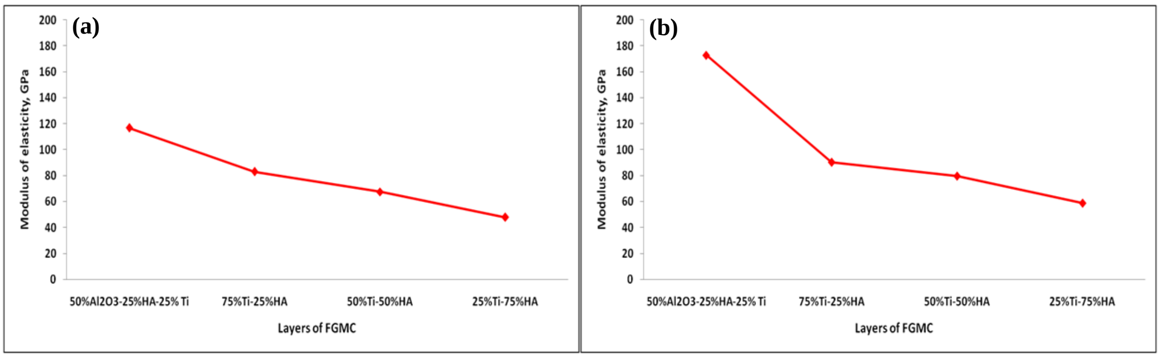

Figure 3.53 Modulus of elasticity of FGMC (Al_2O_3-Ti-HA) sintered under a) pressureless sintering and b) hot isostatic press.

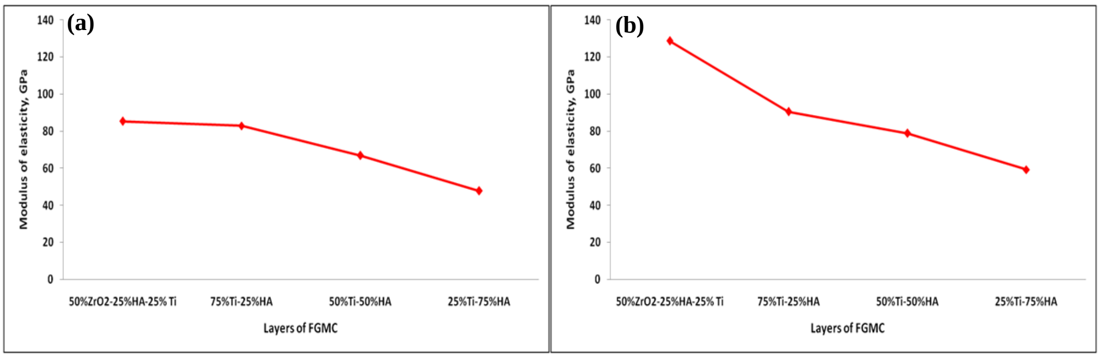

Figure 3.54 Modulus of elasticity of FGMC (ZrO_2-Ti-HA) sintered under a) pressureless sintering and b) hot isostatic press.

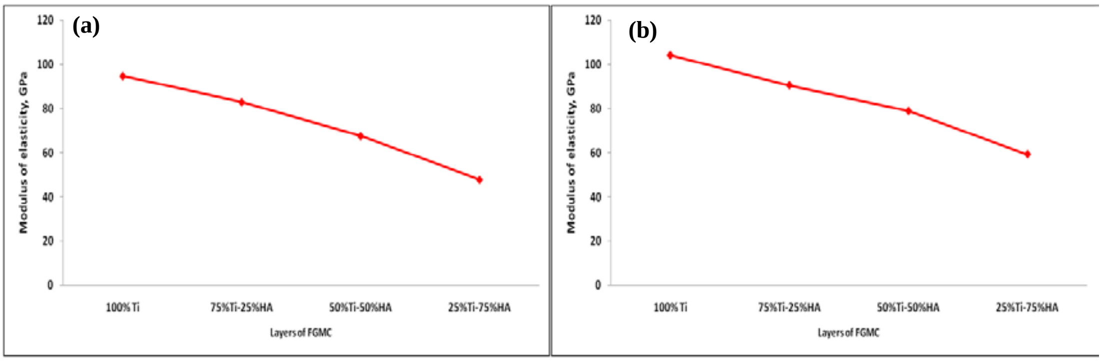

Figure 3.55 Modulus of elasticity of FGMC (Ti-HA-Ti) sintered under a) pressureless sintering and b) hot isostatic press.

3.5.3 Comparison of pressureless sintering and hot isostatic pressing

3.5.3.1 Experimental density

Table 3.2 shows the mean value of density of the Al_2O_3-HA-Ti, ZrO_2-HA-Ti and Ti-HA-Ti FGMCs specimens sintered by pressureless sintering and hot isostatic press. When sintering technique was compared, the mean value of the density of specimens sintered by pressureless sintering was lower than those sintered by hot isostatic press.

The assumption of normality for the data was checked and histogram generated indicated that the data approximates the normal distribution curve and Shapiro-Wilk test was also carried out, $p > .05$. Since the main purpose of this study was the effect of sintering technique on experimental density of each layer, therefore, the independent sample *t*-test was carried out. Independent sample *t*-test showed that experimental density of the FGMCs sintered by hot isostatic press was significantly higher ($p < .05$) compared to specimens sintered by pressureless sintering as represented in Table 3.2.

Table 3.2 The effect of sintering techniques on the experimental density

Experimental density	Pressureless sintering Mean (SD) (n=10)	Hot isostatic press Mean (SD) (n=10)	Mean diff. (95% CI)	*t*-test*	*P* value
First layer (Al_2O_3-HA-Ti)	3.01 (±.09)	3.29 (±.04)	-.28 (-.22,-.35)	-9.05 (18)[a]	<.001
First layer (Ti-HA-Ti)	3.95 (±.06)	4.38 (±.04)	-.42 (-.37,-.47)	-18.26 (18)[b]	<.001
First layer (ZrO_2-HA-Ti)	3.73 (±.07)	4.13 (±.06)	-.39 (-.33,-.45)	-13.33 (18)[c]	<.001
Second layer (HA-Ti)	3.61 (±.05)	4.04 (±.07)	-.43 (-.37,-.49)	-15.64 (18)[d]	<.001
Third layer (HA-Ti)	3.32 (±.06)	3.65 (±.05)	-.32 (-.27,-.38)	-12.93 (18)[e]	<.001
Fourth layer (HA-Ti)	2.81 (±.07)	3.07 (.±07)	-.29 (-.19,-.32)	-8.00 (18)[f]	<.001

**Independent sample t-test was applied.* *a. Equal variances assumed (Levene's test, p = .077). b. Equal variances assumed (Levene's test, p = .288). c. Equal variances assumed (Levene's test, p = .808). d. Equal variances assumed (Levene's test, p = .119). e. Equal variances assumed (Levene's test, p= .522). f. Equal variances assumed (Levene's test, p = .930).*

3.5.3.2 Experimental porosity

Table 3.3 reveals the mean percentage of experimental porosity of the first layer (ZrO_2-HA-Ti) sintered by pressureless sintering and hot isostatic press. When sintering technique was compared, the mean percentage of the porosity of specimens sintered by pressureless sintering was higher than those sintered by hot isostatic press.

Table 3.3 Mean percentage of the experimental porosity for first layer (ZrO_2-HA-Ti) sintered by pressureless sintering and hot isostatic press

Experimental porosity	**Pressureless sintering Mean (SD) (n=10)**	**Hot isostatic press Mean (SD) (n=10)**
First layer (ZrO_2-HA-Ti)	.25 (±.01)	.16 (±.01)

The assumption of normality for the data for first layer (ZrO_2-HA-Ti) was checked and the histogram generated indicated that the data does not approximate the normal distribution curve and Shapiro-Wilk test was also carried out, $p < .05$. Since the main purpose of this study was the effect of sintering technique on experimental porosity of each layer, therefore, Mann-Whitney *U* test was carried out. Mann-Whitney *U* test showed that experimental porosity of first layer (ZrO_2-HA-Ti) of the FGMC sintered by hot isostatic press was significantly lower ($P < .05$) compared to specimens sintered by pressureless sintering as illustrated in Table 3.4.

Table 3.4 The effect of sintering techniques on the experimental porosity for first layer (ZrO_2-HA-Ti)

Experimental density	Mean Rank	Sum of Ranks	*U*-test* (Z)	*P* value
Pressureless sintering	15.50	155.00	55.00 (-3.82)	<.001
Hot isostatic press	5.50	55.00		

**Mann-Whitney U test was applied.*

Table 3.5 shows the mean percentage of experimental porosity of the other layers of Al_2O_3-HA-Ti, ZrO_2-HA-Ti and-HA-Ti FGMCs sintered by pressureless sintering and hot isostatic press. When sintering technique was compared, the mean percentage of the porosity of specimens sintered by pressureless sintering was higher than those sintered by hot isostatic press.

The assumption of normality for the data was checked and histogram generated indicated that the data approximates the normal distribution curve and Shapiro-Wilk test was also carried out, $p > .05$. Since the main purpose of this study was the effect of sintering technique on experimental porosity of each layer, therefore, the independent sample *t*-test was carried out. The independent sample *t*-test showed that experimental porosity of the FGMCs sintered by hot isostatic press was significantly lower ($P < .05$) compared to specimens sintered by pressureless sintering as illustrated in Table 3.5.

Table 3.5 The effect of sintering techniques on the experimental porosity

Experimental porosity	**Pressureless sintering Mean (SD) (n=10)**	**Hot isostatic press Mean (SD) (n=10)**	**Mean diff. (95% CI)**	***t*-test***	***P* value**
First layer (Al_2O_3-HA-Ti)	.24 (±.02)	.17 (±.01)	.07 (.09,.05)	8.09 (18)[a]	<.001
First layer (Ti-HA-Ti)	.12 (±.01)	.03 (±.01)	.09 (.10,.08)	18.05 (18)[b]	<.001
Second layer (HA-Ti)	.15 (±.01)	.05 (±.01)	.10 (.12,.09)	14.50 (18)[c]	<.001
Third layer (HA-Ti)	.16 (±.01)	.08 (±.01)	.08 (.09,.07)	14.10 (18)[d]	<.001
Fourth layer (HA-Ti)	.17 (±.02)	.09 (±.02)	.08 (.10,.06)	7.99 (18)[e]	<.001

***Independent sample t-test was applied.** *a. Equal variances assumed (Levene's test, p = .059). b. Equal variances assumed (Levene's test, p = .511). c. Equal variances assumed (Levene's test, p = .173). d. Equal variances assumed (Levene's test, p = .735). e. Equal variances assumed (Levene's test, p = .796).*

3.5.3.3 Relative density

Table 3.6 shows the mean percentages of relative density of the Al_2O_3-HA-Ti, ZrO_2-HA-Ti and-HA-Ti FGMCs sintered by pressureless sintering and hot isostatic press. When sintering technique was compared, the mean percentages of relative density of specimens sintered by hot isostatic press were higher than those sintered by pressureless sintering.

The assumption of normality for the data was checked and histogram generated indicated that the data approximates the normal distribution curve and Shapiro-Wilk test was also carried out, $p > .05$. Since the main purpose of this study was the effect of sintering technique on relative density of each layer, therefore, the independent sample *t*-test was carried out. Independent sample *t*-test showed that percentages of the relative density of the FGMCs specimens sintered by hot isostatic press was significantly higher ($P < .05$) for all layers compared to specimens sintered by pressureless sintering as presented in Table 3.6.

Table 3.6 The effect of sintering techniques on the relative density

Relative density	**Pressureless sintering Mean (SD) (n=10)**	**Hot isostatic press Mean (SD) (n=10)**	**Mean diff. (95% CI)**	***t*-test***	***P* value**
First layer (Al_2O_3-HA-Ti)	.76 (.02)	.83 (.01)	-.07 (-.05,-.09)	-8.81 (18)[a]	<.001
First layer (Ti-HA-Ti)	.88 (.01)	.97 (.01)	-.09 (-.08, -.10)	-18.05 (18)[b]	<.001
First layer (ZrO_2-HA-Ti)	.76 (.01)	.84 (.01)	-.08 (-.07,.09)	-14.20 (18)[c]	<.001
Second layer (HA-Ti)	.85 (.01)	.95 (.02)	-.10 (-.09,-.12)	-14.50 (18)[d]	<.001
Third layer (HA-Ti)	.84 (.01)	.92 (.01)	-.08 (-.07,-.09)	-14.10 (18)[e]	<.001
Fourth layer (HA-Ti)	.83 (.02)	.91 (.02)	-.08 (-.60, -.10)	-7.99 (18)[f]	<.001

**Independent sample t-test was applied. a. Equal variances assumed (Levene's test, p = .059). b. Equal variances assumed (Levene's test, p = .511). c. Equal variances assumed (Levene's test, p = .902). d. Equal variances assumed (Levene's test, p = .173). e. Equal variances assumed (Levene's test, p = .735). f. Equal variances assumed (Levene's test, p = .796).*

3.5.3.4 Microhardness

Table 3.7 displays the mean values of the microhardness of the Al_2O_3-HA-Ti, ZrO_2-HA-Ti and-HA-Ti FGMCs specimens sintered by pressureless sintering and hot isostatic press. When sintering technique was compared, the mean values of microhardness of specimens sintered by hot isostatic press were higher than those sintered by pressureless sintering.

The assumption of normality for the data was checked and histogram generated indicated that the data approximates the normal distribution curve and Shapiro-Wilk test was also carried out, $p > .05$. Since the main of this study was the effect of sintering technique on microhardness of each layer, therefore, the independent sample *t*-test was applied. Independent sample *t*-test showed that values of the microhardness of the FGMCs specimens sintered by hot isostatic press was significantly higher ($P < .05$) for all layers compared to specimens sintered by pressureless sintering as noticed in Table 3.7.

Table 3.7 The effect of sintering techniques on the microhardness

Microhardness	**Pressureless sintering Mean (SD) (n=10)**	**Hot isostatic press Mean (SD) (n=10)**	**Mean diff. (95% CI)**	***t*-test***	***P* value**
First layer (Al_2O_3-HA-Ti)	238.30 (±8.45)	401.20 (±10.33)	-158.60 (-154.04, -171.76)	-38.62 (18)[a]	<.001
First layer (Ti-HA-Ti)	130.30 (±10.31)	148.70 (±5.31)	-5.02 (-10.70,-26.10)	-18.40 (18)[b]	<.001
First layer (ZrO_2-HA-Ti)	231.10 (±10.22)	389.70 (±6.72)	-158.60 (-150.47, -166.73)	-40.99 (18)[c]	<.001
Second layer (HA-Ti)	188.60 (±20.11)	273.90 (±5.72)	-85.30 (-71.41, -99.19)	-12.90 (18)[d]	<.001
Third layer (HA-Ti)	250.80 (±32.86)	345.30 (±10.61)	-94.50 (-7043,-118.57)	-8.65 (10.86)[e]	<.001
Fourth layer (HA-Ti)	320.10 (±29.50)	477.00 (±7.12)	-156.90 (-135.53, -178.26)	-16.35 (10.01)[f]	<.001

**Independent sample t-test was applied.* *a. Equal variances assumed (Levene's test, p = .269). b. Equal variances assumed (Levene's test, p = .095). c. Equal variances assumed (Levene's test, p = .269). d. Equal variances not assumed (Levene's test, p = .009). e. Equal variances not assumed (Levene's test, p = .009). f. Equal variances not assumed (Levene's test, p = .007).*

3.5.3.5 Flexural strength

Table 3.8 shows the mean values of flexural strength of the Al_2O_3-HA-Ti, ZrO_2-HA-Ti and Ti-HA-Ti FGMCs specimens sintered by pressureless sintering and hot isostatic press. When technique was compared, the mean values of flexural strength of specimens sintered by hot isostatic press were higher than those sintered by pressureless sintering.

The assumption of normality for the data was checked and histogram generated indicated that the data approximates the normal distribution curve and Shapiro-Wilk test was also carried out, $p > .05$. Since the main purpose of this study was the effect of sintering technique on flexural strength of each layer, therefore, the independent sample *t*-test was carried out. Independent sample *t*-test showed that values of the flexural strength of the FGMCs specimens sintered by hot isostatic press was significantly higher ($P < .05$) in all layers compared to specimens sintered by pressureless sintering as seen in Table 3.8.

Table 3.8 The effect of sintering techniques on the flexural strength

Flexural strength	**Pressureless sintering Mean (SD) (n=10)**	**Hot isostatic press Mean (SD) (n=10)**	**Mean diff. (95% CI)**	***t*-test***	***P* value**
First layer (Al_2O_3-HA-Ti)	150.10 (±10.49)	252.00 (±11.89)	-101.9 (-91.37, -122.44)	-20.32 (18)[a]	<.001
First layer (Ti-HA-Ti)	977.00 (±6.65)	1070.10 (±7.29)	-93.10 (-86.54,-99.66)	-29.83 (18)[b]	<.001
First layer (ZrO_2-HA-Ti)	236.50 (±8.03)	356.90 (±15.31)	-120.40 (-108.91, -131.90)	-22.02 (18)[c]	<.001
Second layer (HA-Ti)	132.30 (±9.46)	204.30 (±10.40)	-62.00 (-62.66, -81.34)	-16.19 (18)[d]	<.001
Third layer (HA-Ti)	84.60 (±7.63)	149.00 (±5.81)	-34.40 (-58.03, -70.77)	-21.23 (18)[e]	<.001
Fourth layer (HA-Ti)	63.40 (±7.23)	122.90 (±6.69)	-38.10 (-52.96, -66.04)	-19.10 (18)[f]	<.001

**Independent sample t-test was applied.* *a. Equal variances assumed (Levene's test, p = .726). b. Equal variances assumed (Levene's test, p = .497). c. Equal variances not assumed (Levene's test, p = .045). d. Equal variances assumed (Levene's test, p = .937). e. Equal variances assumed (Levene's test, p = .299). f. Equal variances assumed (Levene's test, p = .512).*

3.5.3.6 Modulus of elasticity

Table 3.9 shows the mean values of modulus of elasticity of the Al_2O_3-HA-Ti, ZrO_2-HA-Ti and Ti-HA-Ti specimens sintered by pressureless sintering and hot isostatic press. When sintering technique was compared, the mean values of modulus of elasticity of specimens sintered by hot isostatic press were higher compared to pressureless sintering.

The assumption of normality for the data was checked and histogram generated indicated that the data approximates the normal distribution curve and Shapiro-Wilk test was also carried out, $p > .05$. Since the main purpose of this study was the effect of sintering technique on modulus of elasticity of each layer, therefore, the independent sample *t*-test was carried out. Independent sample *t*-test showed that values of the modulus of elasticity of specimens sintered by hot isostatic press was significantly higher ($P <. 05$) in all layers compared to specimens sintered by pressureless sintering as shown in Table 3.9.

Table 3.9 The effect of sintering techniques on the modulus of elasticity

Modulus of elasticity	**Pressureless sintering Mean (SD) (n=10)**	**Hot isostatic press Mean (SD) (n=10)**	**Mean diff. (95% CI)**	***t*-test***	***P* value**
First layer (Al_2O_3-HA-Ti)	116.80 (±6.49)	172.97 (±9.80)	-56.17 (-48.36, -63.99)	-15.11 (18)[a]	<.001
First layer (Ti-HA-Ti)	94.72 (±2.56)	104.22 (±3.59)	-9.50 (-6.57, -12.43)	-6.81 (18)[b]	<.001
First layer (ZrO_2-HA-Ti)	85.30 (±8.16)	128.75 (±6.14)	-43.46 (-36.66, -50.23)	-13.46 (18)[c]	<.001
Second layer (HA-Ti)	82.96 (±3.12)	90.59 (±2.48)	-7.63 (-4.98, -10.27)	-6.05 (18)[d]	<.001
Third layer (HA-Ti)	66.84 (±5.89)	78.86 (±3.24)	-14.03 (-9.60, -18.49)	-6.60 (18)[e]	<.001
Fourth layer (HA-Ti)	47.83 (±6.45)	59.23 (±3.40)	-16.40 (-11.56, -21.24)	-7.12 (18)[f]	<.001

**Independent sample t-test was applied. a. Equal variances assumed (Levene's test, p = .170). b. Equal variances assumed (Levene's test, p = .411). c. Equal variances assumed (Levene's test, p = .260). d. Equal variances assumed (Levene's test, p = .445). e. Equal variances assumed (Levene's test, p = .052). f. Equal variances assumed (Levene's test, p = .167).*

3.6 Discussion

According to Kieback et al. (2003), there are several methods that can used to process and fabricate functionally graded materials (FGMs) such as powder processing techniques, coating processes, and lamination processes. Powder processing techniques are good for FGM fabrication, because they are fairly quick and cheap. As it requires inexpensive equipment and only a few items are required for the fabrication. The only material required are powders that form the basis of the FGM composite material system. These materials are mixed together in various concentrations to create the desired FGM composites. Rabin & Heaps (1993) reported that the utilization of powder processing technique by combining various quantities of the powders, with different particle sizes of the constituent materials. The use of layering technique of each of the powder mixtures allows the operator to be in control of the microstructure in the final material. For these reasons this methods was used in this current study for fabrication of FGMCs. Powder processing technique also permits for shape-forming capability. Since the powders do not begin in a solid geometry, they can be placed into a geometrical die and pressed into a desired shape.

Layering techniques offered the capability to build up the graded composite incrementally, which can be performed without using expensive equipment and by utilizing this technique the microstructure of each layer can be controlled easily. Mixture powders can be layered in a desired way. Layering technique needs only amount of the mixture powders to be known, because that mixture powders is simply added on to the other. In order to use same procedure in a continuous gradual structure, an unlimited amount of powder mixtures require being prepared. Williamson et al. (1993), Markworth et al. (1995) and Bruck (2000) found, through their modeling studies, that a discretely layered functionally graded composite offers benefits compared to those composite with a sharp interface. These properties can be interpolated between temperatures to understand the behaviour of the composite material system throughout and assists to restrict deformation to alleviate the stresses that may cause fracture.

The geometry of the die used for creating FGMCs also has an effect on the stress evolution and fracture behaviour of the FGMCs. When geometrical die with sharp corners are used for fabricating a layered graded composite material system, the fracture will initiate at the intersection of free surfaces and interfaces. This will create stress concentrations at those locations that will amplify the probability of crack growth. Differential stresses between layers lead to debonding between them, particularly at interfaces where are highly susceptible to these kinds of failures. Thus, the stress concentrations at the interfacial layers can increase the weakness between them, because they provide an initiation site for cracking. To mitigate these effects, the fabrication of the FGMCs with circular geometries was applied. Therefore, cylindrical die was used in this study to produce a substantial number of gradient structure specimens. These specimens were produced on a systemic basis by varying composition parameters. Due to the lack of sharp edges that concentrate stress, the cylindrical rod geometry is well suited for specimen characterization.

In this study, pressureless sintering was used to fabricate the FGMCs (Pines and Bruck, 2006a, b). Pressureless sintering requires a high temperature furnace, but does not need any preconditioning of the materials. Depending on the material system used, an inert atmosphere may be necessary to prevent oxidation, without any material preparation, thus requiring less time and lower cost. Furthermore since there is no external pressure applied to the FGMC specimens, there is no restriction on the deformation behaviour of the material, and there is no force to mitigate the differential stresses between layers.

In the present study, hot isostatic press was then utilized to refine and optimize the FGMCs. This is in accordance with many researchers that have fabricated graded materials using hot isostatic press (Rabin and Heaps, 1993; Winter et al., 2000). Hot isostatic press applies pressure to the specimen during the heating cycle. The externally applied pressure helps to restrict deformation and alleviate the stresses that lead to fracture and at same time reduce the porosity and increase the relative density leading to an improvement of mechanical properties (Rabin and Heaps, 1993; Winter et al., 2000).

During fabrication of the FGMC, the interfacial layers of the FGMC may be subjected to possible failure due to the stresses generation in different times during the sintering cycle particularly for pressureless sintering. During the initial stage, when the FGMC undergoes consolidation, the interfacial of FGMC layers are more susceptible to crack due to the lower fracture properties of each composite interlayer. Since the FGMC begins as a powder compact, it does not yet possess the material properties of the fully dense composite material system. Rather, the properties should be developed during sintering. This development in fracture properties puts the FGMCs more prone to failure, since the differential stresses cannot be withstood by the weak fracture properties of the interfacial layers. Consequently, when the amount of shrinkage begins to differ greatly between adjacent layers, and the stresses build up, the FGMC is likely to fracture due to stresses during sintering cycle. On the other hand, once the FGMC has reached the final sintering temperature and it undergoes maximum consolidation, the temperature should be decreased gradually down to room temperature. During this stage, residual stresses that have gathered during sintering cycle may lead to form cracks as a result of mismatches in the coefficient of thermal expansion.

Williamson et al. (1993) and Drake et al. (1993) studied the effect of graded distributions on the residual stresses in FGMs. They found, through their residual stress modeling, that the main difference between the heating and cooling stresses are related to the amount of consolidation of the material and the related strength, in addition to the presence of residual stresses during cooling that are not present in the sintering cycle. They also stated that the properties of the FGMs are based upon fully dense composite materials with predictable properties. These properties can be interpolated between temperatures to realize the behaviour of the material throughout cooling. Watanabe (1995) and Mizuno et al. (1995) also showed that shrinkages of each layer during sintering cycle had different rates and in different amounts resulting in large deformations in the specimens. If the differential shrinkages take place prior to the FGMCs fracture properties becoming strong enough to withstand the stresses, the FGMCs will be unable to consolidate crack-free. Drake et al. (1993) showed that the stress distribution could be optimized by selecting the proper exponent and by increasing the overall thickness of the graded region of the FGM. The stresses can be dissipated more easily if the thickness graded region of FGMs were increased. However, Bruck & Gershon (2002) mentioned that the cracks at interfaces are not a result of differential sintering shrinkage. They estimated by using FEA that the cracks are the result of the thermal expansion coefficients of the composite layers. The differences in the thermal expansion coefficients are much smaller than the differences in the shrinkage rates. The formation of these cracks likely occurs after the materials have consolidated, and it propagates through the fully dense material. To minimize the possibility of the cracks arising, the interface areas should be thicker that can better dissipate the stress evolved during sintering or change the composition to match the thermo-mechanical properties at the interfaces.

In this study during fabrication of the FGMCs, the mismatch in the properties between the materials can generate large stresses especially at the interface. These stresses may result from the large differences in coefficient of thermal expansion or any other residual stresses that have accumulated during combining and processing. This is likely to result in the inherent weakness at the interfaces. Therefore, tensile force can cause fracture easily as it prevents the optimal energy being absorbed by the compacted FGMCs. Moreover, in layered FGMCs, the reflections and transmissions of the initial stress wave will interact with each other from each interface in a material, eventually leading to fracture at an interface as shown in Figure 3.11.

In this present study, the analysis of this fracture reveals a coarse surface. The rough layer indicates that along this interface; the layers began to be sintered, and were pulled part as they consolidated at various rates. The second crack is located in the second layer composition. These cracks are most probably due to differential shrinkage stresses that arise during sintering due to the mismatch in the material properties and consolidation rates. The layers generally started to shrink at different temperature and they shrink at various rates. The high stress concentration normally concentrated, due to the difficulty in transmitting a load across it. Therefore, the interfaces in the multilayer composition are the weakest point. If there are no match in thermo-mechanical properties between adjacent layers, cracks will occur.

As shown in Figure 3.13 and 3.15, combination in the first materials matches better than pure materials. Nevertheless, the added Ti to the first layer alleviated stress evolution in interface between first and second layers, but 10% and even 50% was not enough to completely prevent delaminating cracks between first and second layers.

The variations in thermo-mechanical responses result in stresses at the interfaces of the layers (Rabin and Heaps, 1993). Therefore, thermal-matching can be used to modify the sintering starting temperature, sintering rate, and volumetric shrinkage to minimize differential shrinkage. Watanabe (1995) used particle size control to match the sintering behaviours of composite powders. Minimizing this differential shrinkage will reduce residual stresses that can cause premature cracking or debonding during the sintering process as shown in Figures 3.17 and 3.18 when 25% HA and 25% Ti were added into 50% either or ZrO_2 or Al_2O_3. By the gradient distribution of composition and microstructure, FGMCs likely relax the thermal stress induced by the difference of the thermal expansion coefficient between the ceramic and metal during the process of fabrication.

The FGMCs with the optimum graded composition was fabricated by pressureless sintering and hot isostatic pressing under the optimal sintering techniques. Therefore, to achieve a high sintering density and to avoid or reduce the decomposition reaction of HA as much as possible, the sintering temperature of FGMCs should be chosen near the beginning temperature of the decomposition of HA phase. Based on the structural stability of HA phase in FGMCs, the sintering technique was optimized using pressureless sintering and hot isostatic pressing at 1100^{o}C.

In this present study, microstructure depended on the volume fractions of each composite material; the final structure has a different appearance that can easily be compared to the adjacent layers. These observations are used to determine if the desired microstructure was obtained after fabrication. The microstructure of sintered FGMCs varied gradually from riched Ti side to HA side with the diversification of chemical compositions. No sharp interface between second, third and fourth layers were observed, whilst the microstructure of the first, second, third and fourth layers showed a gradual change in the Ti concentration that confirms the functionally graded design of the multilayered composite. In the Ti riched region, FGMCs has a dispersive microstructure of HA particles in the Ti matrix. As the HA content increases to 75%, the microstructure alters inversely in which the Ti particles dispersed in the HA matrix. Obviously in this study, Ti metal particles were distributed homogeneously in HA ceramic matrix for specimens sintered by hot isostatic press compared to specimens sintered by pressureless sintering. There were also remarkably less residual porosity observed in sintered under hot isostatic press compared to that sintered under pressureless sintering. This gradual change of microstructure of the FGMCs specimens likely leads to a continuous distribution of the properties.

In this present study, the phase analyzed by X-ray diffraction indicates that ZrO_2, Al_2O_3, Ti and HA phases were the predominant phases in sintered FGMCs, and no chemical contamination or reactions had taken placed between all phases. To realize the actual distributions of Zr, Al, O, Ca, P and Ti elements, the surface distribution of each element in the FGMCs was examined using EDX. It was found that each element in the FGMCs exhibits a graded distribution. The contents of Ti decrease gradually throughout the layers. This likely confirms graded change of the elemental and phases in the FGMCs.

In this current study, densities of the sintered FGMCs exhibited various graded distributions corresponding to the constitutional change. The relative density reaches its maximum value in the Ti. At the same time, the interlayers of HA and Ti FGMCs had a low relative density, which indicates they have some porosity.

Apparently, densities for specimens sintered by hot isostatic press approximate the theoretical densities. The actual densities of hot pressed FGMCs were 90%-97% of its theoretical density. It may be possible that the actual densification is higher when pressure is applied to specimens during sintering. Therefore, this will definitely reduce the amount of porosities in the specimens.

Densities are also affected by many factors, including the characteristics of the powders and the compaction conditions. In this present study, the compaction conditions were the same for all the specimens, therefore, the green density would be determined essentially by the powder characteristics. Due to the irregular shape of the Ti particles and the significant particle size difference between Ti and HA powders, the mixture of the Ti and HA powders could form a multi-modal packing effectively. In other words, the cavities between large Ti particles could be easily filled by the much smaller HA particles. When the concentration of HA was relatively low in the FGMCs, the small spherical HA particles would enter the interstitial cavities between the Ti particles and would led to improved density. However, when the HA concentration reached a critical value where all the voids between the large Ti particles were occupied by HA particles, further increase in the HA concentration will force the Ti particles apart and hence lead to a decrease in the density of the FGMCs.

Porosity models used in this study were adapted to characterize the sintering behaviour of FGMCs. Using porosity models give an idea about sintering behaviours and differential shrinkage problems that will happen during the sintering.

The shrinkage and their relative shrinkage were approximately linear. The linear shrinkage after sintering along the layers confirms the linearity of properties changes inside the FGMCs.

The hardness test used in this characterization is a Vickers microhardness test. A microhardness test is used in this study because it is a non destructive test that can give an overall idea of the hardness of each layer. This type of microhardness test, however, may lead to incorrect measurements if the microhardness tests are performed in agglomerate regions. Therefore, the microhardness value may read higher than the real value for the FGMCs. An indentation that incorporates both matrix and reinforcing phases in a homogeneous-type composite would provide an optimal measurement, but it may violate constitutive assumptions on too large a scale. By minimizing the agglomerations, the errors in the microhardness measurements can be minimized. Also, each specimen was divided longitudinally into four quarters and hardness was measured in each quarter separately in order to minimize the error of reading due to agglomerations.

In this study, the microhardness of FGMCs increased with increasing HA particles. This is attributed to the fact that the hardness of the metallic particles was less than that of HA ceramic. These results are in accordance with Callister (2007), who found that the hardness of composites should decrease with the increasing in metallic particles. The specimens sintered by hot isostatic press showed higher microhardness compared to specimens sintered by pressureless sintering. This is also in agreement with others that reported that using hot isostatic press enhances the mechanical properties (Rabin and Heaps, 1993; Winter et al., 2000).

Flexural strength is sensitive to the microstructure of the composite materials. Flexural strength is related to the configuration and distribution of the constitutional phases and the pores in the composite materials with a given chemical composition. The porosities decrease the effective area bearing the load and can lead to the stress concentration in the materials. In the present study, flexural strength and modulus of elasticity of FGMCs were significantly higher for specimens sintered by hot isostatic press compared to those sintered by pressureless sintering. This may be due to the higher percentages of the porosity in specimens sintered by pressuresless sintering. These findings concurred with Hirano & Suzuki (1990) who found that the flexural strength of the material with a porosity of 10% can decrease down to 50% of the one of the material without pores.

It should be pointed out that flexural strength of a compact human bone for heavy load-bearing applications could reach up to 121–149 MPa (Hench, 1991; Fung, 1993) and for human dentine 87 MPa (Grigoratos et al., 2001). Modulus of elasticity of adult dentine is 36 GPa (Grigoratos et al., 2001). From the point of view of the requirements towards the materials for hard tissue replacement implant, a biomaterial with low modulus of elasticity is anticipated (Hench, 1991; Fung, 1993). The flexural strength and modulus of elasticity of FGMCs decreased gradually with increasing HA. These findings are in agreement with Callister (2007).

3.7 Conclusions

Within the limitation of this study, the following conclusions may be drawn:

1. FGMCs with the optimum graded composition were satisfactorily fabricated by pressureless sintering and hot isostatic press.
2. SEM micrographs demonstrated satisfactory integration between grains and interface among the layers.
3. The microstructure of sintered FGMCs with the diversification chemical composition and phases varied gradually, which eliminates the macroscopic interfaces.
4. XRD and EDX results proved the presence of expected elements and phases in FGMCs and exhibited a graded distribution in Ti-HA-ZrO_2-Al_2O_3.
5. The linear shrinkage after sintering along the layers confirms the linearity of properties changes inside the FGMCs indicating a functional graded material.
6. Densities, porosities, microhardness, flexural strength and modulus of elasticity change corresponding to the relative density and exhibit gradual variation in FGMCs indicating a functional graded material.
7. The volume fraction porosity was associated with the matrix and the reinforcing particles. The measured porosity values showed similar trends to the theoretical models.
8. The physical and mechanical properties of the FGMCs sintered by hot isostatic press were significantly better compared to pressureless sintering.

Chapter Four

Thermo-Mechanical Stress in Functionally Graded Dental Posts Due to Temperature Gradient

4.1 Introduction

Wide variations of temperature in the oral cavity may occur due to the ingestion of hot and cold food or fluids. Hence, restorative materials in the mouth may show thermal expansion or contraction due to the thermal stimuli. The difference of thermal expansion and contraction between a restoration and the tooth structure may lead to development of stresses at the interface and this may have unfavourable effects on the margins and can finally lead to failure of the restorative materials.

Many studies focussed on the mechanical behaviour and failure characteristics of post and core systems (Pegoretti et al., 2002; Fujihara et al., 2004; Genovese et al., 2005; Lanza et al., 2005; Santos et al., 2010; Al-Omiri et al., 2011; Dejak and Młotkowski, 2011). In addition, some studies investigated temperature changes in restored tooth using finite element method (Spierings et al., 1984, 1986; Yang et al., 2001a; Toparli and Sasaki, 2003; Genovese et al., 2006). Spierings et al. (1984, 1986) predicted the transient heat conduction problems within the teeth restored with various materials using an axisymmetric models and the finite element method. Fenner et al. (1998) also predicted the temperature and thermal stress distribution in a premolar restored with Class II composite resin restoration when subjected to temperature fluctuations, similar to the effect of drinking hot liquid. Toparli et al. (2000, 2003) calculated the temperature distribution and associated thermal stress of intracoronal restored tooth and crowned tooth. Arola & Huang (2000) determined the relative significance of both mechanical and thermal loads on the stress distribution that results in molars with amalgam restorations.

There are significant difference in thermal conductivity and thermal expansion of dentine, and metallic and non-metallic restorative materials. “Thermal conductivity is the heat, in calories per second, passing through a body; 1 mm thick with a cross-section of 1 mm" as defined by Craig & Powers (2002). Metals tend to be better heat conductors than non-metals. "Heat flow is defined as the thermal conductivity divided by the product of specific heat time's density" and "The specific heat of a substance is the quantity of heat needed to raise the temperature of a unit mass of substance by 1°C" (Craig and Powers, 2002).

The coefficient of thermal expansion is used to describe the dimensional changes of a material due to thermal change. Tooth structure and restorative materials in the mouth expand when warmed by hot stimuli and contract when exposed to cold stimuli. If there are mismatch in volumetric thermal expansion by different temperature changes and/or different coefficients of thermal expansion, the induced thermal stress may cause fracture of the restoration or tooth (Craig and Powers, 2002). Therefore, it is important to ascertain the thermal behaviour of FGSPs in order to predict their performance in the oral environmental.

4.2 Aim

The aim of this chapter was to evaluate the thermo-mechanical stress in endodontically treated teeth when restored with functionally graded structured dental posts (FGSPs), titanium and zirconia posts using finite element method (FEM).

4.3 Objectives

The objectives are:

1. To analyse temperature gradient of endodontically treated tooth restored with modelled FGSPs and compare with modelled titanium and zirconia posts under hot and cold conditions using FEM.

2. To evaluate thermal stress distributions of endodontically treated tooth restored with FGSPs and compare with titanium and zirconia posts under hot and cold conditions using FEM.

3. To determine thermal strain distributions of endodontically treated tooth restored with FGSPs and compare with titanium and zirconia posts under hot and cold conditions using FEM.

4.4 Materials and method

4.4.1 Model geometry

An axi-symmetric three dimensional (3D) model of a maxillary central incisor consisting of alveolar bone, periodontal ligament (PDL), dentine, post, core, crown and gutta-percha was developed using Pro/Engineer software (Parametric Technology Corporation, Kendrick St., Needham, USA). The dimensions of each part of the geometric 3D model illustrated in Table 4.1 were based on the data taken from the literature.

4.4.2 Mesh generation

As shown in Figure 4.1, the refined mesh in the 3D model was discretized into 121589 nodes and 76796 elements using FE package (ANSYS Workbench™ 11.0, ANSYS®, Inc., USA). Since the convergence of the FEM analysis was largely dependent on the mesh grid, a standard convergence study was conducted by running FE analyses for the mesh grids using different mesh refinement levels. The convergence was considered acceptable when the relative errors were less than 1%.

Table 4.1 Dimensions of the geometric three dimensional model

Part		**Dimension (mm)**
Crown	Height	10.5
	Thickness at the top	2
	Thickness at the bottom edge	1.5
Core	Height	8.5
	Diameter	6
	Thickness over the post	2
Root	Length	14.5
	Width	8.5
	Ferrule height	3
Post	Length	16
	Diameter	1.5
Gutta-percha	Length	5
	Diameter	1.5
PDL	Thickness	0.18
Bone	Thickness	3.5

Sicher & Du Brul (1970), Wheeler (1974), Ingle & Bakland (2002), Asmussen et al. (2005).

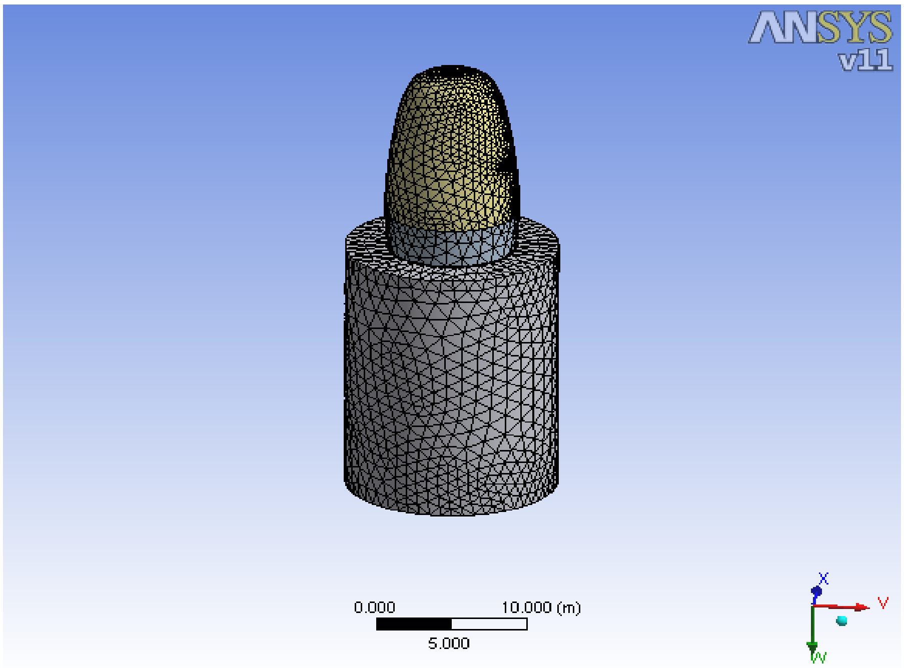

Figure 4.1 Three dimensional finite element mesh representing endodontically treated tooth.

4.4.3 Materials and properties

The mechanical and thermal properties of dentine and the restorative materials included in this study are presented in Table 4.2. The material properties of the FGSPs modelled varies in the longitudinal direction (Figure 4.2). The mechanical and thermal properties of FGSPs were estimated by applying the rule of mixture based on the theory of composite materials as follows (Wakashima et al., 1990);

$$P = P_A V_A + P_B V_B \tag{4.1}$$

where;

P_A *and* P_B are the material properties of the metal and ceramic phases.

V_A *and* V_B are the volume fractions follow a power law distribution.

Three FGSPs were modelled for the restoration of endodontically treated teeth (Models A-C) as shown in Figure 4.2. They were then compared to the homogenous-type zirconia (Model D) and titanium (Model E) posts.

Table 4.2 Mechanical and thermal properties

Materials	Density (g/mm^3)	Young Modulus (Gpa)	Poisson ratio	Thermal expansion (Alpha) (1/C)	Thermal conductivity j/ (s.mm.C)	Specific heat j/(g.C)
PDL [a-d]	1.1E-3	0.69e-4	0.45	10E-6	5.87E-4	1.84
Root [e,f]	2E-3	18.6	0.31	10.6E-6	6.3E-4	1.17
Gutta-percha[g, h, d]	0.97E-3	0.14	0.45	54.9E-6	1.53E-4	1.828
Resin core[i]	2.1E-3	14.8	0.24	39.4E-6	1.0878E-4	0.2
Ceramic Crown[i]	2.4E-3	120	0.19	7.1E-6	10.04E-4	0.21
Alveolar bone[c, j]	1.3E-3	1.37	0.3	10E-6	5.87E-4	1.84
Zirconia[k]	5,89	200	0.32	13.5E-6	1.7E-3	0.502
Alumina[k]	3.89	375	0.25	8.4E-6	35E-3	0.88
Titanium [m-p]	4.51	116	0.33	11.9E-6	0.42E-2	0.52
Hydroxyapatite [n, q, r]	3.156	40	0.27	13.3E-6	12.57E-2	0.8799

[a]Farah et al. (1989), [b]Gale and Darvell (1999b), [c]Yang et al. (2001a,b), [d]Ruse (2008), [e]Fenner et al. (1998), [f]Lin et al. (2001), [g]Asmussen et al (1999), [h]Er et al. (2007), [i]O'Brien (1997), [j]Benzing et al (1995), [k]Material properties, http;//accuratus.com, [m]Toparli (2003), [n]Moroi et al. (1993), [o]Bever (1986), [p]Boyer and American Society for Metals (1985) [q]Hedia and Mahmoud (2004), [r]Babushkin et al. (1994).

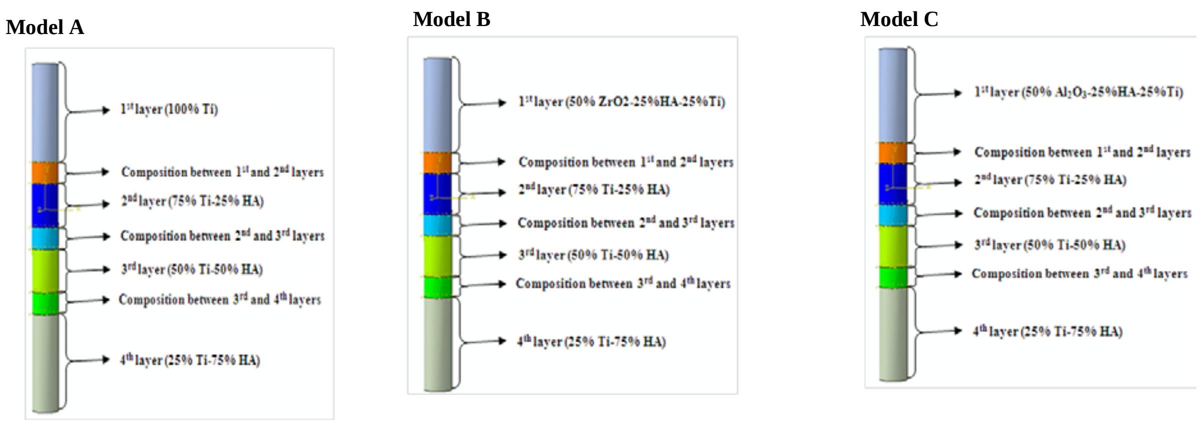

Figure 4.2 Functionally graded composite formulation.

4.4.4 Boundary condition

The boundary condition for the nodes were chosen to be along the bottom end line of the models referred to as alveolar bone as advocated by Yang et al. (2001a) thus allowing no displacement. All components were assumed to be perfectly bonded without any gaps between the components.

The 3D FE model created by using ANSYS FE software program was assumed to be isotropic, homogenous, elastic, axisymmetric and thermally solid following a 3D thermo-mechanical axi-symmety transient FE thermal analysis (ANSYS Workbench™ 11.0, ANSYS®, Inc., USA).

4.4.5 Thermal stimuli

Temperatures of 15°C and 60°C were chosen to represent the cold and the hot stimuli respectively with the normal human body temperature, 36°C, as the initial temperature (Toparli et al., 2000; Toparli and Sasaki, 2003; Güngör et al., 2004). It was assumed that these temperatures could be kept constant for a period of one second in the oral cavity and five seconds was determined to be an appropriate length of time to generate a temperature difference between tooth and restorative system (Spierings et al., 1986; Toparli et al., 2000, 2003; Toparli and Sasaki, 2003). The hot or cold stimuli were applied to all the nodes on the superficial surface of the crown (Figure 4.3). Once the thermal stimulus was removed, it was considered to be normal oral physiology for the temperature in the oral cavity and restorative materials to return to body temperature. A transient FE thermal analysis was carried out to estimate the change in temperature within the models. The thermal stress and strain distributions were also determined as a result of temperature change using FEM.

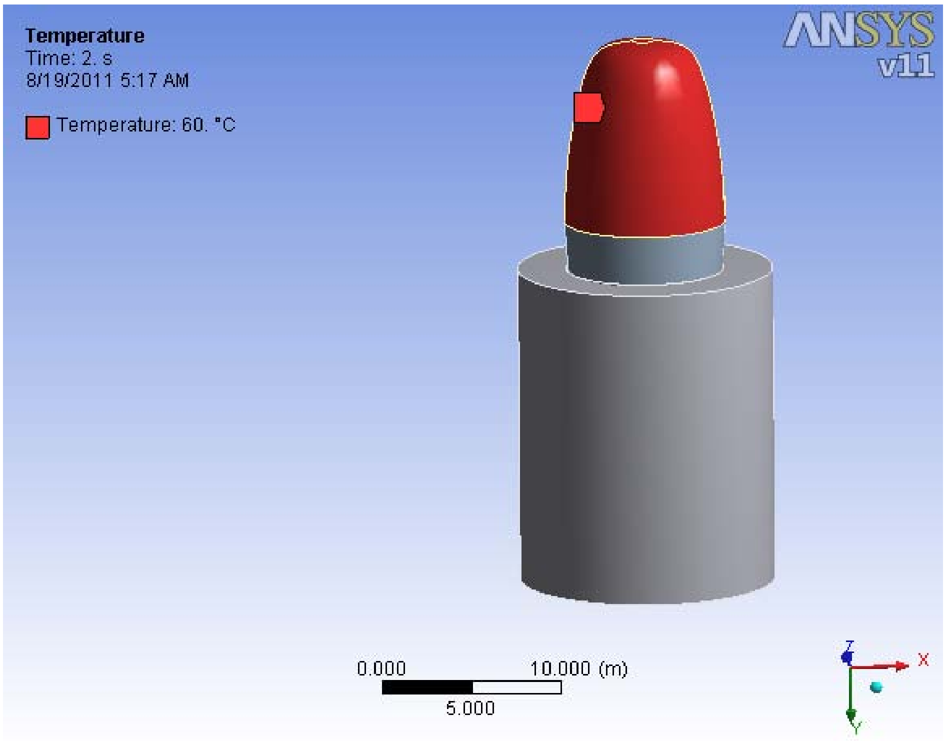

Figure 4.3 Application of thermal stimuli on three dimensional finite element model.

4.5 Results

4.5.1 Hot stimuli and temperature distribution

Figure 4.4 shows the temperature distributions on the 3D model restored with various FGSPs (Model A-C), zirconia (Model D) and titanium (Model E) posts when hot stimuli (60^{o}C) were applied over time. For all the models, there was temperature increase during the first second approximately up to 60°C and then the temperature remained constant for one second at 60^{o}C before declining gradually.

FGSPs (Models A-C) dissipated heat more efficiently compared to zirconia and titanium posts (Models D and E). It was observed that the minimum temperature at the fifth second was 40^{o}C, which was lower than the values recorded for zirconia (Model D) and titanium (Model E) posts; 48^{o}C and 41.5^{o}C respectively within the stipulated time frame of 5 seconds.

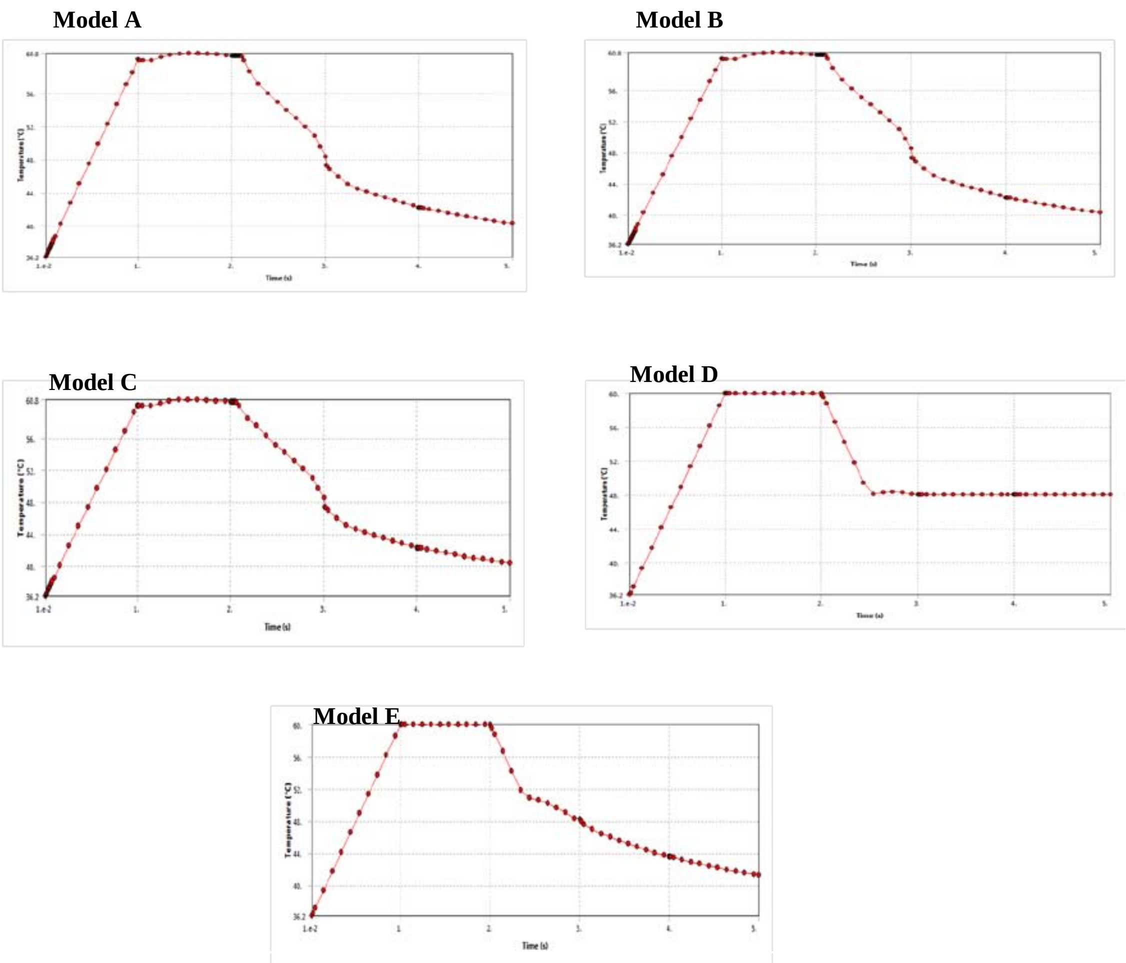

Figure 4.4 Time-dependent temperature distributions on the model restored with FGSPs (Models A-C), zirconia (Model D) and titanium (Model E) posts under hot stimuli.

4.5.2 Hot stimuli and thermal stress and strain distributions analysis

The thermal stress and strain distributions for various posts were recorded as a result of temperature gradient. Figures 4.5-4.14 illustrated thermal stress and strain distributions in teeth due to thermal response of 60^{o}C for the 3D models restored with various posts. Thermal changes generated stress that was located primarily within the post. FGSPs recorded the lowest von Mises stress and strain compared to zirconia and titanium posts. The magnitude of thermal stress and strain distributions in both titanium and zirconia posts were greater than those in FGSPs particularly at middle area of the posts. The peak dentinal stresses generated by hot stimuli for titanium and zirconia posts were approximately twice as much compared to the FGSPs. However, the behaviour of thermal stresses and strains in various FGSPs was similar. The thermal stress and strain in the zirconia post were greater than those recorded for other investigated posts. Zirconia post also generated the highest stress and strain distribution at the post-dentine interface followed by titanium and FGSPs.

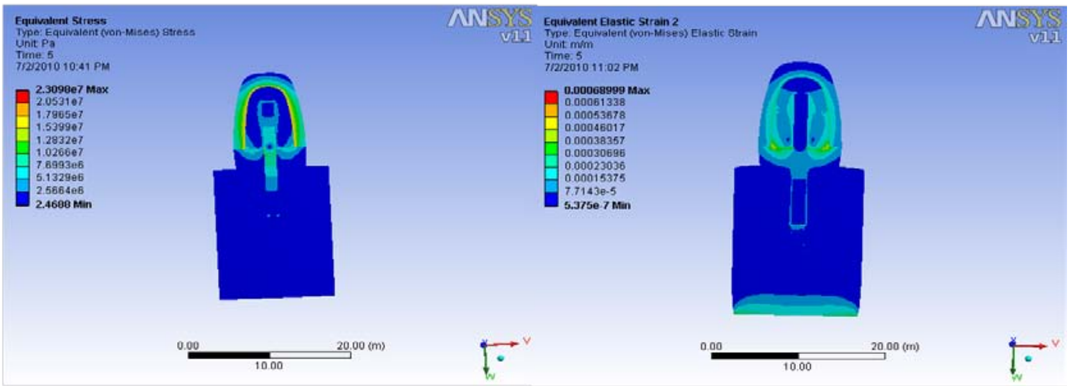

Figure 4.5 Von Mises stress and strain distributions for FGSP in Model A.

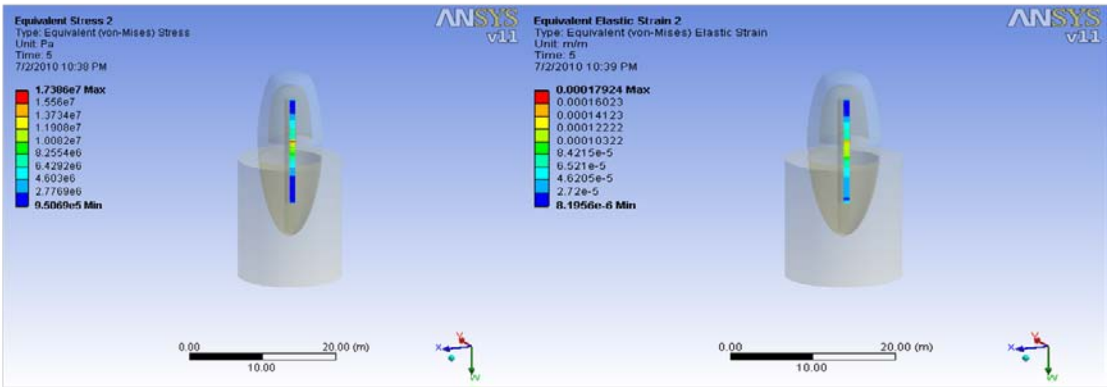

Figure 4.6 Interface von Mises stress and strain distributions for FGSP in Model A.

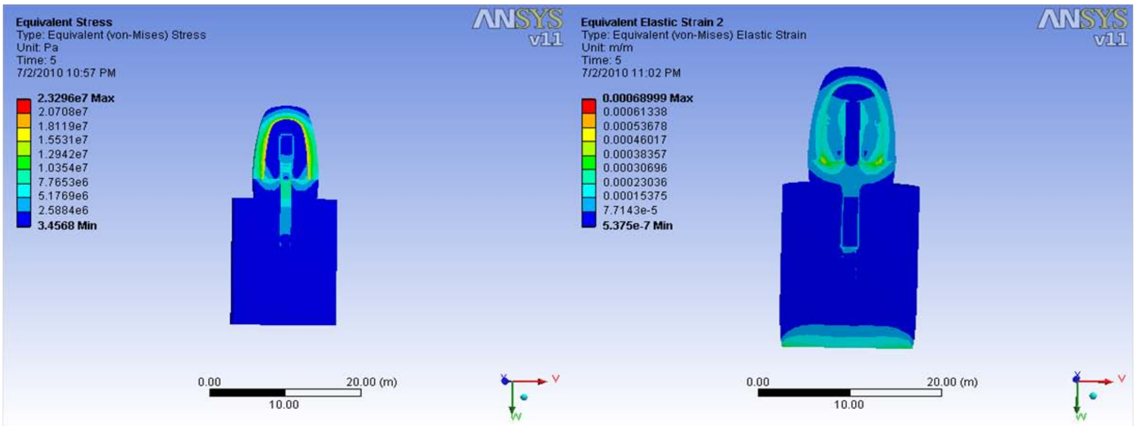

Figure 4.7 Von Mises stress and strain distributions for FGSP in Model B.

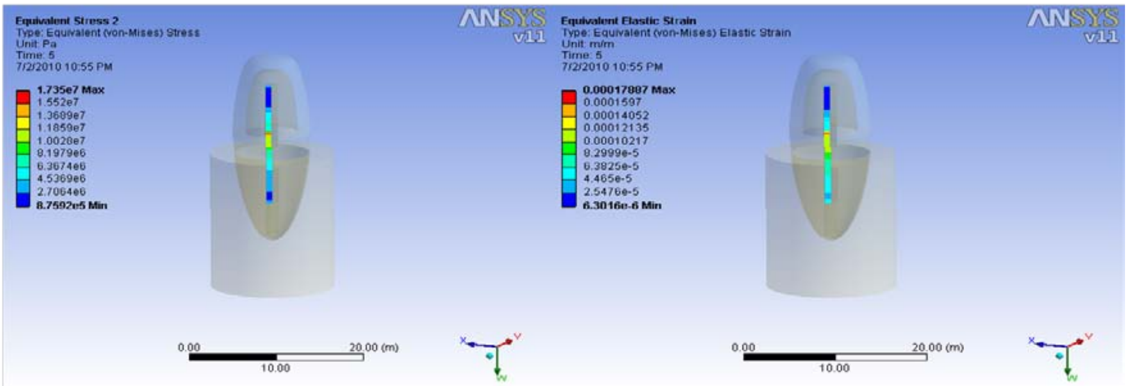

Figure 4.8 Interface von Mises stress and strain distributions for FGSP in Model B.

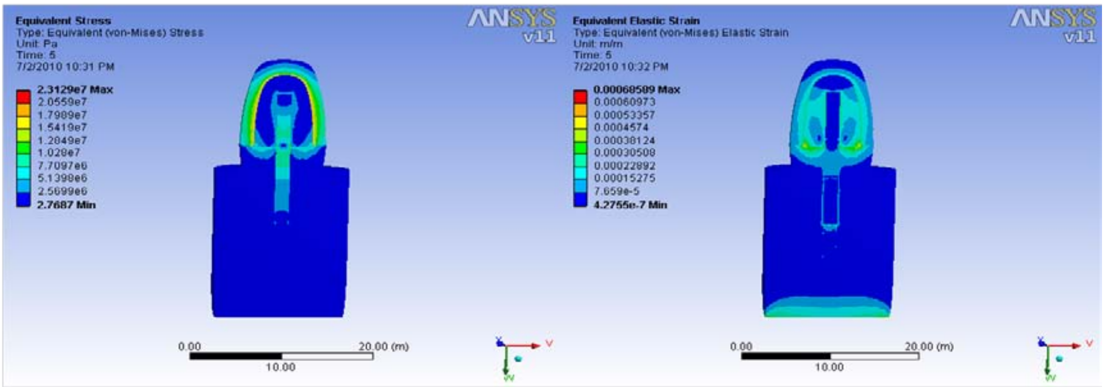

Figure 4.9 Von Mises stress and strain distributions for FGSP in Model C.

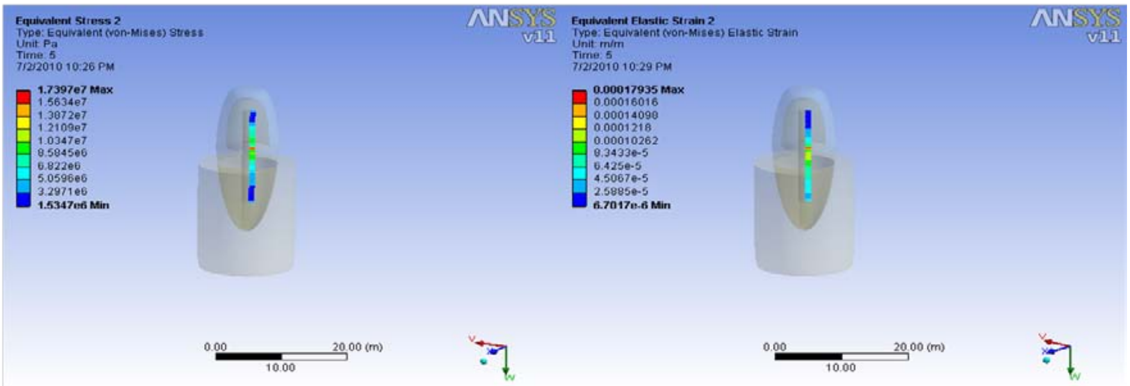

Figure 4.10 Interface von Mises stress and strain distributions for FGSP in Model C.

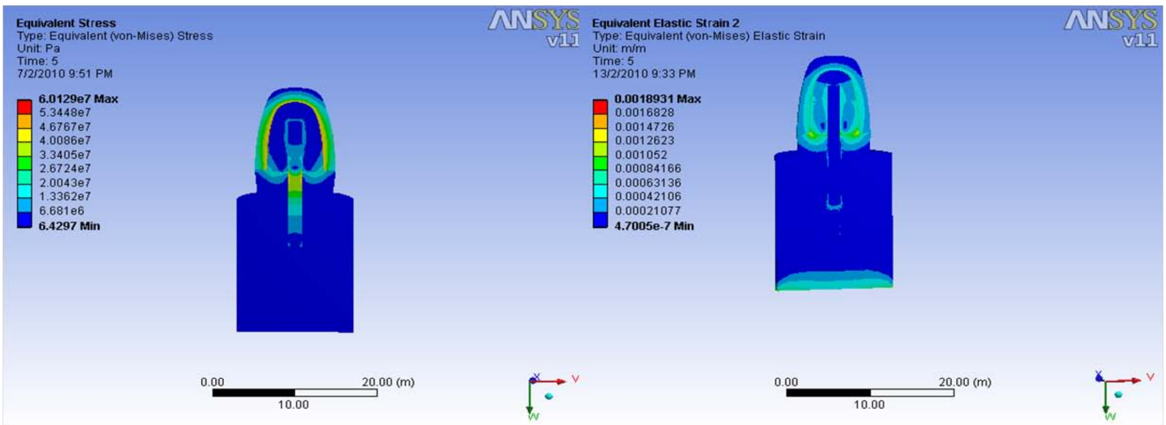

Figure 4.11 Von Mises stress and strain distributions for zirconia post in Model D.

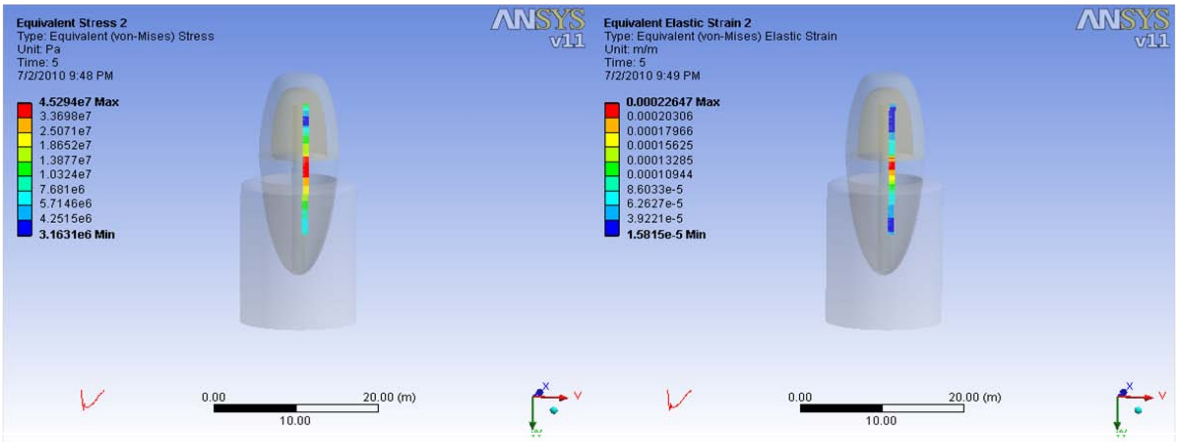

Figure 4.12 Interface von Mises stress and strain distributions for zirconia post in Model D.

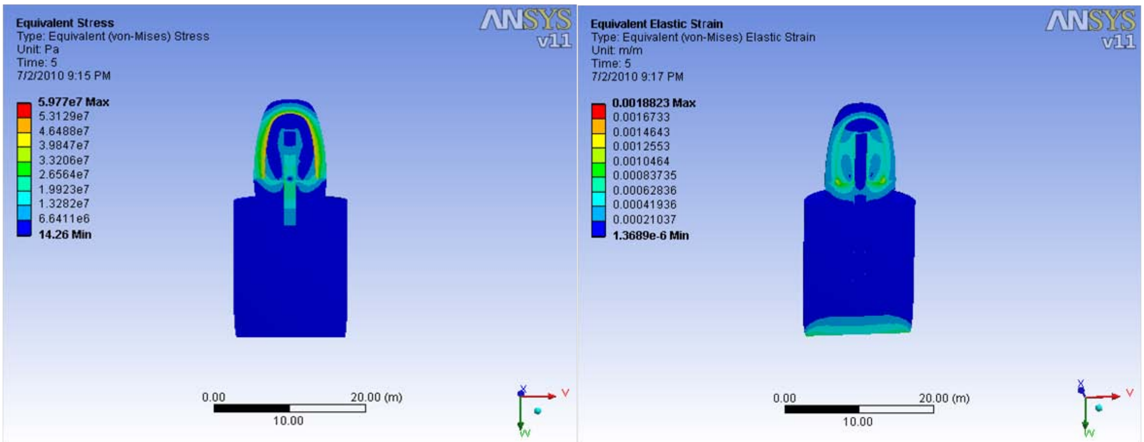

Figure 4.13 Von Mises stress and strain distributions for titanium post in Model E.

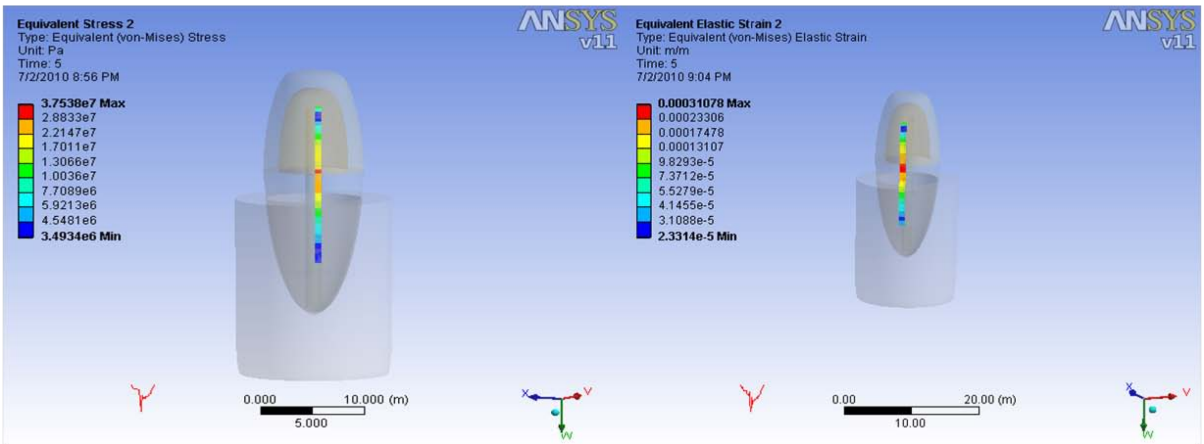

Figure 4.14 Interface von Mises stress and strain distributions for titanium post in Model E.

4.5.3 Cold stimuli and temperature distribution

Figure 4.15 illustrated the temperature distribution in the 3D model restored with FGSPs (Models A-C), zirconia (Model D) and titanium (Model E) posts under cold stimuli over time. For all models, the temperature decreased during the first one second approximately to 15°C and then the temperature remains constant at 15^{o}C for one second before increasing gradually.

FGSPs (Models A-C) exhibited better recovery when exposed to cold stimuli compared to zirconia (Model D) and titanium (Model E) posts. It was observed that at the fifth second the FGSPs (Models A-C) recovered to the temperature of 32.5^{o}C compared to the zirconia (Model D) and titanium (Model E) posts which recorded 26^{o}C and 31^{o}C respectively within the stipulated time frame of 5 seconds as illustrated on Figure 4.15.

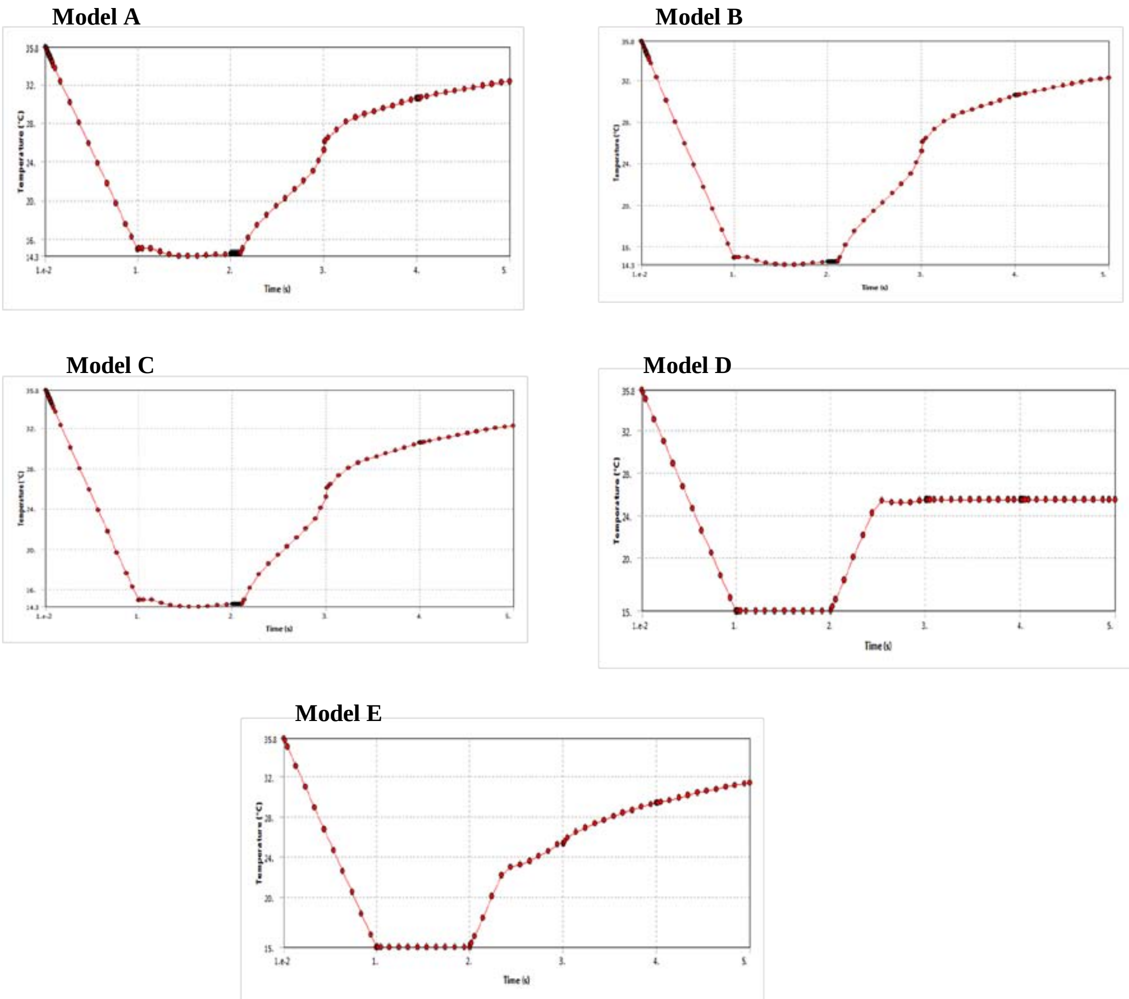

Figure 4.15 Time-dependent temperature distributions on the model restored with FGSPs (Models A-C), zirconia (Model D) and titanium (Model E) posts under cold stimuli.

4.5.4 Cold stimuli and thermal stress and strain distribution analysis

Thermal stress and strain distributions were recorded as a result of temperature change and Figures 4.16-4.25 illustrated thermal stresses and strains in the models. The lowest von Mises stresses and strains were recorded for FGSPs compared to zirconia and titanium posts. The magnitude of thermal stresses and strains at post-dentine interface in both zirconia and titanium posts were greater than those FGSPs especially at middle area of the post. The peak dentinal stresses and strains caused by cold stimuli for zirconia and titanium were approximately twice as much compared to the FGSPs. The thermal stress and strain in zirconia post were the highest amongst the investigated posts.

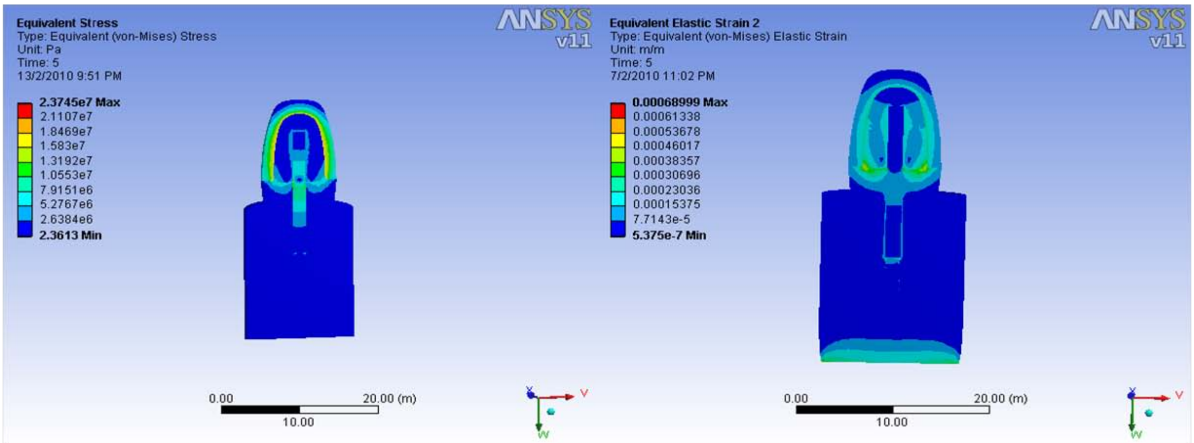

Figure 4.16 Von Mises stress and strain distributions for FGSP in Model A.

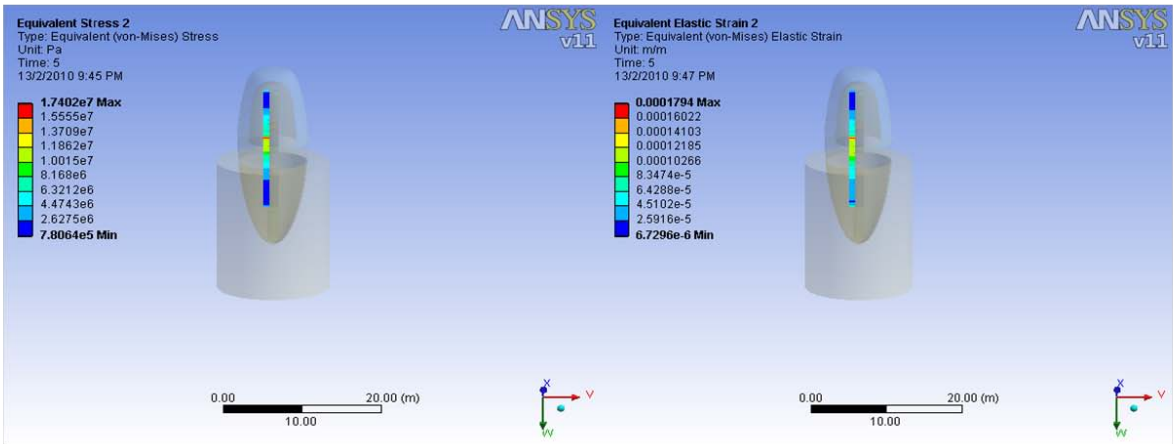

Figure 4.17 Interface von Mises stress and strain distributions for FGSP in Model A.

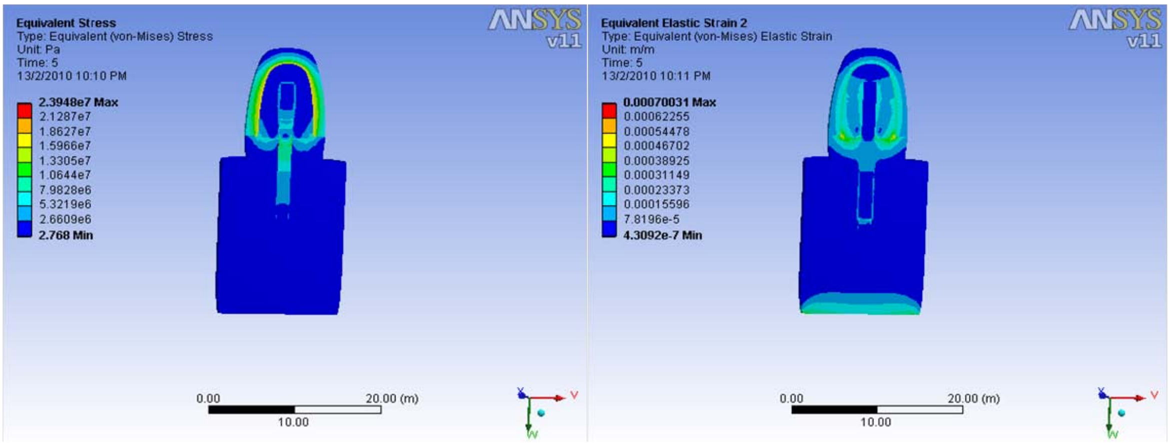

Figure 4.18 Von Mises stress and strain distributions for FGSP in Model B.

.

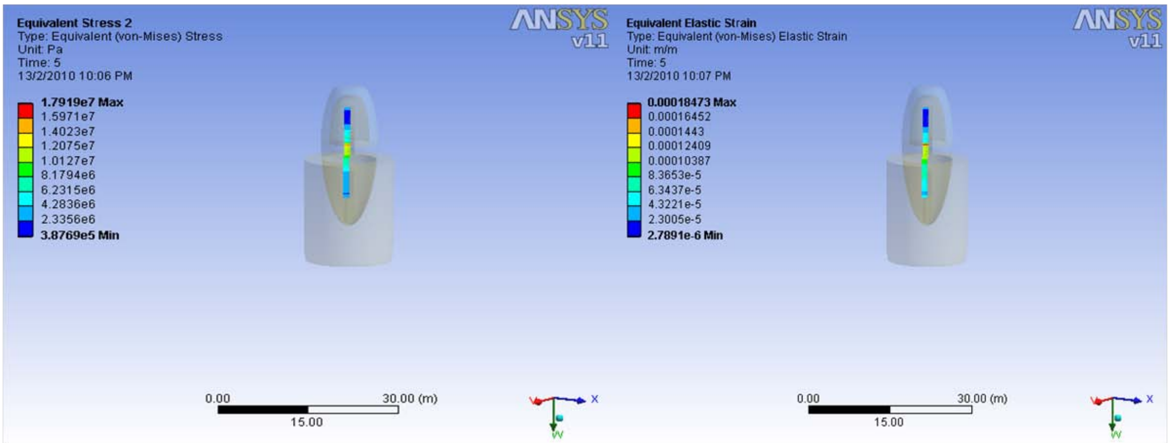

Figure 4.19 Interface von Mises stress and strain distributions for FGSP in Model B.

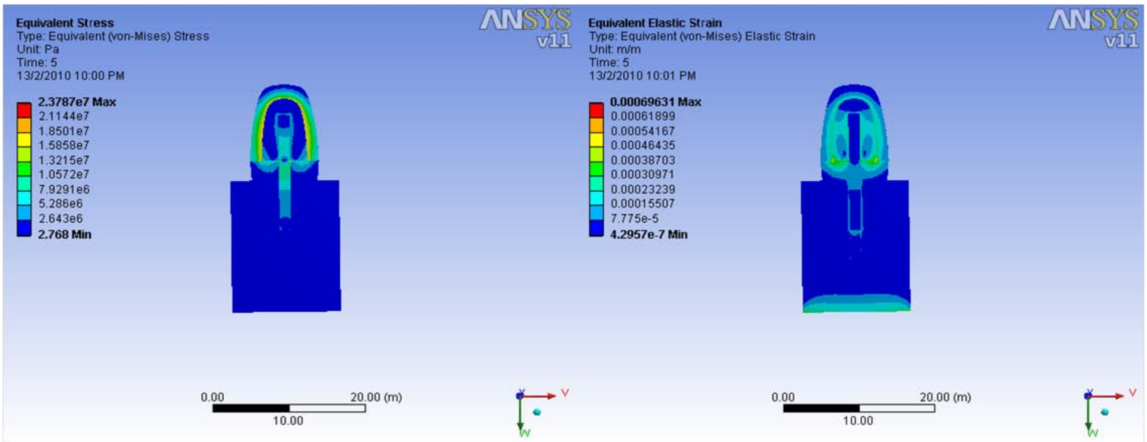

Figure 4.20 Von Mises stress and strain distributions for FGSP in Model C.

.

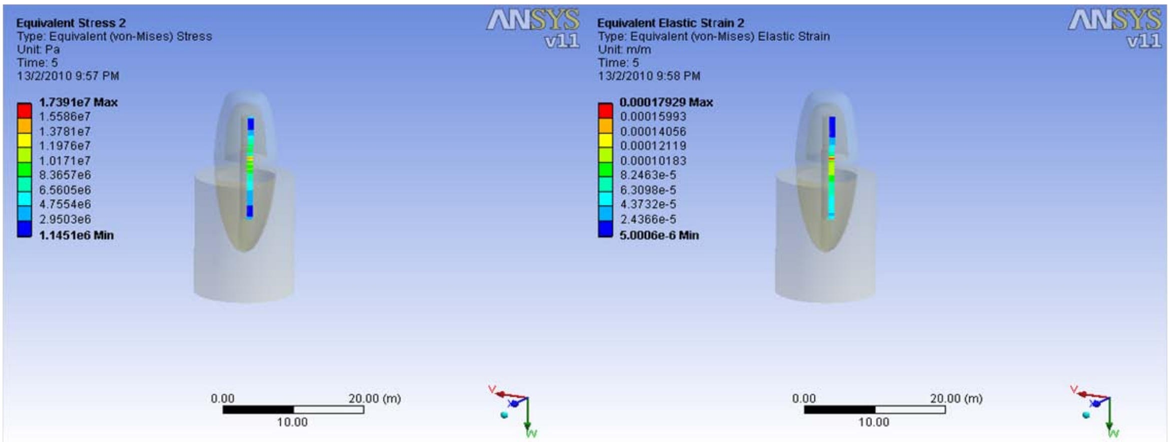

Figure 4.21 Interface von Mises stress and strain distributions for FGSP in Model C.

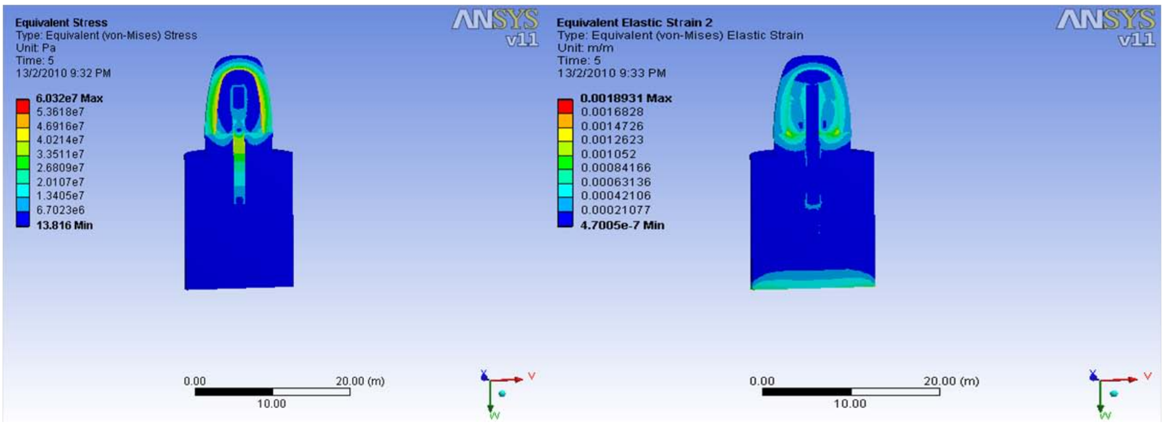

Figure 4.22 Von Mises stress and strain distributions for zirconia post in Model D.

.

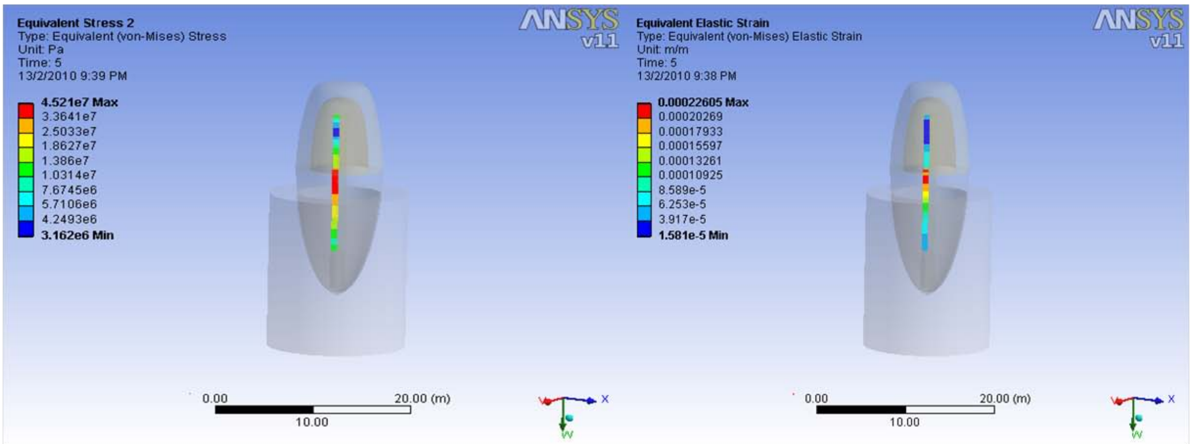

Figure 4.23 Interface von Mises stress and strain distributions for zirconia post in Model D.

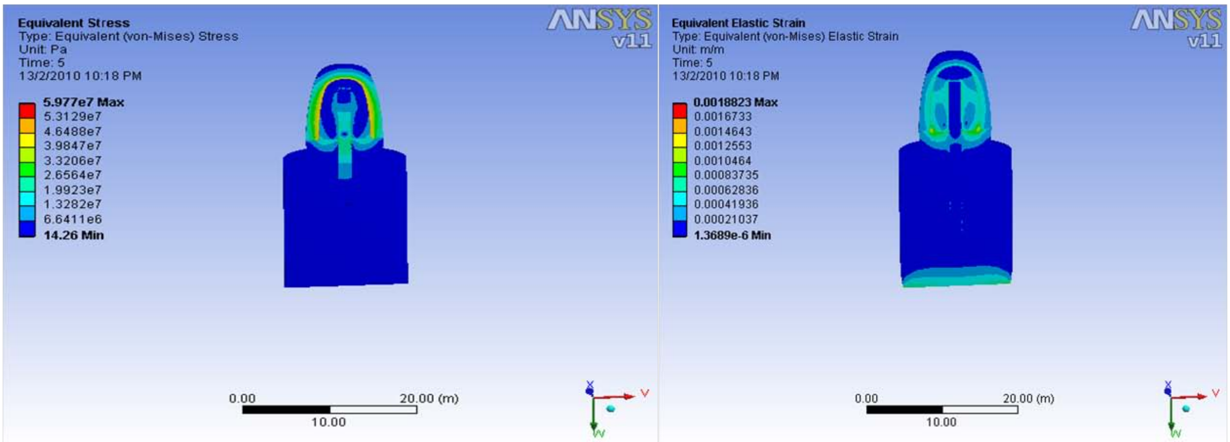

Figure 4.24 Von Mises stress and strain distributions for titanium post in Model E.

.

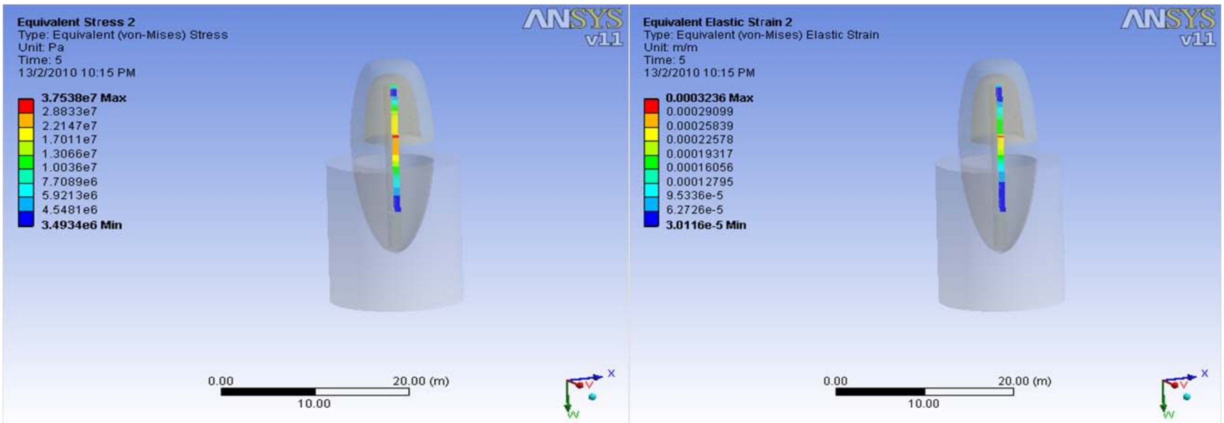

Figure 4.25 Interface von Mises stress and strain distributions for titanium post in Model E.

4.6 Discussion

The oral cavity may be subjected to thermal irritation from hot or cold foods and beverages. Palmer et al. (1992) reported temperature change ranging between 0 and 67°C when they measured the maximum and minimum temperatures on the natural tooth surface of 13 subjects as they ingested hot and cold beverages. Since the normal temperature of the oral cavity is 36±1°C, it appears that there may be a considerable gradient of temperature when teeth come into contact with thermal stimuli. Consequently, thermal stresses may develop at the interfaces between different materials because of thermo-physical property mismatch.

As enamel and dentine reveal slightly mismatch coefficient of thermal expansion, thermal loads may even generate stresses in the intact sound tooth (Magne et al., 1999). This problem is increased if the tooth is restored with various restorative materials. The effect of thermal stimuli may be further amplified in the presence of mastication as functional load could create tensile stresses on the buccal side of the teeth and compressive stresses on the labial side. However, masticatory situations were not considered in this study. Further study could be carried out to evaluate the affect of mastication and stress distribution.

As stated by Craig & Powers (2002), the dentine has different thermal conductivity and thermal expansion from restorative materials. This difference is further amplified in endodontically treated teeth as there is a higher degree of inhomogeneity within the restored tooth (Hood, 1991). From the perspective of structural mechanics, an endodontically treated tooth restored with post, a core and a crown can be treated as a multi-component structure made of complex geometry. If there are differences in volumetric thermal expansion by different temperature changes and/or different coefficients of thermal expansion, the induced stress may cause fracture of the dental structure or leakage of the restoration (Craig and Powers, 2002). These thermal changes finally might lead to post and core failure.

There are difficulties in investigating the effects of thermal changes on restored teeth both *in vitro* and *in vivo* (Toparlı et al., 2003). However, with the advent of powerful computers and software programming, very complicated structures can easily be modelled and the actual working conditions can be simulated precisely. One of those programming methods, FEM, offers solutions for the engineering problems and its use in biomechanical applications has been widely accepted. FEM is fast, accurate, and can be considered reliable alternative *in vivo* and *in vitro* studies (Darendeliler et al., 1992; Yaman et al., 1995, 1998; Toparlı et al., 2003; Yaman et al., 2004).

Evaluation of thermal stress and strain distributions in the endodontically treated tooth restored with post depends on the level of heterogeneity and specific combination of restorative materials included in the tooth structure. These two factors define the overall thermal properties of the restored tooth that finally drive temperature change rates as the tooth is exposed to thermal irritants. Generally, tensile thermal stresses may develop when the crown is in contact with hot irritants while cold irritants may generate compressive stresses. For this reason, both the cold and hot stimuli were investigated in the present study.

Many studies reported that the coefficient of thermal expansion of gold and titanium dental posts is almost comparable to dentine (Yang et al., 2001a; Toparli and Sasaki, 2003; Genovese et al., 2006). However, the high modulus of elasticity of these dental posts often results in root fractures (Genovese et al., 2005).

In the present study, as expected, the thermal stress and strain concentrations at post-core, core-dentine and core-crown interfaces are much higher than at the apical region, because the crown and core are the first to respond when thermal perturbation is applied. Also, the thermal stress in the restorations and coronal portion of the dentine increased markedly than did stress levels in the supporting bone. These results are in accordance with Toparli et al. (2000), who investigated the thermal stress distribution on restored tooth and reported that maximum stress differences were at the restorative material-enamel interface.

In this study, the lower thermal stress and strain were observed in titanium (Model E) compared to zirconia (Model D) posts. Overall, zirconia post (Model D) showed the highest thermal stress and strain distributions compared to other models. These findings may be attributed to the fact that zirconia possesses the highest density and lowest thermal conductivity amongst posts materials included in this study. This is due to high thermal inertia associated with large mass density which may limit temperature gradients and, finally, magnitude of stresses. Thermal conductivity will dominate if there is some preferential transmission path. High thermal conductivity as mentioned may result in high stresses because it tends to increase thermal gradients. In addition, the higher stress and strain developed within Model D are likely to be contributed by the thermal retention even after removal of stimuli as zirconia; a non-metallic post could not efficiently dissipate the heat into dentine.

Remarkably, FGSPs (Models A-C) exhibited minimal thermal stress and strain distributions. These types of posts were able to redistribute thermal stresses over time. Stress concentrations at the crown-core, post-core and post-core interfaces were visualized, whereas stresses were reduced in post itself and dentine. This may be due to the compositional gradients arising from the combination of multiple material properties to avoid the thermal stress and strain concentrations that occur at sharp interfaces of different materials. Drake et al. (1993) used the power law distribution to show that significant stress and plastic strain reductions can be achieved by increasing gradient thickness and tailoring the exponent to provide gradual compositional change near phases that exhibit high modulus and little plasticity, such as ceramic materials.

Functionally graded materials composed of different components such as ceramics and metals which have continuous or gradual change in materials composition across its thickness. Such a microstructure is expected to reduce thermo-mechanical stresses and to improve the thermal shock onto the materials and at the end tailored functional performance.

In this study, there was lower interfacial thermal stress and strain concentrated at the middle and apical parts of the FGSPs (Models A-C) compared to Model D and Model E. This would support the findings that failures of these systems occurred cohesively within the interface with dentine rather than in the dentine as reported by Oilo (1978). The HA concentration variation in xTi-yHA provided a smooth change in the properties of FGSP resulting in reduction of thermal stress and strain concentration at interfaces with the surrounding structures (Kim and Paulino, 2002). In this study, the FGSPs possibly improved the heat flow into dentine because of the gradual change in thermal conductivity. Thus thermal stresses and strains could be transmitted into the surrounding structures successfully. Although considerable thermal stress and strain peak concentration were noted at the coronal part, in FGSPs these peaks (Models A-C) were negligible compared with the zirconia (Model D) and titanium (Model E) posts.

In this study, thermal analysis showed that thermal stress level is closely related to the amount of temperature gradient. The peak stress by thermal stimuli for the zirconia and titanium posts are approximately three times higher than FGSPs.

4.7 Conclusions

Within the limitation of this study, the following conclusions may be drawn:

1. FGSPs were able to recover to near normal body temperature more efficiently within the allocated time frame than the titanium and zirconia posts.

2. Zirconia and titanium posts produced greater thermal stresses and strains than FGSPs.

3. Difference in the temperatures gradient during the recovery phase for all FGSPs was not evident.

4. Only slight differences in thermal stress and strain distributions were observed for all FGSPs.

Chapter Five

Evaluation of the Stress and Strain Distributions of Endodontically Treated Tooth Restored with Functionally Graded Dental Posts Compared to Homogenous-Type Dental Posts

5.1 Introduction

Endodontically treated teeth are at higher risk of biomechanical failure than vital teeth (Llena-Puy et al., 2001). The placement of a dental post creates an unnatural restored structure since it fills the root canal space with a material that has a defined stiffness unlike the pulp. Hence it is difficult to recreate the original stress distribution within the tooth in order to avoid fractures. Therefore, post systems must be carefully selected to reduce the incidence of root fractures and to preserve the root if failure occurs.

Commercially, there are two types of post systems; cast and prefabricated posts are usually adopted to rehabilitate the root canal and provide retention for the crown. Cast post, made directly by the dentist or indirectly by a dental technician, was considered to be the safest way to restore an endodontically treated tooth (Shillingburg et al., 1970). However, prefabricated posts have become more popular due to their clinical convenience and promising results in *in vitro* root fracture resistance studies (Fredriksson et al., 1998; Fokkinga et al., 2004). The main advantage deriving from its usage is that a limited preparatory work is generally required, subsequently saving time and money (Baraban, 1988; Stockton, 1999; Torbjörner, 2000; Torbjörner and Fransson, 2004a). Metal and ceramic prefabricated posts exhibit higher elastic moduli than dentine and studies have shown that there are greater stress around the apices of these posts during loading resulting in oblique and middle root fractures (Cormier et al., 2001; Akkayan and Gulmez, 2002; Newman et al., 2003). Fibre posts are another type of prefabricated posts currently available in the market. They are characterized by different physical properties, chemical composition and handling (Asmussen et al., 1999; Drummond et al., 1999). However, stress concentration may be focused at the cervical region leading to either fracture of the crown and post at coronal region or at the post-dentine interface causing debonding of posts and movement of the core which could then result in microleakage (Sorensen et al., 2001).

In order to overcome at least one of the above mentioned shortcomings, the concept of FGMs was applied as described in the earlier Chapters.

Computerized models have proven to be useful in simulating the simultaneous interaction of the many variables affecting a restorative system. Finite element analysis (FEA) is a computer-based numerical method developed to solve the different equations. The geometric model of the structure is built and subdivided into small elements. Stress and strain distributions in response to various loading conditions can be simulated with the assistance of computers provided by dedicated software. As a consequence, evaluations in detail of the mechanical behaviour of the restorative systems may be performed (Ausiello et al., 2001). If correctly validated, FEA could be helpful in optimizing restorative design criteria and material choice and in predicting the fracture potential of restorations under given conditions (Zarone et al., 2006).

5.2 Aim

The aim of this chapter was to determine the mechanical behaviour of three newly designed FGSPs as alternative type of posts compared to titanium and zirconia posts which can be considered as homogenous-type in design when subjected to various directions of loading.

5.3 Objectives

The objectives are:

1. To investigate the von Mises stress distribution within the tooth and along the centre of the posts.
2. To analyse the von Mises stress distribution at the post and surrounding structures interface.
3. To investigate the compressive stress distribution within the tooth and along the centre of the posts.
4. To analyse the compressive stress distribution at the post and surrounding structures interface.
5. To investigate the tensile stress distribution within the tooth and along the centre of the posts.
6. To analyse the tensile stress distribution at the post and surrounding structures interface.
7. To analyse the shear stress distribution at the post and surrounding structures interface.
8. To analyse the strain distribution at the post and surrounding structures interface.

5.4 Materials and method

5.4.1 Generation of external volume of 3D model

A CT scan (Siemens, Germany) of a patient who attended the Department of Biomedical Imaging, University of Malaya Medical Centre was obtained (Ethics NO: DF OS0901/0006(1). The inclusion criteria were patient with complete dentition and fully formed maxillary incisors. The CT scan images of pixels size of 0.4235 and 512 resolutions were imported into the image processing software (Mimics® 13.1, Materialise, Leuven, Belgium) by using digital imagining and communication (DICOM) and 361 images was imported to Mimics® (Figure 5.1). The different hard tissues visible on the scans were then identified using Mimics® based on image density thresholding (Figure 5.2). This tool gives effective information in non-invasive mapping of the anatomy of various subjects. Hence, the right maxillary central incisor and its supporting structure were reconstructed by cropping the selected areas (Figure 5.3).

Once the tooth and its supporting structures were isolated, segmentation process was commenced. Segmentation is a process that consists of separating an object of interest from other adjacent anatomical structures in different groups or masks, such as tooth, bone as illustrated in Figure 5.4 (a-c). A 3D image was automatically generated in the form of masks by growing a threshold region on the entire stack of scans.

After that, smoothing, triangle reduction and remeshing (Figure 5.5 a-c) were carried out on model in Mimics® 13.1 to create a suitable model for FEA. The remesh module attached to Mimics® 13.1 was used to automatically reduce the amount of triangles and simultaneously improve the quality of the triangles while maintaining the geometry. During remeshing, the tolerance variation from the original data was specified. The quality is defined as a measure of a triangle's height/base ratio so that the file could be imported in the FEA software. After creating the external volume of the 3D model which are tooth and bone components in Mimics® 13.1, the model was saved as a (*.INP) file prior to importing into ABAQUS/CAE software, Professional Version (Simulia, Valley St., Providence, USA).

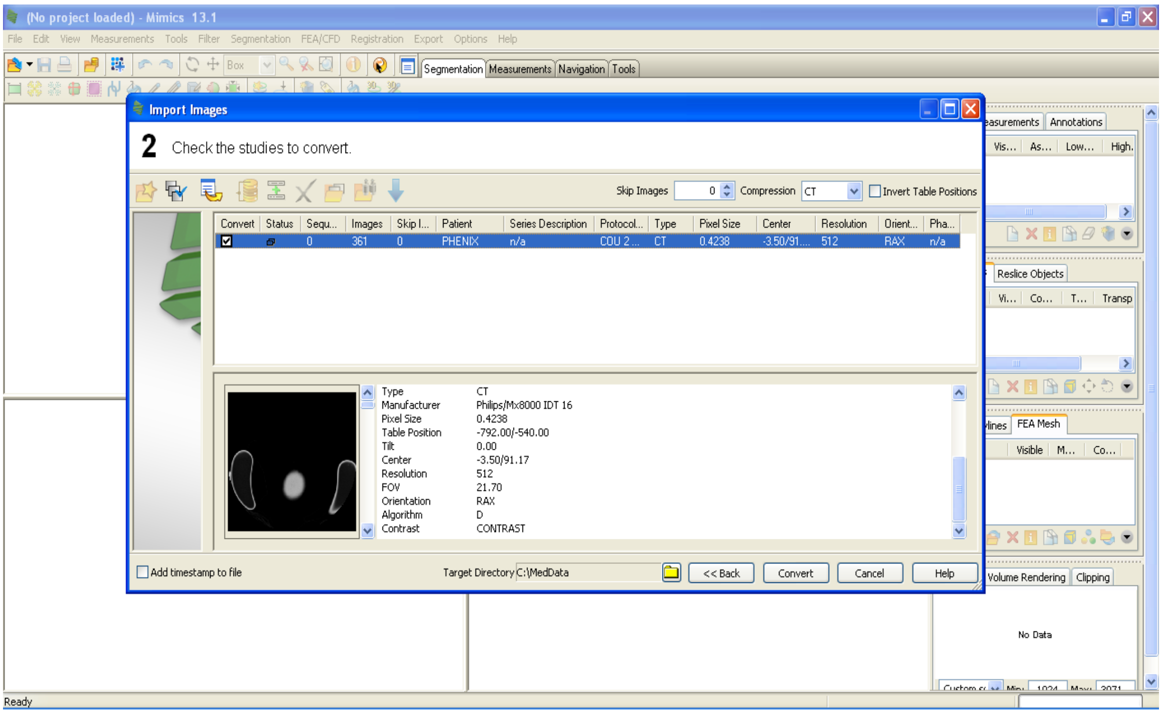

Figure 5.1 Image slices inserted into image processing software (Mimics® 13.1).

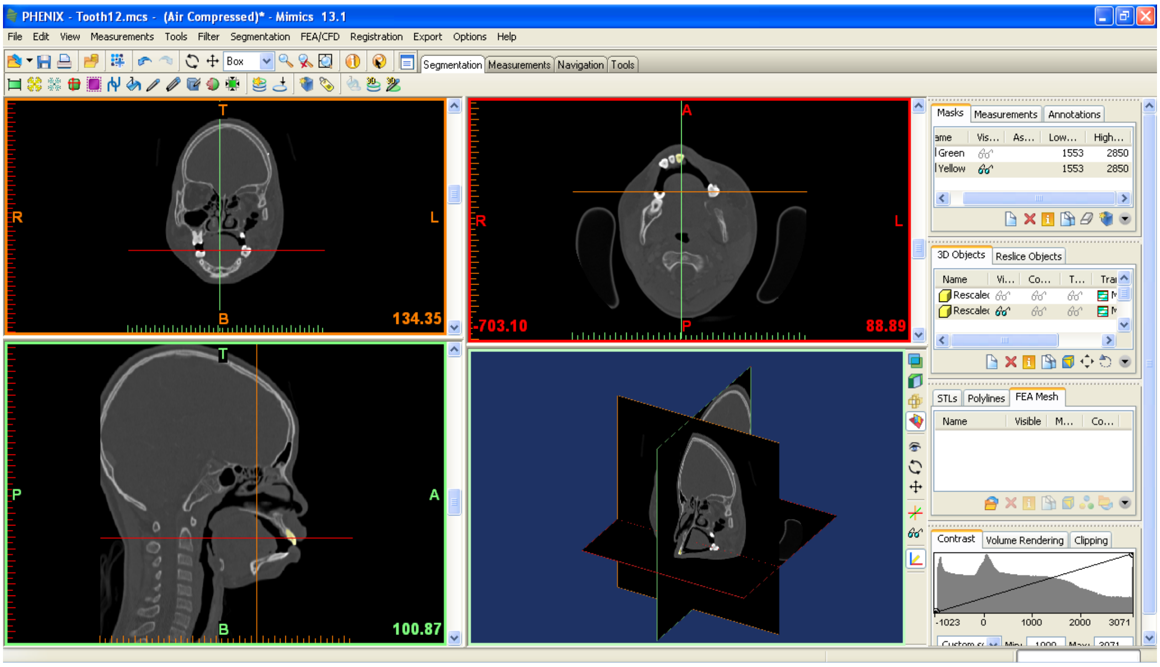

Figure 5.2 CT scan data as seen in Mimics® 13.1 where the selected maxillary central incisor is isolated. Masked was applied to the tooth and supporting structures.

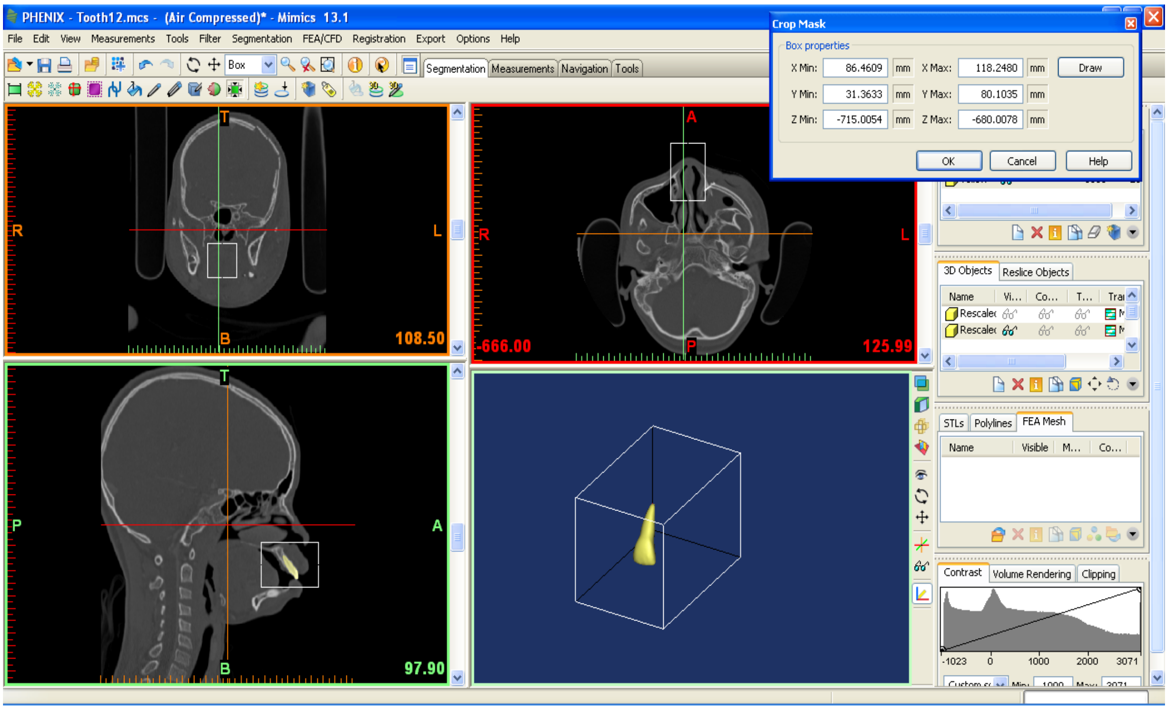

Figure 5.3 Images of tooth and bone are isolated from each other by defining the proper range of threshold values.

(a) Tooth

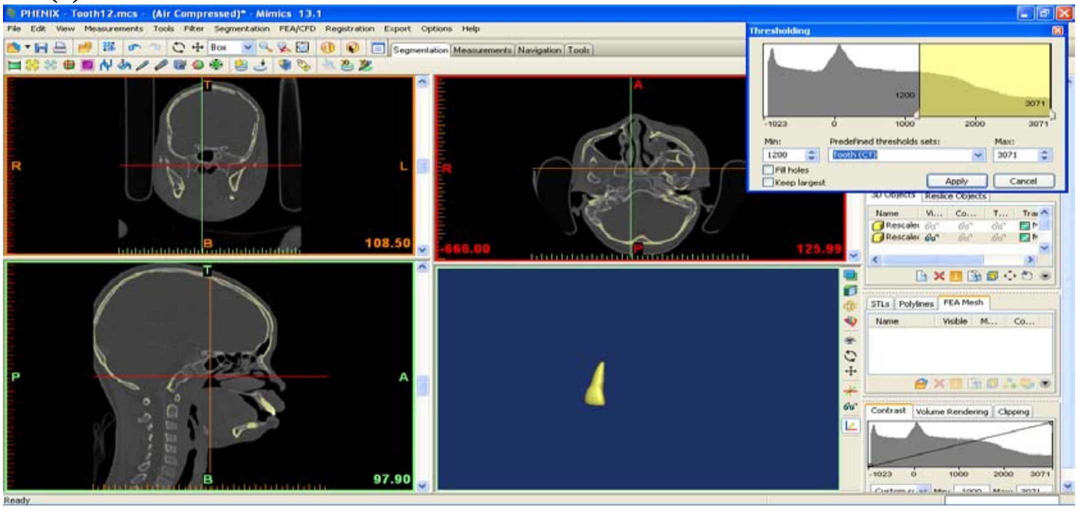

(b) Cancellous bone

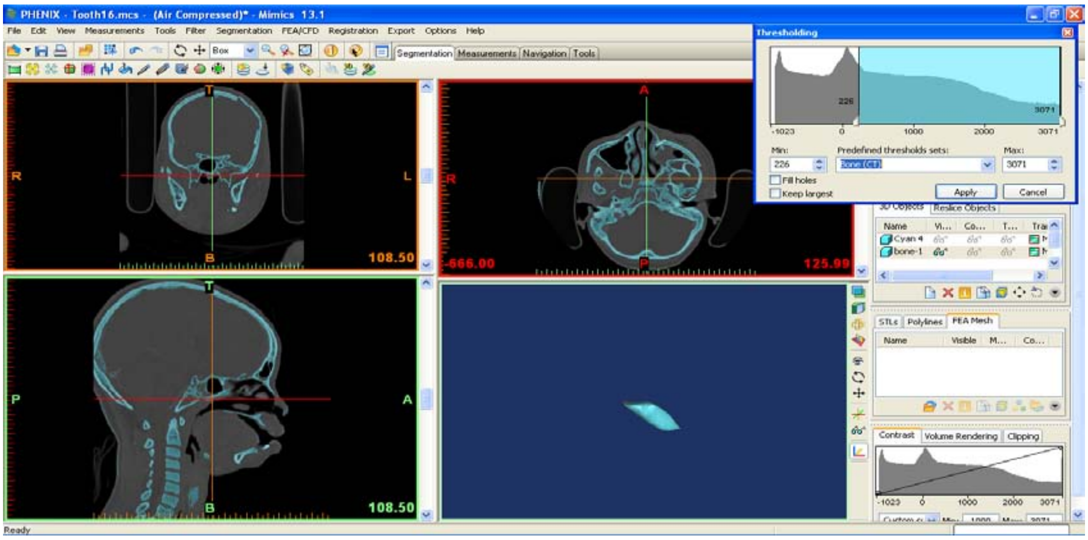

(c) Compact bone

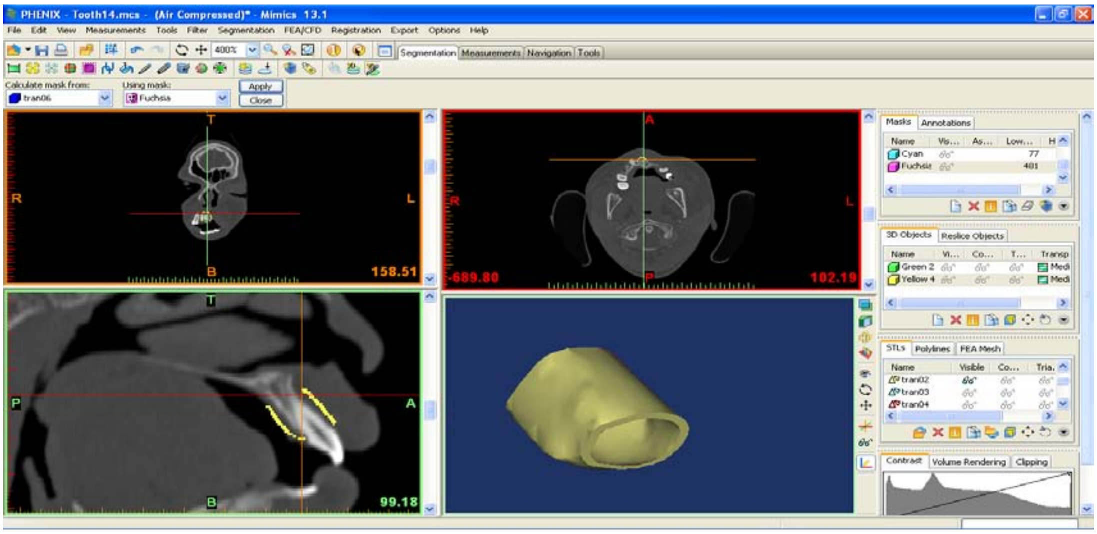

Figure 5.4 Segmentation of object of interest (tooth, cancellous bone and compact bone) from other adjacent anatomical structures by applied masks.

(a) Smoothing

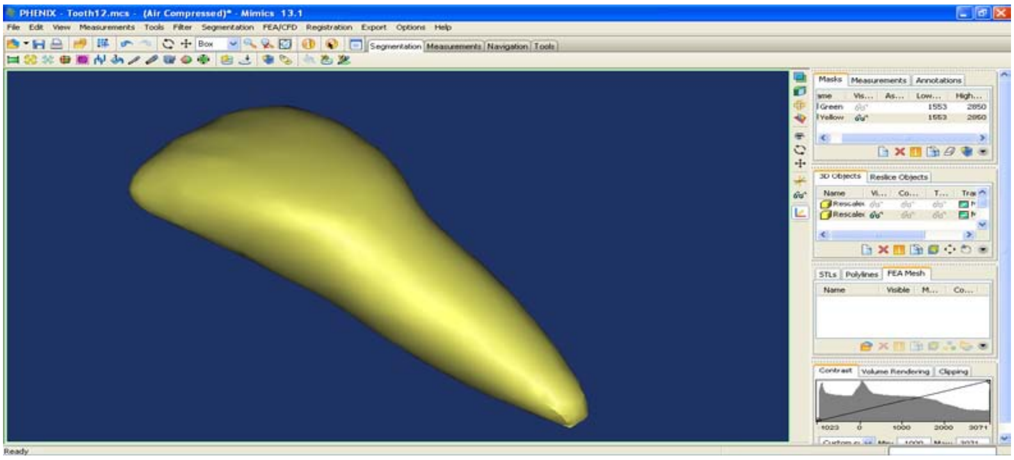

(b) Triangle reduction

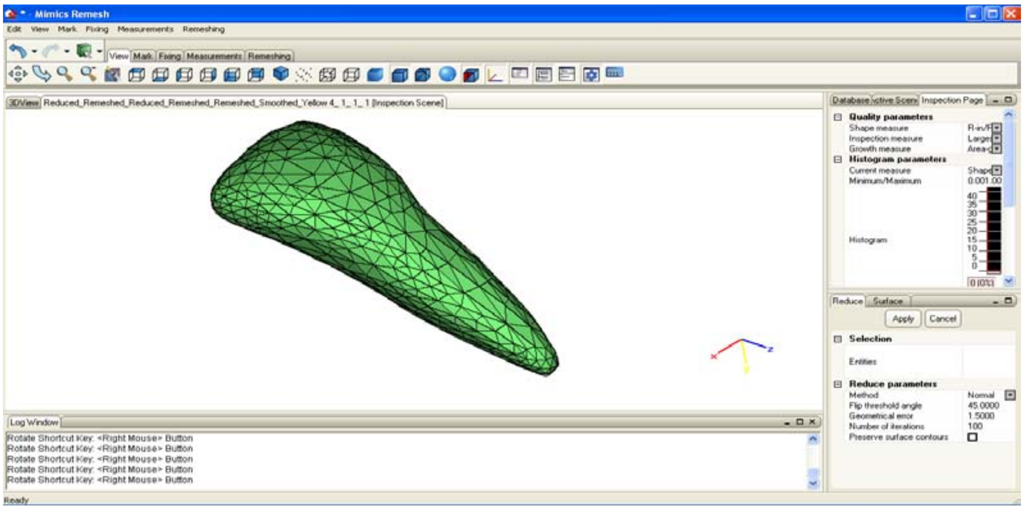

(c) Remeshing

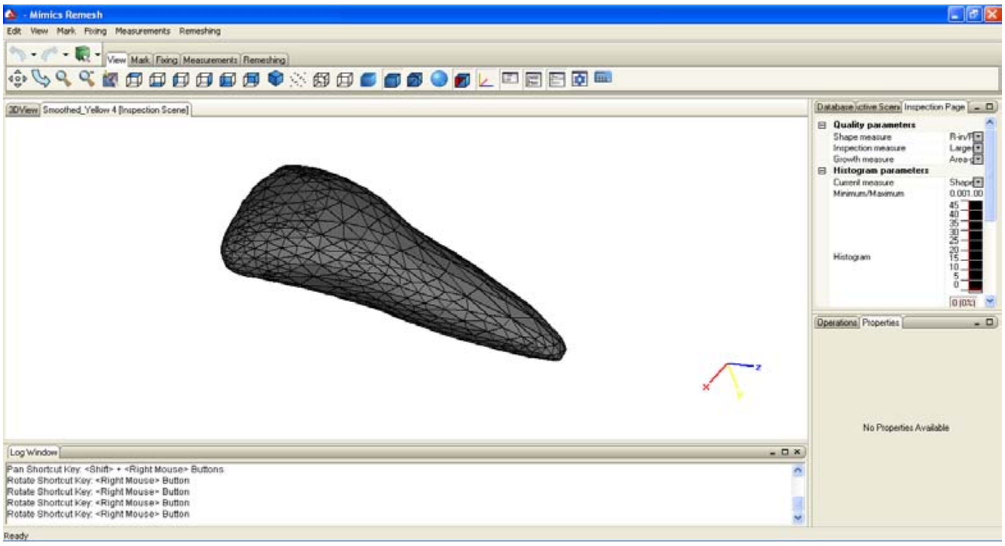

Figure 5.5 Smoothing, triangle reduction and remeshing are carried out in mimics® 13.1 creating a suitable three dimensional model for finite element analysis.

5.4.2 Generation of internal volume of 3D model

Defining the periodontal ligament from CT scan images is difficult due to its thin structure and the pixel size of 0.4235 mm. Thus periodontal ligament of 0.18 mm thick was generated based on the isocurves of the dentine in ABAQUS (Rees and Jacobsen, 1997). The internal volume of the 3D model was then generated by adding dentine, enamel and restorative components (Figure 5.6). The dimension of each component were based on the data from literature (Wheeler, 1974; Pegoretti et al., 2002; Asmussen et al., 2005; Genovese et al., 2005; Zarone et al., 2006; Santos et al., 2009).

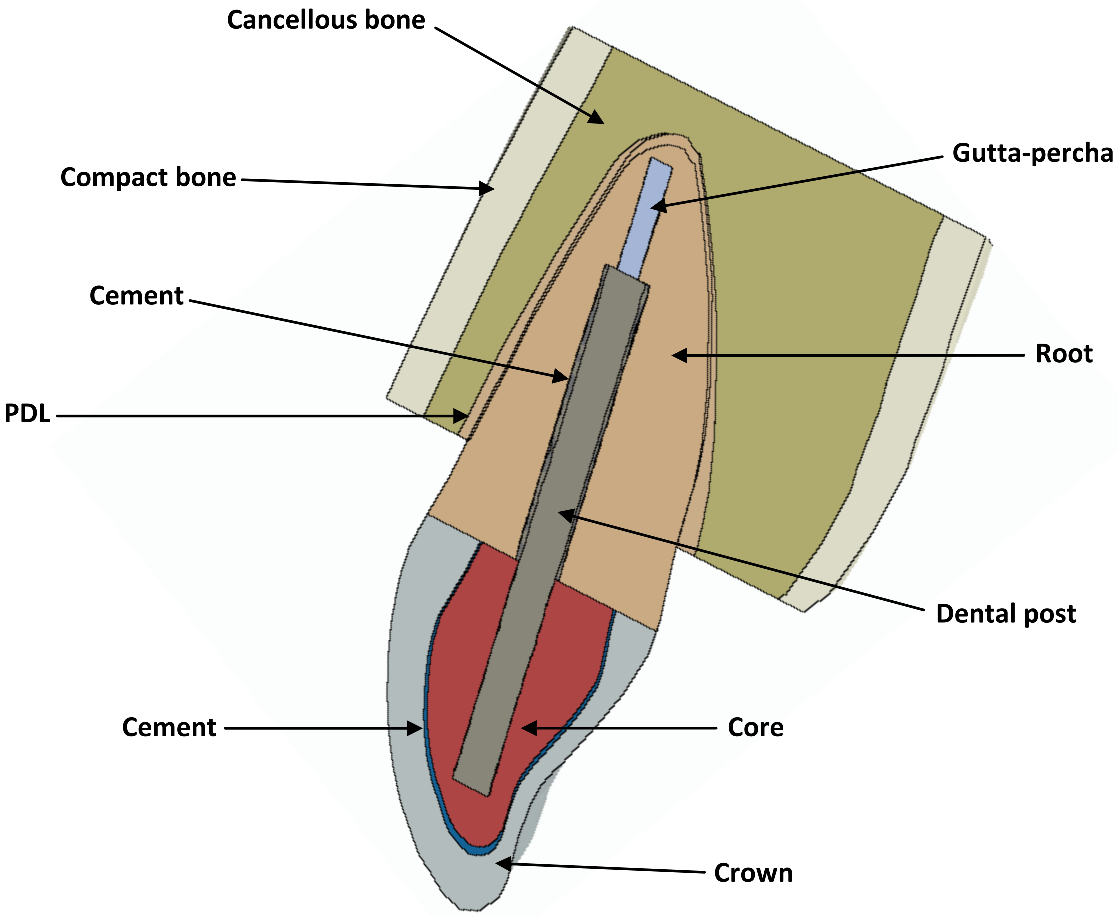

Figure 5.6 Schematic illustration of the three dimensional geometric model.

5.4.3 Mesh generation

Mesh generation is an important procedure to subdivide the solid geometry of a FE model into smaller elements and ABAQUS provides a number of different meshing techniques. Free meshing technique was adopted and tetrahedral elements were used to separate the model due to the complicated geometries of the models thus the convergence was achieved. In this study, it was preferred to use four nodes first order linear tetrahedral solid elements (C3D4) for the stress analysis. The C3D4 was used with fine meshes to obtain accurate data as constant stress tetrahedral elements exhibit slow convergence (ABAQUS, 2005). A tetrahedral mesh of 150465 was used after a pilot study revealed that the error remained below 0.1% for two mesh sizes of 150465 and 239906 (Figure 5.7).

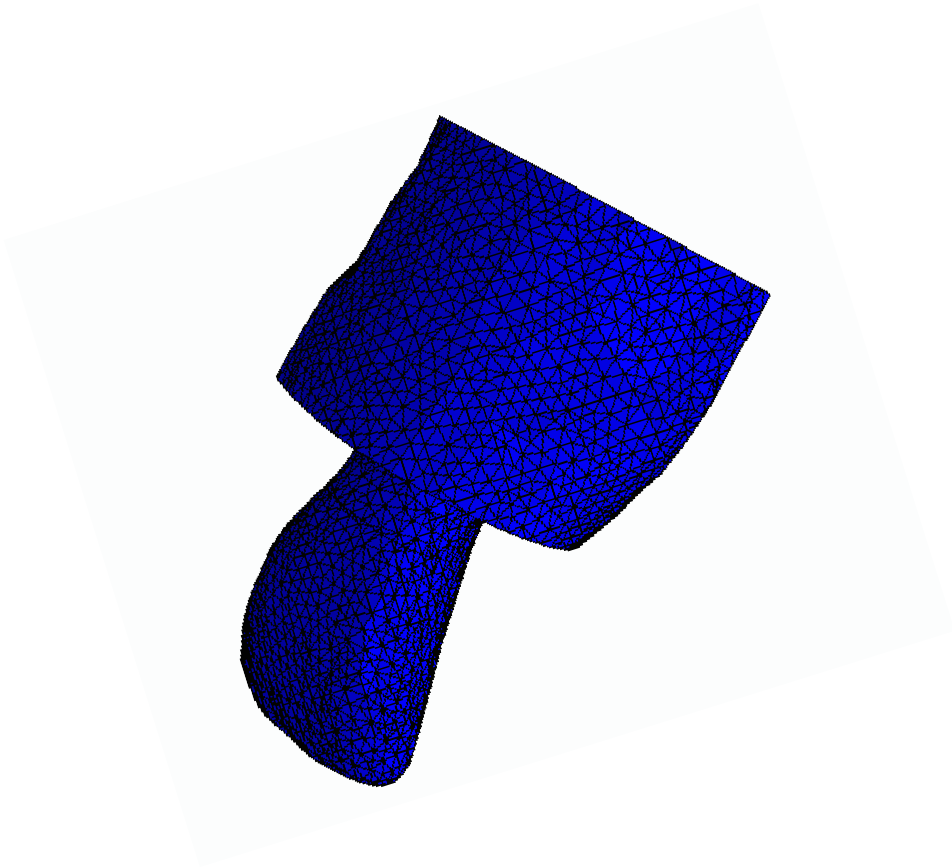

Figure 5.7 Tetrahedral mesh structure of the three dimensional finite element model.

5.4.4 Boundary condition

Displacements were disregarded as the boundary conditions for the nodes were along the bottom end line of the models, fixed to the supporting structure of the central incisor as prescribed by the system (Yang et al., 2001a).

Three different loading conditions were chosen:

(i) A vertical load applied on the top of the crown to simulate loading during bruxism; P_1 = 100 N (Joshi et al., 2001; Genovese et al., 2005).

(ii) An oblique load, angled at 45°, to simulate the masticatory force; P_2 = 100 N (Joshi et al., 2001).

(iii) A horizontal load to simulate external traumatic forces; P_3 = 100 N (Joshi et al., 2001; Genovese et al., 2005).

All forces were applied on the aforementioned area as distributed pressure. Any stresses that are likely to be introduced during the endodontic treatment were neglected.

5.4.5 Restorative materials and elastic properties

Mechanical properties of the restorative materials were created for each part of the FE model. The materials used for modeling each part of model tooth parts were assumed to be linearly elastic, isotropic and homogeneous. The modulus of elasticity of FGSPs (Models A-C) was obtained experimentally as mentioned in Chapter 3. However, the Poisson's ratio of FGSPs (Models A-C) was calculated by rule of mixture (Wakashima et al., 1990). The elastic properties of titanium (Model D) and zirconia (Model E) posts and other restorative materials used in the geometric model are presented in Table 5.1. Any stresses that are likely to be introduced during the endodontic treatment were neglected.

A natural tooth (Model F), whose stiffness is equal to those of enamel and dentine was considered as a reference model.

Table 5.1 Elastic properties of restorative materials

No	Materials	modulus of elasticity (GPa)	Poisson's ratio
1	Root[a, b]	18.60	0.32
2	Enamel[a, b]	84.1	0.33
3	Titanium[c]	116	0.33
2	Periodontal ligament[e]	0.69×10^{-4}	0.45
3	Compact bone[d]	13.70	0.30
	Cancellous bone[d]	1.37	0.30
4	Gutta-percha[e]	0.14	0.45
5	Composite resin core[f]	16.60	0.24
6	Zirconia[g]	200	0.33
7	Ceramic crown[h]	120	0.24
8	Alumina[i]	380	0.25
9	Hydroxyapatite[j]	40	0.27
10	Cement[d]	22.4	0.25

[a] Asmussen et al. (1999), [a, b] Ferrari et al. (2000a, b), [c] Toparli (2003), [d] Holmes et al. (1996), [e] Ruse (2008), [g] Christel et al. (1989), [h] Pegoretti et al. (2002), [i] Hench (1991), [j] Hedia and Mahmoud (2004)

5.4.6 Finite element analysis

The generation of the FE model, calculation of the various stress distributions and processing were carried out using ABAQUS/CAE software, Professional Version (Simulia, Valley St., Providence, USA). Von Mises, compressive and tensile stresses were evaluated within the tooth, along the centre of the posts and at post and surrounding structures interfaces. The shear stress and strain distributions was also investigated at the post and surrounding structures interfaces.

5.5 Results

5.5.1 Stress distribution in the tooth and at the centre of the posts

5.5.1.1 Von Mises stress distribution

Figure 5.8 shows the von Mises stress distribution on an obliquely loaded tooth model restored with various types of posts (Models A-E) and a natural tooth (Model F). Maximum von Mises stress concentrated at the coronal third of the root both on the labial and palatal aspect of the tooth near to the cemento-enamel junction (CEJ) level and spreading towards the apical third.

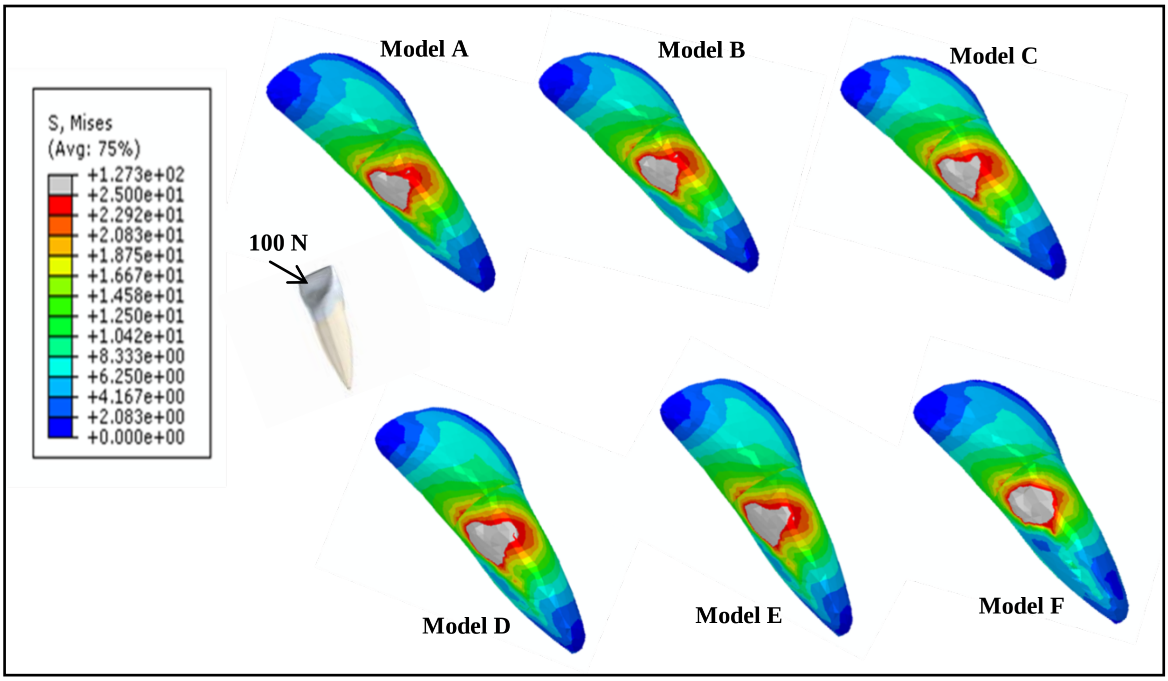

Figure 5.8 Contour plots of the von Mises stress distribution under oblique loading.

Higher stress distribution was observed at the CEJ and coronal third of the root, both on the palatal or labial aspect, progressively decreased towards the inner part of the tooth (Figure 5.9). The maximum von Mises stress concentration was seen inside the zirconia and titanium posts (Figure 5.9). However, lower von Mises stress concentration were observed for FGSPs (Models A-C) and natural tooth (Model F).

The von Mises stress distribution for the FGSPs (Models A-C), titanium (Model D) and zirconia (Model E) along the centre of the posts when loaded obliquely is shown in Figure 5.10. The maximum von Mises stress concentration within the post was observed in models D and E. However, the FGSPs models revealed lower von Mises stress at different regions along the posts (Figure 5.10). In general, the von Mises stress started to build up from coronal region and slightly decrease towards the apical with maximum stress of 34.50 MPa (Model E), 26.94 MPa (Model D), 16.86 MPa (Model C), 16.92 MPa (Model B) and 16.96 MPa (Model A).

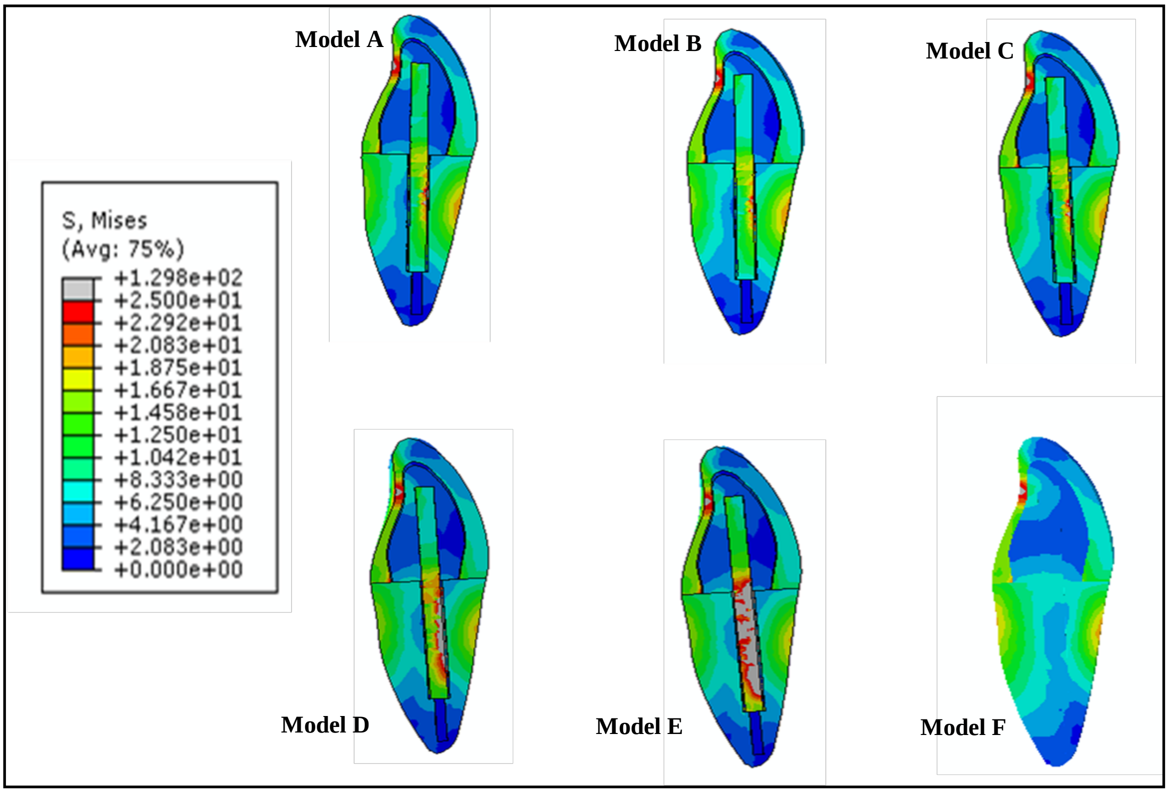

Figure 5.9 Von Mises stress distribution within the tooth and the posts under oblique loading.

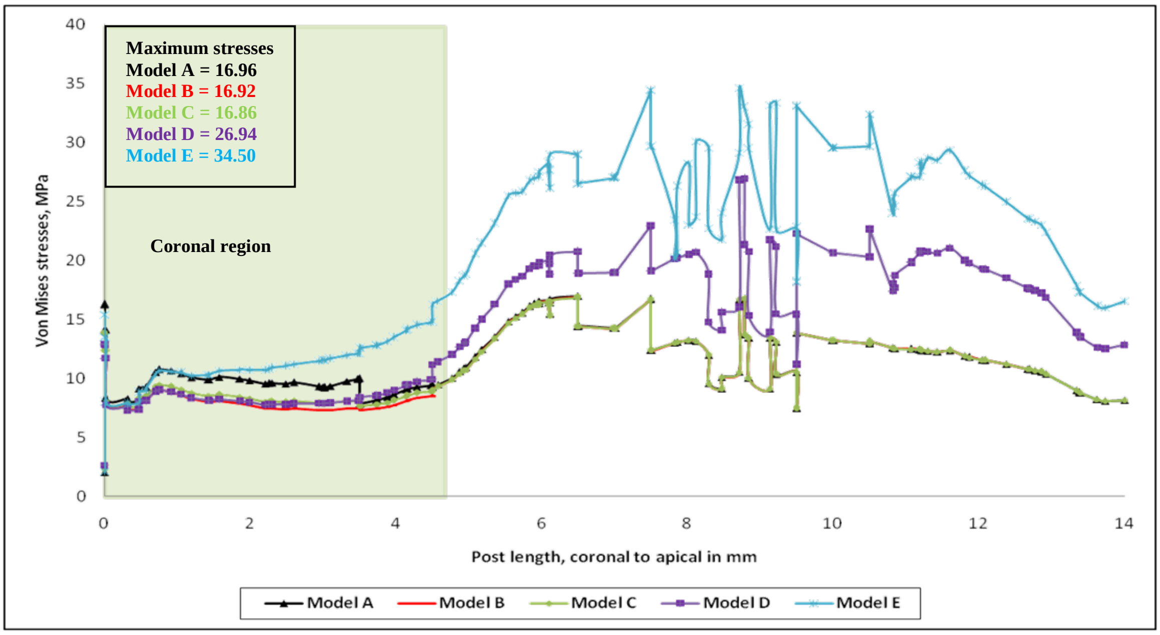

Figure 5.10 Von Mises stress distribution along the centre of the post when loaded obliquely.

When horizontal loading was applied, similar von Mises stress distribution was observed (Figures 5.11 and 5.12). However, the magnitude of the von Mises stress distribution under horizontal loading was higher than oblique loading. This was also reflected in the von Mises stress distribution along the centre of the posts (Figure 5.13). The maximum von Mises stress distribution was the highest in Model E (46.98 MPa) followed by Model D (29.26 MPa). However, the maximum von Mises stress in the three FGSPs models remains almost similar at 19.83 MPa, 19.85 MPa and 19.64 MPA for Models A, B and C respectively.

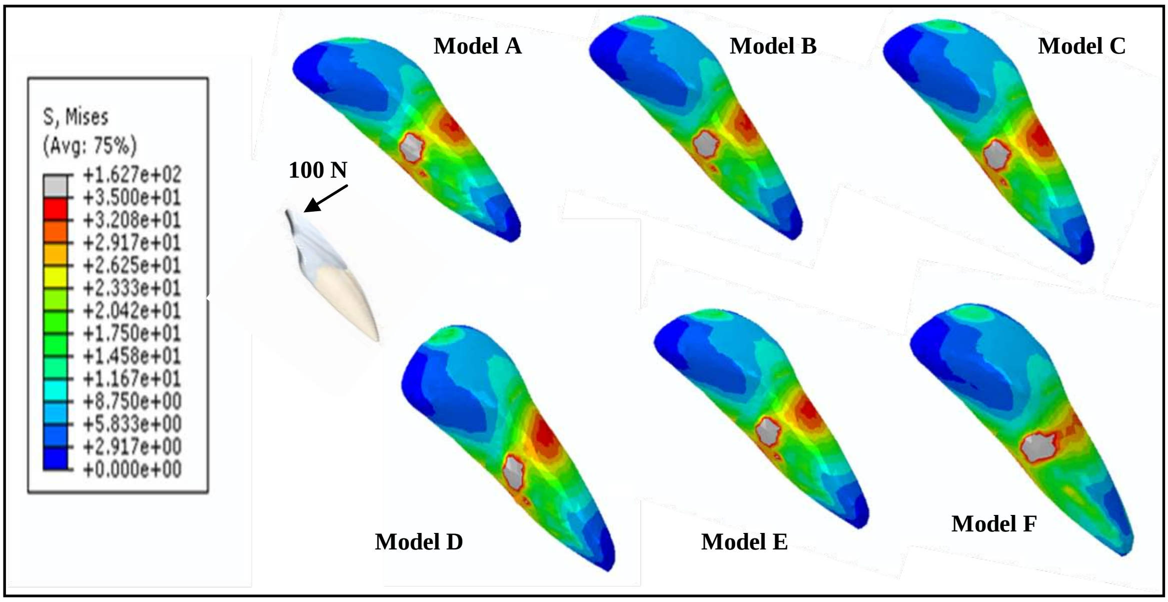

Figure 5.11 Contour plots of the von Mises stress distribution under horizontal loading.

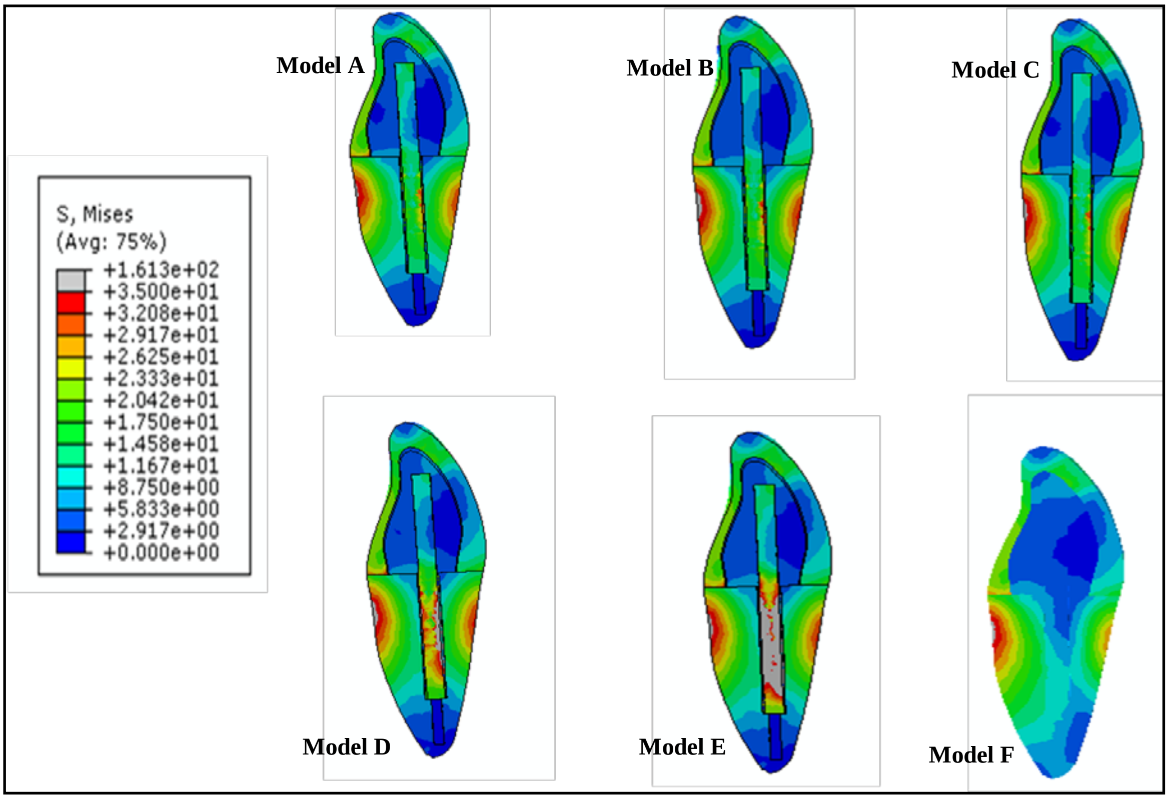

Figure 5.12 Von Mises stress distribution within the tooth and the posts under horizontal loading.

.

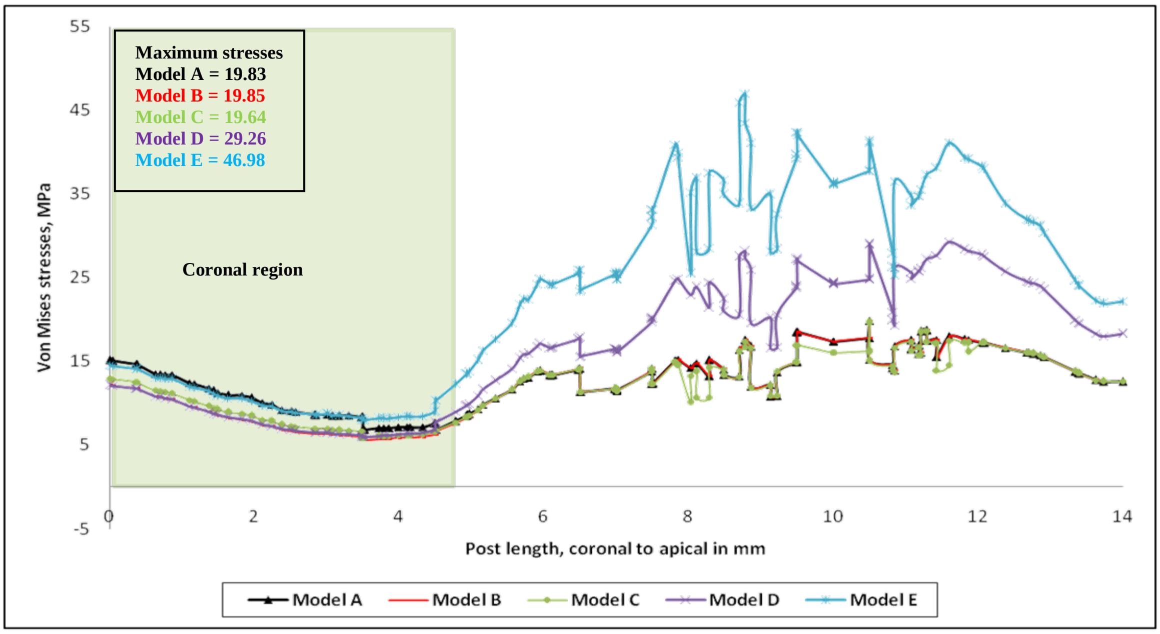

Figure 5.13 Von Mises stress distribution along the centre of the post when loaded horizontally.

Although the von Mises stress distribution was similar when the tooth was loaded vertically (Figures 5.14 and 5.15), the magnitude of the von Mises stress distribution was higher than oblique loading, but it was lower than horizontal loading. This is again reflected in the von Mises stress distribution along the centre of the post where the maximum stress of 45.26 MPa (Model E), 29.01 MPa (Model D), 18.04 MPa (Model C), 18.03 MPa (Model B) and 18.07 MPa (Model A) as shown in Figure 5.16.

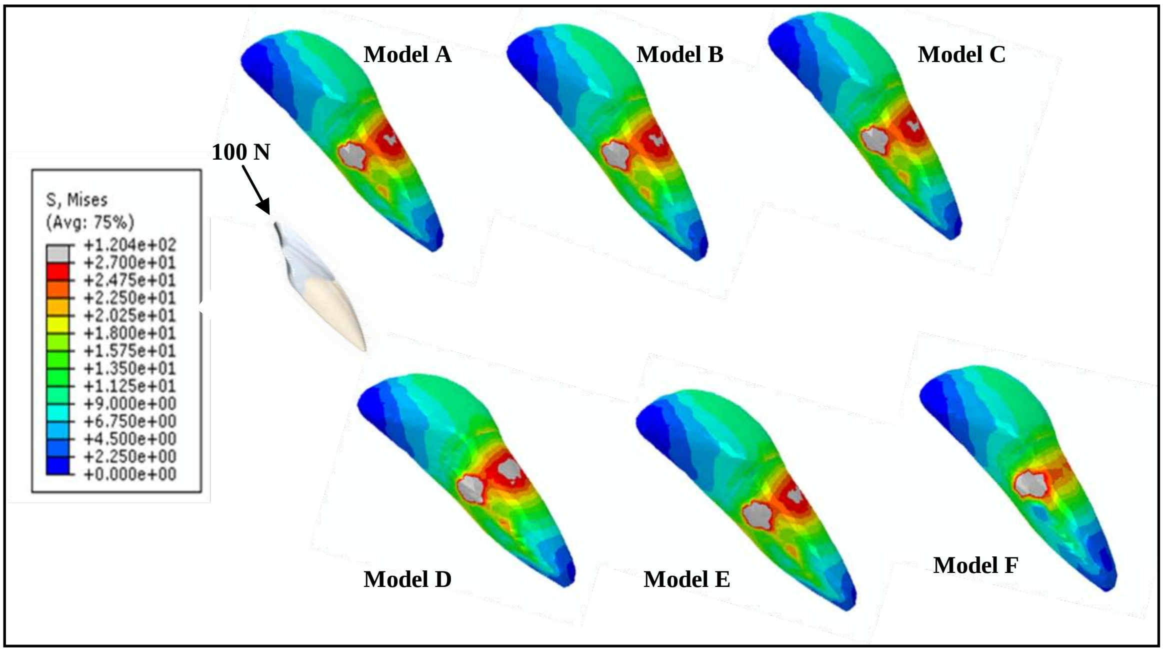

Figure 5.14 Contour plots of the von Mises stress distribution under vertical loading.

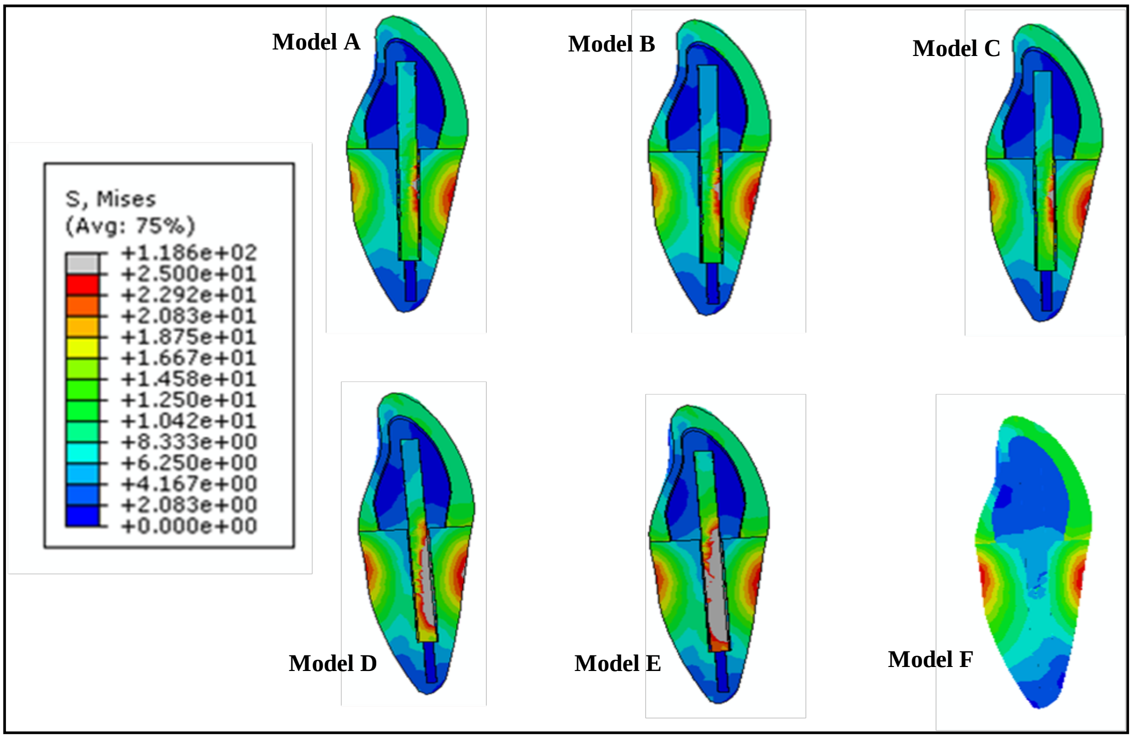

Figure 5.15 Von Mises stress distribution within the tooth and the posts under vertical loading.

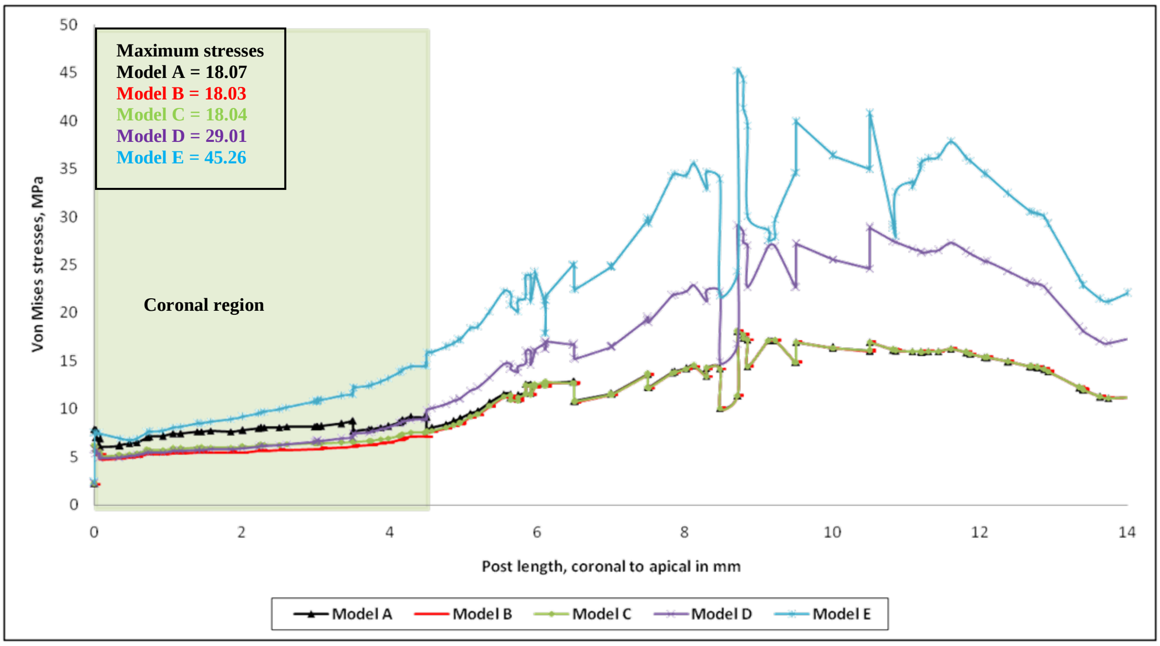

Figure 5.16 Von Mises stress distribution along the centre of the post when loaded vertically.

The improvement in the average von Mises stress values under oblique, horizontal and vertical loadings for FGSPs (Models A-C) compared to titanium (Model D) and zirconia (Model E) posts was calculated in percentage as shown in Table 5.2. The reduction in the average von Mises stress values by FGSPs compared to titanium and zirconia posts is highlighted in Table 5.2. The percentage difference in average von Mises stress values amongst the three FGSPs was not high.

Table 5.2 Percentage difference in average von Mises stress value along the centre of the post loaded under various loading directions

Model comparison	**Percentage difference in average von Mises stress values (MPa)**		
	Oblique loading	**Horizontal loading**	**Vertical loading**
A and B	4.76	4.96	5.71
A and C	3.47	4.92	5.28
A and D	22.83	24.60	26.64
A and E	44.97	48.12	49.88
B and C	1.33	0.04	1.50
B and D	26.50	28.34	30.84
B and E	47.59	50.69	52.74
C and D	25.51	28.31	29.79
C and E	46.88	50.67	52.02
D and E	28.69	31.19	31.67

5.5.1.2 Compressive stress distribution

Figure 5.17 shows the compressive stress distributions under oblique loading for all models, where high compressive stress were recorded at the middle third of the labial aspect of the root surface. Models D and E showed considerably higher compressive stress concentration at the middle and apical regions of the posts compared to FGSPs (Models A-C) as illustrated in Figure 5.17. Generally, these stress progressively decreased from the outer to the inner part of the root dentine and from the CEJ towards the incisal margin of the crown as well.

Compressive stress distribution along the centre of the posts for FGSPs (Models A-C), titanium (Model D) and zirconia (Model E) when loaded obliquely is shown in Figure 5.18. The maximum compressive stress concentrations were observed in the Models D and E. However, the FGSPs models displayed low compressive stress distribution at different regions along the post. The compressive stress started to build up from coronal region and slightly decreased towards the apical with maximum stress of -31.45 MPa (Model E), -20.87 MPa (Model D) -13.12 MPa (Model C), -13.13 MPa (Model B) and -13.32 MPa (Model A).

Similar compressive stress distribution was observed when horizontal loading was applied (Figure 5.19) except that the compressive stress was observed at the middle third of the palatal aspect of the root. However, compressive stress distribution under oblique loading was higher than horizontal loading. This was also reflected in the compressive stress distribution along the centre of the posts (Figure 5.20) where the compressive stress distribution was higher for Model E (-21.09 MPa) and Model D (-12.01 MPa) compared to Models A, B and C (-11.99 MPa, -10.38 MPa, -11.10 MPa) respectively.

Similarly, when the tooth was loaded in the vertical direction, the same pattern of compressive stress distribution was observed (Figure 5.21). However, the magnitude of the compressive stress was higher than oblique and horizontal loadings. This was also observed in the compressive stress distribution along the centre of the posts (Figure 5.22). The maximum compressive stress was higher for Model E (-37.82 MPa) and Model D (-26.81 MPa). Interestingly, the maximum compressive stress in the FGSPs; Models A, B and C remains almost the same constant at -15.27 MPa, -15.27 MPa and -15.26 MPa respectively.

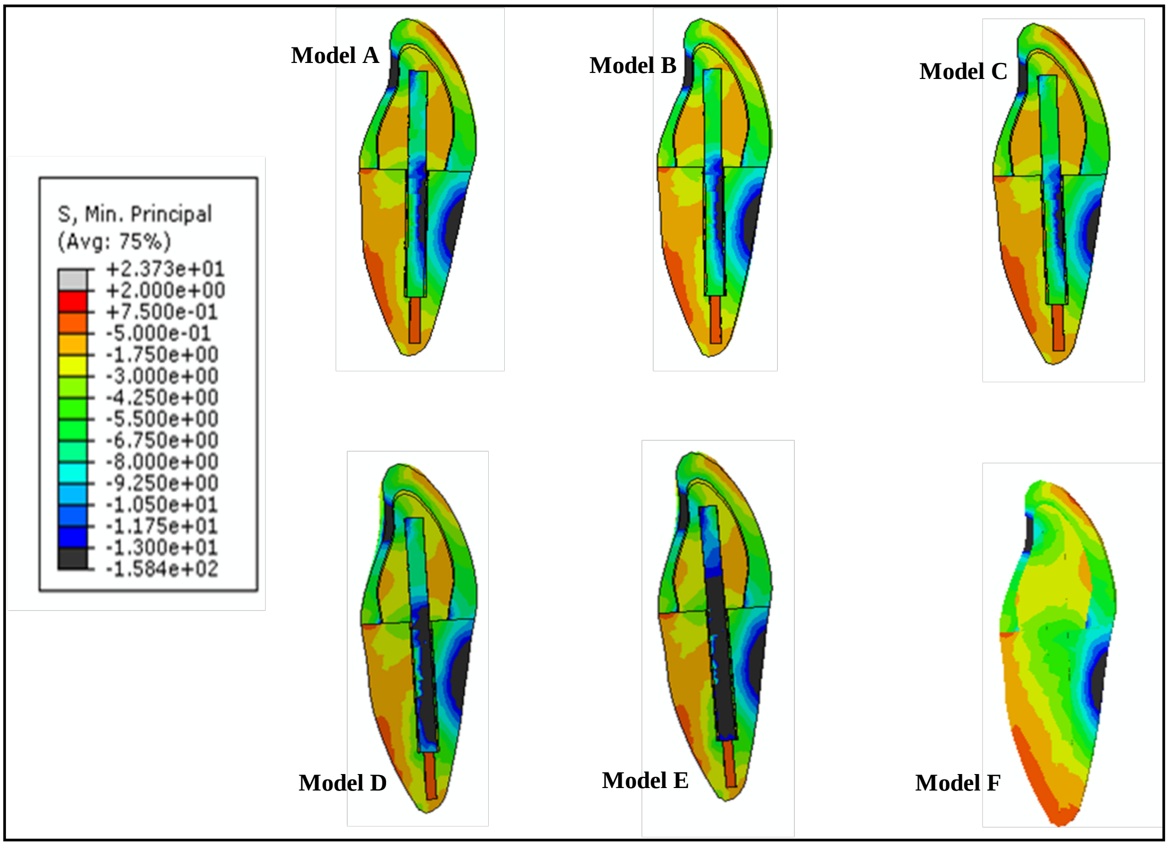

Figure 5.17 Contour plots of the compressive stress distribution within the tooth and the posts when loaded obliquely.

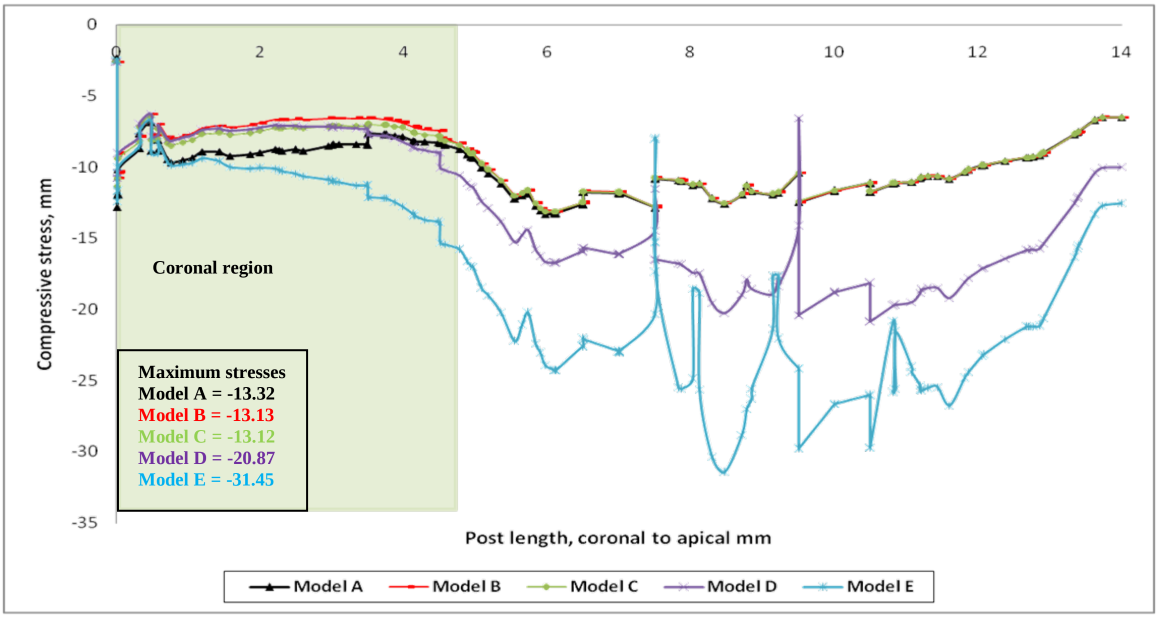

Figure 5.18 Compressive stress distribution along the centre of the post when loaded obliquely.

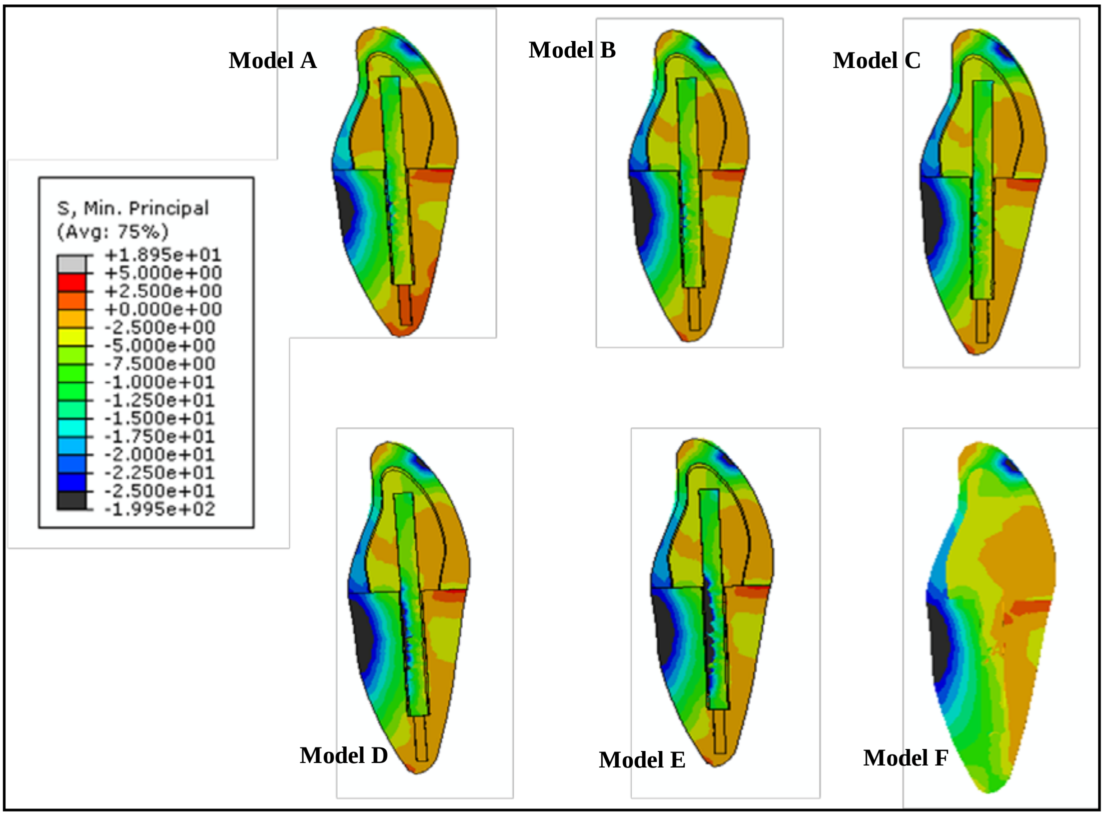

Figure 5.19 Contour plots of the compressive stress distribution within the tooth and along the centre of the posts when loaded horizontally.

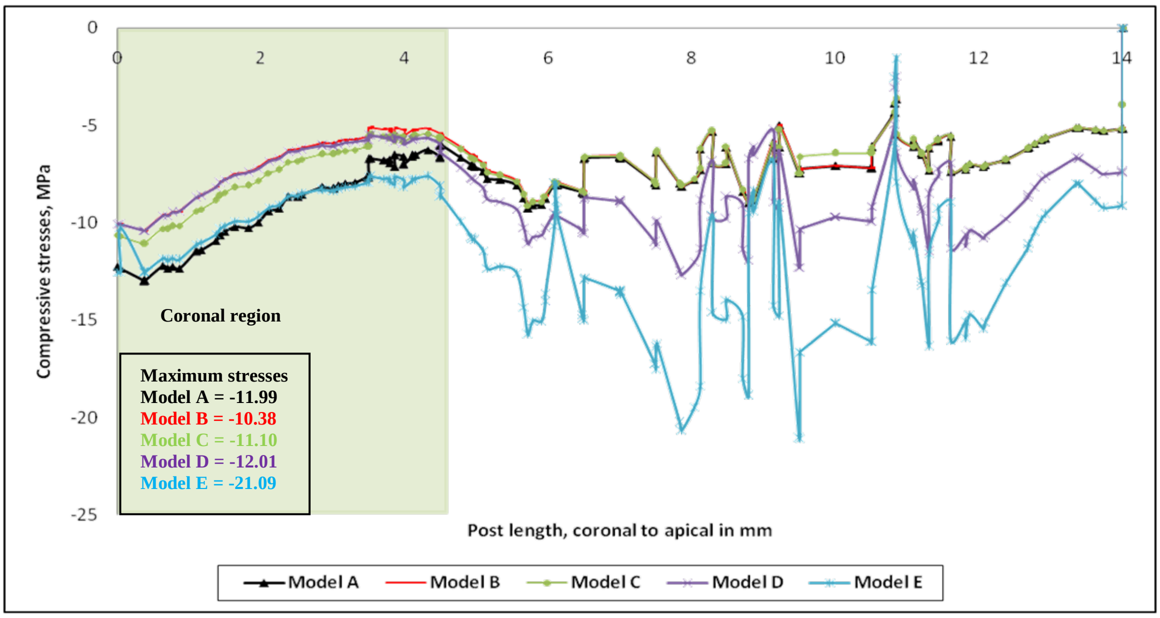

Figure 5.20 Compressive stress distribution along the centre of the post when loaded horizontally.

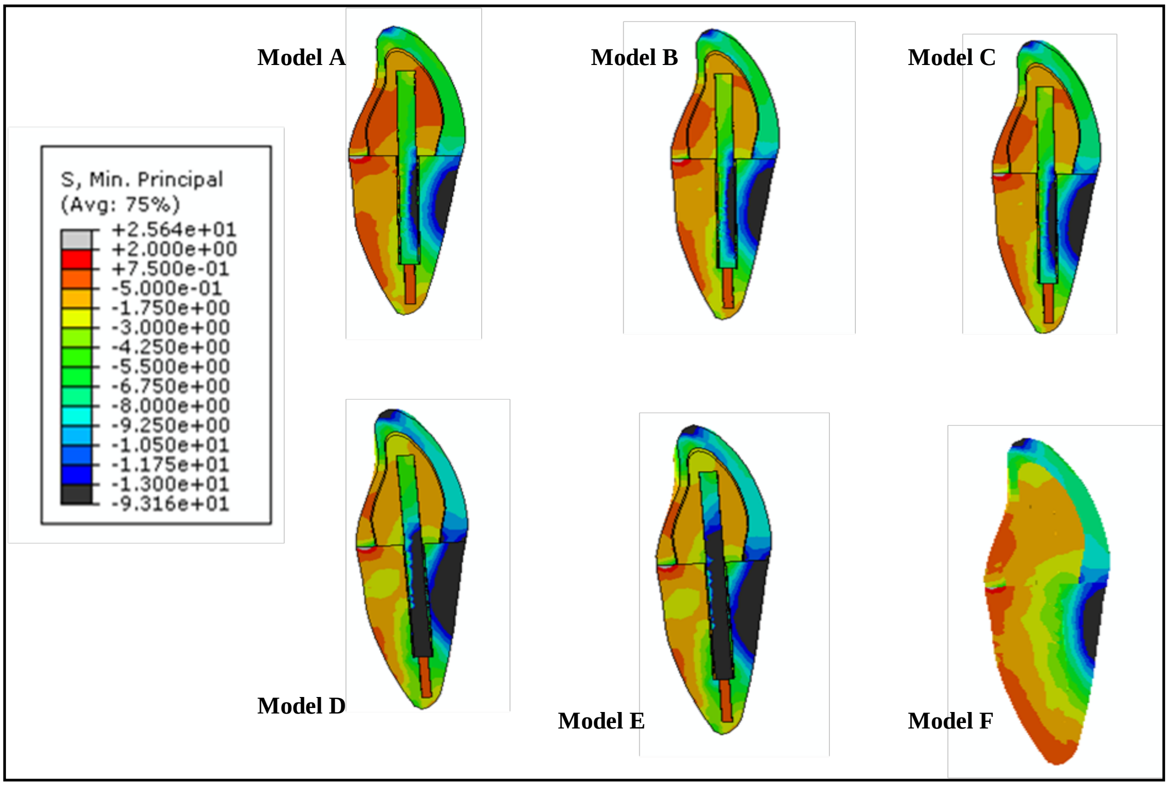

Figure 5.21 Contour plots of the compressive stress distribution within the tooth and the posts when loaded vertically.

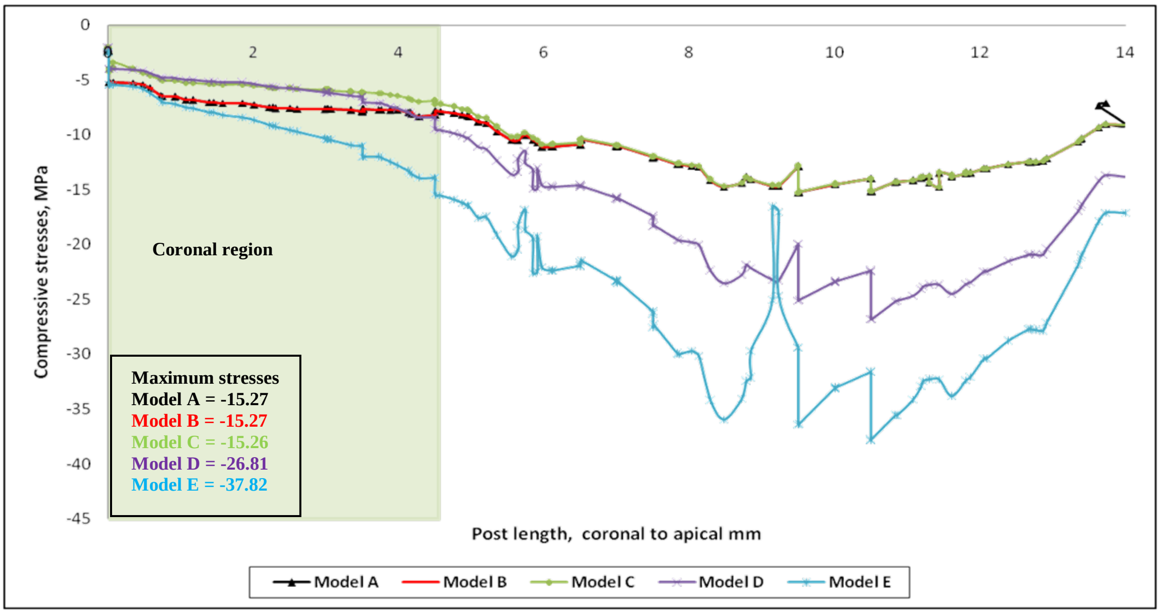

Figure 5.22 Compressive stress distribution along the centre of the post when loaded vertically.

The improvement in the average compressive stress values under oblique, horizontal and vertical loadings for FGSPs (Models A-C) compared to titanium (Model D) and zirconia (Model E) posts was calculated in percentage as demonstrated in Table 5.3. The reduction in the average compressive stress values by FGSPs compared to titanium and zirconia posts is highlighted in Table 5.3. The percentage difference in average compressive stress values among FGSPs was not high.

Table 5.3 Percentage difference in average compressive stress value along the centre of the post loaded under various loading directions

Model comparison	**Percentage difference in average compressive stress values (MPa)**		
	Oblique loading	**Horizontal loading**	**Vertical loading**
A and B	5.88	9.87	6.13
A and C	4.21	9.84	7.03
A and D	22.23	20.14	31.49
A and E	44.72	35.91	47.50
B and C	1.74	0.03	0.47
B and D	26.80	19.01	26.67
B and E	47.97	42.24	49.27
C and D	25.50	18.99	27.01
C and E	47.05	42.22	52.60
D and E	28.92	28.68	30.82

5.5.1.3 Tensile stress distribution

Figure 5.23 shows the tensile stress distribution under oblique loading for all models, where the higher tensile stress was recorded at the middle third of the palatal aspect of the root surface. Models D and E showed considerably higher tensile stress concentration at the middle and apical regions of the zirconia and titanium posts compared to FGSPs. Generally, the stress progressively decreased from the outer to the inner part of the root dentine and from the CEJ towards the incisal margin of the crown as well. Tensile stress distribution along the centre of the FGSPs, zirconia and titanium posts under oblique loading is shown in Figure 5.24. The maximum tensile stress concentrations within the posts were observed in the Models D and E. However, the FGSPs models displayed lower tensile stress distribution at different areas of the post in comparison to models D and E. The tensile stress started to build up from cervical region and slightly decreased towards the apex with maximum stress of 16.79 MPa (Model E), 10.50 MPa (Model D), 6.86 MPa (Model C), 6.87 MPa (Model B) and 6.85 MPa (Model A).

Tensile stress distribution tends to be centred at the root dentine area when loaded horizontally (Figure 5.25). Although, the tensile stress distribution were mainly recorded at the middle third of the labial aspect of the root when loaded horizontally. Tensile stress distribution under oblique loading was lower than horizontal loading. This was reflected in the tensile stress distribution along the centre of the posts (Figure 5.26). The maximum tensile stress was higher for Model E (32.31) and Model D (22.09 MPa) compared to Models A, B and C (12.45 MPa, 12.46 MPa and 12.26 MPa) respectively.

The tensile stress distribution concentrated at the middle third of the palatal aspect of the root when loaded vertically (Figure 5.27). Tensile stress distribution under vertical loading was lower than horizontal loading. This was again revealed in the tensile stress distribution along the centre of the posts (Figure 5.28). The maximum tensile stress distribution was higher for Model E (13.52) and Model D (9.12 MPa) compared to Models A, B and C (5.52 MPa, 5.11 MPa and 5.11 MPa) respectively.

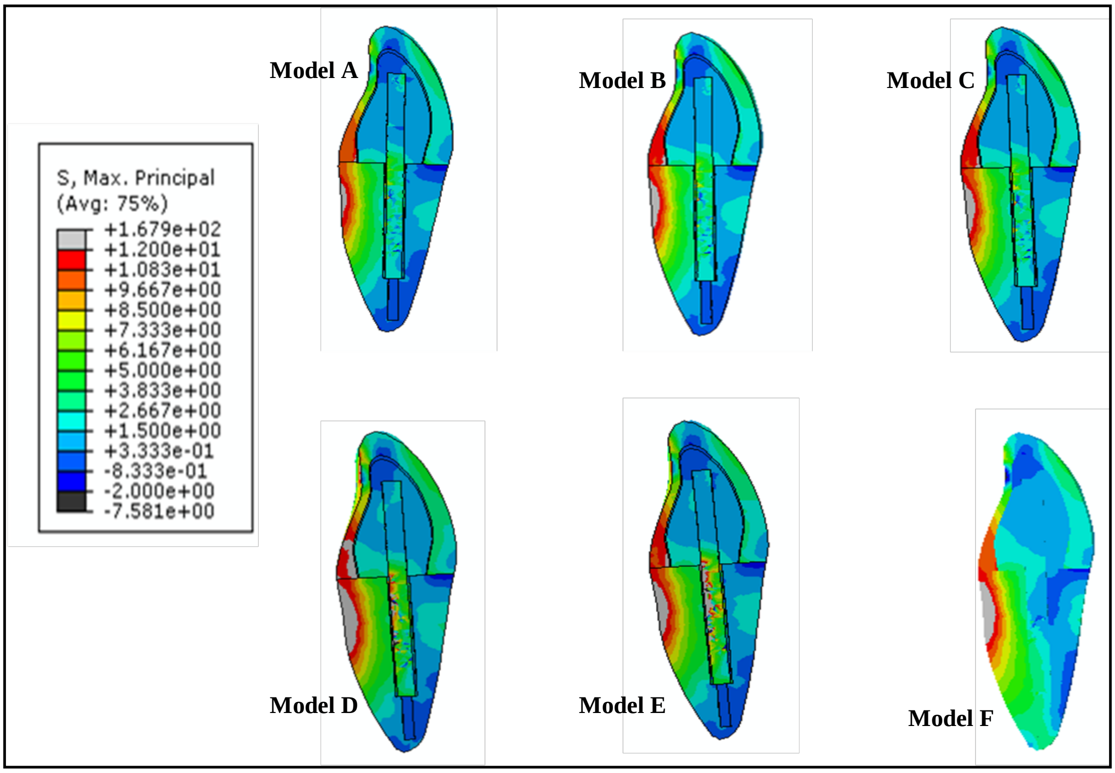

Figure 5.23 Contour plots of the tensile stress distribution within the tooth and the posts when loaded obliquely.

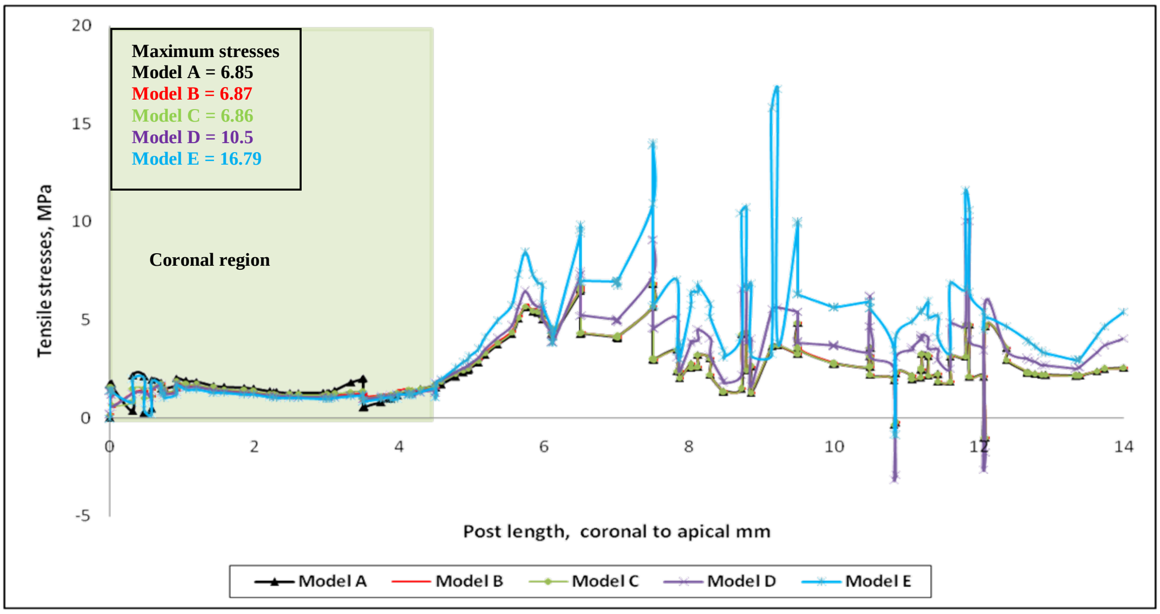

Figure 5.24 Tensile stress distributions along the centre of the post when loaded obliquely.

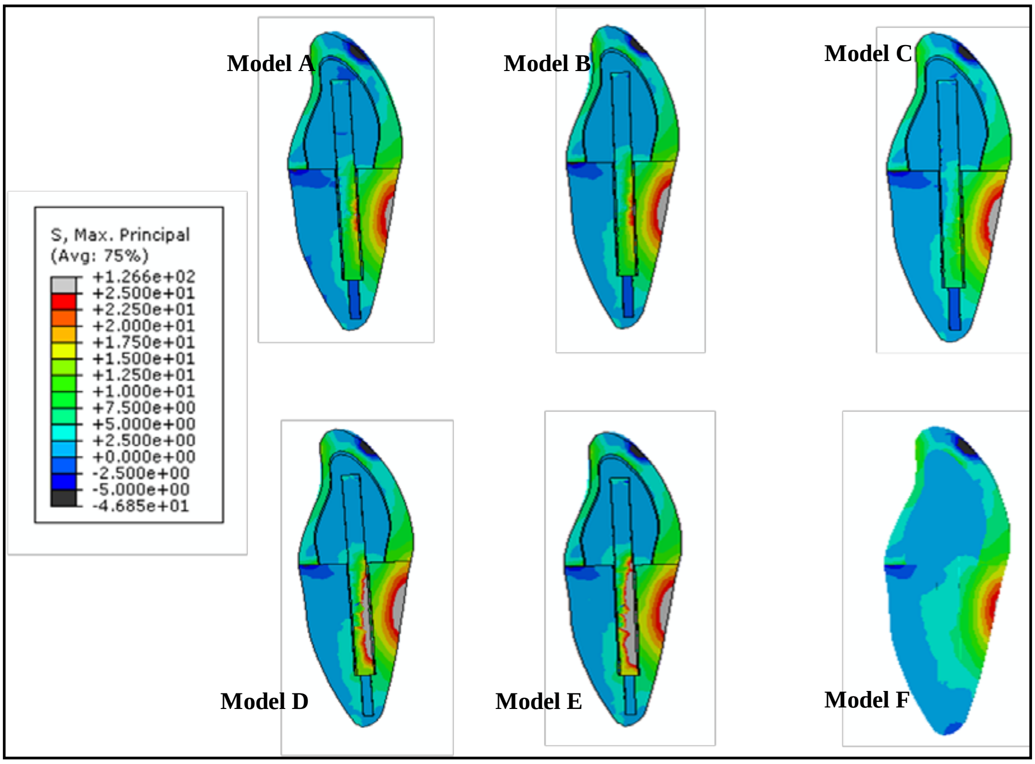

Figure 5.25 Contour plots of the tensile stress distribution within the tooth and the posts when loaded horizontally.

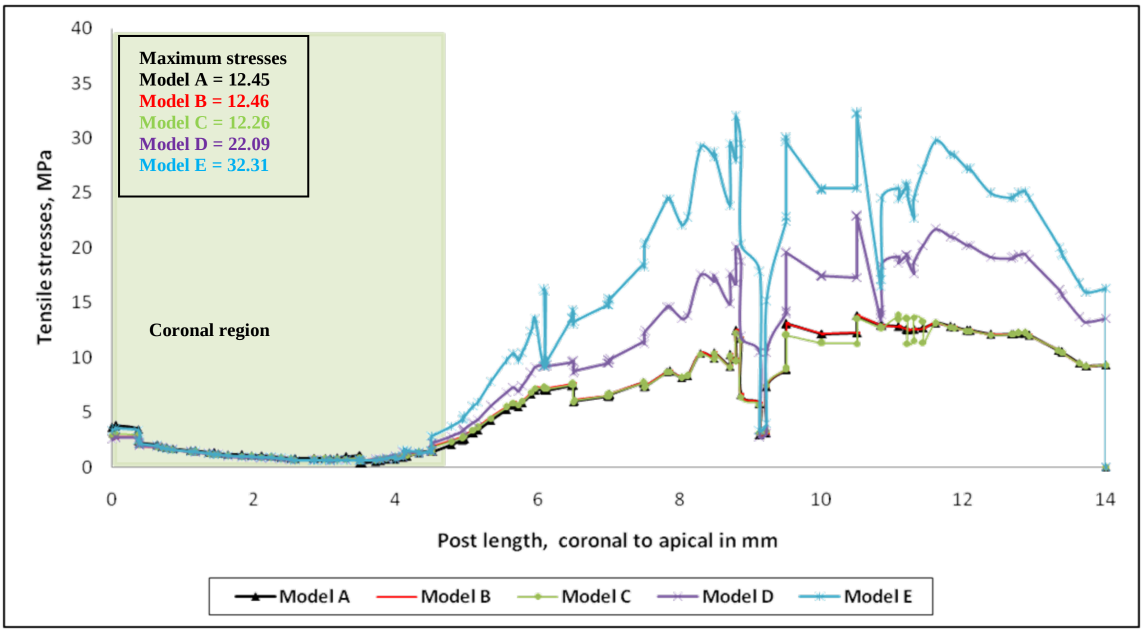

Figure 5.26 Tensile stress distributions along the centre of the post when loaded horizontally.

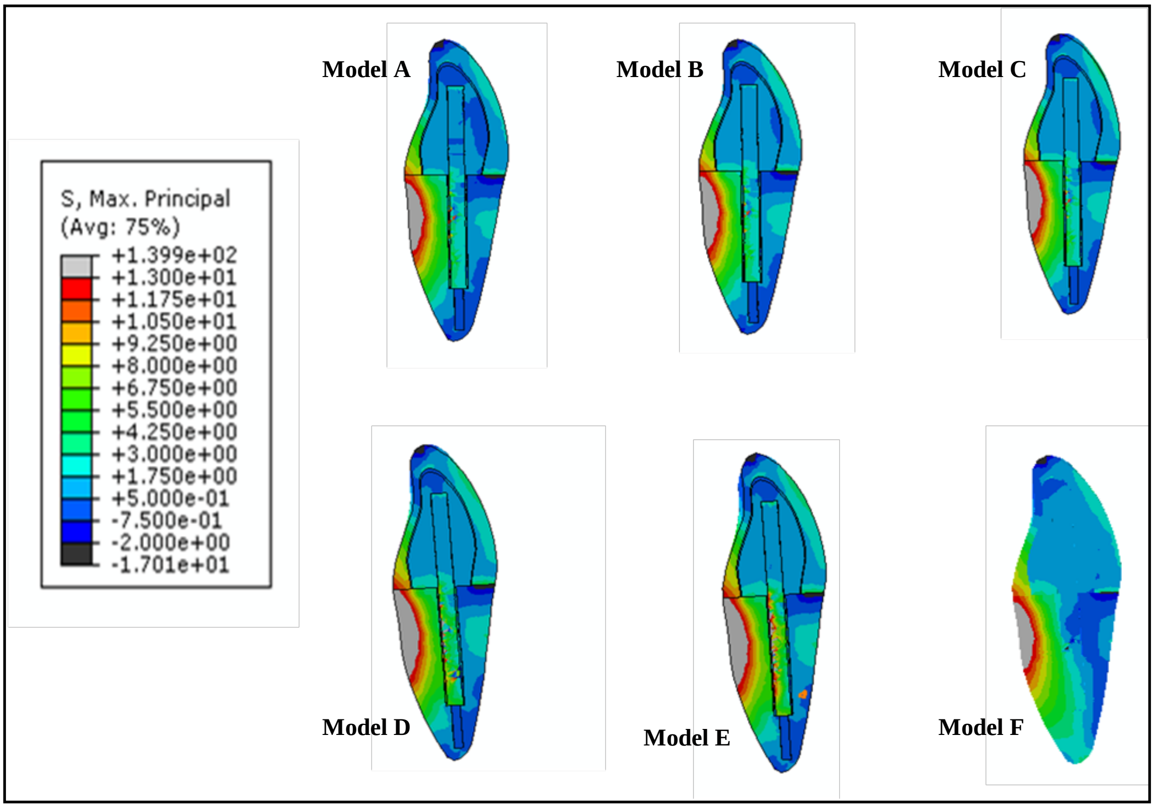

Figure 5.27 Contour plots of the tensile stress distribution within the tooth and the posts when loaded vertically.

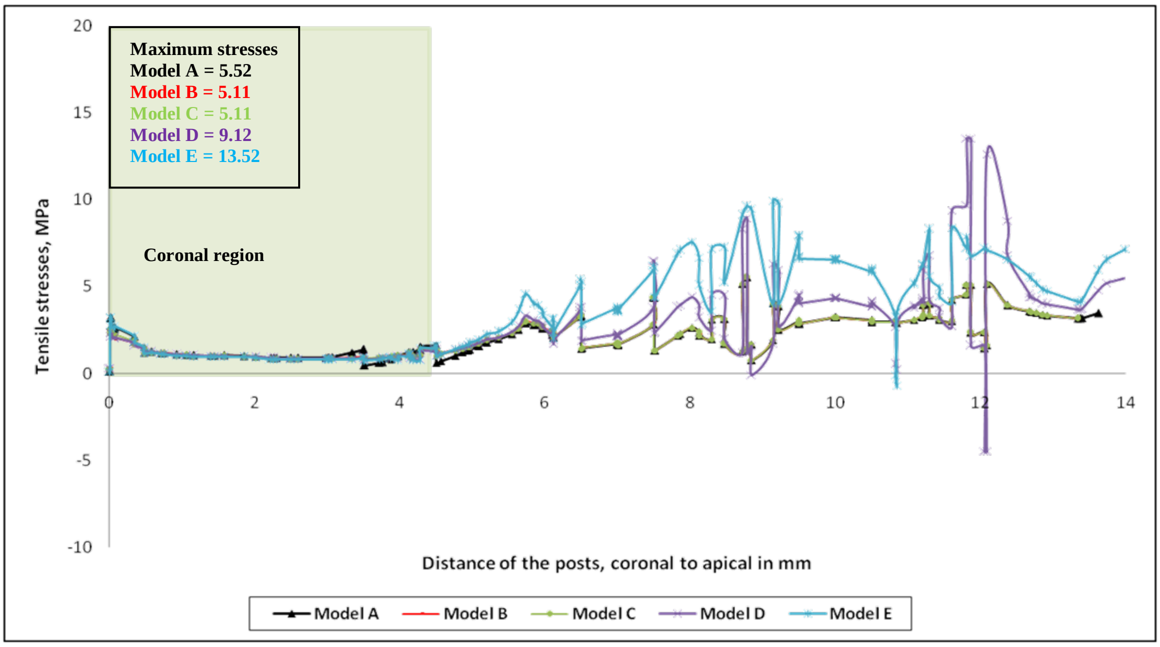

Figure 5.28 Tensile stress distributions along the centre of the post when loaded vertically.

The improvement in the average tensile stress values under oblique, horizontal and vertical loadings for FGSPs (Models A-C) compared to titanium (Model D) and zirconia (Model E) posts was calculated in percentage as presented in Table 5.4. The decrease in the average tensile stress values by FGSPs compared to titanium and zirconia posts is highlighted in Table 5.4. The high difference in average tensile stress values amongst FGSPs can be considered small.

Table 5.4 Percentage difference in average tensile stress values along the centre of the post loaded under various loading directions

Model comparison	**Percentage difference in average tensile stress values (MPa)**		
	Oblique loading	**Horizontal loading**	**Vertical loading**
A and B	1.42	1.31	2.08
A and C	0.72	-1.07	2.12
A and D	16.86	32.10	20.81
A and E	38.72	53.69	41.09
B and C	0.70	2.35	-0.04
B and D	18.04	32.99	22.46
B and E	39.59	54.30	42.32
C and D	17.47	31.38	22.47
C and E	39.16	53.19	42.34
D and E	26.29	31.79	25.61

5.5.1.4 Comparison among all average stresses along the centre of the post

Figures 5.29-5.31 show all the average stresses along the centre of the post under oblique, horizontal and vertical loadings. FGSPs showed lower von Mises stress compared to titanium and zirconia posts. Similarly this was also observed for the compressive and tensile stresses.

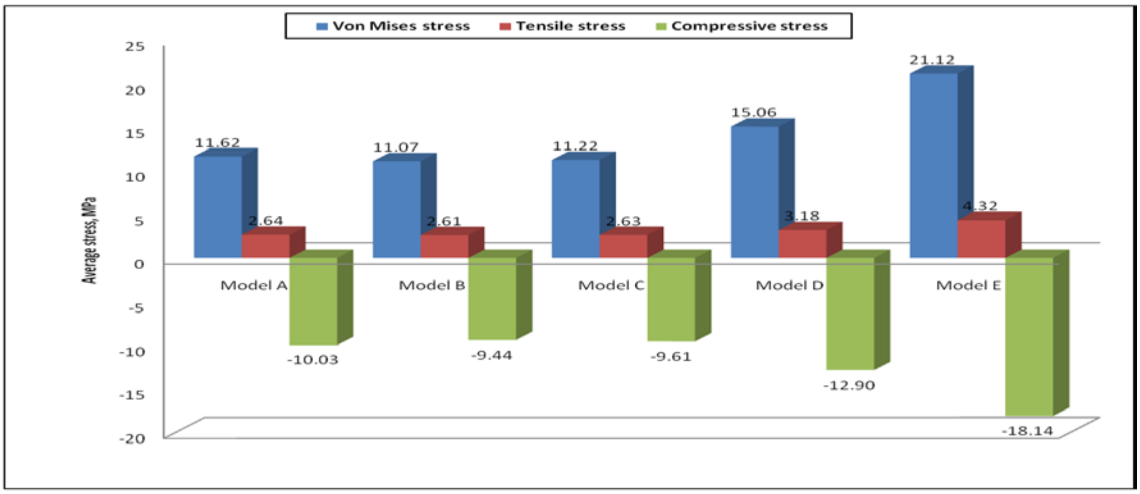

Figure 5.29 Comparison amongst all average stresses along the centre of the post under oblique loading.

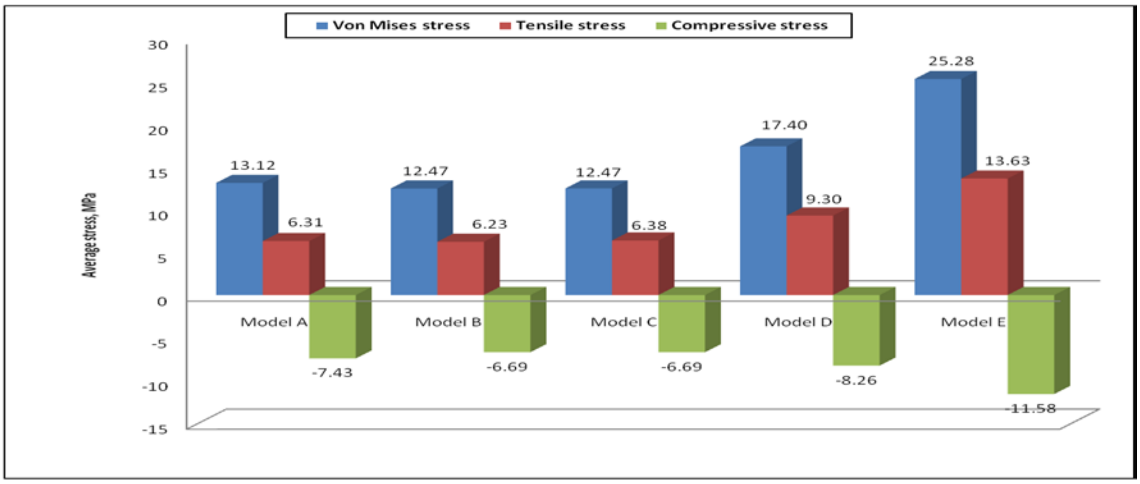

Figure 5.30 Comparison amongst all average stresses along the centre of the post under horizontal loading.

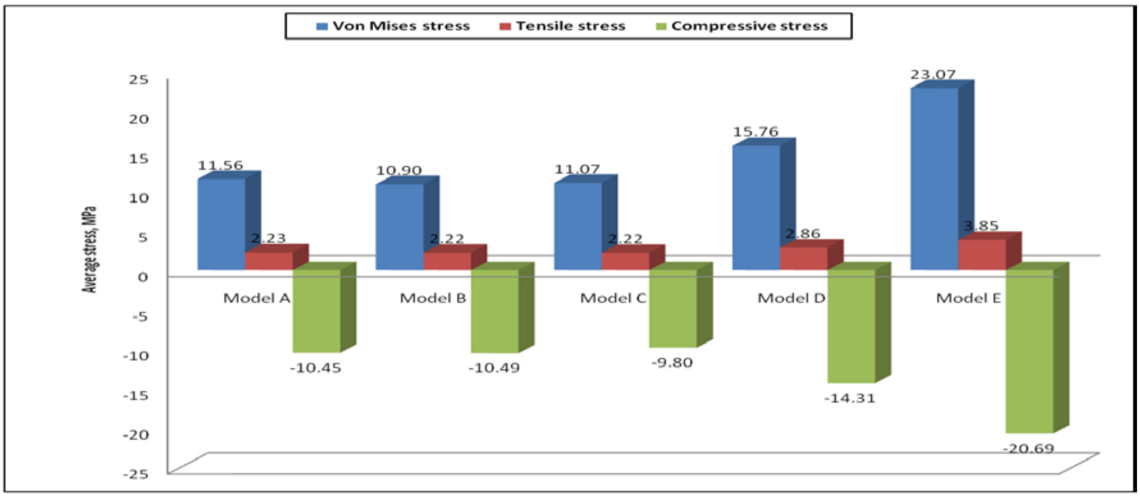

Figure 5.31 Comparison amongst all average stresses along the centre of the post under vertical loading.

5.5.2 Stress distribution at post and surrounding structure interfaces

5.5.2.1 Von Mises stress distribution

Von Mises stress distribution was investigated at the posts and surrounding structures interfaces for obliquely loaded tooth as illustrated in the Figure 5.32. Models A-C showed a lower von Mises stress compared to models D and E. In FGSP models, the von Mises stress at the post/core interface were negligible, while it increased slightly at middle part of the post/dentine interface and almost negligible value at the apical. The maximum von Mises stress was 30.04 MPa (Model A), 30.02 MPa (Model B) and 30.01 MPa (Model C), 50.00 MPa (Model D) and 80.80 MPa (Model E).

Similarly when tooth was loaded in the horizontal direction, the same von Mises stress distribution was observed (Figure 5.33). However, the magnitude of the von Mises stress distribution under horizontal loading was higher than oblique loading with maximum value of 32.02 MPa (Model A), 32.05 MPa (Model B), 31.59 MPa (Model C), 53.02 MPa (Model D), and 87.58MPa (Model E).

Von Mises stress distribution again displayed the same trend at posts and surrounding structures interfaces when loaded vertically (Figure 5.34). The maximum tensile stress distribution under vertical loading was higher than oblique loading but lower than horizontal loading with the value of 31.53 MPa (Model A), 31.68 MPa (Model B), 31.50 MPa (Model C), 51.95 MPa (Model D) and 82.95 MPa (Model E).

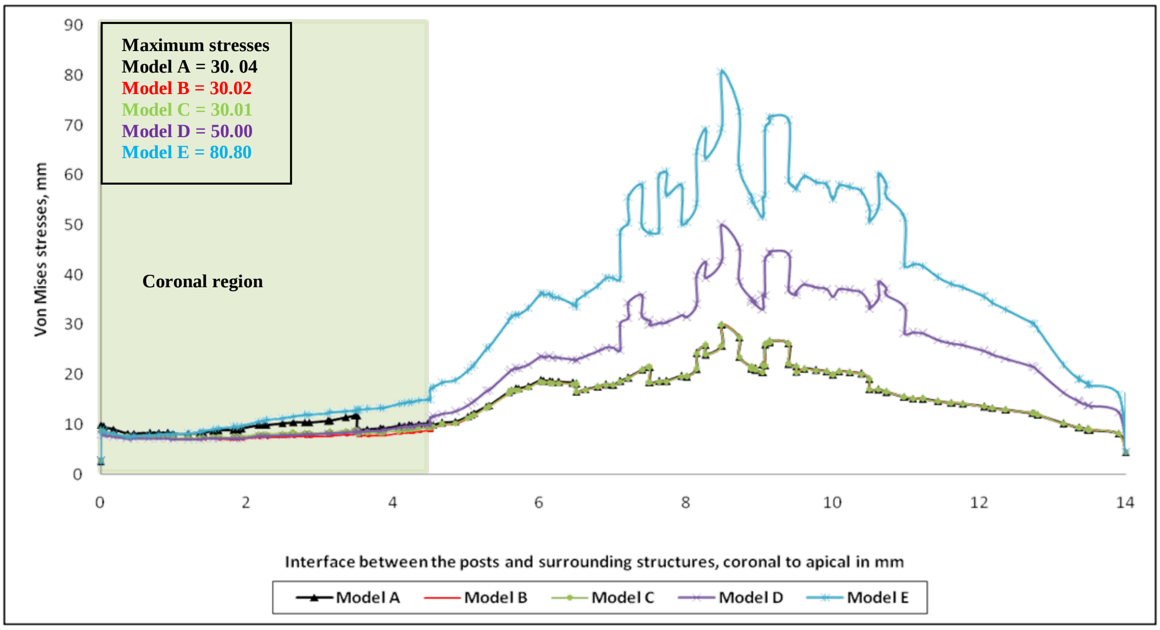

Figure 5.32 Von Mises stress distributions at the posts and surrounding structures interfaces when loaded obliquely.

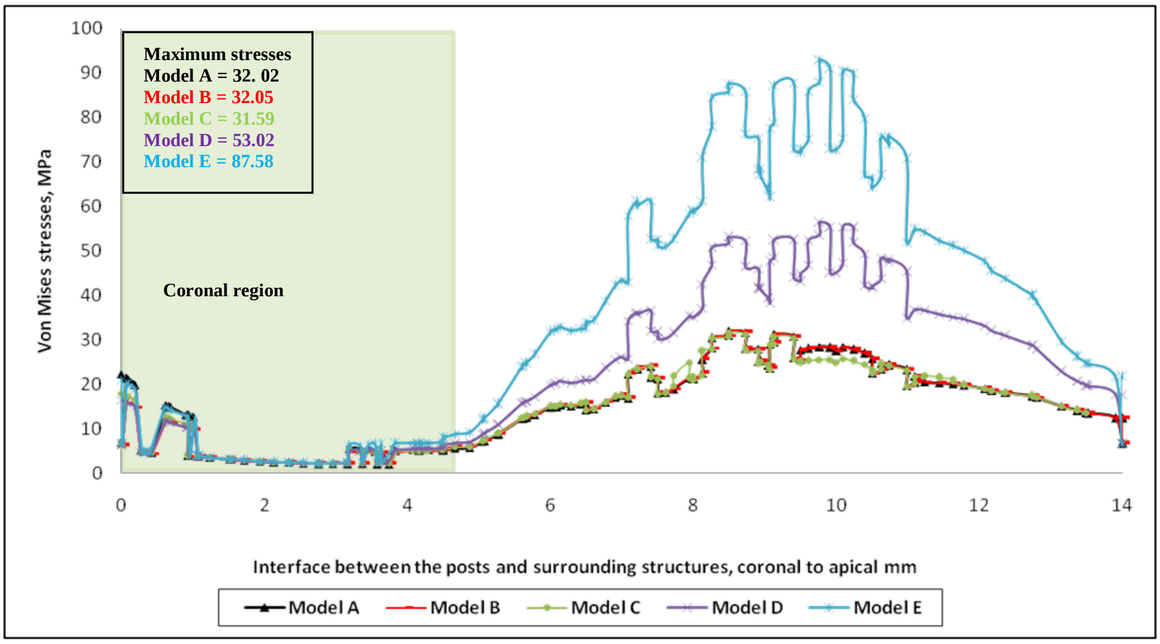

Figure 5.33 Von Mises stress distributions at the posts and surrounding structures interfaces when loaded horizontally.

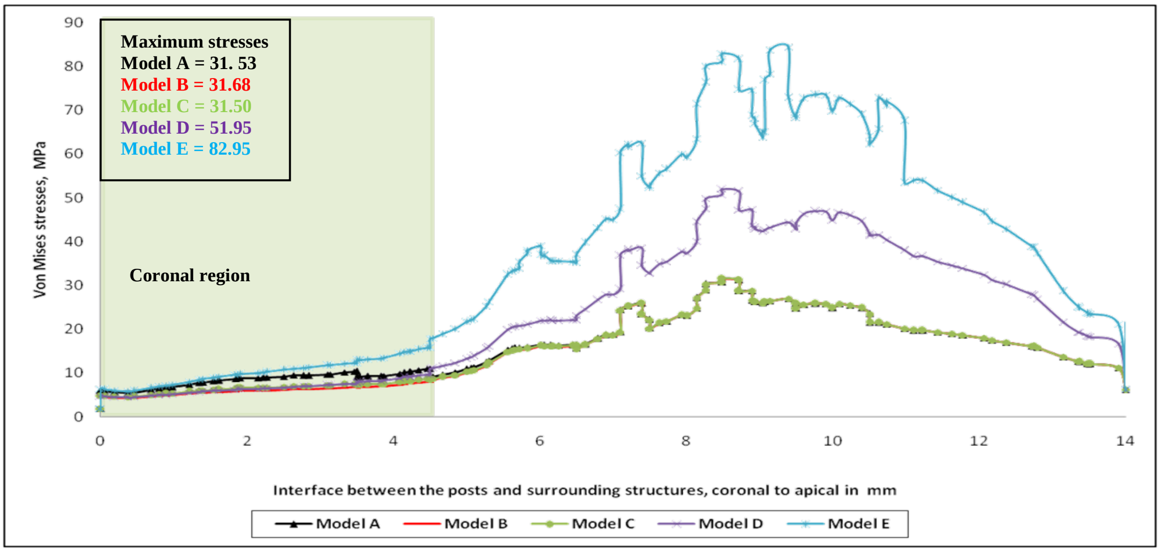

Figure 5.34 Von Mises stress distributions at the posts and surrounding structures interfaces when loaded vertically.

Table 5.5 shows the improvement in the average von Mises stress for FGSPs (Models A-C) compared to titanium (Model D) and zirconia (Model E) posts values under oblique, horizontal and vertical loadings at posts and surrounding structures interfaces. The reduction in the average von Mises stress values by FGSPs compared to titanium and zirconia posts is highlighted in Table 5.5. The percentage difference in average von Mises stress values among FGSPs was also not high.

Table 5.5 Percentage difference in average von Mises stress values at the posts and surrounding structures interfaces loaded under various loading directions

Model comparison	**Percentage difference in average von Mises stress values (MPa)**		
	Oblique loading	**Horizontal loading**	**Vertical loading**
A and B	4.42	1.96	5.59
A and C	3.26	0.79	4.31
A and D	31.98	36.94	31.68
A and E	55.91	59.11	58.34
B and C	1.20	1.80	1.34
B and D	34.99	37.69	35.50
B and E	57.86	59.91	60.67
C and D	34.20	36.94	34.62
C and E	57.35	59.43	60.13
D and E	35.17	35.66	39.03

5.5.2.2 Compressive stress distribution

Compressive stress distribution was also investigated at the posts and surrounding structures interfaces (Figure 5.35). In FGSPs models, the compressive stresses were considerably diminished in all regions of the interface compared to titanium and zirconia posts. The maximum compressive stress was -20.37 MPa (Model A), -20.35 MPa (Model B) and -20.34 MPa (Model C), -36.21 MPa (Model D) and -72.87 MPa (Model E).

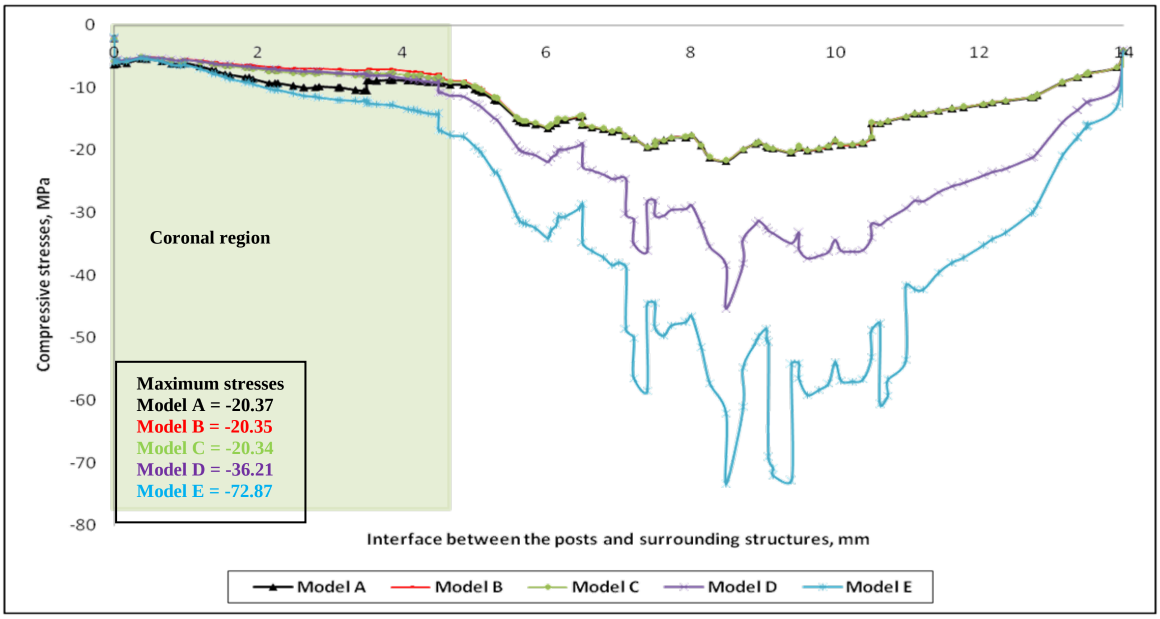

Figure 5.35 Compressive stress distribution at the posts and surrounding structures interfaces when loaded obliquely.

Compressive stress distribution also had same trend when loaded horizontally and vertically (Figures 5.36 and 5.37). The maximum compressive stress under horizontal loading was -27.56 MPa (Model A), -27.24 MPa (Model B), -27.53 MPa (Model C), -48.77 MPa (Model D), and -88.14 MPa. (Model E). However under vertical loading, the maximum compressive stress was -26.08 MPa (Model A), -26.04 MPa (Model B), -26.05 MPa (Model C), -46.04 MPa (Model D), and -86.26 MPa (Model E).

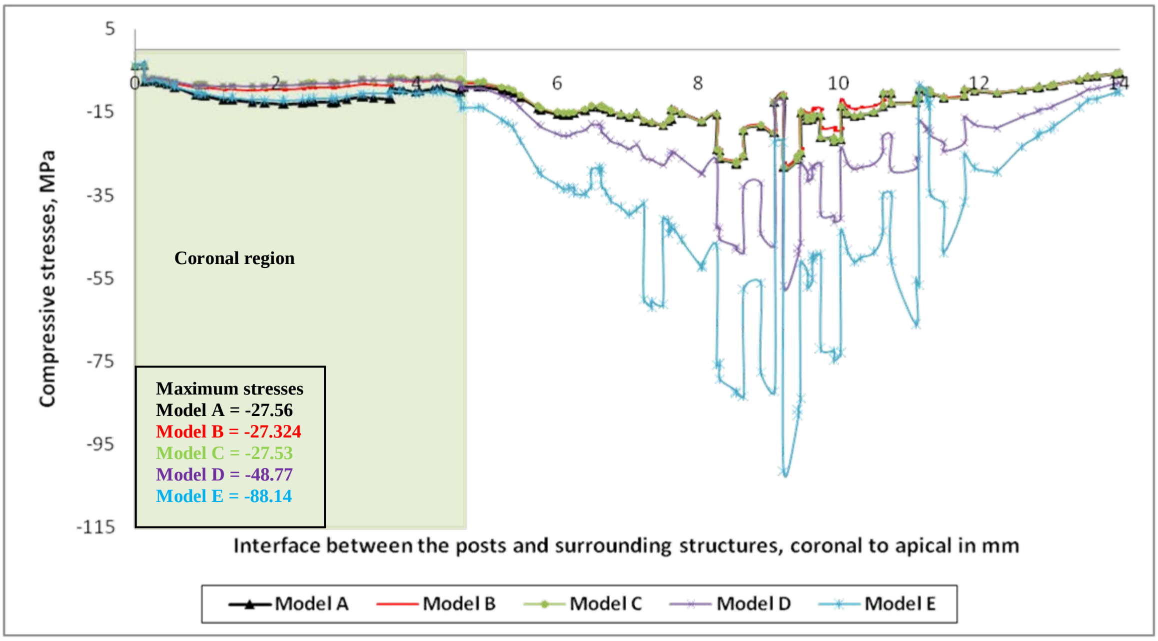

Figure 5.36 Compressive stress distribution at the posts and surrounding structures interfaces when loaded horizontally.

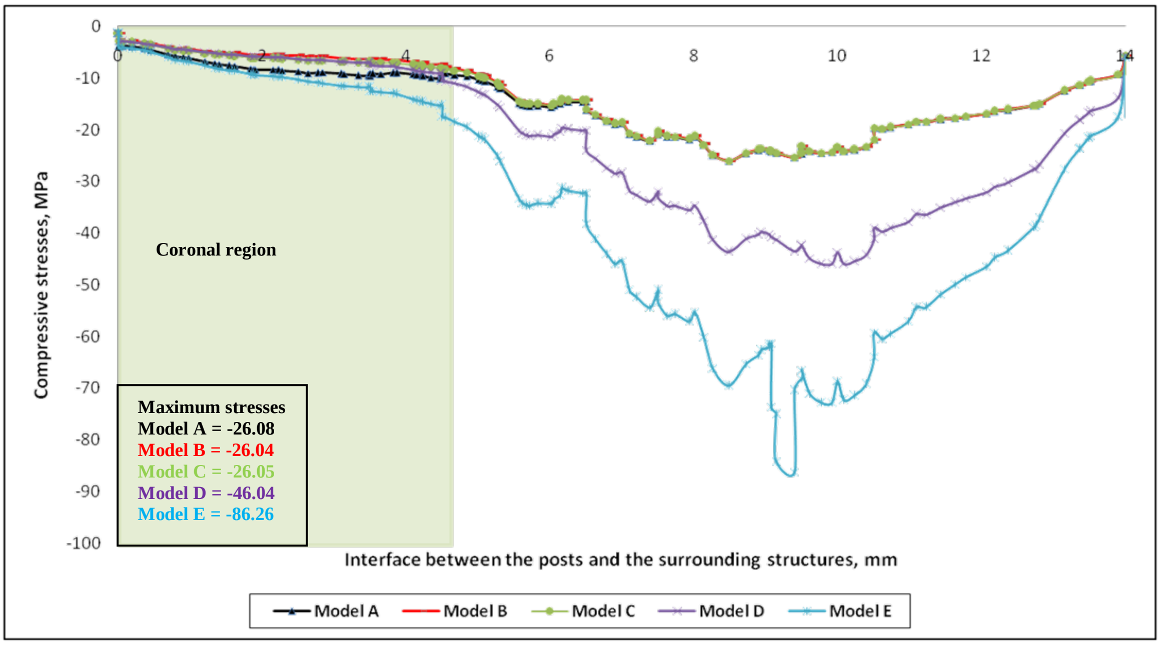

Figure 5.37 Compressive stress distribution at the posts and surrounding structures interfaces when loaded vertically.

Table 5.6 shows the improvement in the average compressive stress for FGSPs (Models A-C) compared to titanium (Model D) and zirconia (Model E) posts values under oblique, horizontal and vertical loadings at post and surrounding structures interfaces. The decrease in the average compressive stress values by FGSPs compared to titanium and zirconia posts is highlighted in Table 5.6.

Table 5.6 Percentage difference in average compressive stress values at the posts and surrounding structures interfaces loaded under various loading directions

Model comparison	**Percentage difference in average compressive stress value (MPa)**		
	Oblique loading	**Horizontal loading**	**Vertical loading**
A and B	5.24	6.94	6.77
A and C	3.83	6.84	5.15
A and D	33.56	27.80	32.12
A and E	59.31	56.46	58.55
B and C	1.46	0.10	1.70
B and D	37.04	32.80	37.21
B and E	61.44	59.48	61.36
C and D	36.10	32.73	32.65
C and E	60.87	59.44	60.69
D and E	38.76	39.70	38.46

5.5.2.3 Tensile stress distribution

Tensile stresses distributions were also investigated at the posts and surrounding structures interfaces (Figure 5.38). In FGSPs models, the stress were noticeably diminished in all regions of the post and surrounding structures interface compared to zirconia and titanium posts. The maximum tensile stress was 12.38 MPa (Model A), 12.38 MPa (Model B), 12.38 MPa (Model C), 23.29 MPa (Model D), and 42.33 MPa (Model E).

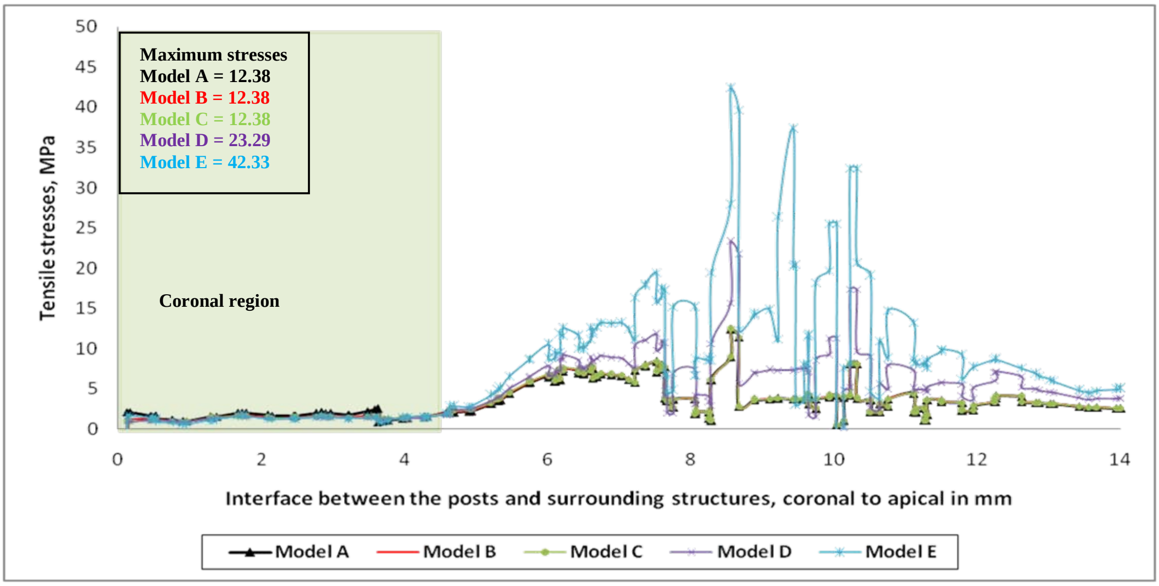

Figure 5.38 Tensile stress distribution at the post and surrounding structures interface when loaded obliquely.

Tensile stress distribution again displayed the same trend when loaded horizontally and vertically (Figures 5.39 and 5.40). The maximum tensile stress under horizontal loading was 28.71 MPa (Model A), 28.73 MPa (Model B), 27.99 MPa (Model C), 50.68 MPa (Model D), and 95.01 MPa (Model E). However under vertical loading, the maximum tensile stress was 14.34 MPa (Model A), 14.34 MPa (Model B), 14.35 MPa (Model C), 25.78 MPa (Model D) and 50.12 MPa (Model E).

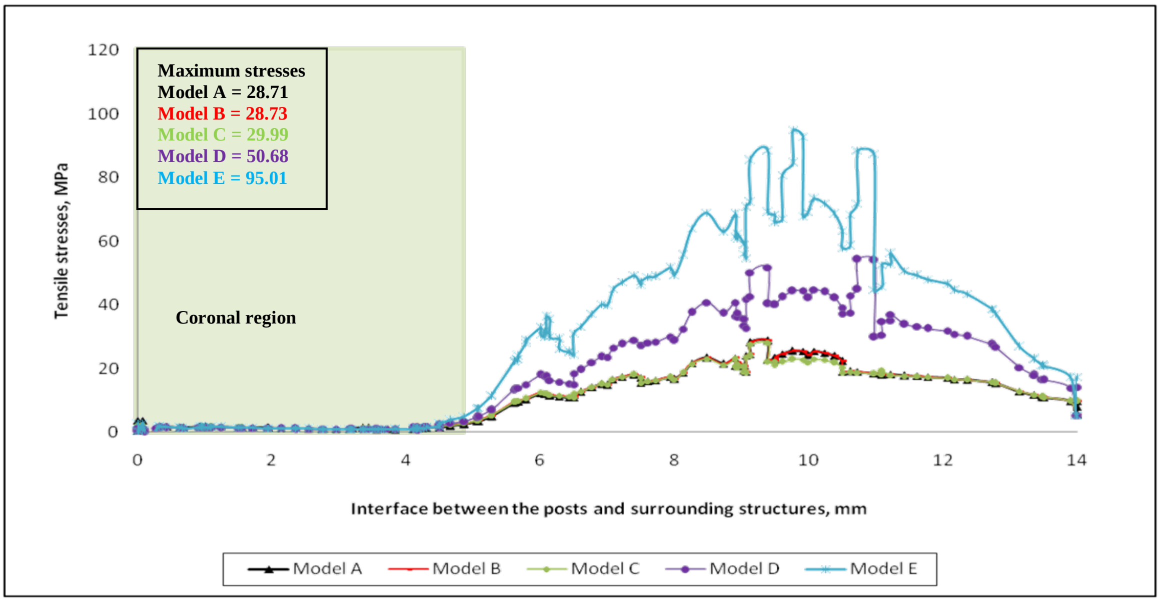

Figure 5.39 Tensile stress distribution at the post and surrounding structures interface when loaded horizontally.

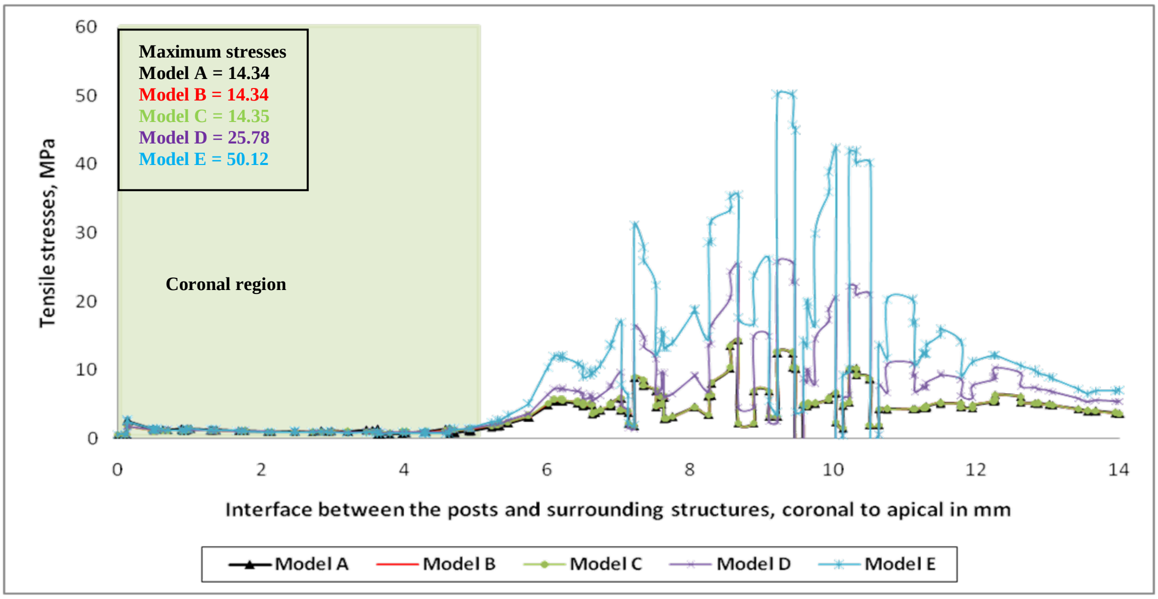

Figure 5.40 Tensile stress distribution at the post and surrounding structures interface when loaded vertically.

Table 5.7 shows the improvement in the average tensile stress for FGSPs (Models A-C) compared to titanium (Model D) and zirconia (Model E) posts values under oblique, horizontal and vertical loadings at post and surrounding structures interfaces. The decrease in the average tensile stress values by FGSPs compared to titanium and zirconia posts is highlighted in Table 5.7.

Table 5.7 Percentage difference in average tensile stress values at the posts and surrounding structures interfaces loaded under various loading directions

Model comparison	**Percentage difference in average tensile stress values (MPa)**		
	Oblique loading	**Horizontal loading**	**Vertical loading**
A and B	-0.98	3.77	0.21
A and C	-0.06	5.28	0.03
A and D	28.84	40.28	38.00
A and E	56.30	64.78	62.81
B and C	0.70	-0.16	-0.09
B and D	28.91	42.53	37.81
B and E	56.33	66.10	62.70
C and D	29.56	43.43	37.87
C and E	56.72	66.63	62.73
D and E	38.57	41.63	40.02

5.5.2.4 Comparison among all average stresses values at post and surrounding structure

Figures 5.41-5.43 illustrates all the average stresses at the post and surrounding structures interfaces under oblique, horizontal and vertical loadings. FGSPs showed lower von Mises compared to zirconia and titanium posts. Similarly this was also seen for the compressive and tensile stresses.

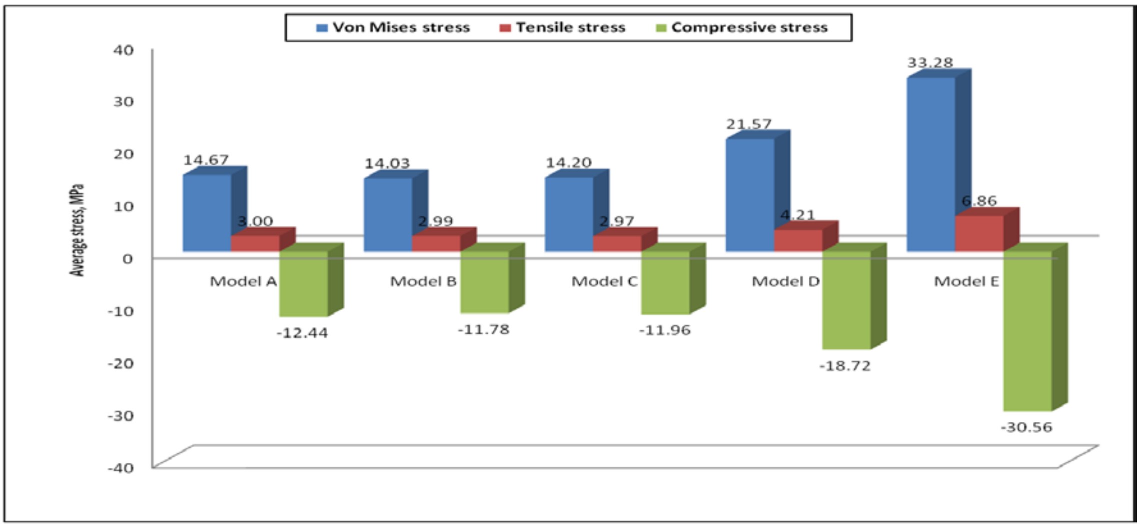

Figure 5.41 Comparison among all average stresses at the post and surrounding structures interfaces when loaded obliquely.

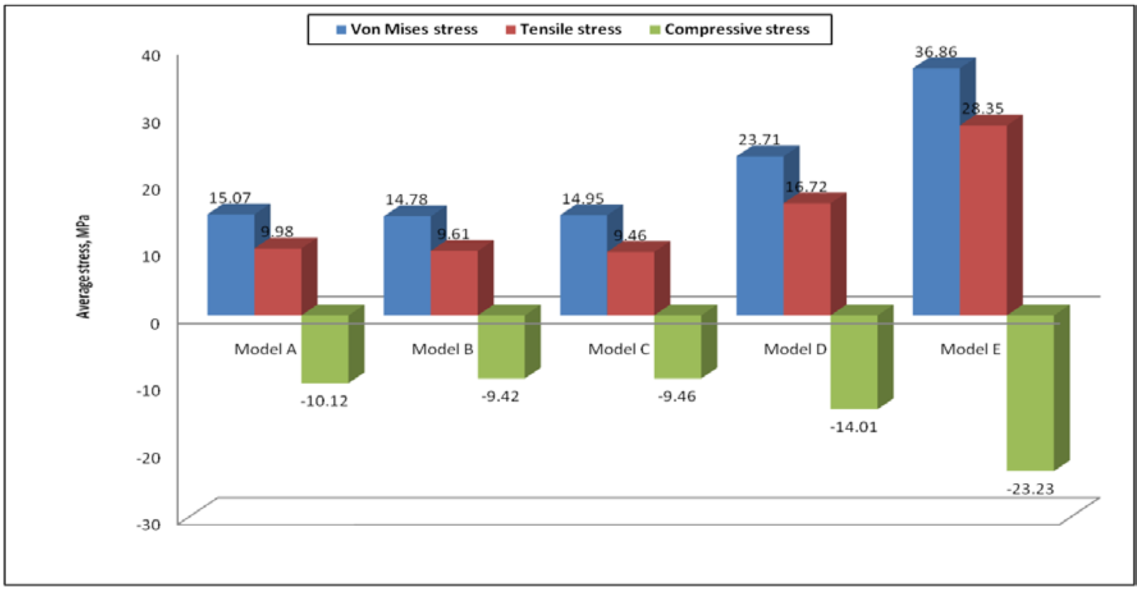

Figure 5.42 Comparison among all average stresses at the post and surrounding structures interfaces when loaded horizontally.

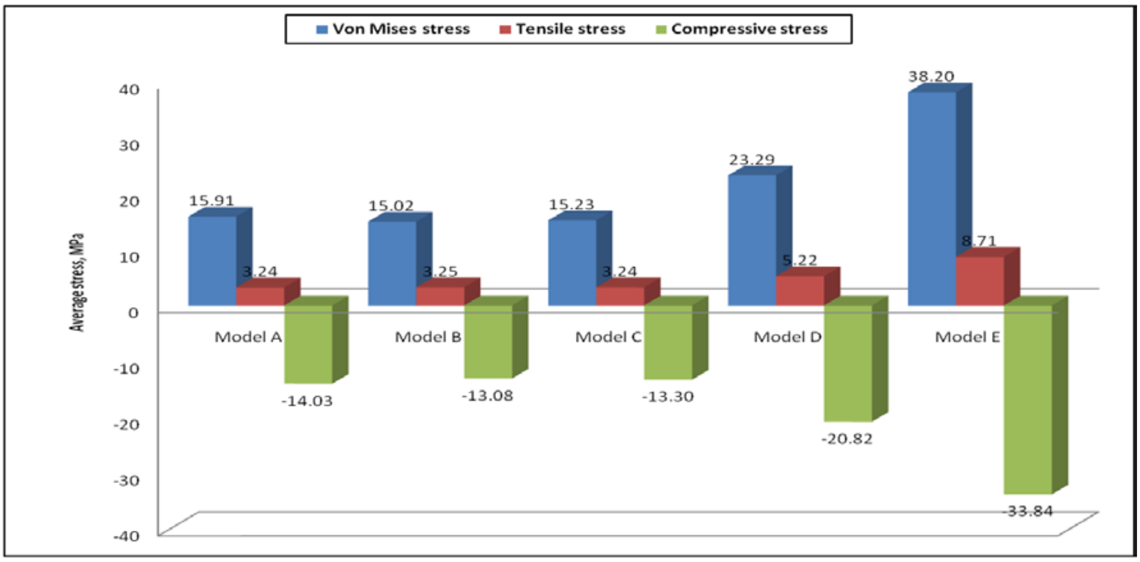

Figure 5.43 Comparison among all average stresses at the post and surrounding structures interfaces when loaded vertically.

5.5.2.5 Shear stress distribution

Shear stress of FGSPs at posts and surrounding structures (Models A-C) was lower than titanium (Model D) and zirconia (Model E) posts when tooth loaded obliquely as illustrated in (Figure 5.44). It was observed that the peak shear stress for the FGSPs reduced approximately three times of those for titanium and zirconia posts.

When horizontal loading was applied similar shear stress distribution were observed (Figure 5.45). However, the magnitude of the shear stress distribution under horizontal loading was higher than oblique loading. Shear stress distribution also had same trend at area when loaded vertically (Figure 5.46). However, the magnitude of the shear stress distribution under vertical loading was lower than oblique and horizontal loadings. The reduction in the interface shear stress reduces the probability of post loosening from dentine as the stress on bonding cement is reduced.

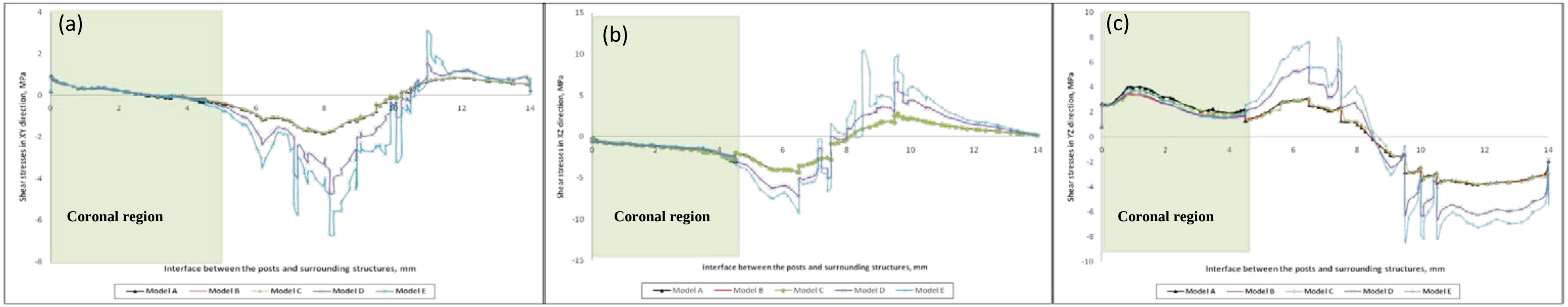

Figure 5.44 Shear stress distributions at a) at XY direction b) XZ direction c) YZ direction at the posts and surrounding structures when loaded obliquely.

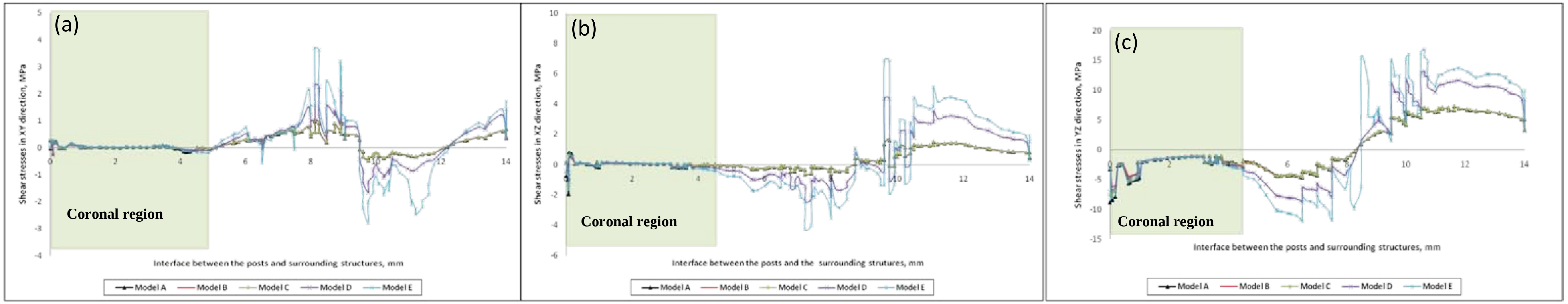

Figure 5.45 Shear stress distributions at a) XY direction b) XZ direction c) YZ direction at the posts and surrounding structures when loaded horizontally.

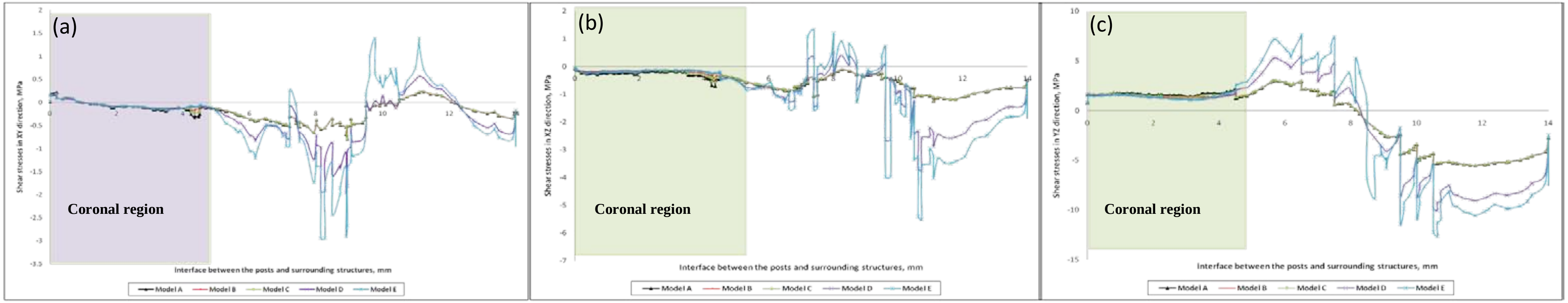

Figure 5.46 Shear stress distributions at a) XY direction b) XZ direction c) YZ direction at the posts and surrounding structures when loaded vertically.

5.5.3 Strain analysis

Figure 5.47 (a-b) shows strain distribution on obliquely loaded tooth model restored with various posts (Models A-E) and natural tooth (Model F). In all the models, strain distribution was recorded at the cervical third of the palatal aspect of the root surface and spread towards the middle third. On the contrary, the minimum values were noticed at level of both the apical portion of the post and the root apex. Maximum strain was evident at the level of CEJ on both the labial and palatal aspects of root. Strains progressively decreased from the outer to the inner part of the root and from the CEJ towards the incisal margin of the crown as well.

Strain distribution on obliquely loaded tooth was investigated at the posts and surrounding structures interfaces as illustrated in Figures 5.48 and 5.49. All models showed same trend for strain distribution under oblique loading at junction between middle and coronal parts of the root, all models showed localized higher strain. At the middle and apical regions strain was reduced gradually but fluctuates.

Similar strain distribution was observed when horizontal and vertical loadings were applied (Figures 5.50-5.55) except that under horizontal loading the strain was seen at the cervical third of the labial aspect of the root surface of the root surface and spread towards the middle third (Figure 5.50).

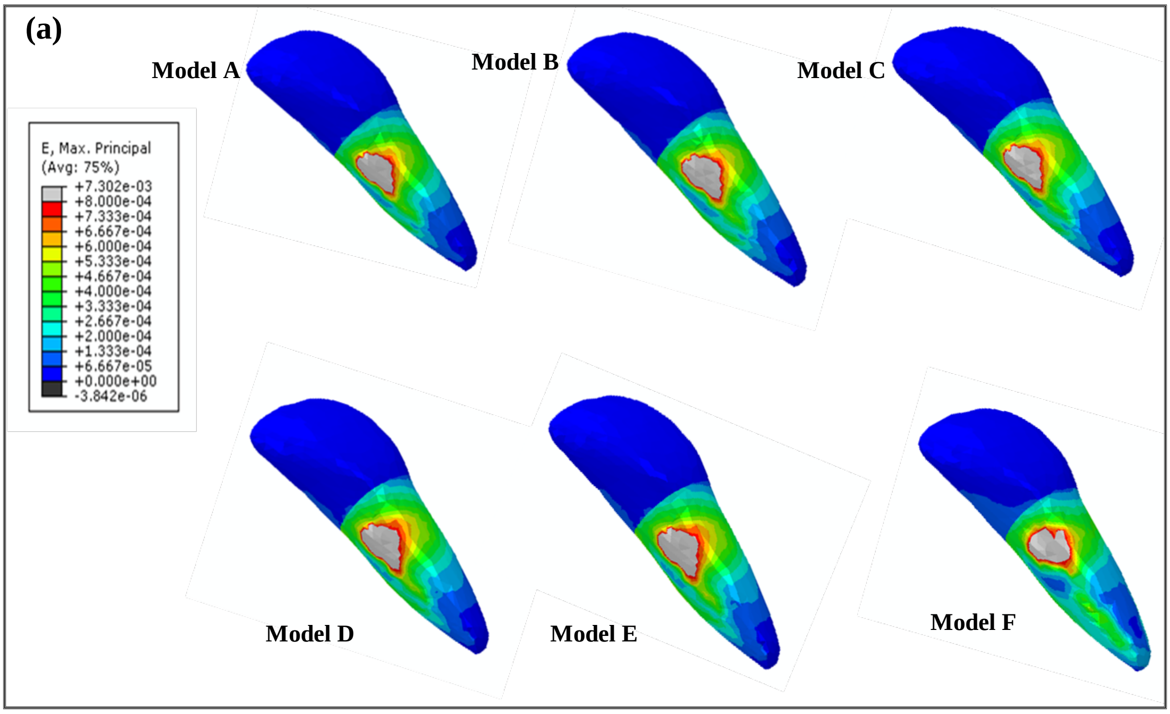

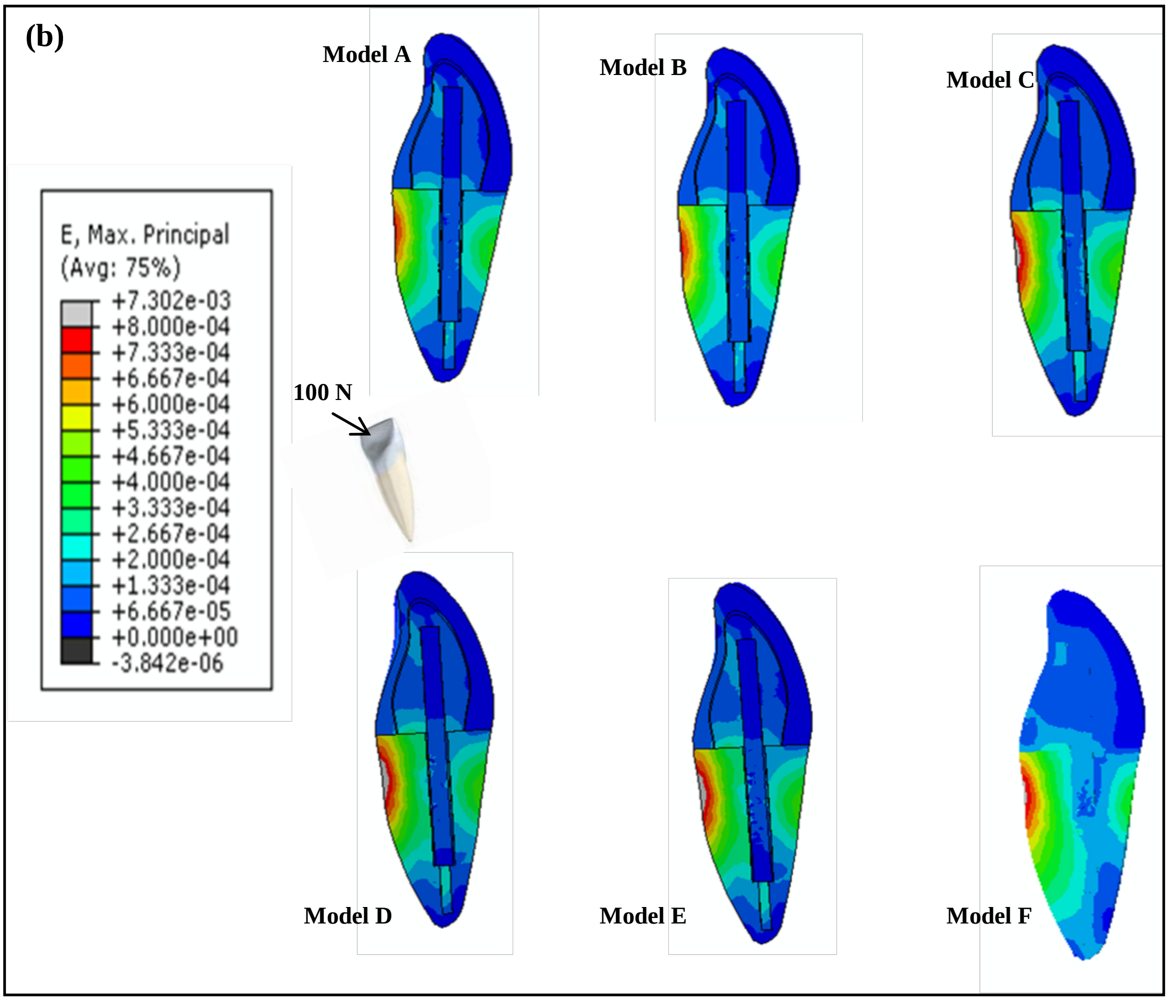

Figure 5.47 Tooth loaded obliquely a) Contour plots of the strain distribution; b) strain distribution within the tooth and the posts.

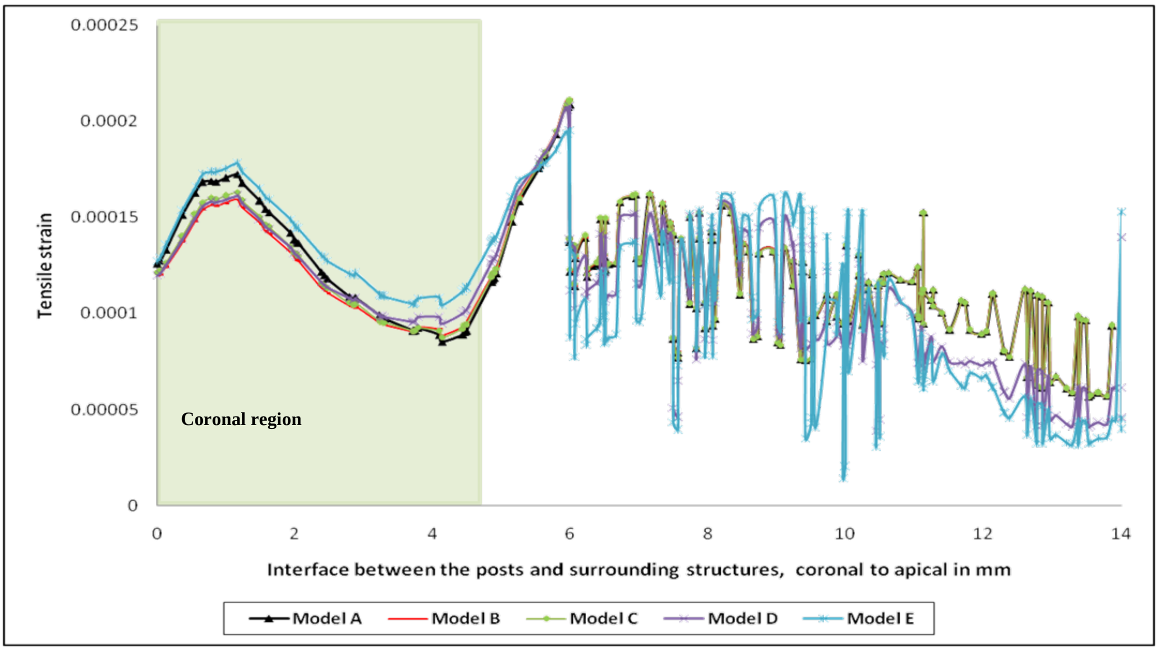

Figure 5.48 Tensile strain distributions at the post and surrounding structures interfaces when loaded obliquely.

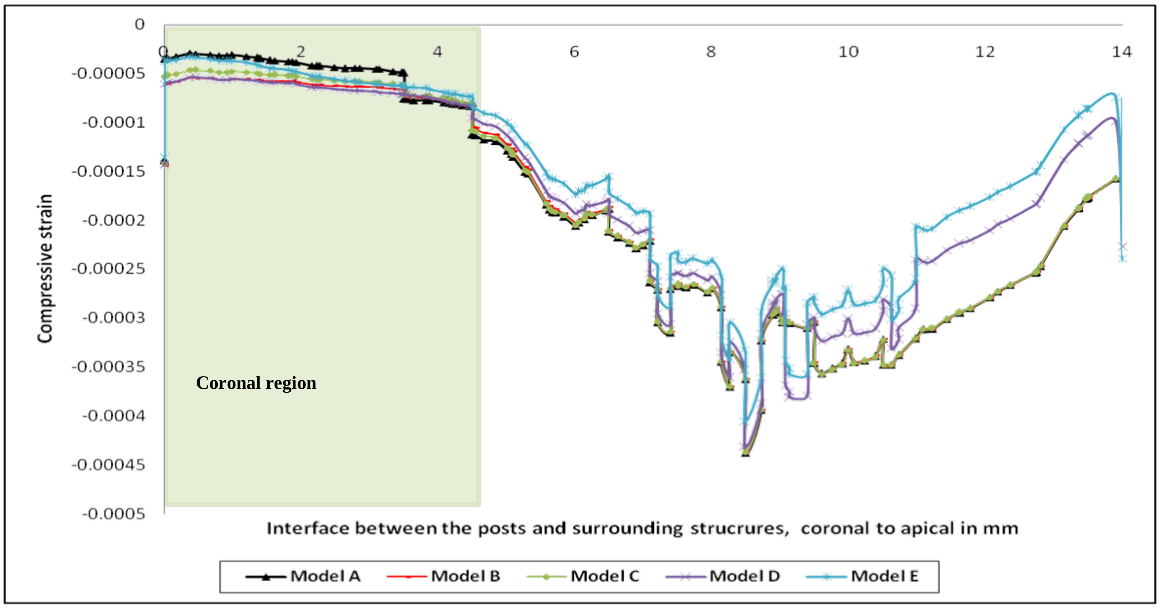

Figure 5.49 Compressive strain distributions at the post and surrounding structures interfaces when loaded obliquely.

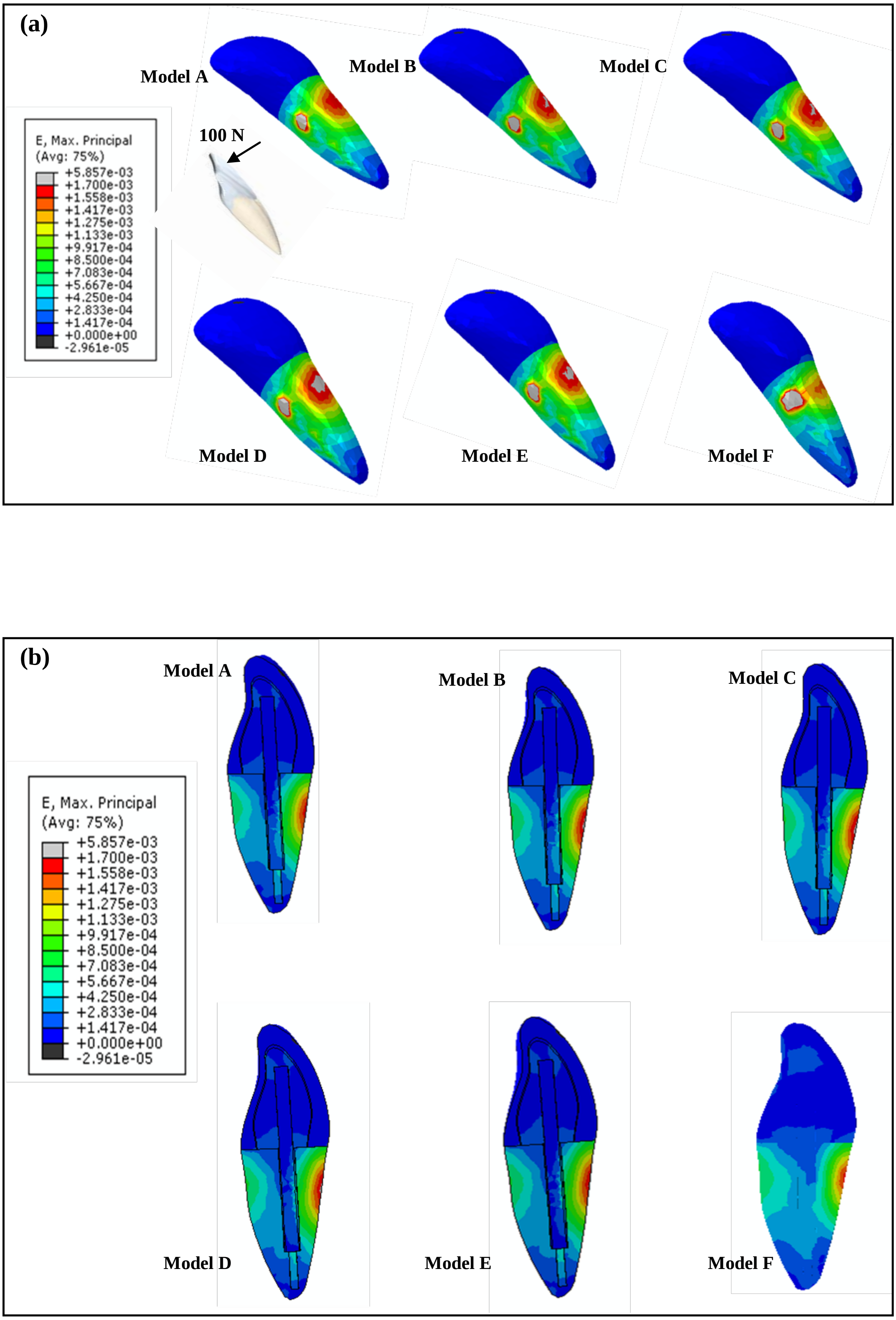

Figure 5.50 Tooth loaded horizontally a) Contour plots of the strain distribution; b) strain distribution within the tooth and the posts.

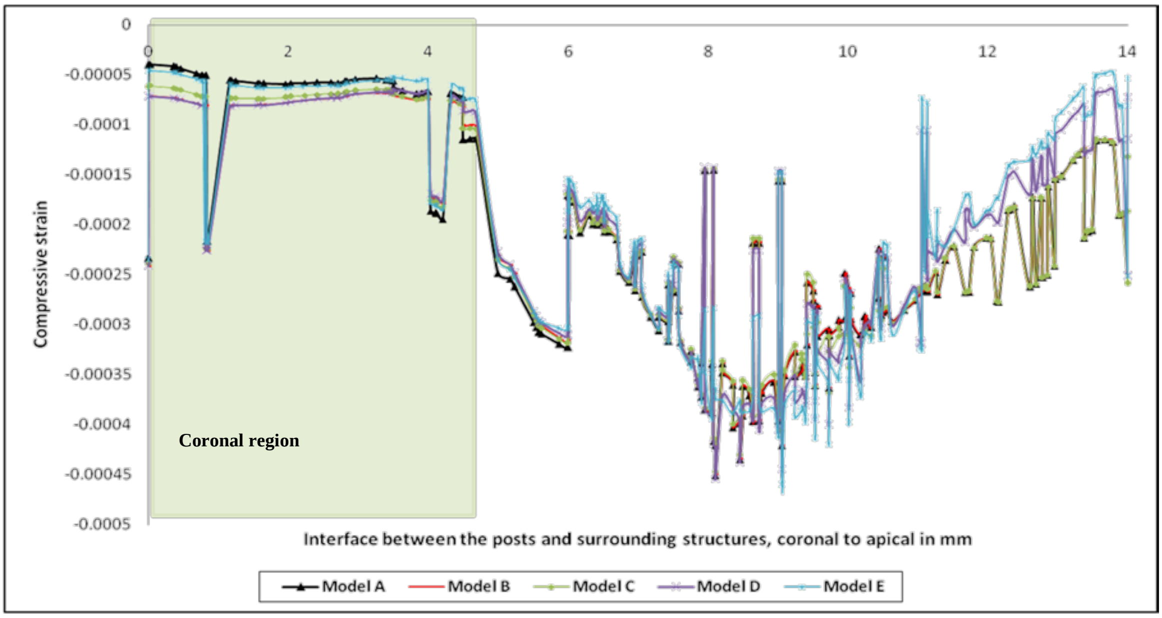

Figure 5.51 Tensile strain distributions at the post and surrounding structures interfaces when loaded horizontally.

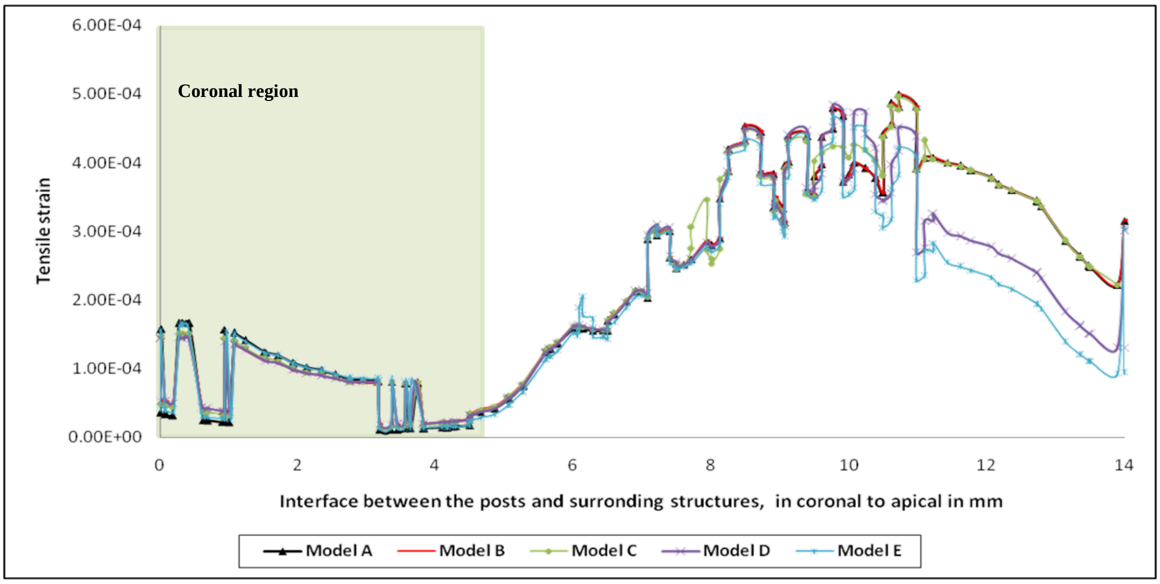

Figure 5.52 Compressive strain distributions at the post and surrounding structures interfaces when loaded horizontally.

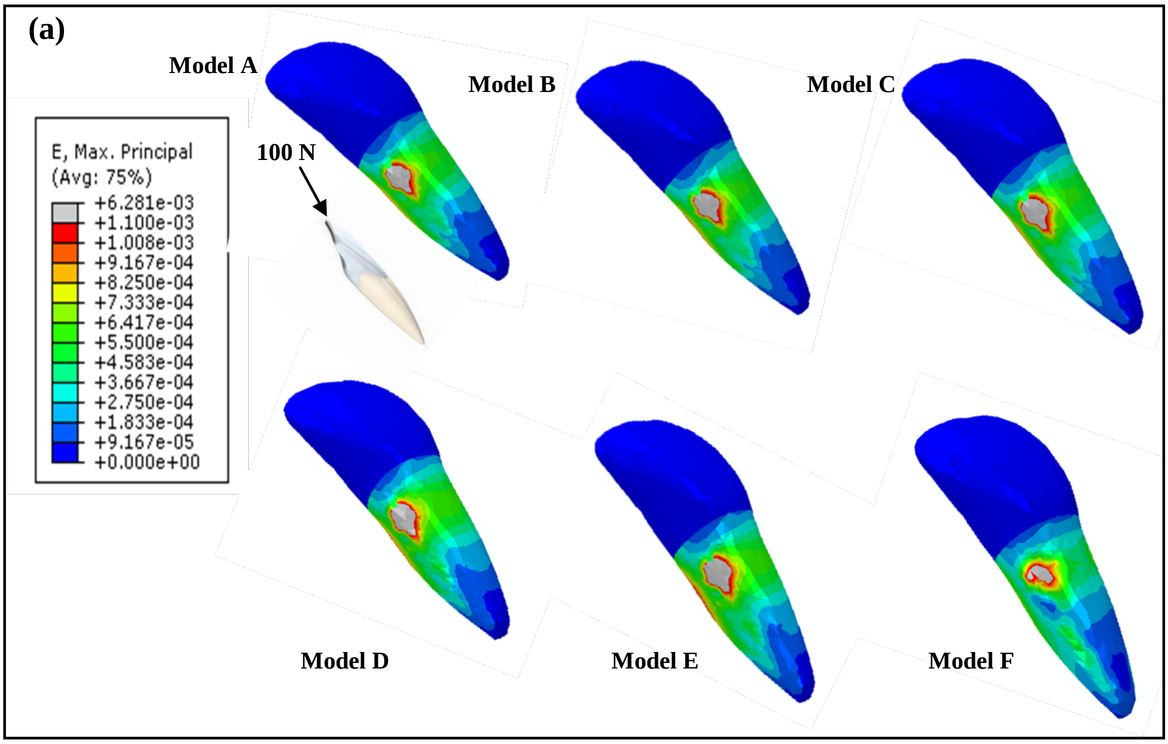

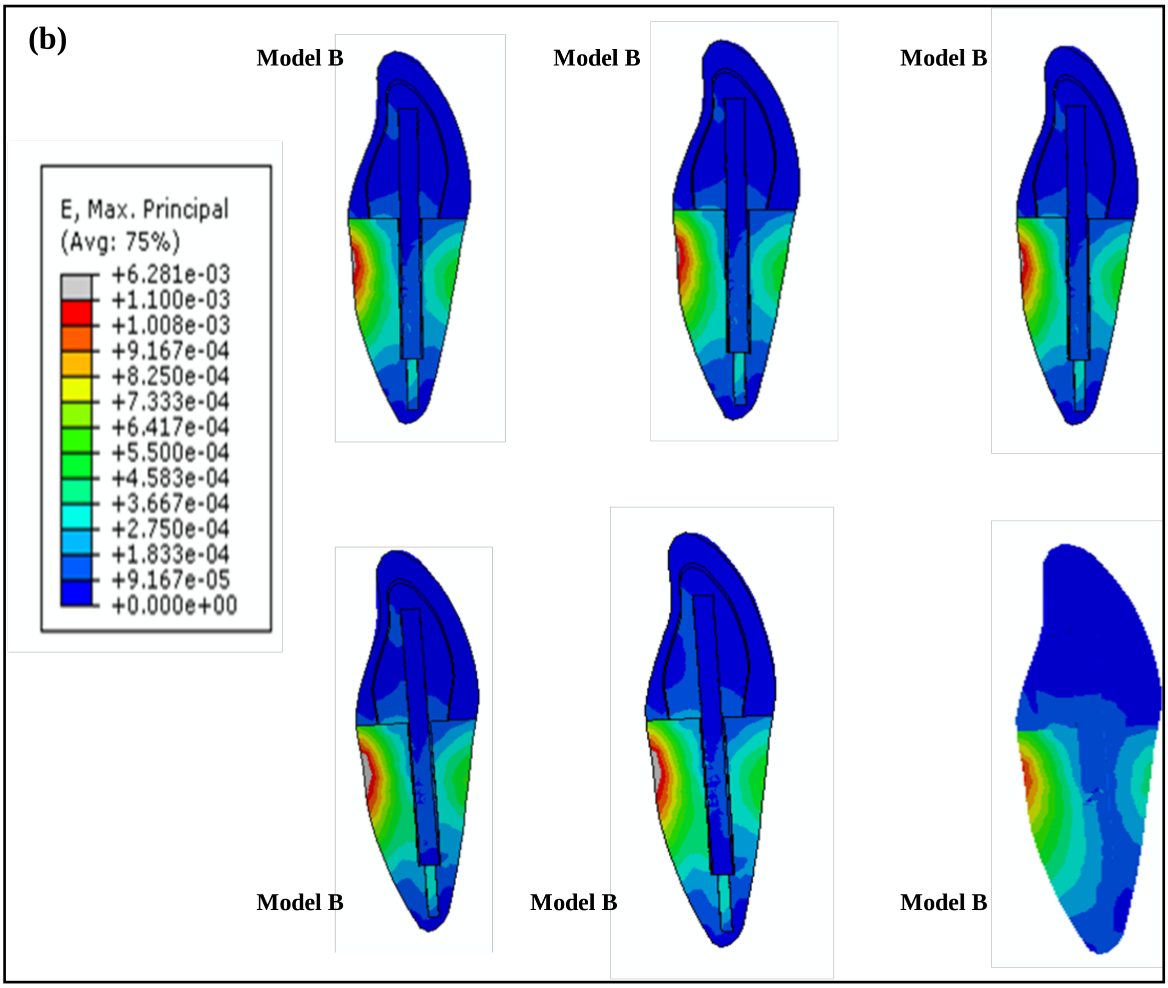

Figure 5.53 Tooth loaded vertically a) Contour plots of the strain distribution; b) strain distribution within the tooth and the posts.

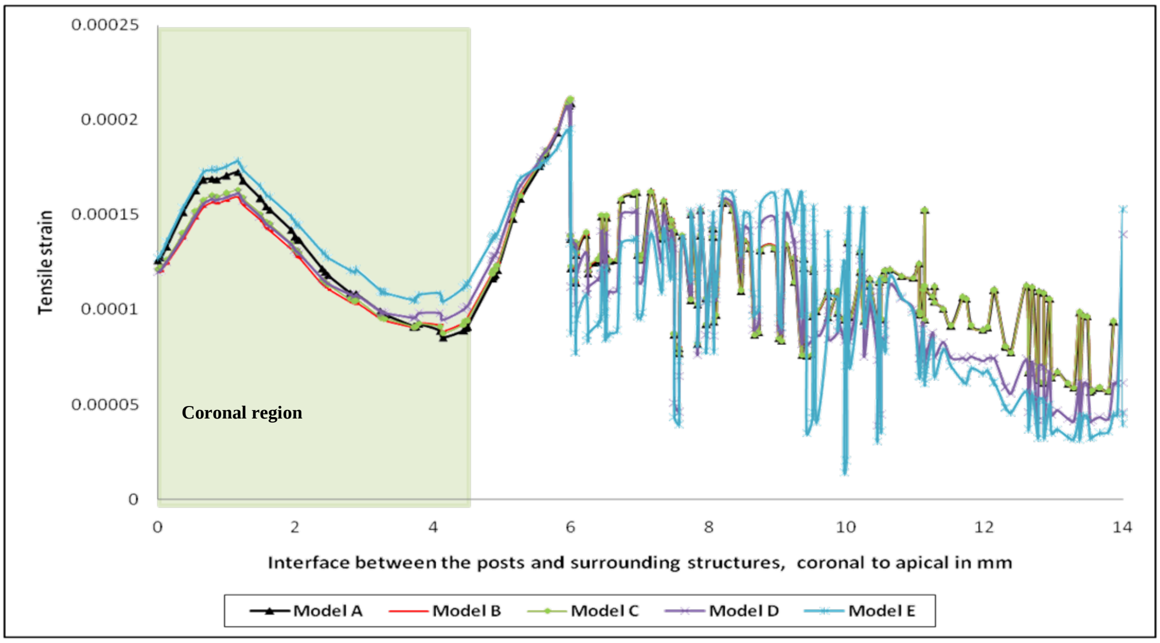

Figure 5.54 Tensile strain distributions at the post and surrounding structures interfaces when loaded vertically.

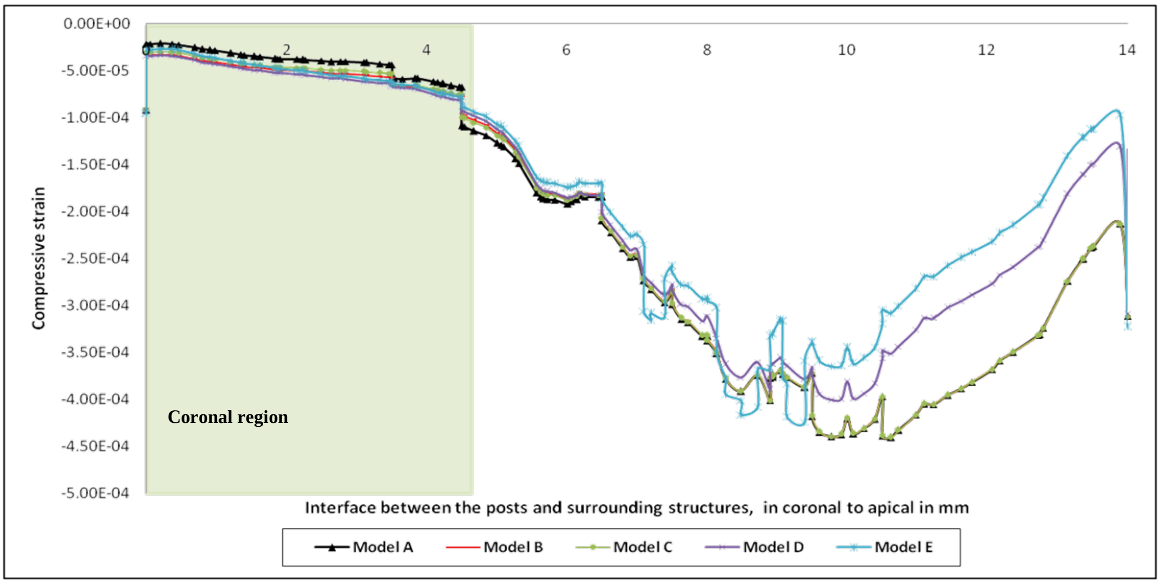

Figure 5.55 Compressive strain distributions at the post and surrounding structures interfaces when loaded vertically.

5.6 Discussion

The primary role of teeth in the oral cavity is to serve as a mechanical device for the mastication of food. The main role of post is to provide retention to the core of an endodontically treated tooth. When occlusal force is applied coronally, the force is transferred to dentine through the core and post system. In such cases, stress tends to be concentrated at the coronal and the apical regions. Stress concentrations at the coronal region of the root are likely to be due to the increased flexure of the compromised root structure, while stress concentrations at the apical region are generally due to taper of the root canal and characteristics of the post (Kishen, 2006). The regions of high stress concentration were also observed at the apical termination of the post (Kishen and Asundi, 2002). In such cases, stress concentration which occurred at the apical end, could initiate root fracture. This phenomenon is dependent on post geometry, material choice of the post and adhesion between a post and dentine. Considerable controversy exists with regards to the ideal choice of material and design of post and core.

In the oral environment, restorations are subjected to fatigue stress, which may produce microcracks causing the failure of the restoration (Ausiello et al., 2001). Such microcracks nucleate at locations of highest stress and lowest strength. Restorations investigated either in static and fatigue loading conditions showed underposable highest stress concentration areas and similar failure patterns (De Iorio et al., 2002; Reis et al., 2002). Although dynamic or cyclical tests may closely model the manner in which dental restorations fail, the static test also validates the relative resistance to stress of various restorations (Loney et al., 1995).

Many studies used the FEM to study the stress generation in the endodontically treated teeth restored with various posts under various load conditions (Pegoretti et al., 2002; Fujihara et al., 2004; Genovese et al., 2005; Lanza et al., 2005; Jager et al., 2006). It has been shown to be a useful tool when investigating complex systems that are difficult to be standardized during *in vitro* and *in vivo* studies (Genovese et al., 2005; Zarone et al., 2006). However, two main problems for the FEM are its accuracy and validity. Accuracy of the model in this study was confirmed by convergence tests where subsequent refinements of the mesh were made resulting in the mesh size of 150,465 elements. This is comparable to other previous studies where the elements and nodes ranged from 4400 to 185,000 nodes respectively (Pegoretti et al., 2002; Maceri et al., 2007; Sorrentino et al., 2007b). Validity is dependent upon the extent to which the model of the tooth approximates the real conditions. In this study, the model of the incisor tooth was created from a CT scan image of an adult maxillary central incisor along with its surrounding structures. It is felt this provided a realistic rendition of the clinical conditions.

The results of the FEA are expressed as stresses distributed in the structures under investigation. Stress is produced within a structure as a result of load acting upon it. The direction of the load applied and the shape of the structure influence the nature of the distribution of stress within the structure. Also, any imperfections such as notches or cracks within the structure can cause a localized increase in the magnitude of the stress, referred to as the stress concentration. Area of stress concentrations from a biomechanical perspective indicates regions of potential failure due to the formation of cracks or fatigue.

The stresses that act on teeth may be tensile, compressive, shear, or a combination known as equivalent von Mises stresses (Figure 5.56). Von Mises stress depends on the entire stress field and is a widely used indicator to predict damage occurrence (Pegoretti et al., 2002). The compressive strength of dentine is considerably higher than tensile strength, and the calculated tensile and von Mises stresses may be compared with the tensile strength of dentine to assess the risk of fracture (Kinney et al., 2003b). While shear stresses could result in defective dentine/post interface (Pegoretti et al., 2002). Calculated shear stresses may be compared to values of adherence obtained with resin based materials (Asmussen and Peutzfeldt, 2001) or zinc phosphate cement to assess the risk of loss of retention of the post (Drummond et al., 1999).

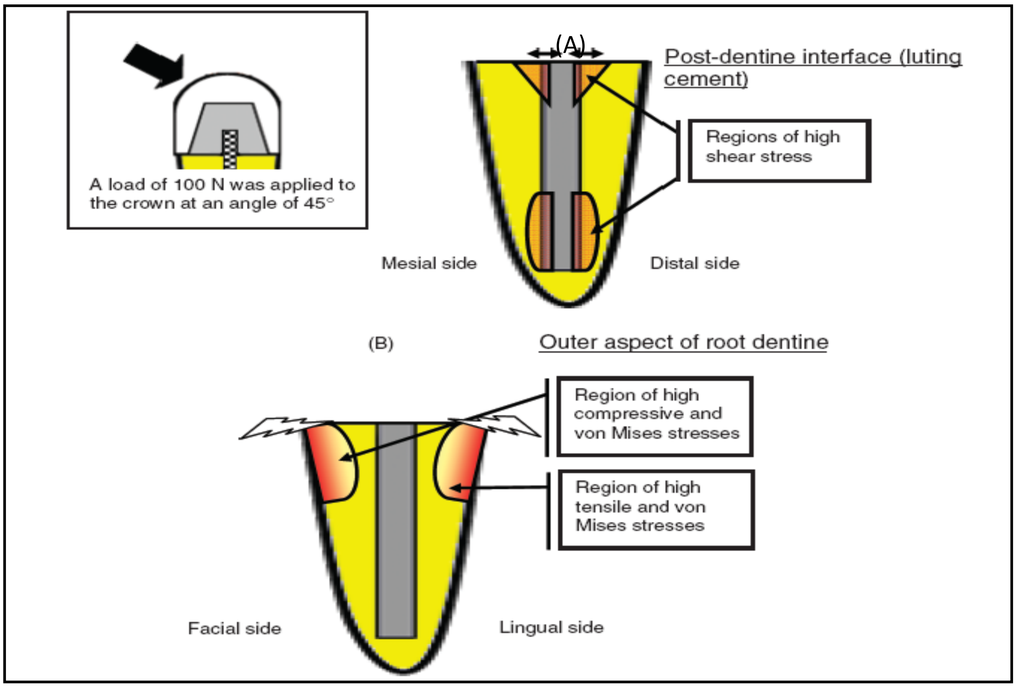

Figure 5.56 Schematic diagram obtained from FEM analysis showing the typical distribution of (A) shear and (B) tensile, compressive and von Mises stresses in a post and core restored teeth.

In the present study, the compressive stress along one side is substantially higher compared to tensile stress along the other side in the labio-lingual direction of the root depending on the direction of the load. The apical region of the root showed a notable reduction in bending and manifested particularly compressive stress (Asundi and Kishen, 2001). The increased tendency to compressive in comparison with tensile stresses is due to the shape and angulations of the tooth and supporting bone. An increase in tensile stress associated with post and core system in endodontically treated tooth could be deleterious to the remaining dentine structure.

In this study, the von Mises, compressive and tensile stresses distributions in the natural tooth (Model F) and endodontically treated teeth restored within posts (Models A-E) were analyzed. Most of the stresses on the root surface were distributed along the coronal and middle thirds and diminished towards the apical third. The stresses concentration in the coronal region of the root was in congruence with the 3D FEA conducted by Ho et al. (1994). These findings also concurred with Pierrisnard et al. (2002). The same authors used 3D FEA to compare how the mechanical parameters of different degrees of coronal tissue loss and restoration with different materials affected the restoration. Regardless of the models designed, the greatest stress was observed in the coronal region. The analysis confirmed that the reconstructed tooth was subjected to the most stress in the coronal region of the root. The findings reported in this study were also in agreement with the results obtained from the *in vivo* strain gauge experiments (Asundi and Kishen, 2000). The same authors confirmed that most of the axial bite forces are distributed along the coronal and middle thirds of the root. This pattern of stresses distributions can cause increased loading of the alveolar bone in the cervical region, relieving the apical region from any undue stress.

Stresses tend to concentrate in areas where the distribution of materials is unhomogeneous such as at the interfaces. At the interfaces materials have different moduli of elasticity represent the weakest link of the restorative systems and the stiffness mismatch influences the stress distribution (Assif and Gorfil, 1994; Ausiello et al., 1997). The highest stress distribution in the current study was recorded at the post and surrounding structures interfaces. These findings concurred with Zarone et al. (2006), who observed high stress concentration at the post-cement/dentine interface.

They stated that high modulus materials used for the restoration of endodontically treated teeth strongly alter the natural biomechanical behaviour of the tooth. The findings reported in this present study also concurred with Genovese et al. (2005), who reported that most stresses concentrated at post-dentine interface. The modulus of elasticity mismatch of the adjacent parts, particularly at the post-cement/dentine interfaces, was considered to be the weakest interface in the restored tooth. The stress concentration at this interface increases the probability of debonding failure. Pegoretti et al. (2002) also reported that the gold cast post and core produce the greatest stress concentration at the post dentine interface. Similarly, Lanza et al. (2005) noticed that the stiffer systems work against the natural function of the tooth and create zones of tension and shear both in the dentine, and at the interfaces of the luting cement during oblique loading of the post.

In this study, the homogenous-type (titanium and zirconia) post showed higher stress distribution regardless of the loading directions. The highest stress concentration was noticed within the zirconia post (Model E) followed by the titanium post (Model D). These results are in agreement with the findings reported by Cailleteau et al. (1992), who studied the stresses along the inner canal wall of a maxillary central incisor using FEM. They calculated the maximum tensile, compressive and shear stresses using a general purpose FE program. They reported that the stress patterns within the root were changed as a result of the posts insertion. Post placements did not result in a uniform distribution of stress along the canal wall. The results of this study also coincide with Ersoz (2000), who showed that the highest value of stress of 100 MPa was recorded when the tooth was restored with a stainless steel post. The highest stress caused by titanium post was found to be 60 MPa, which was much lower. Joshi et al. (2001) also evaluated the mechanical performance of endodontically treated teeth using 3D FEM. They reported that stainless steel post showed highest stress followed by titanium post.

In this present study, the strain distribution pattern in the natural tooth (Model F) and endodontically treated teeth restored within posts (Models A-E) was also analyzed. Strain mainly occurred at the coronal third of the root and gradually diminished towards the apical third. This strain may result from the increased displacement of the alveolar bone in the cervical region, relieving the apical third from any undue strain. These results are in accordance with Thresher & Saito (1973), who have conducted FEA and concluded that the maximum physiological tooth displacement takes place in the upper one-half of the root.

In this study, although FGSPs and natural tooth models distributed stress and strain uniformly in the tooth structure, the stress and strain were found to concentrate at the coronal third of the root, where the CEJ creates a physiological discontinuity of the mechanical properties of natural tissue. These results are consistent with Zarone et al. (2006), who reported that natural tooth distributed stress uniformly; however it concentrated at the coronal third of the root due to discontinuity in the mechanical properties between enamel and dentine. This is further substantiated by Drake et al. (1993), who used the power law distribution to show that significant reduction in stress and plastic strain can be achieved by increasing gradient thickness and tailoring the exponent to provide a gradual compositional change near phases that exhibit high modulus and little plasticity of ceramic materials.

Ideally, dental post should have varying stiffness along its length. Specifically, the coronal end of the post should have higher stiffness for better retention and rigidity of the core, and this stiffness should reduce apically. A post with graded stiffness is only possible by designing functionally graded multilayered composite materials. Compositional gradient of multilayer materials achieved in post has been identified as a possible solution for this problem.

In this present study, FGSPs showed a reduction in peak von Mises, compressive, tensile and shear stresses compared to the homogenous-type posts. FGSPs results are in agreement with those of others which mentioned that graded designed structure such as dental implants and crowns could improve the stress dissipation and barred stress propagation into the surrounding structures successfully (Yang and Xiang, 2007). The same authors investigated the biomechanical behavior of a functional graded biomaterial (FGBM) dental implant by using 3D FEM and the interaction between the implant and surrounding bone was taken into account. The computational results showed that the use of an FGBM implant effectively reduces the stress difference at the implant-bone interfaces where the maximum stresses occurred. Huang et al. (2007) added a FGM layer forming an enamel-like dental ceramic layer. FE simulations of the structure showed that the addition of FGM adhesive layer could significantly reduce the stress concentrations in the sub-surface of ceramic. This increases the resistance of the structure to radial cracking. This suggests the possibility of building synthetic bio-inspired functionally graded dental multilayers that have comparable or better durability than those of natural teeth. Traini et al. (2008) used a laser metal sintering technique to construct titanium alloy dental implant incorporating a gradient of porosity, from the inner core to the outer surface. The functionally graded materials were proven to give better approximate to the elastic properties of the bone.

The property gradient in a continuously non homogeneous material will cause a continuous change in acoustic impedance as a function of position. Hugh (2000) developed a model for designing FGMs to manage stress waves. He considered stress waves as linearly elastic longitudinal waves propagating in one dimension through a discretely layered FGM as depicted in Figure 5.57. At each interface, the stress waves are partially reflected and partially transmitted as shown in the same figure due to the following reasons:

i. The peak stress of waves reflected from the FGM interface was greater than for materials with sharp interfaces.

ii. The benefit of the FGM over the sharp interface was to introduce a time delay to the reflected wave propagation when stresses approached peak level.

iii. The time delay was highly dependent on the composition gradient and the differences in base material properties.

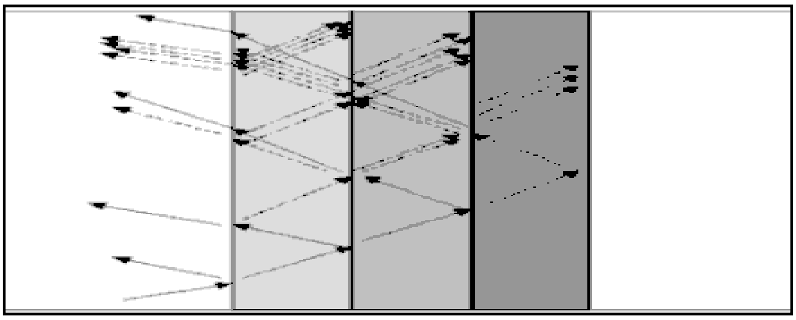

Figure 5.57 Stress wave propagation through discretely layered FGM.

This may be practically true because the changes in mechanical properties between each composite will introduce a time delay to the stress propagation. This will reduce the velocity of the stress transmutation and therefore will minimize the stress peak. This may well explain why FGSPs perform better results than homogonous-type posts.

5.6.1 Stress under various load directions

The highest von Mises stress were observed mainly at the middle and apical parts of the post in models D and E under oblique, horizontal and vertical loadings. However, for models A-C, there was lower stress concentration at the middle and apical parts of the posts. This is likely to be due to functionally graded structured design of models A-C. The Ti concentration variation in xTi-yHA provided a smooth change in the properties of FGSP offering advantages such as reduction of stress concentration (Kim and

Paulino, 2002). In this study, the FGSPs (Models A-C) improved the stress dissipation and barred stress into the structure successfully. However, small stress concentration was observed at the palatal aspect of models A-C. Small stress noticed in FGSPs (Models A-C) could be considered to be negligible compared to homogenous-type posts (Models D and E).

The von Mises stress concentration along the symmetrical axis inside the post was studied in more detail for all the models under the oblique, horizontal and vertical loadings. FGSPs models demonstrated better stress distribution compared to the homogenous-type posts. Although there was higher stress observed at the middle portion of models A-C, this value is almost negligible if compared to the stress in models D and E where considerably high stress concentration was detected. This means the stresses from the applied load were distributed through the homogonous-type posts. Possibly this is the main reason for stress concentration on the coronal and apical thirds which could lead to fracture of the root when homogonous-type posts were employed.

The von Mises stress distribution in the interface of the post and its surrounding structure after exerting the oblique, horizontal and vertical loads for all models was also investigated. The stresses were higher on the post at the post and surrounding structures interface on the opposite side of the loading. This is due to the contact conditions and difference between the stiffness of the post and cement, which cause amplification of stress magnitudes. The zirconia and titanium posts generated higher stresses than FGSPs. The FGSPs dissipated the interface stresses remarkably from the coronal to the apical regions of the post. The homogenous-type posts transferred the stress through the entire interface with maximum point located at the middle third. The behaviour of models A-C was similar while models D demonstrated similar behaviour with model E at the coronal and apical regions.

The three FGSPs appeared to be able to dissipate the compressive and tensile stresses excellently at the coronal and apical parts of the post. Although the stresses at the middle part of the post were slightly higher, the differences between the three FGSPs could be considered negligible compared to homogenous-type posts where the shear stress were three times more. The reduction in tensile stress for FGSPs is advantageous as it likely to be able to resist cyclic loading and reduce the probability of root failure. Kinney et al. (2003b) reported that tensile strength of dentine is in the range of 50 to 100 MPa and suggested that tensile loads in the range of 150 to 300 N could increase the risk of tooth fracture. It is probably prudent to investigate further the performance of FGSPs under higher loading compared to 100 N used in this study. It would also be interesting to observe if the behaviour of FGSPs mimics that of dentine during tensile loading.

As mentioned previously, the maximum shear stresses were found to be primarily located at post and surrounding structures interface. The bonding strength of dentine bonding systems has been reported to be in the range of 15 to 30 MPa, and posts luted with zinc phosphate cement have been reported to lose retention at a stress level of approximately 5 to 25 MPa (Asmussen and Peutzfeldt, 2001). Thus, every effort should be made to reduce stresses in the dentine and the post and surrounding structures interface. The maximum shear stresses were lower compared to the tensile, compressive and von Mises stresses for FGSPs. Thus, the shear stresses presumably do not predispose the root to fracture, however, shear stresses located at the post and surrounding structures interface to a level where the bond may break and the post will lose retention.

In general, irrespective of loadings directions, stresses started to increase dramatically at the middle part of the posts and reduced significantly towards the apical part. However, the direction of the loadings has greater effect on stresses distribution. The stress concentration within posts and in posts-cement/surrounding structures interface caused by horizontal loadings was higher than that caused by vertical and oblique loadings. During horizontal loadings, bending of the core and post generate the higher stresses to develop with the post and at the interface between post and cement. The findings of the present study are in agreement with the results reported by Yang et al. (2001b), who observed that greater deflection and higher stresses generated under horizontal loading. They also reported that the loading direction had a much greater effect than post design on maximum stress generated and displacement. Thus, horizontal loading should be avoided as much as possible. Posts material should also be chosen carefully so that posts can support the restored tooth and will prevent the generation of high stresses along the post and surrounding structures interfaces.

Ramakrishna et al. (2001) suggested that ideally dental post should be stiff at the coronal region, i.e. in the region of the core, so that the core is not stressed excessively when occlusal force is applied to the crown and its stiffness should be reduced apically. The high stiffness eradicates the stress from the core and the gradual reduction of stiffness along the post would dissipate the stress from the post to the dentine uniformly. The gradual dissipation of stress would also help to eliminate local stress concentration area and reduce the interfacial shear stress growth.

5.7 Conclusions

Under the limitations of this study, the following conclusions may be drawn:

1. FGSPs reduced the von Mises stress distribution within the tooth and along the centre of the posts compared to homogeneous-type titanium and zirconia posts.
2. FGSPs decreased the compressive stress distribution within the tooth and along the centre of the posts compared to homogeneous-type titanium and zirconia posts.
3. FGSPs reduced the tensile stress distribution within the tooth and along the centre of the posts compared to homogeneous-type titanium and zirconia posts.
4. FGSPs diminished the von Mises stress distribution at the post and surrounding structures interfaces compared to homogeneous-type titanium and zirconia posts.
5. FGSPs decreased the compressive stress distribution at the post and surrounding structures interfaces compared to homogeneous-type titanium and zirconia posts.
6. FGSPs also reduced the tensile stress distribution at the post and surrounding structures interfaces compared to homogeneous-type titanium and zirconia posts.
7. FGSPs diminished the shear stress distribution at post and surrounding structures interfaces compared to homogeneous-type titanium and zirconia posts.
8. The strain distributions of FGSPs were not considerably different from homogeneous-type titanium and zirconia posts.

Chapter Six

Fracture Resistance of Endodontically Treated Teeth Restored with Prototype Functionally Graded Dental Posts

6.1 Introduction

Endodontically treated teeth are considered to have a higher risk of fracture because of their inherently poor structural integrity due to pre-existing caries and/or tooth preparation (Tidmarsh, 1976). Loss of the roof of the pulp chamber and/or the marginal ridges is further factors that are likely to influence the fracture resistance of such teeth (Reeh et al., 1989a, b; Donald et al., 1997). Sound coronal dentine should be conserved during restorative procedures to extend the crown margin below the junction of the core and the remaining tooth structure (Aykent et al., 2006). However, the clinicians often find that horizontal loss of the clinical crown has occurred and that little ferrule can be created on the remaining tooth structure (Libman and Nicholls, 1995). In these situations, there are few alternatives for restoration with a post and core buildup. The fracture potential of endodontically treated teeth have been studied, yet to date, no specific causal relationship between the type of restorations and the fracture has been established, and arguments remain as to which material or technique would be ideal for their rehabilitation.

Generally, there are significant mismatch between material properties of these types of posts, e.g. stiffness, and surrounding dental tissues resulting in the poor stress distribution and root fracture. In order to overcome the shortcomings of available dental posts, the concept of functionally graded materials (FGMs) was applied. Compositional gradient of multilayer materials achieved in dental post has been identified as a possible solution for this problem.

FGMs arose in the mid 1980’s as a way of improving the thermo-mechanical performance of aerospace structures. FGMs is recent advances in materials processing and engineering have led to a new class of materials which can display continuously or discretely varying compositions and/or microstructures and related properties including hardness, density, thermal conductivity, resistance, Young's modulus and etc., over definable geometrical distances according to the desired function. The gradients can be continuous on a microscopic level, or in the form of laminates which comprised of gradients of metals, ceramics, polymers, or variations of porosity/density (Narayan et al., 2006). FGM allows the integration of dissimilar materials without formation of severe internal stress and combines diverse properties into a single material system. Therefore, fabrication of dental posts prototypes with multilayered structured where the properties change gradually throughout the post from the coronal to apical is most desirable.

6.2 Aim

The aim of this chapter was to investigate the fracture resistance of endodontically treated teeth restored with three FGSPs prototypes.

6.3 Objectives

1. To compare the fracture resistance of endodontically treated bovine teeth restored with FGSPs prototypes, prefabricated titanium post, cast post, endodontically treated teeth without post and extracted sound teeth.

2. To evaluate and compare the failure modes of endodontically treated bovine teeth restored with FGSPs prototypes, prefabricated titanium post, cast post, endodontically treated teeth without post and extracted sound teeth.

6.4 Materials and method

6.4.1 Fabrication of prototype functionally graded dental posts

Functionally graded blocks with thickness of 14-16 mm and width of 12.7 mm were prepared as described in Chapter 3. The functionally graded blocks were then manually milled until a dimension of 2.5 mm in diameter was achieved (Figure 6.1). Finally, the FGSPs prototypes were then hot pressed utilizing hot isostatic pressing machine at 1100^{o}C under a pressure of 180 MPa in Argon atmosphere for one hour and the final diameter of the FGSP is 2.3 mm.

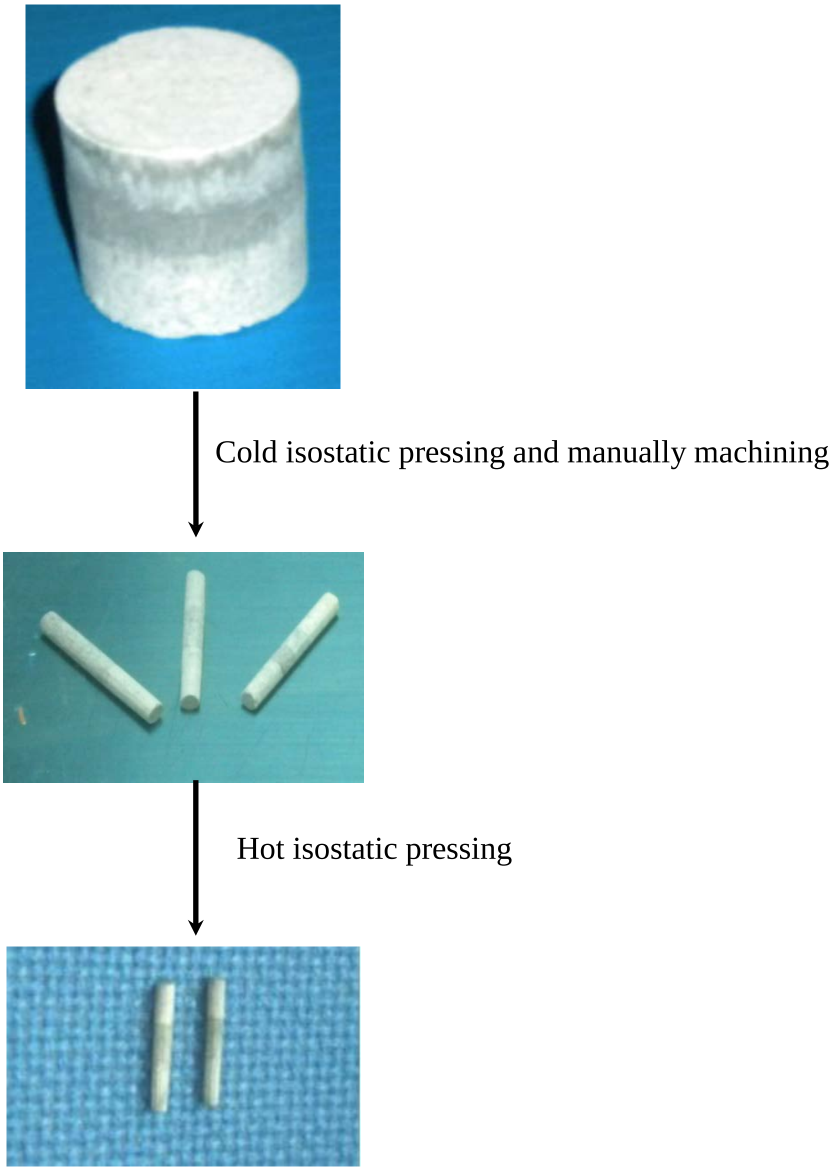

Figure 6.1 Sequence of the fabrication of FGSP prototype

6.4.2 Sample preparation

6.4.2.1 Collection and selection of the teeth

One hundred fifty recently extracted bovine incisors were collected. The teeth were disinfected by using 0.5% Chloramine T trihydrate solution for one week. Soft and hard deposits were removed by using an ultrasonic scaler (Piezon® Master 400, Nyon, Switzerland). The teeth were then stored in distilled water at 4ºC until used to prevent dehydration. The distilled water was changed weekly.

The selected incisors had similar dimensions, roots without curvature, were free of cracks or defects, and had been stored for no longer than 3 months. The inclusion criteria for tooth selection were teeth with single canals, without root surface caries or fractures. The selected specimens were examined at 10x magnification using a stereomicroscope (Kyowa Optical, Tokyo, Japan) to ensure fracture-free roots. Those with crazing or crack lines were excluded from the study. Buccolingual and mesiodistal radiographs (Eastman Kodak, Rochester, New York, USA) were made from each of the specimen teeth to exclude any tooth with internal resorption or canal abnormality. Seventy bovine incisors were selected for this study.

In order to make the specimens length standardized, the anatomical crowns of the selected teeth were removed using a separating disc (BEGO, Breman, Germany) under cooling water to minimize heating at the level of the CEJ perpendicular to the long axis of the root canal to obtain a relatively standard root canal length (16 mm) for all specimens. An attempt was made to select teeth with similar size and shape. Buccolingual (7.5 - 8 mm) and mesiodistal (5.5 - 6 mm) diameters of root canals were measured at the CEJ using digital caliper (Mitutoyo/Digimatic, Tokyo, Japan).

6.4.2.2 Canal preparation and obturation

Prior to endodontic preparation, each tooth was then mounted in impression compound (Hoffmann Harvard Dental, Berlin, Germany) to facilitate handling during root canal preparation and root canal obturation.

All the root canals were prepared with Gates-Glidden instruments (Dentsply Maillefer, Ballaigues, Switzerland) and K-files (Dentsply Maillefer, Ballaigues, Switzerland) using the step-back technique. The pulp was first extirpated with a barbed broach (Dentsply/Maillefer, Switzerland). The canal patency was established with a size 10 K-file. The file was placed in the canal with light pressure till its tip was just apparent at the apical foramen; the true working length was set 1 mm short of this file’s length.

Root canals were instrumented to the full extension using no. 2 and 3 Gates-Glidden drills (Dentsply Maillefer, Ballaigues, Switzerland). This was followed by no. 4 Gates-Glidden drill (Dentsply Malleifer) for the preparation of the cervical and middle thirds of the root canal.

After each filing, the canals were repeatedly irrigated with 3 mL of 1% sodium hypochlorite solution (NaOCl) (Clorox (M) Industries Sdn Bhd, Malaysia) and the canal were recapitulated with a 10 K-file to ensure canal patency. After completion of the preparation, each canal was irrigated in the following sequence, initially with 3 mL 1% NaOCl for one minute, then with 3 mL of 17% ethylenediaminetetraacetic acid (SmearClear™, SybronEndo, Orange, USA) for one minute in order to remove the smear layer and finally, with 3 mL distilled water for one minute to ensure complete removal of the NaOCl residue. Each endodontic file and Gates-Glidden drill was discarded after preparation of five canals.

The teeth were obturated using the warm compaction technique with gutta-percha cones (Dentsply/Asia) and AH-Plus™ sealer (Dentsply De Trey, Konstanz, Germany) using Bee Fill™ (VDW, Munich, Germany) system. Then the gutta-percha at the canal orifice was vertically compacted with a heated condenser. The canal orifices were sealed with IRM (Dentsply Caulk, Milford, USA). Then the teeth were stored in a 100% humid environment at $37^{o}C$ for 24 hours to ensure that the sealer set fully.

6.4.2.3 Grouping of samples

The specimens were randomly divided into seven groups of 10 specimens each as follows:

Group 1: endodontically treated teeth restored using the prototype FGSP (ZrO_2-Ti-HA) cemented with zinc phosphate cement and composite core.

Group 2: endodontically treated teeth restored using the prototype FGSP (Al_2O_3-Ti-HA) cemented with zinc phosphate cement and composite core.

Group 3: endodontically treated teeth restored using the prototype FGSP (Ti-HA-Ti) cemented with zinc phosphate cement and composite core.

Group 4: endodontically treated teeth restored using cast post obtained through direct modeling with a prefabricated plastic patterns, which was adjusted to the prepared root canal with self-cure acrylic resin (Pattern Resin, Tokyo, Japan) until passive retention was obtained. The final resin pattern had an intraradicular portion with passive taper and coronal portion with a standardized height of 5 mm. These resin patterns were invested and casted with nickel-chromium alloy (Columbium, Tokyo, Japan).

Group 5: endodontically treated teeth restored using prefabricated parallel-sided titanium post cemented with zinc phosphate cement and composite core.

Group 6: endodontically treated teeth without posts.

Group 7: extracted sound teeth.

6.4.2.4 Post space preparation

The gutta-percha was removed using Gates-Glidden drills to prepare standardizing the post space in all the teeth. The working length of the drills was measured and matched with a rubber stop according to the post length assigned (14 mm). Post spaces in all of the specimens were then sequentially prepared with the drills. The length of the prepared post canal with in root (10 mm) was further confirmed using drill of the titanium dental post system (Coltène/Whaledent, Cuyahoga Falls, OH). The post space was flushed with distilled water. The coronal part of the post was 4 mm.

6.4.2.5 Post placement and cementation

All the posts were cemented with zinc phosphate cement (GC Corporation, Tokyo, Japan). A trial insertion of the post was made to ensure passive complete seating to a depth corresponding to the post length of 10 mm in root canal. The cement was mixed according to the manufacturer's instructions. The canals were coated with zinc phosphate cement by using a Lentulo spiral. The posts were then coated with the same cement and inserted in the prepared canal, allowed to rebound in order to release hydraulic pressure and then gently reseated. This procedure was repeated until the post seated passively without rebound. The post was immediately seated into cement filled canal using finger pressure for 5 minutes to allow the cement to set. The excess cement was removed using an ultrasonic scaler after initial setting was achieved.

6.4.2.6 Core fabrication

A simplified anatomical build-up technique was used to restore all the crowns. Composite cores were prepared approximately by hand to resemble as closely to the final shape as possible.

The enamel was etched for at least 15 seconds. The composite restorations were then bonded using a universal self-priming dental adhesive (Prime and Bond®, Dentsply De Trey, Konstanz, Germany) according to the manufacturer's instructions. A standardized incremental composite build-up technique was employed by light-curing the resin composites at 2 mm increments. Each increment was light cured for 40 seconds up to 5 mm. The intensity of the light curing unit was not less than the 500 mW/cm^2 monitored periodically throughout the specimens' preparations. Then the specimens were ready to receive a metal coping (Figure 6.2).

Figure 6.2 Resin composite build-up.

6.4.2.7 Crown preparation

After complete polymerization of resin composite, similar cylindrical shape of composite cores were made. A circular line was marked using a permanent marker on the occlusal surface of the core, 1 mm away from the peripheral surface. The shank of diamond instrument was placed perpendicularly to the circular line to ensure standard preparation. All specimens were prepared with a diamond rotary cutting instrument in a high speed handpiece with water spray. A standardized 1 mm chamfer preparation was performed using a chamfer diamond bur on 2 mm below the composite margin (Figure 6.3). This is to ensure a proper dentine ferrule design was obtained.

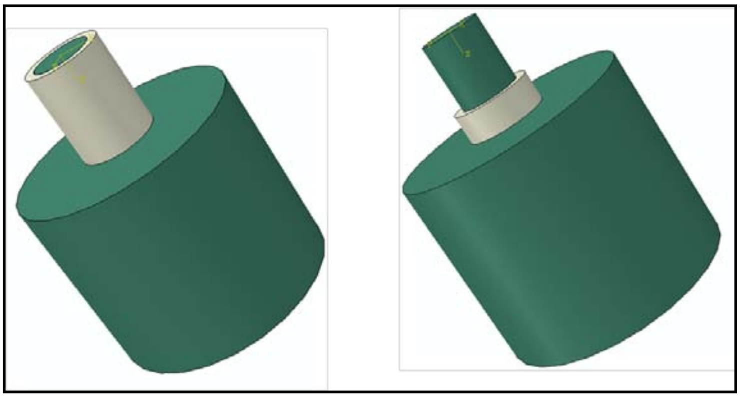

Figure 6.3 Schematic illustration of the tooth preparation.

6.4.2.8 Impression, die fabrication and waxing

After preparation, an impression of the specimens was made using polyether impression material (Impregum Soft; 3M ESPE, Seefeld, Germany). The impression material was allowed to set for 10 minutes and then poured in Type IV stone (Durone IV; Dentsply), and then all dies were waxed. Wax patterns (Degussa, Hanau, Germany) were then formed in the shape of a composite resin incisor crown (Figure 6.4) and standardized notch was placed across the palatal surface of each crown 2 mm from the incisal edge for load application in mechanical tests.

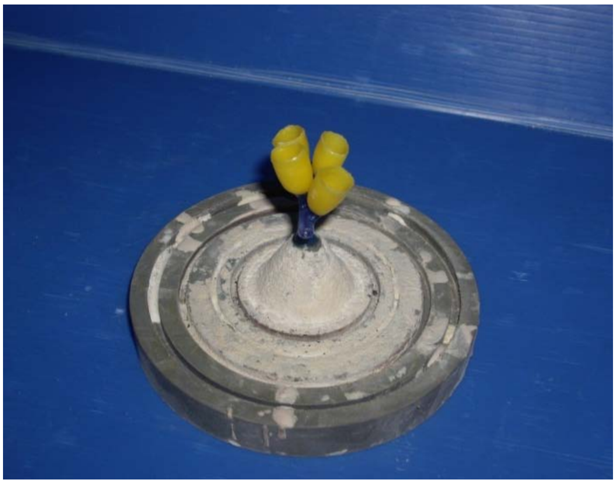

Figure 6.4 Wax pattern.

6.4.2.9 Investing and casting

Once the full wax-ups were completed, were sprued, and invested in Castorit Super C (Dentaurum, Pforzheim, Germany). The investment were allowed to set, and then were placed in the burnout oven, heated to 980^{o}C and held for 45 minutes at the final temperature entire. The crowns were then casted with Ni-Cr alloy (Remanium CD, Dentaurum, Germany) using an induction casting machine (Krupp, Essen, Germany) at 1370^{o}C. After devesting, the fitting surfaces of the coping were sandblasted with 50 µm Al_2O_3 at 2.5 Bar for 15 seconds. The fitting of the coping were checked and finalized to resemble a crown.

6.4.2.10 Copings cementation

All copings were cemented with zinc phosphate cement (GC Corporation, Tokyo, Japan). The cement was mixed on a glass slab for 20 s. The fitting area of copings was filled with cement and was then seated using finger pressure for 60 seconds. After 10 minutes, the excess cement was removed from the margin with a dental explorer No. 1. Prior to thermocycling, all specimens were stored in 100% humidity at 37^{o}C for 24 h. The specimens were then thermocycled according to (IS0/TS 11405:2003) at 5 and 55^{o}C for 500 cycles.

6.4.2.11 Periodontal membrane simulation

The specimens were first removed from the compound blocks. A thin layer (200 to 400 µm) of light body silicon paste (Aquasil Ultra XLV Dentsply/Caulk) was then painted on the root surface to simulate the periodontal membrane, and to provide a space between root surface and embedded resin and 3 mm short of the CEJ as described by Heydecke et al. (2001), Heydecke et al. (2002), Hayashi et al. (2006) and Sorrentino et al. (2007a).

6.4.2.12 Tooth mounting

Each of the specimens was then embedded in cold-cure epoxy resin (Mirapox A and B, Miracon, Kuala Lumpur, Malaysia) using cubic molds of 23 mm width X 23 mm length X 25 mm depth (Figure 6.5). Specimens were stabilized on a fixator with vertically moving rods, from the most coronal tip of each crown, with sticky wax to ensure that the long axis of the root was perpendicular to the horizontal plane. The specimens were left for 24 hours to allow complete setting of the epoxy resin.

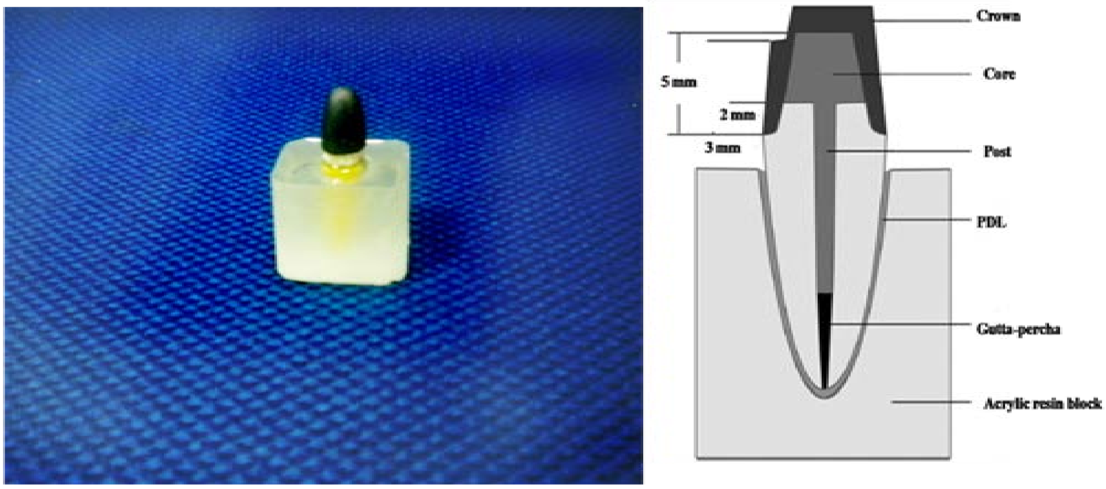

Figure 6.5 Specimen embedded in cold-cure epoxy resin and it’s diagrammatic illustration.

6.4.3 Testing procedure

6.4.3.1 Fracture resistance

Each of the mounted specimens was fixed in a customized fabricated jig to align long axis of the tooth at an angle 45^{o} to the horizontal plane and 135^{o} to the loading rod tip. This jig was secured to the lower compartment of the universal testing machine (Shimadzu, Japan) as shown in Figure 6.6. A steel flat ended rod of 2 mm diameter was fixed to the moving upper compartment of the testing machine. The tip of the loading rod was applied at the center of the beveled palato-incisal surface of each crown to standardize loading point for all specimens. An increasing compressive load was applied at a crosshead speed of 0.5 mm/min. The load at failure (N) was recorded at the point where a sudden sharp drop of the stress-strain curve was displayed.

Figure 6.6 Universal testing machine (Shimadzu) machine.

6.4.3.2 Failure mode

All specimens were examined by visually to classify and record the mode of failure. Then the specimens were evaluated under a stereomicroscope to confirm the visual findings. The failure mode was further confirmed using SEM. The failure mode was classified into either repairable or non repairable failures; a classification adopted from Fokkinga et al. (2004) as shown in Figure 6.7. The repairable failure modes were considered as those occurring by complete or partial post and core debonding or post-core-tooth complex fracture above the resin level. The non repairable failure modes were those with displayed fracture of the post core/root below resin block, vertical root fractures or crack within the resin block.

In order to investigate the failure pattern within epoxy resin block, the block were sectioned using a diamond precision cutting saw (ISOMET™, Buehler® Ltd, Evanston, USA) leaving the tooth intact. The teeth were placed in 2% methelene blue to mark the fractures lines. All teeth were examined at 10x magnification under a stereomicroscope.

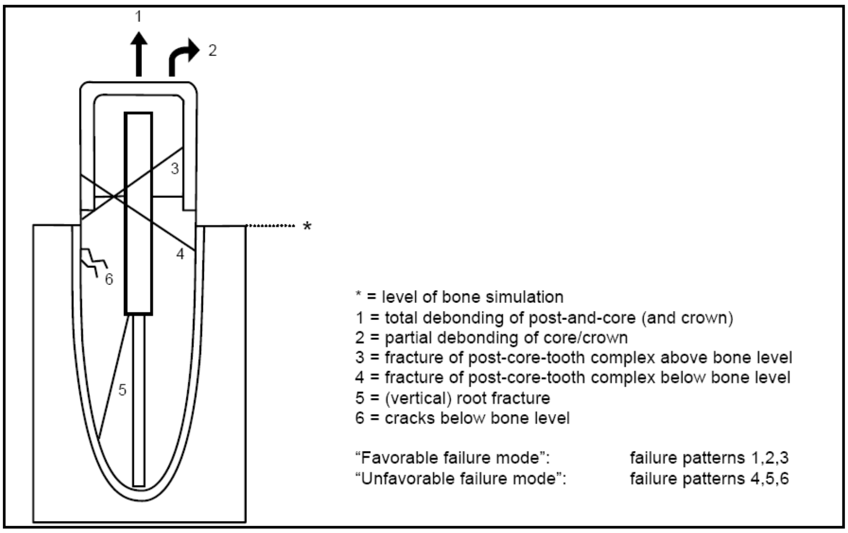

Figure 6.7 Schematic presentation of failure modes.

6.4.4 Data analysis

The data were subjected to statistical analysis in SPSS, version 12 (SPSS Inc., Chicago, USA) as follows:

6.4.4.1 Fracture resistance

The mean fracture resistance of various groups will be analyzed using the one-way analysis of variances (ANOVA) at $p = .05$. This will be followed by multiple comparisons if a significant difference among the groups is detected.

6.4.4.2 Failure mode

A chi-square test ($p = .05$) will be used to analyze the association between repairable and non repairable failures. If required Fisher's exact test will also be employed to compare between groups when the cells is less than 5.

6.5 Results

6.5.1 Fracture resistance

The mean fracture resistance for the various groups is shown in Figure 6.8. Mean fracture resistance for titanium (1408.65 N ± 226.39) and cast (1398.59 N ± 314.29) posts were the highest compared to the FGSPs; ZrO_2-HA-Ti (1299.31 N ± 251.74), Al_2O_3-HA-Ti (1242.53 N ± 196.55), Ti-HA-Ti (1267.68 N ± 173.00) and endodontically treated tooth without post (1051.40 N ± 207.78). Extracted sound teeth showed the lowest mean fracture resistance (922.48 N ± 261.59).

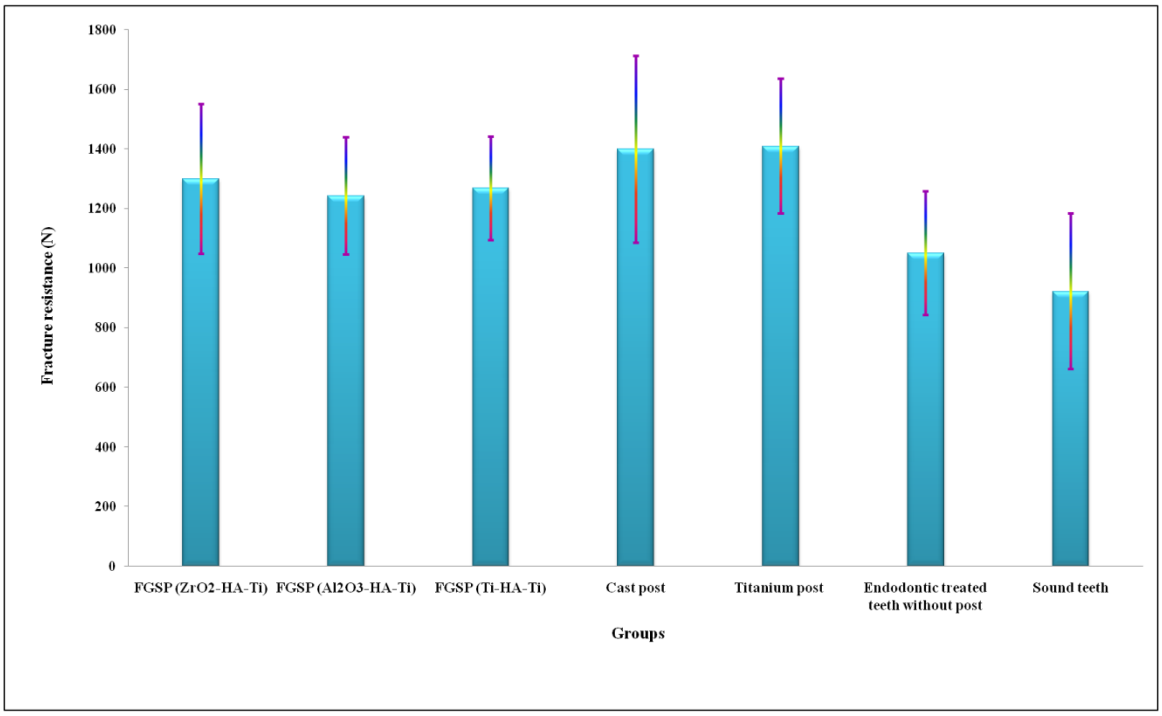

Figure 6.8 Mean fracture resistance for all groups.

The assumption of normality was checked and indicated that the data approximate normal distribution curve and it was further confirmed using the Shapiro-Wilk test, $p > .05$ (Appendix IV, Table A and Figure A). The values of Skewness and Kurtosis were within acceptable range, -1.92 to 1.83 (Tabachnick and Fidell, 2001).

One-way analysis of variances (ANOVA) showed that there is significant difference amongst the various groups ($p < .01$) as shown in Table 6.1. Levene's test showed that the assumption of homogeneity of variances was met, $p > .05$, (Table 6.2). Thus, the LSD Post Hoc for multiple comparisons was undertaken. Mean fracture resistance for the FGSPs; ZrO_2-HA-Ti (1299.31 N ± 251.74), Al_2O_3-HA-Ti (1242.53 N ± 196.55), Ti-HA-Ti (1267.68 N ± 173.00), cast post (1398.59 N ± 314.29) and titanium post (1408.65 N ± 226.39) were significantly higher than the endodontic treated teeth without post (1051.40 N ± 207.78) and extracted sound teeth (922.48 N ± 261.59) at $p < .05$.

Even though the mean fracture resistance of endodontically treated tooth restored with either cast post, or titanium post was higher than that for FGSPs no significant difference ($p > .05$) was detected between the groups as shown in Appendix IV Table B. There was no significant difference between endodontically treated teeth without post and extracted sound teeth ($p > .05$) as illustrated in Appendix IV Table B.

Table 6.1 One-way ANOVA analysis

	Sum of squares	df	Mean square	F	Sig.
Between groups	1931329.072	6	321888.179	5.725	.000
Within groups	3542110.181	63	56223.971		
Total	5473439.253	69			

Table 6.2 Test of homogeneity of variances

Levene's statistic	df1	df2	Sig.
1.118	6	63	.362

6.5.2 Failure mode

6.5.2.1 Percentage of repairable against non repairable failures

The percentage of non repairable against repairable is shown in Figure 6.9. Two specimens restored with FGSPs; Ti-HA-Ti, Al_2O_3-HA-Ti showed non repairable, whereas for FGSP (ZrO_2-HA-Ti), there was only one specimen that was showed non repairable failures. For endodontically treated teeth without post, there were three specimens exhibited non repairable failure. However there were nine non repairable failures for the titanium post and cast post groups. All the extracted sound teeth exhibited non repairable failures.

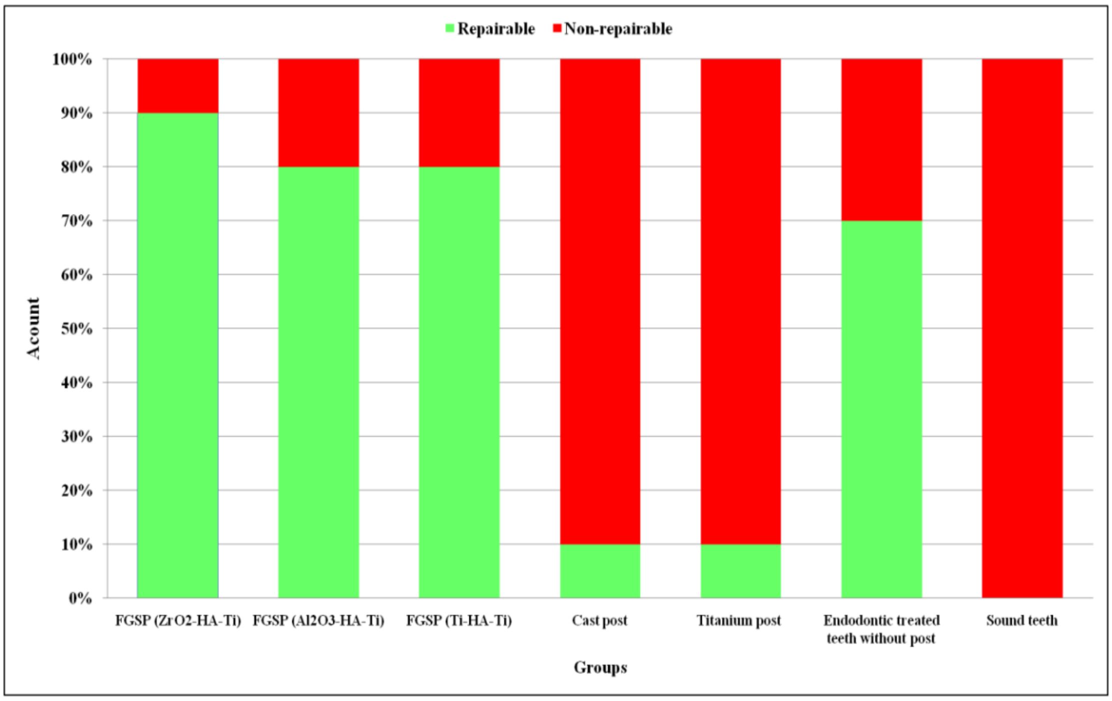

Figure 6.9 Failure mode of root restored with various restoration.

6.5.2.2 Failure mode behaviour

Distinct differences in failure patterns amongst experimental groups were observed. No fractures were seen in the middle or apical third of the roots for most of the FGSPs specimens and endodontically treated tooth without posts. In 80%-90% of specimens fracture was confined to the crown margin involving only core and posts or specimens, fracture extending into the root surface just below the crown margin. Only five specimens of the FGSPs were non repairable as the fracture extended from the palatal margin to the labial surface below the acrylic resin into middle parts of the root (Figures 6-10 and 6-13)

Only one specimen from each of the cast post and titanium post groups was repairable where the post was dislodged from the root canal. No serious damage was observed both visually and microscopically for these specimens. Oblique root fractures were apparent in the titanium and cast posts groups, with fracture lines occurring in the middle third of the root extending to the apical (Figures 6.14 and 6-15). The most catastrophic failure was seen in specimens from the titanium post and cast post groups.

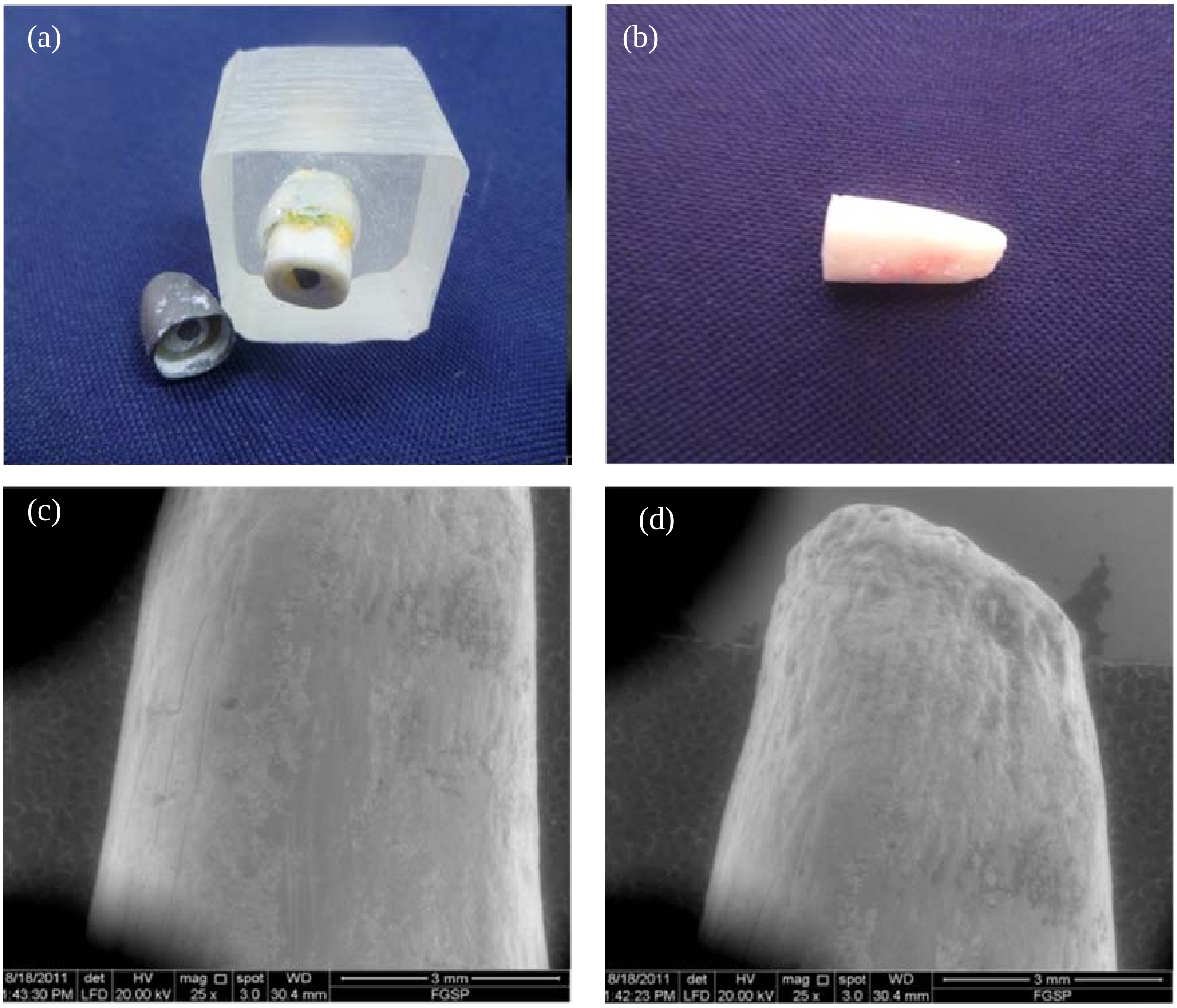

Figure 6.10 Representative specimen for the FGSP formulation, ZrO_2-HA-Ti; a) specimen after failure where the fracture is within the post, b) specimen without the embedding block prior to microscopy, c) scanning electron micrograph at the middle third and d) scanning electron micrograph at the apical third showing that the root is free from cracks indicating a repairable failure.

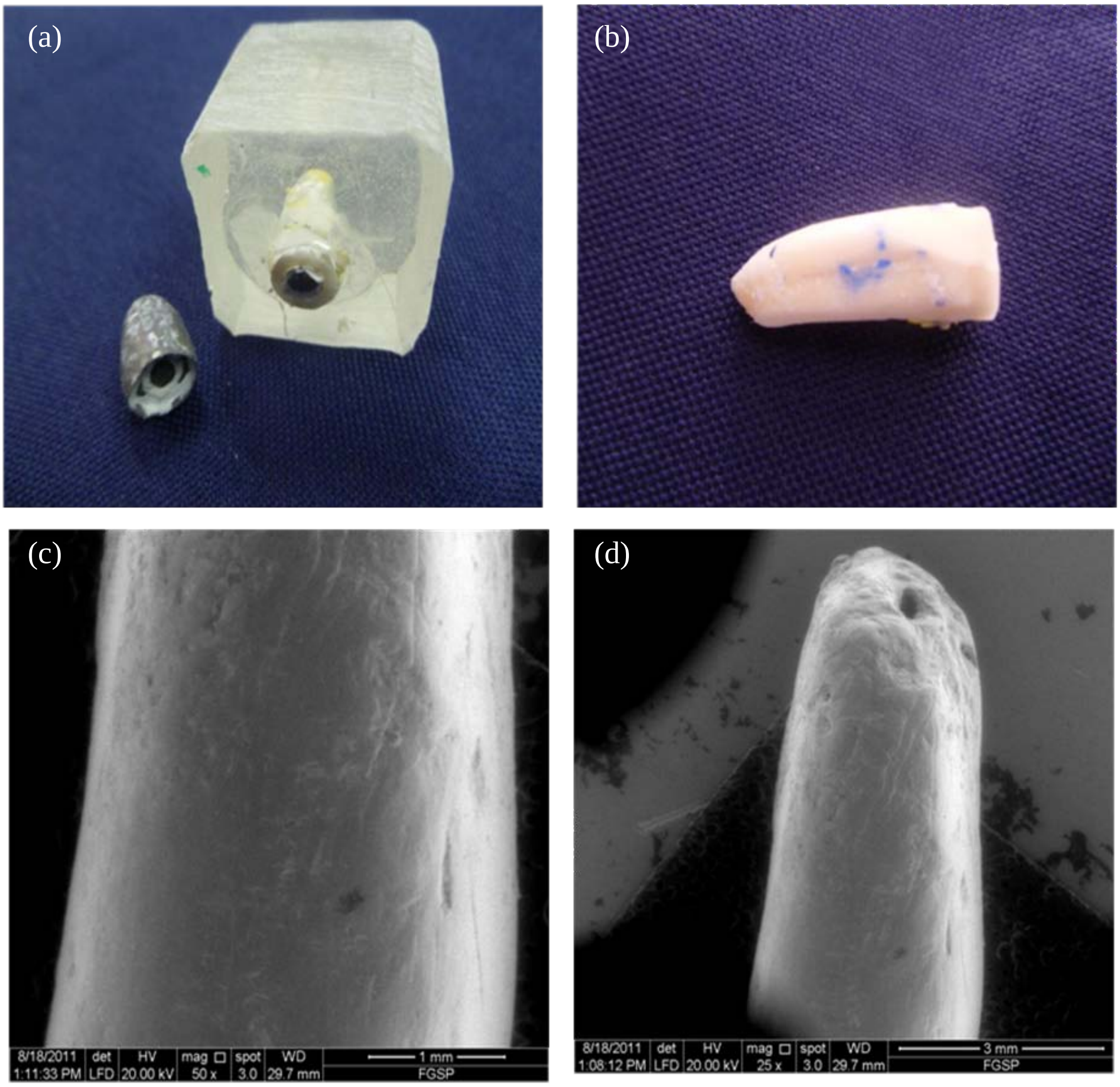

Figure 6.11 Representative specimen for the FGSP formulation, Al_2O_3-HA-Ti; a) specimen after failure where the fracture is within the post, b) specimen without the embedding block prior to microscopy, c) scanning electron micrograph at the middle and coronal thirds and d) scanning electron micrograph at the apical third showing that the root is free from cracks indicating a repairable failure.

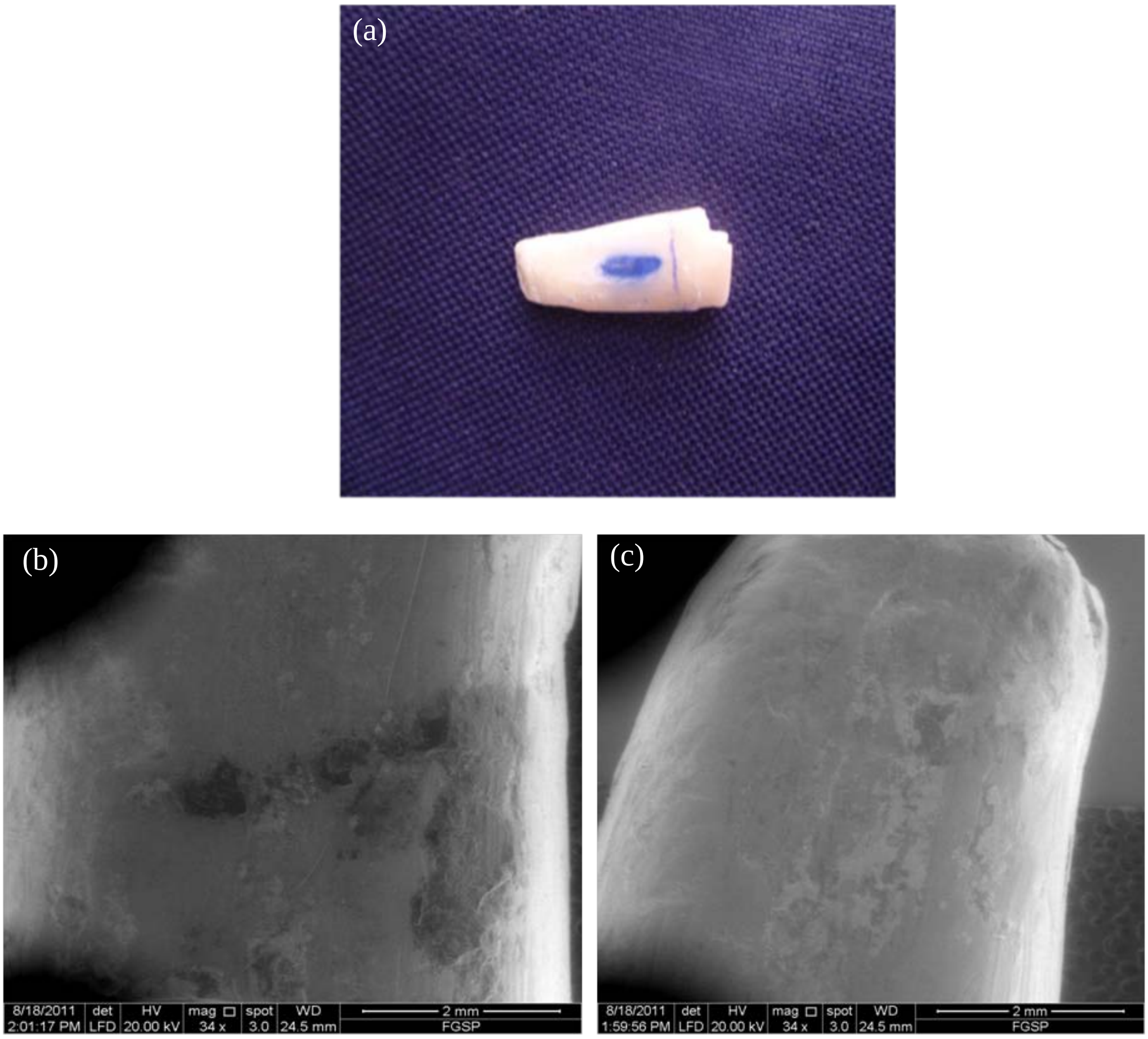

Figure 6.12 Representative specimen for the FGSP formulation, Ti-HA-Ti; a) specimen without the embedding block prior to microscopy, b) scanning electron micrograph at the coronal third and c) scanning electron micrograph at the apical third showing that the root is free from cracks indicating a repairable failure.

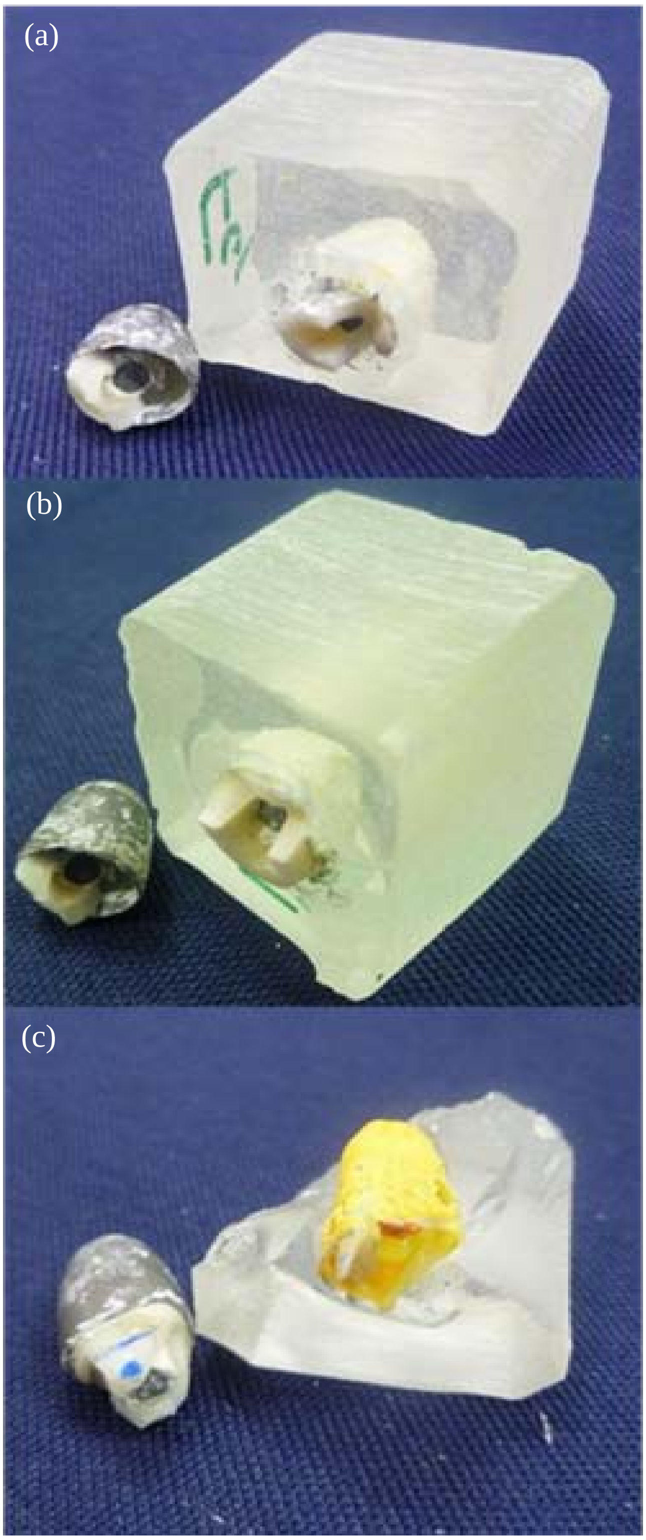

Figure 6.13 Representative specimens for the FGSP formulations, a) ZrO_2-HA-Ti, b) Al_2O_3-HA-Ti and c) Ti-HA-Ti specimens after failure where the fracture is within the root indicating a non repairable failure

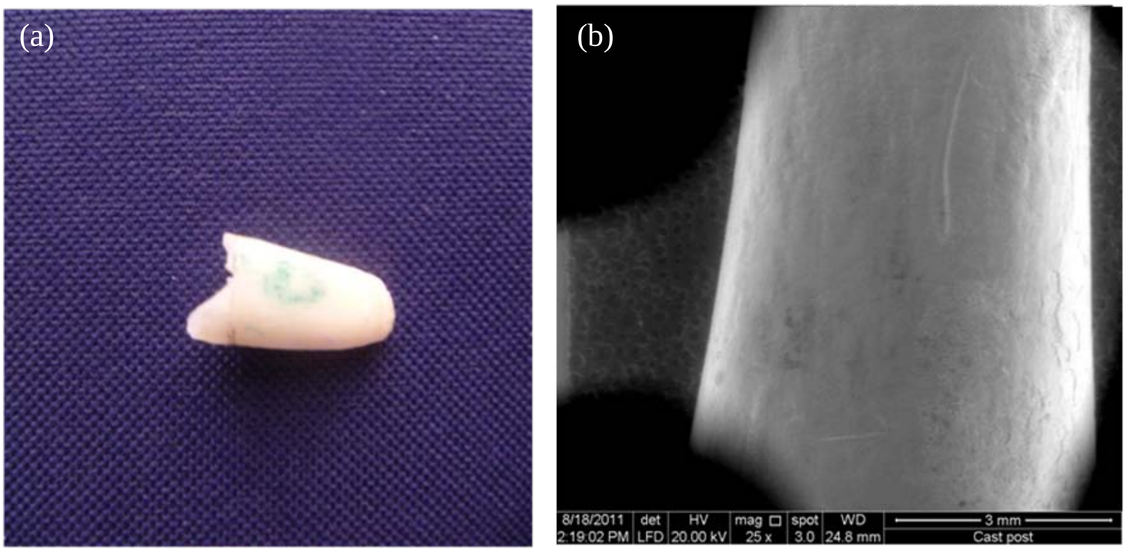

Figure 6.14 Representative specimen for the cast post a) specimen without the embedding block prior to microscopy, c) scanning electron micrograph showing that the root is free from cracks indicating a repairable failure.

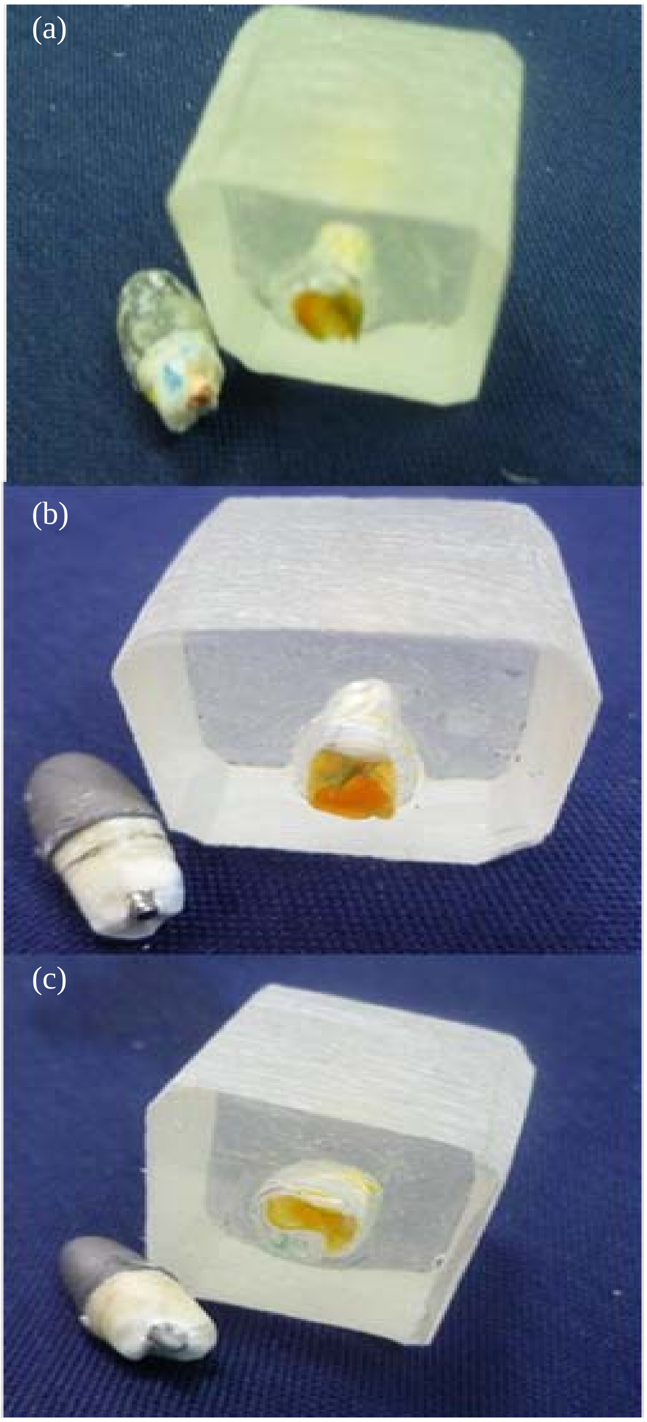

Figure 6.15 Representative specimens for the a) endodontically treated teeth without post, b) titanium post, c) cast post specimens after failure where the fracture is within the root indicating a non repairable failure

6.5.2.3 Effect of various dental post on failure mode

The chi-square test (Appendix IV, Table C) showed significant differences amongst all groups. In order to determine where the significant difference lies, the Fisher's exact test was carried out. There were no significant difference between the FGSPs (ZrO_2-HA-Ti, Al_2O_3-HA-Ti, Ti-HA-Ti) and endodontic treated teeth without post ($p > .05$). The same was observed between cast and titanium posts ($p > .05$). However, when the cast post and titanium post were compared to FGSPs (ZrO_2-HA-Ti, Al_2O_3-HA-Ti, Ti-HA-Ti) and endodontic treated teeth without post, non repairable failure mode of titanium and cast posts was significantly higher ($p < .05$). The same was observed between endodontic treated teeth without post and extracted sound teeth ($p > .05$) (Appendix IV, Tables D-X).

6.6 Discussion

6.6.1 Methodology

6.6.1.1 Extracted teeth

In this study, recently extracted bovine incisors were used in accordance with other *in vitro* studies when evaluating the fracture behaviour of various post and core systems (Bortoluzzi et al., 2007; Soares et al., 2007; Santos-Filho et al., 2008; Martelli et al., 2008; Clavijo et al., 2009; Soares et al., 2010; Nothdurft et al., 2011).

Bovine incisors were used for convenience as human incisors in large numbers are difficult to collect. Bovine dentine is often used for *in vitro* tests, and is generally considered similar to the human dentine in composition and geometric root configuration (Schilke et al., 2000; Fonseca et al., 2004; Fonseca et al., 2008). Several studies have reported that the mechanical properties of bovine dentine when used for laboratory testing such as bond strength, ultimate tensile strength and modulus elasticity of bovine dentine was similar to human dentine (Nakamichi et al., 1983; Saunders, 1988; Ruse and Smith, 1991; Sano et al., 1994; Schilke et al., 2000). In addition, bovine incisors also showed less variation in anatomical morphology than human teeth. Therefore, bovine teeth could provide a standard and reproducible anatomy that allows evaluation of different treatment modalities. The greater availability of bovine teeth also made it possible to standardize specimen size and shape (Soares et al., 2007; Santos-Filho et al., 2008).

6.6.1.2 Canal irrigation

The canal was irrigated with 3 mL of NaOCl after each instrumentation. This was done throughout the endodontic treated (Baumgartner and Cuenin, 1992). NaOCl is the most used employed root canal irrigant; it is usually used in concentrations ranging between 0.5-5.25% (El-Karim et al., 2007). Studies reported that NaOCl reduced the flexural strength and elastic modulus of dentine by depleting the organic content of dentine (Sim et al., 2001). However, its effects were reported to be concentration dependent (Sim et al., 2001). Many studies reported comparable debridement capabilities and intracanal antimicrobial effect for 1%, 2.5% and 5.25% solutions (Baumgartner and Cuenin, 1992; Berber et al., 2006). Therefore in the current study, copious amounts of a relatively low concentration (1% NaOCl) were used to minimize any possible effects on the physical or mechanical properties of the tooth whilst achieving the desired debridement effect.

6.6.1.3 Cementation of posts

Cements play a significant role in enhancing retention, stress distribution, and sealing irregularities between the post and the tooth (Trope et al., 1985). Many studies reported that resin based cements could influence failure mode and increase the fracture resistance of endodontically treated tooth restored with a post (Al-Hazaimeh and Gutteridge, 2001; Mezzomo et al., 2003; Naumann et al., 2008). According to these studies, the repairable behaviour of fibre reinforced resin posts might be related to the resin cements used to lute them rather than the post material itself. As this present study was addressed to investigate the fracture resistance and failure mode of FGSPs prototypes, therefore, zinc phosphate was used to prevent any effect of resin cement on the fracture resistance and failure mode. Moreover, zinc phosphate cement has also been used as gold standard for cementation of posts. It is also still the luting agent of choice for most conventional fixed prosthesis because of its easy handling characteristics and adequate long term clinical results (Jokstad and Mjör, 1996).

6.6.1.4 Tooth preparation and final restoration

Teeth prepared with adequate ferrule can effectively withstand functional forces and enhances the fracture strength of posts and cores in endodontically treated teeth. Sorensen & Engelman (1990) found that the key factor in failure threshold was coronal extension of the tooth structure above the crown margin. Libman & Nicholls (1995) examined the effects of various ferrule heights (0.5 to 2.0 mm) on the load resistance of endodontically treated teeth restored with cast posts and cores. They reported that a ferrule height of at least 1.5 mm is required to ensure good prognosis for restoration. Assif et al. (1993) stated that complete crown coverage with a 2 mm ferrule on sound tooth structure alters the distribution of forces to the root and post and core complex.

Although many studies supported the use of ferrules, some studies questioned the advantage of ferrules because they did not offer additional support for restored teeth (Al-Hazaimeh and Gutteridge; 2001; Mezzomo et al., 2003). Al-Hazaimeh & Gutteridge (2001) examined the effect of a ferrule on central incisors when a direct post and composite resin core was utilized. They reported no significant difference between the ferruled and non ferruled specimens. Mezzomo et al. (2003) found no significant difference in fracture resistance of ferruled specimens and non ferruled specimens restored with resin cemented posts. Ng et al. (2004) found a higher frequency of root fracture among teeth restored with bonded posts and cores when ferrules were included. Qing et al. (2007) examined the failure loads of anterior endodontically treated teeth prepared with a 2 mm ferrule, restored with glass fibre and zircon posts and composite resin cores or cast posts and cores. They found that glass fibre and zircon posts and composite resin cores showed significantly lower fracture resistances than those with cast Ni-Cr alloy posts and cores. Naumann et al. (2006) reported that incomplete ferrules, that do not encircle 360 of the tooth, were associated with higher failure loads when compared with ferrules that totally encircle the tooth. They reported that tooth structure preservation is more important for the fracture resistance of post and treated teeth. The findings of the above studies underlie that the incorporation of ferrules in conjunction with resin cemented posts for the sake of tooth reinforcement might constitute an unjustifiable insult to the remaining tooth structure. When zinc phosphate cement was used, ferruled specimens showed significantly higher fracture resistance than non ferruled ones (Al-Hazaimeh and Gutteridge; 2001).

In this current study, 2 mm ferrule was prepared for all specimens as recommended by the literature for better resistance form. The final restoration was constructed a full coverage non-precious metal crowns.

6.6.1.5 Artificial periodontal membrane

It has been proven that rigid embedding materials, such as acrylic resin may affect the mode of the failure of the specimens during the mechanical testing (Newman et al., 2003). In order to imitate the physiologic tooth mobility, silicon was used as artificial periodontal membrane was used in this study (Heydecke et al., 2001; Heydecke et al., 2002; Hayashi et al., 2006; Sorrentino et al., 2007a).

6.6.1.6 Loading area and direction

When evaluating the fracture resistance of restored endodontically treated teeth, the area for load application has been widely described as one of the paramount factor to be considered in order to achieve reliable results (Hannig et al., 2005; Nagasiri and Chitmongkolsuk, 2005; Hayashi et al., 2006). The direction of load application area is also dependent on the tooth anatomy (Hannig et al., 2005; Nagasiri and Chitmongkolsuk, 2005; Hayashi et al., 2006).

In this present study, the chosen area for loading was on the palatal aspect, 2 mm away from the incisal edge as recommended by other studies (Heydecke et al., 2001; Heydecke et al., 2002). This area coincides with the area of incisor guidance during stomatognatic functions.

It has also been well documented that fracture resistance of teeth depends on the angle of applied load and axial forces are less detrimental than oblique forces (Loney et al., 1995). As a consequence, the loading is a critical factor affecting the longevity of endodontically treated teeth (Krejci et al., 2003). According to the gnatology concepts, teeth are subjected to different loading condition due to their specific function. As a consequence, posterior teeth have to withstand occlusal and masticatory forces (Schwartz and Fransman, 2005) whereas anterior teeth are responsible for tearing and functional guidances (Heydecke et al., 2002). The majority of the studies evaluating the fracture resistance of anterior endodontically treated teeth employed loading angles ranging from 130^{o} to 135^{o} (Fokkinga et al., 2004). In this current study, the teeth were loaded at 135^{o} to the long axis of the root from the palatal direction. The chosen angle also simulates the average interincisal relationship between maxillary and mandibular incisors in Class I occlusal relationship (Bishara, 2001) as illustrated in Figure 6.16.

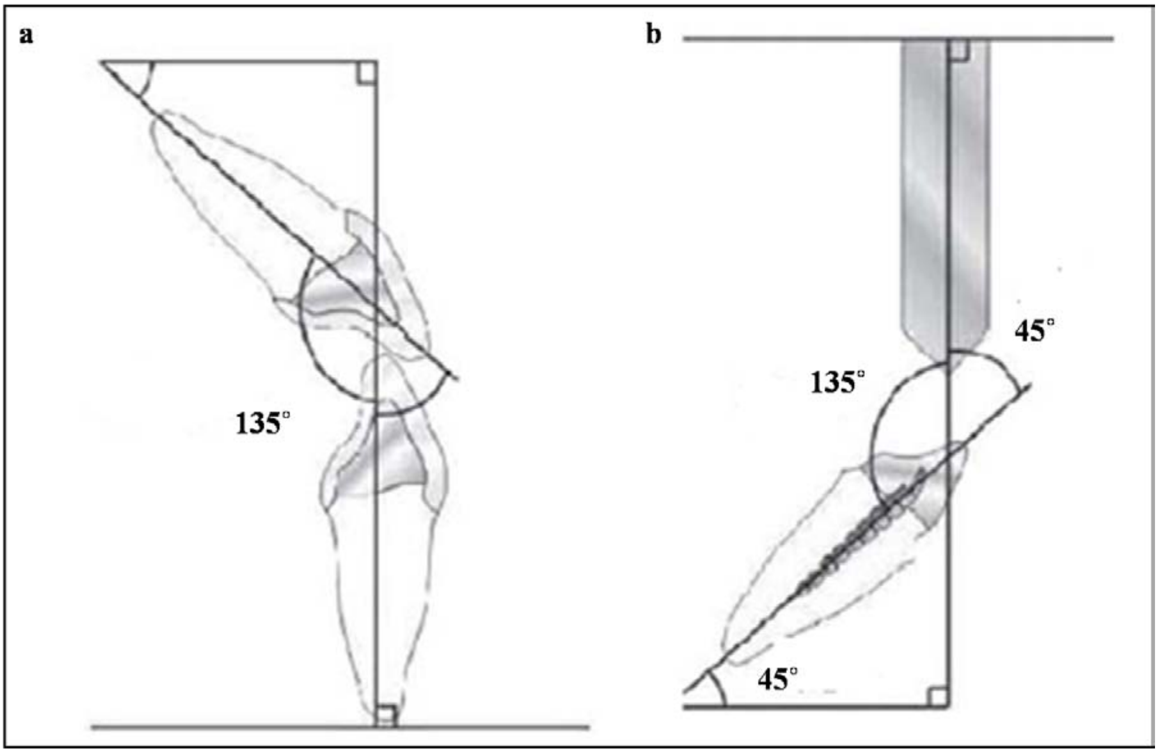

Figure 6.16 Schematic diagram showing the load application a) 135^{o} angle formed by contact between the human maxillary and mandibular central incisors in a Class I occlusal relationship; b) schematic representation of load at an angle of 135^{o} to the long axis of the root.

6.6.2 Results

Fracture behaviour has been widely used in the evaluation of post and core systems (Salameh et al., 2006; Jung et al., 2007). Fracture behaviour can be explained as the relationship between the load-bearing capacity (fracture resistance) and the failure mode of a post and core system (Fokkinga, 2007). Therefore, fracture resistance was measured in order to evaluate the load-bearing capacity of the teeth restored with different types of posts. Assessment of the failure modes was also recorded to assess the influence of post type on the restored teeth.

One of the disadvantages of fracture resistance evaluation using human and or bovine teeth is the large standard deviation (Yoldas et al., 2005). Variation among individual teeth, such as the mechanical and physical properties inside and outside the root canals may be different, and existing microcracks in the dentine may not be visible prior to testing. The observation was also evident in the data collected for this study.

In the present study, titanium and cast posts have higher fracture resistance when compared to other groups. These results might be related to the high rigidity of metallic posts (Lambjerg-Hansen and Asmussen, 1997). However, the failure for titanium and cast posts group was catastrophic and most resulted in extraction of the tooth from the embedding resin. The results of this present study are in accordance with Cohen (1995), who showed that titanium post cemented with zinc phosphate had asymmetric and uneven stresses concentrated apically when vertical or oblique forces were applied. These findings also are in agreement with Cormier et al. (2001) and Ferrari et al. (2000b), who reported that the cast posts and cores were frequently associated with deep catastrophic root fractures. The most common fracture site seen in the titanium and cast posts was at the apical third followed by failures at the junction of the middle and apical thirds. These findings also concurred with Butz et al. (2001) and Lertchirakarn et al.

(2003), who reported that higher incidence of vertical root fractures was reported among teeth restored with titanium, zirconia, and cast posts. This has been attributed to the stress concentration within the radicular dentine during post placement and, consequently, the altered pattern of stress distribution upon loading (Lertchirakarn et al., 2003). Akkayan & Gulmez (2002) and Fokkinga et al. (2004) also reported similar failure mode. A recent retrospective study reported that 13.2% of endodontically treated teeth restored with metal posts had complications, such as root or crown fractures (Willershausen et al., 2005). The results of this present study was further substantiated by Loney et al. (1990). Through 3D FEM, they reported that cast posts demonstrated the highest stress concentrations at the apical part of the post.

Although the titanium and cast posts demonstrated the highest fracture resistance values, nine specimens from each group were non repairable. These findings concurred with Sorensen & Martinoff (1984b) who showed that tapered cast post and cores demonstrated higher failure rates than teeth treated without intracoronal reinforcement. In another study by Sorensen & Engelman (1990), they showed that tapered cast posts exhibited wedging effect that resulted in non repairable root fractures.

In this study, the endodontically treated teeth without post showed lower fracture resistance compared to titanium and cast post group. The observation for the extracted sound teeth group may not be reflected of the clinical situation as their behaviour could be affected by the lost of pulp vitality. These results are in agreement with Ferrari et al. (2007) and Cagidiaco et al. (2008), who showed that the placement of fibre posts did improve the survival rate of endodontically treated premolars. Salameh et al (2007, 2008a, b) also showed that endodontically treated teeth restored with fibre posts and ceramic crowns were more resistant to fracture and had less catastrophic fracture patterns than the ones restored with ceramic crowns and no posts. On the contrary, Fokkinga et al. (2005) reported that the presence or absence of metal and fibre posts did not affect the fracture resistance of endodontically treated premolar teeth even though the coronal tooth structure were replaced with resin composite crowns. Mohammadi et al. (2009) also found no difference in fracture resistance of premolars restored with direct resin composite in the presence or absence of fibre post and cuspal coverage.

In this study, the fracture resistance of the three FGSPs prototypes group did not differ significantly from the fracture resistance of the titanium and cast post group. However, the fracture resistance was significantly higher than endodontically treated teeth without posts.

Interestingly, the results of the failure mode evaluation exhibited significant differences between the groups. In all the groups, most typically, fracture of the sample happened initially at the crown margin on the palatal side where loading was applied. The fracture line then continued towards the buccal surface of the root, above, below or at the simulated bone level. If the fracture terminates above or at the simulated bone level, this fracture mode was considered to be repairable. The three groups restored with FGSPs and the endodontically treated teeth without post showed more repairable failures compared to titanium and cast posts. These findings concurred with the 3D FEM stress analyses as reported in Chapter 5 where the higher stress on FGSPs concentrated at the coronal part of the post (Figure 6.17). This may explain why most specimen exhibit repairable failure for FGSPs. It seem like FGSPs were able to facilitate stress dissipation due to its gradual change in properties along the post. This could also explain the repairable fracture patterns for FGSPs in endodontically treated teeth, further work need to be conducted to confirm this hypothesis.

The location of stress concentration that is likely to cause fracture in the endodontically restored teeth were affected by parts of the post along its length, stiffness of the post and core and the direction of the loading. For titanium and cast posts, the stress was concentrated at the middle and apical regions adjacent to the apical part of the post hence resulting in non repairable fracture. This is in agreement with previous FEM studies (Williams and Edmundson; 1984; Sorensen and Engelman, 1990) and our 3D FEA stress analyses reported in Chapter 5, where stress were concentrated at middle and apical thirds for endodontically treated teeth restored with titanium and cast posts compared to FGSPs and endodontically treated teeth without posts (Figure 6.17).

Anusavice et al. (2003) and Tan et al. (2005) stated from the literature that the maximum incisal forces of anterior teeth almost below 200 N. This occlusal force was much lower than the fracture resistance (N) of all experimental groups in this study, thus indicating that the three FGSPs are likely to be able to withstand incisal force in the oral cavity.

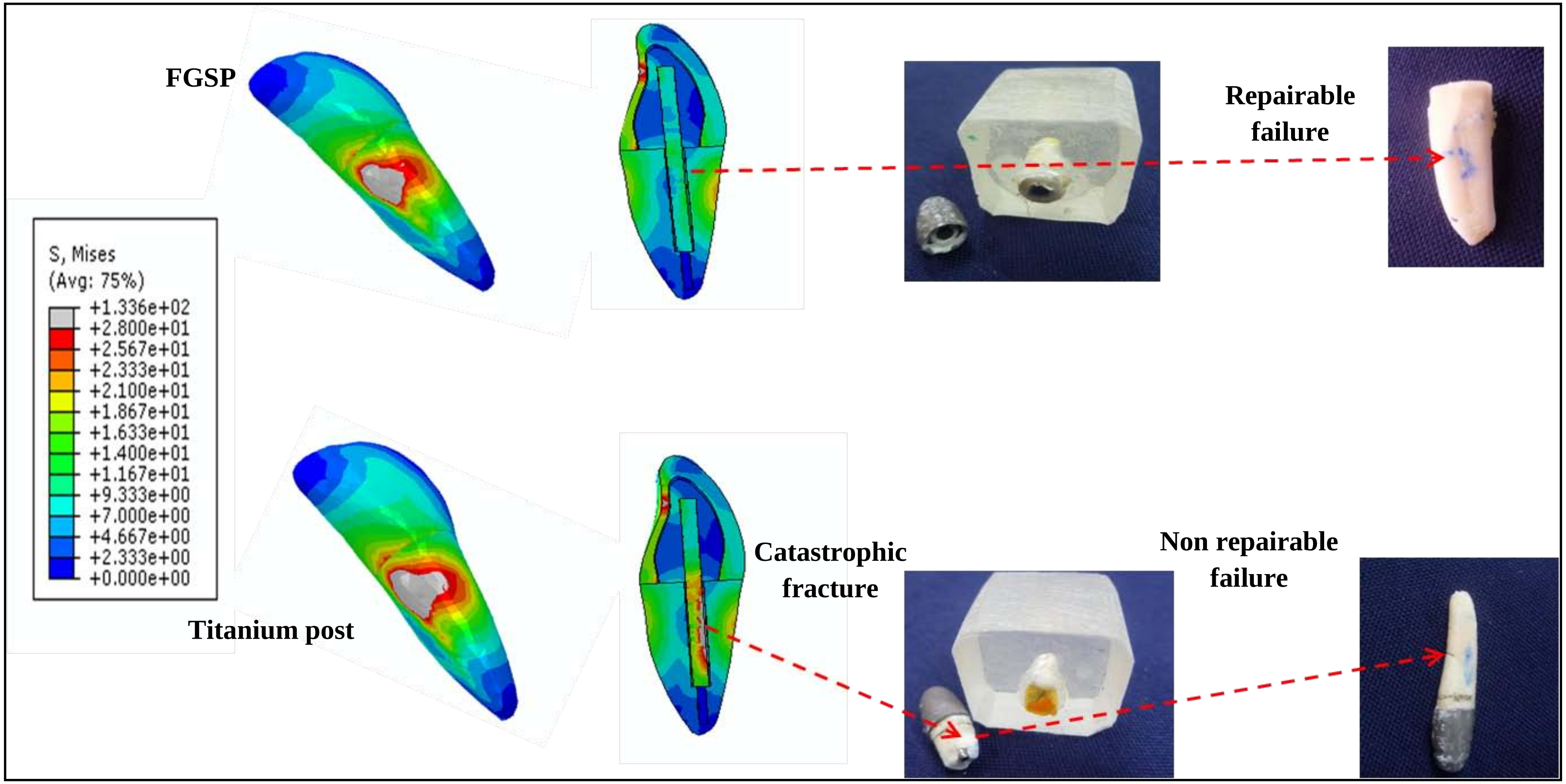

Figure 6.17 Relationship between failure mode and the finite element analysis.

6.7 Conclusions

Under the limitation of this study, the following conclusions may be drawn:

1. There was no significant difference in the mean fracture resistance (N) for endodontically treated restored with FGSPs, titanium and cast posts.

2. The mean fracture resistance of endodontically treated teeth restored with the FGSPs, titanium and cast posts was significantly higher than that endodontically treated teeth without posts and extracted sound teeth.

3. Titanium and cast posts resulted in significantly higher non repairable fracture of the roots whilst the FGSPs and endodontically treated teeth without posts had repairable fractures within resin core, ferrule or post.

Chapter Seven

Summary

7.1 Summary

The concept of functionally graded materials (FGM) has been conceived as a new material design approach to improve performance compared to traditional homogeneous and uniform materials. This technique allows the production of a material with very different characteristics within the same material at various interfaces. FGM is an innovative materials technology, which has rapidly progressed both in terms of materials processing and computational modeling in recent years. However, the fabrication of functionally graded multilayered composites (FGMCs) is most often hindered by the variation of elastic, plastic, thermal, chemical, and kinetic properties within the composite. Across a material interface, these discontinuities in material properties can lead to the formation of residual stresses. Despite these challenges, compositional gradient structures offer significant benefits. In addition to utilizing the beneficial properties of the base materials, the transition of thermal stresses across materials with thermal expansion mismatch was smoothed, the magnitude and critical locations of thermal and mechanical stresses was tailored.

The FGMCs were fabricated and optimized using pressureless sintering and hot isostatic press. Initially, the FGMCs were fabricated using the findings from the preliminary FEA results, and then optimized to various gradient architectures. SEM, EDX and XRD were used for characterization of compositional and microstructural of FGMCs. The SE micrographs showed that interfaces between the first, second, third and fourth layers showed continuous boundaries free of defects and graded phase distribution. The microstructure of the first, second, third and fourth layers also showed a gradual change in the titanium concentration that confirms the functionally graded design of the multilayered composite. EDX and XRD analyses from different areas of the microstructures confirmed the presence and gradual change of Ti-HA-ZrO_2-Al_2O_3

elements and phases in all the specimens. The gradual change of the compositions and microstructure in Ti-HA-ZrO_2-Al_2O_3 can likely lead to a gradual change in material properties. Moreover, the physical and mechanical properties changed gradually which confirms the functionally graded structure of the multilayered composite. As different components, ceramics and metals showed gradual variation in materials composition across its thickness. Such a microstructure, compositional, physical and mechanical properties is expected to reduce thermal and mechanical stresses and at the end tailored functional performance.

In daily consumption of food and drinks at different temperatures, the temperature of the oral cavity varies and this phenomenon is very important to evaluate because it interferes with the strength of the material and might shorten the service period. Since the natural temperature of the oral cavity is 36±1°C, it appears that there may be a considerable gradient of temperature when teeth come into contact with irritants. Consequently, thermal stresses and strain may develop at interfaces between different materials because of thermo-physical properties mismatches. Therefore, it is important to ascertain the thermal behaviour of FGSPs in order to predict their performance in the oral environmental. FGSPs exhibited minimal thermal stress and strain distributions. These types of posts were able to redistribute thermal stresses over time efficiently. This may be due to the compositional gradients arising from the combination of multiple material properties.

When a restorative system is loaded, it is able to absorb the applied forces generating peculiar stresses (von Mises, compressive, tensile and shear) and strains. The evaluation of such patterns by using FEA can be a reliable predictive tool to forecast areas under risk of possible mechanical failures. In this present study, FGSPs showed a reduction in peak von Mises, compressive, tensile and shear stresses compared to the homogenous-type posts.

Consequently, a laboratory investigation was used to validate the simulated mathematical models as in Chapter 5. Data extrapolated from virtual simulations in Chapter 5 was confirmed by *in vitro* results in Chapter 6. In this study, the fracture resistance of the three FGSPs prototypes group did not differ significantly from the fracture resistance of the titanium and cast post group. However, the fracture resistance was significantly higher than endodontically treated teeth without posts.

7.2 Limitations of the present study

1. Stacking the layer by layer was performed manually. This may cause some inaccuracy in the uniform distribution of powders compared to automatical stacking.
2. The specimen was compacted manually by using the hydraulic uniaxial press as it will be more efficient if automatical compaction is used.
3. The powder size of each component had an important role in optimization of FGMCs specimens. Therefore, changing the particle size requires new optimization. Nano-particles may improve the performance although it is more costly.
4. The maximum pressure of hot isostatic press applied to the specimens during the sintering was 180 MPa, while the higher pressure (300 MPa) will decrease the porosity and will enhance the physical and mechanical properties.

7.3 General conclusions

1. FGMCs with the optimum graded composition have been successfully fabricated by both pressureless sintering and hot pressing.

2. The physical and mechanical properties of the sintered FGMCs exhibit gradual variation in FGM architecture.
3. The zirconia and titanium posts produced greater thermal stresses and strains than FGSPs.
4. FGSPs exhibited reduction in terms of stress distribution compared to homogenous-type dental posts under various load directions.
5. There was no significant difference in the mean fracture resistance of endodontically treated teeth between the FGSPs, titanium and cast posts.
6. Titanium and cast posts resulted in significantly higher non repairable fracture of the roots whilst the FGSPs and endodontically treated teeth without posts showed repairable failure fractures as were within the resin core, ferrule or post.

7.4 Recommendations of the present study

1. The fabrication of the FGMCs using micro-injection molding in order to enhance FGSPs production.
2. Further requirement of FGMCs using particle size distributions, binder additives, and nano-particle sintering aids.
3. Fatigue behaviour of FGSPs prototypes and compared with the homogenous-type dental posts should be conducted.
4. Effect of various cements in the bond strength of FGSPs prototypes and compared with the homogenous-type dental posts.
5. Further FEA should be carried out to evaluate the affect of mastication and stress distribution in FGSPs.
6. Study the mechanics of how FGSP facilitate thermal and stress dissipation in trend.